the Hybrid Cutter Dredger

a study on technical and economical feasibility

J.L.S. Gerritsen

DELFT UNIVERSITY OF TECHNOLOGY
Master of Science Thesis Marine Technology
Master in Marine Engineering

Report Number: SDPO.16.027

TU Delft

the Hybrid Cutter Dredger

a study on technical and economical feasibility

by

J.L.S. Gerritsen

to obtain the degree of Master of Science
at the Delft University of Technology,
to be defended publicly on October 31, 2016 at 09:30 AM.

Student number: 4098013
Project duration: December, 2015 – October, 2016
Thesis committee:

Prof. ir. J.J. Hopman,	TU Delft
Ir. K. Visser,	TU Delft, supervisor
Dr. ir. S.A. Miedema,	TU Delft
Ir. J.R. Voormolen,	Van Oord

An electronic version of this thesis is available at http://repository.tudelft.nl/.

TU Delft

Preface

This master thesis marks the end of my study Maritime Technology at Delft University of Technology. The last six years I had the privilege to study and work with a group of enthusiastic fellow students. I learned a lot about the ins and outs of shipping and shipbuilding, not only by the formal lectures and projects that are part of the study program, but also through the excursions and study-trips organised by study association S.G. William Froude.

The last year I had the opportunity to do my internship and graduation project at Van Oord. The first phase of this graduation period was a bit of a struggle. I remember reading the book of Joris Luyendijk, *This Can't be True*, in this period. I recognised the problems he faced while writing his book. Joris Luyendijk summarised it as follows, "it was not a puzzle - in which you search for an answer to a question -, but a mystery: what is actually the question and to whom should it be asked?".[1] Fortunately during the process (*that took almost ten months*) the questions and the answers became clear.

I would like to thank all the people from Van Oord who supported me during my project, by providing information used in this research, but also for the conversations during the breaks. In particular I would like to thank Jop Paauw and Klaas van Dijk for letting me work in their office. Furthermore, I want to express my gratitude to Job Voormolen who was my supervisor at Van Oord, for his management style of supervising!

Not only the people at Van Oord helped with the graduation project, thanks go out to Klaas Visser (Tu Delft) and Hans Hopman (Tu Delft) for their guidance from the academic perspective.

Last but not least I would like to tank my family and my girlfriend for supporting me over the last few years. This wouldn't be a proper preface without it!

J.L.S. Gerritsen
Rotterdam, September 2016

[1] [Luyendijk, 2015]

Executive summary

Growing concern about global warming and climate change intensified the research into more efficient ways of operation in the maritime industry. These researches triggered the use of electrical batteries in hybrid systems. Van Oord aims to operate more efficiently, which implies using less fuel and thus emitting less carbon dioxide. A way to achieve this might be the use of batteries for hybrid power plants on board of their cutter suction dredgers. This will investigate what the potential carbon dioxide reduction of a hybrid system could be. Since the competitiveness of the Van Oord fleet should not be affected a certain cost perspective is taken into account as well. The objective of this thesis is to find a battery capacity that achieves a fuel and running hour reduction in such a way that it is cost effective.

The cutter suction dredger's operational profile has a fluctuating nature in terms of power demand. In this study several operational profiles are examined and one most representative operational profile is constructed. This operational profile has large peaks and troughs which favours the use of a certain peak shaving system like a battery. Moreover, the average loading of the diesel engines is quite frequently far off the optimal 85% load. In order to optimise the power demand from the diesel engines and ensuring efficient operation, models are developed to simulate the behaviour of the diesel engine, the battery and the hybrid system as a whole.

As a start the effect of transients in the load profile of the diesel engine on its efficiency is investigated. It is found that the efficiency of a larger medium speed diesel engine running on constant speed with a sufficient air excess ratio, is not affected by transients in the load profile. The data collected in this analysis is used to develop a fuel consumption model which estimates fuel consumption as function of the load of the engine. In addition, the diesel engine the battery pack is modelled. The model of the battery pack is based on multi dimensional lookup tables that hold the non-linear relations between terminal voltage, state of charge and current. For the battery a separate lifetime calculation is developed, which estimates the battery lifetime for different charge/discharge profiles. The fuel consumption model and the battery model are tested and perform as intended. In order to combine the fuel consumption model and the battery model, a power management system is developed. This power management system uses binary logic to optimise the system performance. The set-points of the power management system are tuned in an iterative way.

Due to a structured simulation approach the simulation results can be converted to trend lines. These trend lines enable the determination of the optimal battery capacity with respect to reduction of fuel consumption, reduction of running hours, investment cost and battery lifetime. The optimal capacity for the battery is 4516 kWh. With this battery the system is not cost effective. However, technical feasibility is proven and fuel consumption is reduced. A yearly fuel reduction of 75 ton HFO and 142 ton MDO is achieved. This results in a reduction of carbon dioxide of 687 ton annually. With this system every ton of carbon dioxide reduction will cost Van Oord €575.

The performance of the hybrid system can be improved by extending the battery lifetime. This is done by adjusting the power management settings according to the actual residual battery capacity. This method reduces the cost per ton carbon dioxide reduction to €128. Furthermore the effect of running on MDO instead of HFO is investigated, this results in a marginal improvement in cost perspective. Every ton of carbon dioxide reduction will cost €554. The actual annual carbon dioxide reduction will not change. Unfortunately the proposed hybrid system will only reduce carbon dioxide emission in a cost effective way when the HFO price rises to €700 per ton and the battery price per kWh halves.

In combination with a Liquefied Natural Gas (LNG) fuelled power plant the hybrid system can be used. It is proven that energy demand can be stored in and provided by a battery with a reasonable size. Due to the response of a gas engine the battery is not an extra any more, but it becomes a necessity.

Contents

List of Figures

List of Tables

Symbols

A	exponential voltage	V
B	exponential capacity	$1/Ah$
B	cylinder bore	mm
C/H	carbon hydrogen ratio	–
CL	battery cycle life	$cycles$
CO_2	carbon dioxide	–
C_1	dynamic response capacitor	F
C_c	charge rate	h
C_d	discharge rate	h
C	nominal discharge curve slope	V/Ah
DOD	depth of discharge	–
ES	energy source in EFD	–
EU	energy use in EFD	–
E_m	open circuit voltage	V
E	electric energy EFD	–
I_c	charge rate	h
I_d	discharge rate	h
J	rotational moment of inertia	J/kgm^2
K_{factor}	number of pulses per litre	$pulses/l$
K	polarization constant	$1/Ah$
LF^t	load factor at current simulation step	–
LF_{max}	maximum load factor	–
LF_{min}	minimum load factor	–
LF_{pref}	preferred load factor	–
L_s	stroke length	mm
MCR	maximum continues rating	kW
M	mechanical energy in EFD	–
Opt^t	option at current simulation step	–
Opt^{t-1}	option at previous simulation step	–
P_b	brake power	kW
P_{ch}	charge power	kW
P_{dem}	power demand	kW
P_{des}	desired power ouput	kW
P_{disch}	discharge power	kW
$P_{maximal}$	maximum power output	kW
$P_{minimal}$	minimum power output	kW
Q_f	potential heat in fuel	kJ
Q_i	indicated heat	kJ
Q_{comb}	combustion heat	kJ
Q	maximum battery capacity	Ah
Q	volume flow	$l/second$
RC	resistor and capacitor	–
R_0	steady state resistor	Ohm
R_1	gas constant dry air	kJ/kgK
R_1	dynamic response resistor	Ohm
R_c	charge air gas constant	kJ/kgK
SOC_{av}	average state of charge	–
SOC_{max}	thermodynamic efficiency	–
SOC_{min}	minimum state of charge	–

SOC	state of charge	$-$
T_1	in cylinder temperature at the moment the inlet valve closes	K
T_a	ambient temperature	K
T_c	charge air temperature	K
T_{ref}	nominal ambient temperature	K
T	kinetic energy	kJ
T	temperature	$degree\ C$
V_1	in cylinder volume at the moment the inlet valve closes	m^3
V_s	stroke volume	m^3
V_{TDC}	volume above the piston in the top dead centre position	m^3
W_e	effective work	kJ
W_i	indicated work	kJ
X	compression stroke effectiveness	$-$
Δp	change in number of pulses	$pulses/s$
Δt	sampling period	s
Δv	change in volume	l
α	Arrhenius rate constant for polarization resistance	$-$
β	Arrhenius rate constant for internal resistance	$-$
$\dot{J}$	energy flow	kJ/s
$\dot{m}_f$	fuel mass flow	kg/s
η_e	engine efficiency	$-$
η_m	mechanical efficiency	$-$
$\eta_{battery}$	battery efficiency	$-$
η_{comb}	combustion efficiency	$-$
η_{hl}	heat loss efficiency	$-$
η_{td}	thermodynamic efficiency	$-$
η_{trap}	trapped air efficiency	$-$
η	geometric compression ratio	$-$
λ^*	pseudo air excess ratio	$-$
λ	battery efficiency weight factor	$-$
λ	air excess ratio	$-$
ω	rotational speed	rad/s
ρ_f^T	density of fuel at a certain temperature	kg/m^3
$\rho_f^{15.6}$	density of fuel at 15.6 degrees	kg/m^3
ρ_f^{15}	density of fuel at 15 degrees	kg/m^3
σ	stoichiometric ratio	$-$
gc	gravity change	$\%/degree\ C$
h^l	lower heating value	kJ/kg
i^*	low frequency current dynamics	A
it	extracted capacity	Ah
i	current	A
k	number of revolutions per cycle, k=1 for 2-stroke engines, k=2 for 4-stroke engines	$-$
$m_{available}^{air}$	available air for combustion	kg
$m_{minimal\ needed}^{air}$	minimal air needed for complete combustion	kg
m_1	air mass in closed cylinder	kg
m_1	in cylinder pressure at the moment the inlet valve closes	Pa
m_σ	minimal air needed for complete combustion	kg
mf	multiplication factor for extrapolating simulation results	$-$
m	mass	kg
nCL	nominal battery cycle life	$cycles$

p_c	charge air pressure	Pa
p_{me}	mean effective pressure	Pa
r	radius	m
t^*	integrated time	s
t^{limit}	minimum time set-point	s
x_s	mass fraction of sulphur	$-$

Abbreviations

AC	Alternating Current
aux.	Auxiliary
BDC	Bottom Dead Centre
CL	Cycle Life
CPP	Controllable Pitch Propeller
CSD	Cutter Suction Dredger
DC	Direct Current
DOD	Depth of Discharge
DP	Dynamic Positioning
ECA	Emission Control Area
ECM	Equivalent Circuit Model
EFD	Energy Flow Diagram
FAT	Factory Acceptance Test
gen.	Generator
HFO	Heavy Fuel Oil
IMO	International Maritime Organisation
LF	Load Factor
LHV	Lower Heating Value
Li-Ion	Lithium Ion
LNG	Liquefied Natural Gas
MCR	Maximum Continues Rating
MDO	Marine Diesel Oil
MGO	Marine Gas Oil, in this thesis assumed to inherit the same properties as MDO
PI	Proportional Integrator
PMS	Power Management System
PSV	Platform Supply Vessel
RMSE	Root Mean Square Error
RPM	Revolutions Per Minute
SCC	Social Cost of Carbon
SECA	Sulphur emission Control Area
SFOC	Specific Fuel Oil Consumption
SOC	State of Charge
TDC	Top Dead Centre
VODAS	Van Oord Data Acquisition System

1 Introduction

1.1. General background

This research is done in cooperation with Van Oord, a well-known dredging company. Van Oord operates a vast amount of dredging equipment around the world. The cutter suction dredger is one of the types of dredge machinery that is used by Van Oord. In this thesis the cutter suction dredger will be the piece of equipment that is analysed. The cutter dredger uses its cutter head to *cut* the seabed. The loose sand or rock is then pumped through a system of pipes and pumps to a certain location. In contrast to a trailing suction hopper dredger which sails while dredging the cutter suction dredger is stationary equipment. The purpose of the cutter dredger is to transport material from the seabed to a designated area by using hydraulic transport. This can either be to deepen a harbour or waterway or for land reclamation. The production of a cutter dredger is therefore expressed in cubic meters of dredge material delivered at for instance a landfill area. Although this is a rather short general introduction to Van Oord and the equipment that is focussed on in this thesis, it gives a starting point for a further introduction to the research itself.

It is a general fact that climate change forms a worldwide problem. Global warming is caused by the emission of carbon dioxide, which is released during the burning of fossil fuels. In addition to climate change, the increase of the worlds population forms another challenge to cope with. The rapid growth of the number of people in the world in fact increases the rate of climate change, since more and more energy has to be produced. It is common knowledge that climate change will lead to rising of the sea level. To accommodate the growing population, more land should be made available and this land should be protected against the rising sea level [UNFPA, 2016]. Dredging companies like Van Oord are responsible for both land reclamation and coastal defence. Unfortunately, dredging equipment consumes fuel and therefore emits carbon dioxide, which has a negative effect on the environment.

Dredging is a necessity to accommodate the growth of the world population. It is inevitable that carbon dioxide is emitted by dredging equipment like cutter suction dredgers. However it appears to be possible to use the energy stored in the fossil fuels in a more efficient way. In this way the amount of fossil fuel burned for a certain amount of cubic meters dredge material produced can be reduced. As explained earlier this will also translate in a reduction of carbon dioxide per cubic meter of material dredged.

Van Oord is aware of its responsibility to become more environmental friendly. This can be achieved by increasing production with the same amount of fuel or by decreasing the fuel consumption while maintaining the same production. The question raised by Van Oord is if it is possible to reduce emission of carbon dioxide and other pollutants caused by the burning of fossil fuels. If the production increases during that process, this is seen as a bonus. The reduction of fuel consumption and carbon dioxide emission is important for Van Oord. However not against every price. If carbon dioxide reduction is possible this should not compromise the competitiveness of Van Oord.

Since the beginning of dredging, several major steps have been taken in the development of dredging equipment. The first cutter suction dredger was introduced between 1870 and 1880 and was powered by steam [The Dutch Association of Contractors in Dredging, 2010]. The development of the cutter suction dredger from the normal suction dredger was already a great improvement with respect to production capabilities. The next development was the introduction of the diesel engine. More efficient operation was achieved since the diesel engine itself was a more efficient way of generating power than the steam engine. The latest step in the development of the cutter dredger was the use of diesel electric installations. The cutter and the dredge pumps are mostly electrically driven which enables the operator to tune the whole system to achieve a higher production. Although the electrical installations and the diesel engines of these vessels have become more efficient the principle of the cutter suction dredger has not been changed since the 1950's [Dredgepoint.org, 2012]. As stated earlier there is a growing need to reduce the air born emission from the cutter suction dredgers operating within the Van Oord fleet. This is probably not possible without re-evaluating the general design as has been introduced in the 50's. Fortunately more and more possibilities and techniques to reduce emissions and increase efficiency have become available in the last few years. Van Oord is looking in to the possibilities to use some of these techniques.

Multiple new techniques were introduced in the shipbuilding industry in order to reduce emissions. One of the ways to reduce carbon dioxide, nitrous oxide and sulphur oxide is to change the fuel that is used. An upcoming trend is the use of LNG. Due to the chemical composition of LNG the formation of greenhouse gasses is lower per amount of energy. Also the formation of sulphur oxide and nitrous oxide will be reduced significantly when using LNG. Another option that is mentioned is the use of bio fuels. These fuels are produced from organic materials. The idea behind this type of fuel is that all the carbon dioxide emitted after burning this fuel has first been taken out of the atmosphere by the plant it was produced from, resulting in a net emission of zero. Although being introduced as a promising option to operate *greener* there is still a debate going on about the competition of bio fuel on the worlds food supply. Naturally land that is used for the production of bio fuels can not be used for the cultivation of crops for human consumption. In this study not much attention will be given to alternative fuels. The reason for this is that the efficiency of the equipment will not increase by using alternative fuels. What might increase the efficiency of the Cutter Suction Dredger (CSD) is the use of energy storage devices. This is commonly referred to as *HYBRID*. In a hybrid system there will still be an engine that burns fossil fuels to generate power. However this engine can operate in a better efficiency point *(which lies mostly around 85% load)*. If there is less power required than is produced at the best efficiency point this surplus of power is stored in the energy storage device. On the other hand if more power is needed than can be provided at the best efficiency point of the engine, the shortage of power can be taken out of the storage device.

A hybrid system in the way it is intended in this thesis uses at least one engine that burns fuel and a certain form of energy storage. Several options for energy storage devices are available. Hybrid systems found in the market use flywheel technology [Thoolen, 2014], compressed air [Trajkovic, 2010], super capacitors [Grbovíc, 2014; Maxwell Technologies, 2009] and/or electrical batteries [CORVUS energy, 2015]. In this thesis the focus will be on a hybrid system as a combination of diesel generators and an electrical battery. The reason for this lies in the fact that the hybrid systems that use batteries are the only ones capable of storing large amounts of energy. The storage capacity of flywheel technology, compressed air and super capacitors is not sufficient. If it would be even possible to scale these systems to the intended storage capacity they would become too heavy since the energy density of these storage devices is very low.

1.2. Problem statement

The introduction that was given in section 1.1 has lead to a problem statement. The general feeling is that a hybrid system using batteries and diesel generators can result in a more efficient operation of a cutter dredger than a system that is purely diesel electric without any energy storage capacity. The idea behind this study is to boost efficiency in order to reduce fuel consumption, which will lead to reduced emission of carbon dioxide. Currently, there are no values available about how large the battery pack should be. Furthermore, no research has been done yet to confirm the fuel saving potential of such a proposed hybrid system for a cutter suction dredger. Also, there is no information available about the effect of the use of batteries on the running hours of the diesel generators and the related maintenance of these diesel generators. These potential gains like reduced fuel consumption, running hour reduction, reduced maintenance should make it economically viable for Van Oord to invest in a hybrid system. The problem statement can be summarized in a main research question.

What should be the size and capacity of a battery in a hybrid electrical grid of a cutter suction dredger to reduce fuel consumption and running hours of diesel engines in such a way that it is cost effective?

1.3. Objective

Obviously the objective of this research is to answer the research question described in section 1.2. To do so multiple steps have to be taken. First of all several sub questions can be distilled from the main research question.

1. *What are the main variables that determine the size of the battery?*
2. *Which variables influence the fuel consumption in a hybrid system?*
3. *Which variables determine the running hours of the diesel generators in a hybrid system?*

The first sub questions can probably be answered using literature. In the past, several studies on the working principles of batteries and diesel engines have been done. The running hours of the diesel engine in a hybrid configuration will probably be determined by the capacity of the battery. In other words, to what extend can the battery replace one or more running diesel engines? So from the start it is obvious that a certain interaction exists between the size of the battery, the fuel consumption and the running hours of the diesel engines. This is not surprising since the general belief is that a hybrid system with a battery will indeed reduce fuel consumption and running hours. This is one of the main reasons that this research is viable. The value of this research lays in the fact that an attempt will be done to quantify the potential of a hybrid system and to prove or reject the hypothesis. The following hypotheses were developed using information from literature;

1. *The use of a battery in a hybrid electrical grid of a cutter suction dredger reduces the total installed power and the need for spinning reserve resulting in a better average loading of the main diesel engines contributing to a better efficiency and a lower specific fuel oil consumption*
2. *When a battery is solely used for peak shaving purposes this will reduce the transient behaviour of the power demand and therefore the transient response of the diesel engine resulting in lower specific fuel consumption and less exhaust emissions of the diesel engine.*
3. *The capacity of the battery will have an effect on the amount of spinning reserve that can be replaced and to what extend peak shaving can be applied. The capacity will not only affect the earning potential, but also the cost of the system. The larger the battery the longer it will last, however more capacity comes with a higher investment.*

1.4. Methodology

As a start an analysis of the working principle of the cutter suction dredger will be done, based on the operation of the Athena and Artemis. These two cutter suction dredgers are the largest in the Van Oord fleet. The Athena and Artemis are the strongest cutters in the fleet in terms of installed power. For this reason it is assumed that the fuel saving potential of a hybrid system will be maximal for these vessels. The evaluation of the working principle will be based on literature and actual data loggings. The Athena and Artemis are both equipped with a data logging system. The system is referred to as Van Oord Data Acquisition System (VODAS). VODAS stores most signals used in the automation of the dredge process and the power management system.

When the working principle is well understood the working profile can be analysed. The result of this analysis will be a data set containing values of power demand in time. This power demand will be a subset of the data that has been logged over the last few years. This subset should be representative for a full year of operation. In fact the data subset represents a trade of between accuracy and computational effort. Nevertheless it enables checking of the data for errors which makes further analysis more reliable.

During the analysis of the power signals the different energy consumers will be identified. Then it will be clear how a cutter suction dredger operates and how much power is needed to execute a specified task. The remaining question is how the power is generated and distributed. The path from fuel to actual process will be analysed using an Energy Flow Diagram (EFD) to introduce the components in the system. Also, a power chain will be constructed to get a feeling for the efficiencies in the system.

In order to know which possibilities are available for a hybrid system, existing systems will have to be analysed. A clear definition of *hybrid* should be established. An understanding of the systems available in the market is necessary to make a decision on the layout of the hybrid system. For the hybrid configuration that is decided on, a functional decomposition will have to be made. This functional decomposition will provide a handle to understand the most important effects of the hybrid system on the overall performance of the system. According to the hypothesis, peak shaving might play an important role in the reduction of fuel consumption. This is already one of the functions to be fulfilled by the hybrid system.

One of the promises of peak shaving is that fuel consumption is reduced. In order to confirm this general feeling, an analysis will be done on the effects of transient loading of a diesel engine on its fuel consumption. Since the Athena and Artemis are not equipped with fuel flow sensors, it is suggested to investigate two other vessels in the Van Oord fleet that are equipped with fuel flow sensors. The result of this analysis will be the foundation for the fuel consumption model.

As stated in section 1.3, a dependency exists between the performance of the battery, the diesel engines and the system as a whole. Therefore it is not possible to evaluate the different system components individually. In addition, the performance of the hybrid system is most probably dependent from dynamically changing variables. Static calculations are therefore not favourable. To evaluate the performance of the system, a time dependent mathematical model should be developed. The first step for the development of a fuel consumption model has already been made in the transient versus fuel consumption analysis. Furthermore, the battery will be modelled. To create the battery model, decisions should be made on the modelling strategies. Literature provides several possibilities for battery modelling. Important criteria to choose a modelling strategy are the input to the model, the output from the model, the accuracy and the computational effort. Keeping in mind that one of the goals of this study is to make an economical analysis of the hybrid system, attention should be paid to the life time expectancy of the battery. From literature it is known that life expectancy of a battery is expressed in an amount of charge/discharge cycles which are dependent from the amplitude and period of these cycles. The last two are again dependent on the size of the battery. An algorithm should be found or developed to estimate the cycle life of the battery. The interface between the battery model, the fuel consumption model and the power demand *(from measurements)* will be the power management system. The power management system should be used to find an optimum between fuel saving, reduction of running hours and battery capacity. Furthermore the power management system will ensure

the robustness of the model. Certain constraints can be introduced to prevent algebraic loops and values going to infinity during simulation.

After the development of the individual models, these will be verified. The verification of the fuel consumption model will be based on the fuel database. The fuel database contains weekly reports about consumed fuel. If the simulation result without the use of a battery is equal to the fuel consumption that was actually measured during operation, the model can be confirmed. The verification of the battery model will be done by testing it against a set charge and discharge profile.

If the cutter model is working as was intended simulations will be done with different battery capacities. The load profile that will be used as input has been described earlier. Different battery capacities will lead to different values of fuel consumption and running hours. The cycle life of these specific battery sizes can also be calculated using the algorithm that will be developed together with the battery model. The simulation results can be translated to investment cost and potential earnings. This makes it possible to answer the research question.

1.5. Contribution to the literature

In this report, five issues are addressed which can be seen as a contribution to the existing literature about hybrid applications in the maritime industry. More specifically, an initial step was taken in the development of new power generation systems for dredging equipment. The main contributions to literature that are described in this report are listed below.

1. A representative working profile for a cutter suction dredger that is fit for time domain simulations is developed.
2. In this thesis an in depth analysis of the fuel consumptions of a diesel engine in transient operation is presented.
3. Different battery modelling strategies are analysed, resulting in the development of a custom model, which can be used with limited information of battery suppliers without compromising on important parameters.
4. Existing battery life cycle prediction algorithms have been extended to be used in really fluctuating non-uniform load profiles for the battery as is the case in a hybrid system for a cutter suction dredger.
5. To the authors best knowledge, this is the first publication solely focussed on the application of batteries in a hybrid system for a cutter suction dredger.

1.6. Content description

This report is build up as follows. Chapter 2 will give a short introduction to Van Oord as a company, continuing with a description of the cutter suction dredger. Furthermore the specifications of the Athena and Artemis will be presented since these two vessels are the benchmark for this research. Using log data from the Athena the working principle of the cutter suction dredger will be explained in detail. In addition, the working principle the working profile or load profile will be introduced. The working profile of the Artemis is analysed to find a representative time window which can be used for further analysis. The result of chapter 2 is a general understanding of Van Oord and the cutter suction dredgers as the Athena and Artemis with their corresponding working principles and load profile. Chapter 3 will focus on hybrid systems in general. A definition for *hybrid* will be introduced as well as multiple examples of hybrid systems in the maritime industry and other industries. In chapter 4 the different models that were described will be discussed. Starting with the description of the proposed hybrid system. Furthermore, the relation between a transient load profile and fuel consumption is presented. Finally the battery model and the power management model will be explained. Chapter 5 described the testing and verification process that was done after the models discussed in chapter 4 were developed. After the models were tested the actual simulations were done. The input and output of these simulations will be presented in chapter 6. Special attention will be given to the battery cycle life calculations in this chapter. In chapter 7 the results of the simulations will be discussed. The discussion will address the physical impact of different battery capacities in terms of size and weight. Also, attention will be given to the financial analysis to estimate investment cost and potential cost reductions as result of fuel savings and the reduction of running hours. The final conclusions and recommendations for future work will be given in chapter 8.

Calculations and information that fall somewhat outside the scope of this project but which still support the conclusions and findings presented in the main body of the report can be found in the appendices. In appendix A an extended analysis of the working profiles, as discussed in chapter 2, will be presented. Appendix B presents the background on the air excess ratio calculations that are done in order to confirm the conclusion made on fuel consumption of a diesel engine in transient operation as is presented in chapter 4. Appendix C displays turbo performance parameters which form the input for the calculations in appendix B. To provide background information on the effect of inertia in rotating systems on the mechanical efficiency of the diesel engine, an analysis of the kinetic energy in different propulsion systems is presented in appendix D. The battery specifications that are used in the battery model that is discussed in chapter 4 are presented in appendix E. Appendix F and appendix G display the Simulink models of the battery and the power management system respectively. The Simulink model that is constructed to validate the fuel consumption model in chapter 5 is presented in appendix H. Appendix I visualises the peak shaving filters that are used for the peak shaving simulations. Finally the results of the battery lifetime calculations are presented in appendix J.

2

Cutter suction dredger background

2.1. Van Oord

Van Oord is a well known company in the maritime industry. The company is known for its dredging, offshore and offshore wind activities. The offshore wind branch of Van Oord focusses on the development of offshore wind parks. These windparks are being build with an eye on the future. in the near future there is a need for more and more energy from renewable energy sources. Not only for the fact that the worlds oil supply is limited as well for the fact that the environment has problems to cope with the pollution from conventional energy sources, e.g. fossil fuels. In this light Van Oord is helping our society to make the transition to a more environmental friendly way of life. On the other hand Van Oord is not only active in the market for renewable energy. As stated before dredging and offshore oil and gas are also markets in which Van Oord operates. These two sectors of the company are not known for their *green image*. Van Oord lives up to its responsibility towards society by investing in more environmental friendly solutions, also in the dredging and offshore oil and gas division. This resulted in the question if it is possible to develop a '*hybrid* cutter suction dredger'.

2.2. Cutter dredger

A cutter suction dredger uses a cutter (*comparable with a milling machine*) to cut material. This material, soil, comes in a vast amount of forms. It can either be loose sand or hard rock and everything in between with different grain size and hardness. One can imagine that the soil conditions of the material to be dredged determines the way the dredger operates. This will be explained further in coming sections. After the dredge material is loosened by the cutterhead and the cutting action it will be transported via hydraulic transport. The soil will be pumped as a solid-liquid suspension from the cutterhead to a certain location. Hence the name of the machine the cutter *suction* dredger. In the section 2.2.1 an introduction will be given to the Athena and Artemis. These two CSDs will be the focus point of this thesis and will therefore be introduced with all their technical specifications. In this introduction the working principle is briefly described in rough form. In section 2.2.2 the operating principles will be explained more thorough. In this section the different energy consumers that were introduced in section 2.2.1 will be discussed in terms of power demand in the cycle time of the cutter dredger.

2.2.1. Athena and Artemis

The Athena and Artemis are the two largest cutter suction dredgers of Van Oord. Both vessels are relatively young. The Athena and Artemis were launched in 2011 and 2012 respectively. Both vessels are self propelled, which means that contrary to their stationary counterpart they can sail to the work area without the need for tugboats. A cutter dredger has multiple energy consumers placed over the entire vessel. For example, the Athena and Artemis are equipped with two inboard dredge pumps, one submerged pump, several winches and of course the cutter.

The layout of the current engine room configuration is presented as an EFD in figure 2.1 [Klein Woud and Stapersma, 2002].

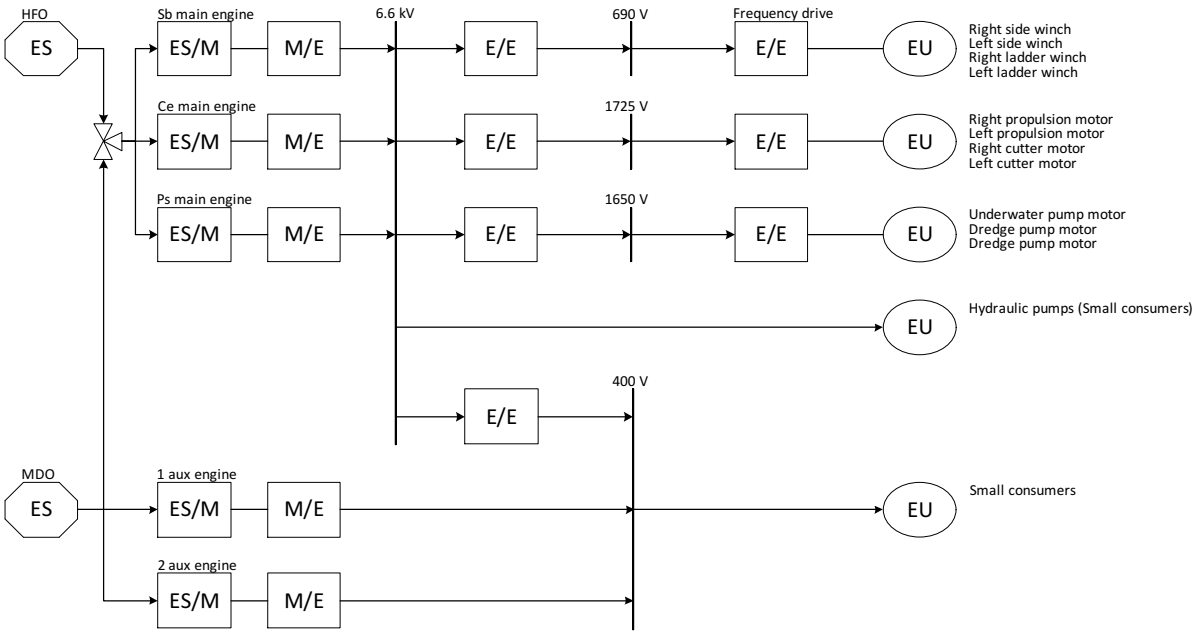

Figure 2.1: Energy flow diagram of the Artemis

2.2.2. Operating principle

The typical cutter cycle can be described in terms of the position of the cutterhead and spud carrier. According to The Dutch Association of Contractors in Dredging [2010] the cutter cycle can be described using a few simple steps. These steps are presented in figure 2.2 and will be discussed subsequently.

1. swinging to port *(Dutch: verhalen)* :
   to swing the vessel with a rotating cutterhead from the center line of the cut to the port side.
2. stepping *(Dutch: stappen)* :
   to push the vessel forward by moving the spud carrier to the aft of the vessel.
3. swinging to starboard :
   to swing the vessel back to the starboard side.
4. stepping :
   repeat step 1 to 3 until the spud carrier is in its maximal aft position.
5. swinging to center :
   to swing the vessel back to the center line of the cut.
6. changing spuds *(Dutch: verpalen)* :
   swing is stopped in the centerline of the cut. The secondary spud is lowered. The primary spud is lifted and moved to its forward position. The primary spud is lowered again and the secondary spud is lifted.
7. new cycle is started.

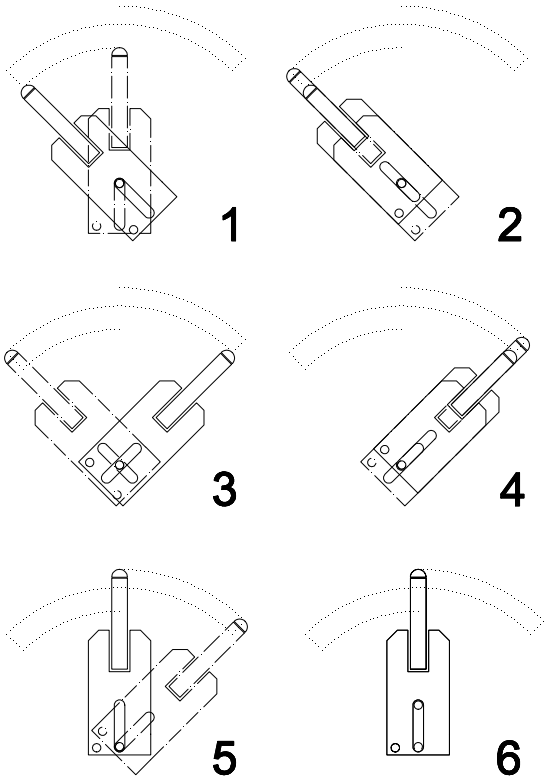

Figure 2.2: Schematic overview of the cutter cycle

To introduce a more specified example of the working principle of the cuttter suction dredger figure 2.3 and 2.4 will be used. In figure 2.3 the position of the cutterhead is plotted. In the same time period the power demand from the main energy consumers of the vessel is plotted in figure 2.4. The numbers in these figures represent the same moment in time. The different points will be discussed in terms of part of the cycle and power demand. In this way the power can be related to the actual phase or position of the cutter during its cycles.

1. The spud carrier is in its most forward position. Pump power, cutter power and the left side winch power will increase. The vessel will make a swing to port side. During the swing the ladder winches and right side winch will use some power in order to keep a constant tension in the wires.
2. The cutterhead is in the left corner. The spud carrier will be moved to the aft of the vessel by one step length, pushing the cutterhead forward. Pump and cutter power stay at their operational level. The roles of the right and left side winch will change since the vessel has to be swung to starboard. The right side winch will use more power than the left side winch.
3. The cutterhead is in the right corner. The spud carrier will be moved to the aft of the vessel by one step length, pushing the cutterhead forward. Pump and cutter power stay at their operational level. the winch power will be changed again between left and right side winch.
4. Step two will be repeated.
5. The power to the cutter and the pump power is reduced to zero. The power to the side winches goes to zero as well, the vessel stops its swing and stops production. It can be seen that the power to the ladder winches is increased. The ladder is lifted out of the water.
6. The cutter head is above the water surface. Most probably the cutterhead has to be inspected and teeth have to be replaced. (*The Athena was working in really hard rock for the coast of Australia when these measurements were taken. Hard rock causes more wear on the cutter teeth, so more maintenance has to be done*)
7. Maintenance to the cutterhead is finished and dredging can commence again. The power to the ladder winches is increased in order to lower the ladder.
8. The cutterhead is at the bottom and in position. The dredging operation is started again and cutter power and pump power will be increased. further step two and three will be repeated till it is either time for maintenance again or till the spud carrier has to be moved forward again. (*Actually the cycle will end around ten o clock when the spuds are changed*)

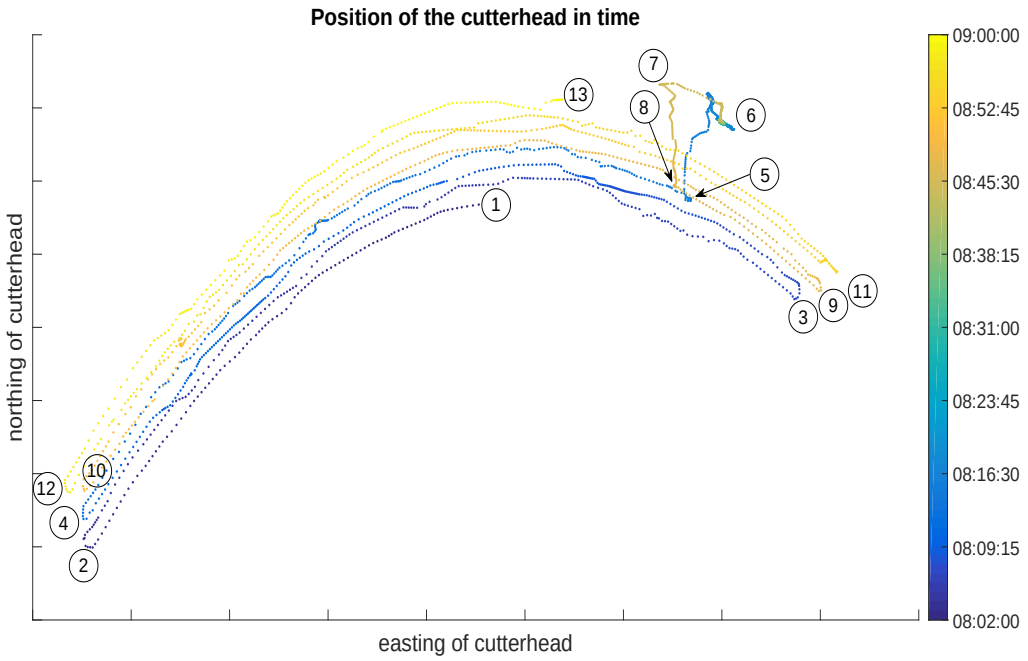

Figure 2.3: Position of the cutterhead from the Athena in time

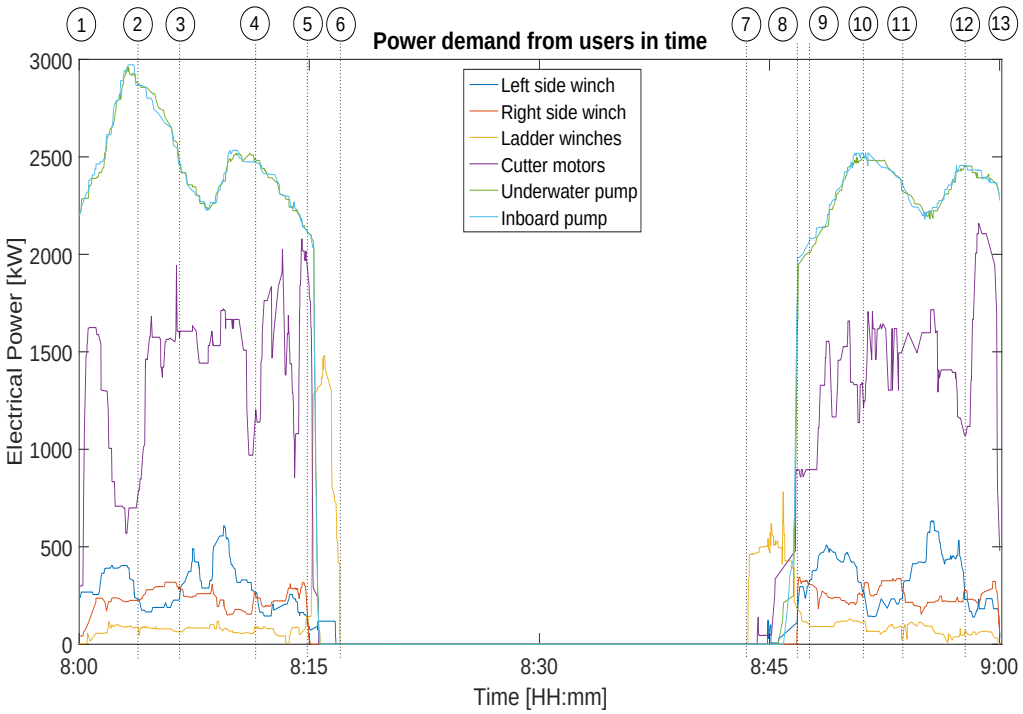

Figure 2.4: Power distribution from the Athena in time (*corresponding with figure 2.3*)

2.2.3. Working profile

To evaluate the performance of the hybrid cutter a mathematical model of such a hybrid system will be developed. This mathematical model will use power measurements as input for the simulation. It is not advisable to run a simulation for the duration of a year due to computational constraints. A full year of measurements consists of 31449600 data points. It is decided to develop smaller sets of data since this will speed up computation. These smaller time windows should represent the working profile of a cutter over the duration of a year. To assure that the chosen time frames are a representable collection a frequency analysis is executed. Histograms will be developed for the power demand measurements over the year 2014. Next to that three projects are chosen.For these projects similar histograms will be constructed. Finally a combination of these projects will be presented in the form of a histogram. With this information a conclusion can be drawn to what extend the chosen projects are valid representations of the full year operational profile. If a combination of these projects is not representable another time frame should be searched for.

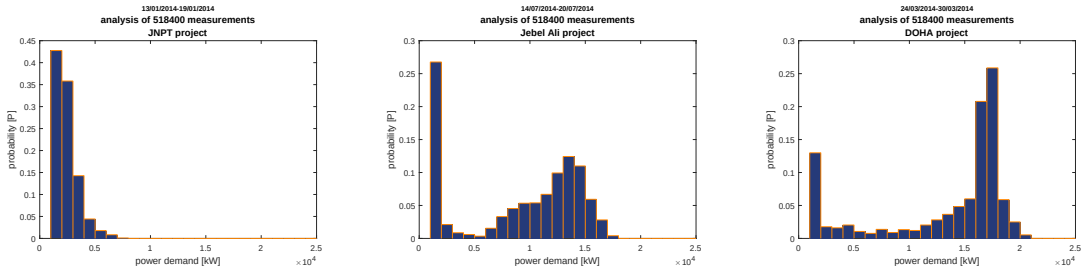

(a) power demand measurements JNPT

(b) power demand measurements Jebel Ali

(c) power demand measurements DOHA

Figure 2.5: Histograms power demand measurements on three different projects

The histogram of the full year operation is presented in figure 2.6. The three different projects are presented in a similar way in figure 2.5. The decision to choose for these three projects was based on the research done by Rensen [2014]. In this research the same projects were evaluated in terms of fuel consumption. This gives the possibility for the comparison of results of this thesis and the conclusions given by Rensen [2014]. As stated in the introduction a combined histogram of the three projects is constructed as well. The probability for a certain power demand when the three projects are combined is presented in figure 2.7. It turns out that the combination of the three projects does not give a valid representation of a full year operational profile as is shown in figure 2.8. The Root Mean Square Error (RMSE) between the full year operational profile and the three projects combined is 0.0271. This gives a measure to what extend the three projects combined represent the actual operational profile. A lower RMSE between the histogram of the full year operation and a smaller time window would increase the accuracy of the simulation results.

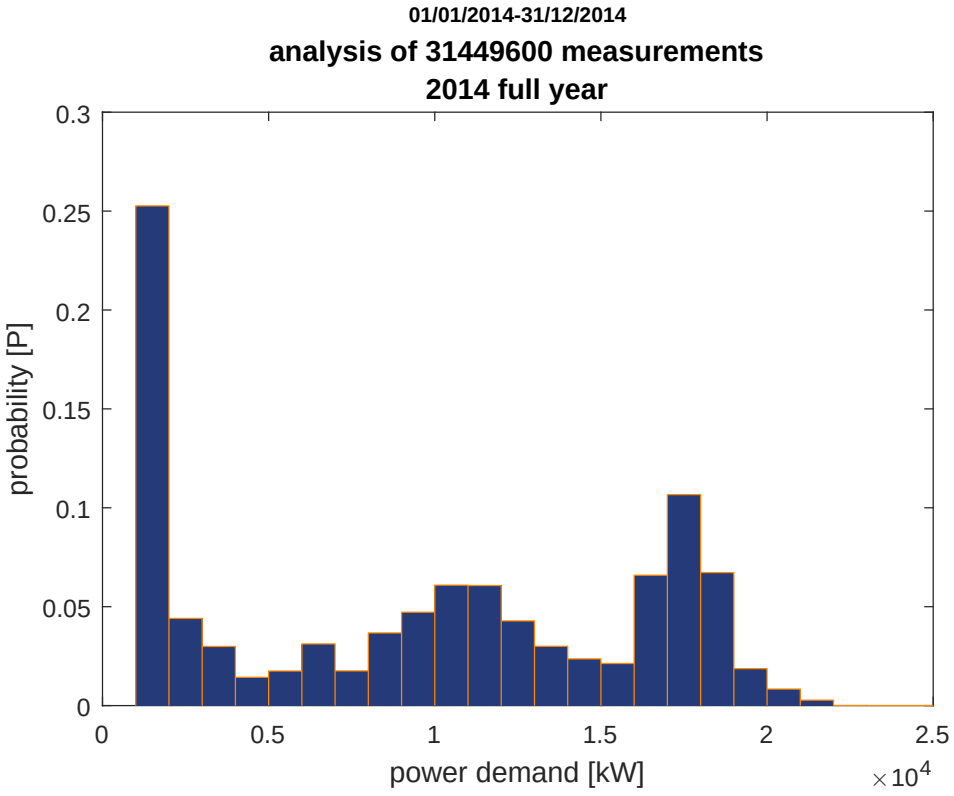

Figure 2.6: Histogram power demand measurements 2014

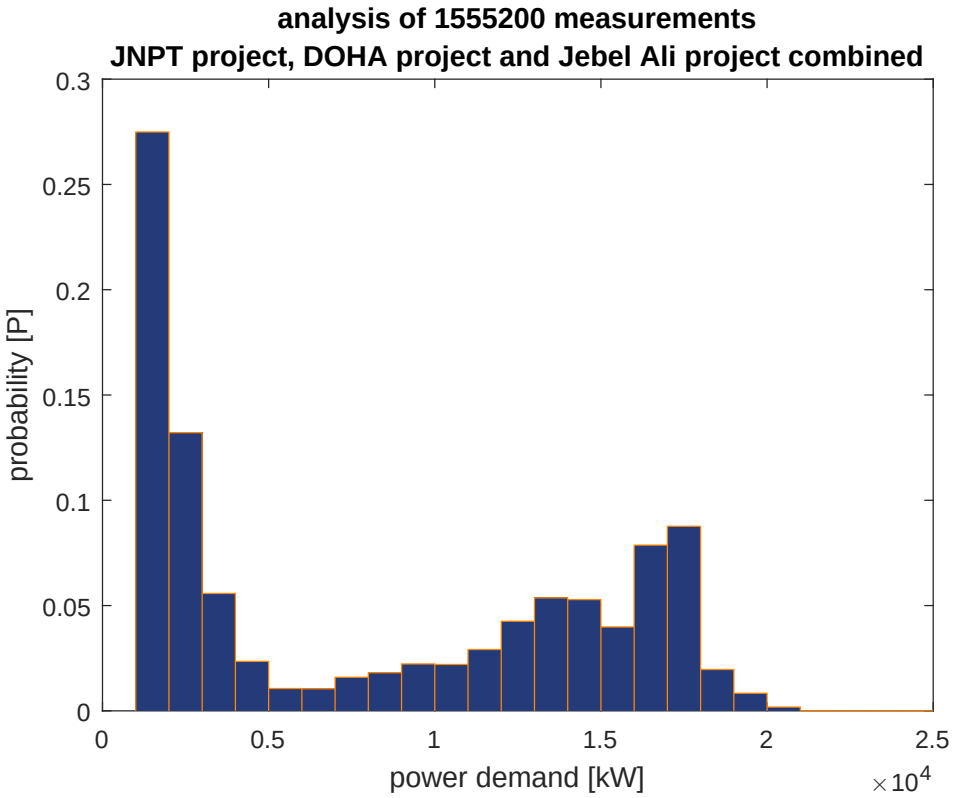

Figure 2.7: Histogram power demand measurements on three different projects combined

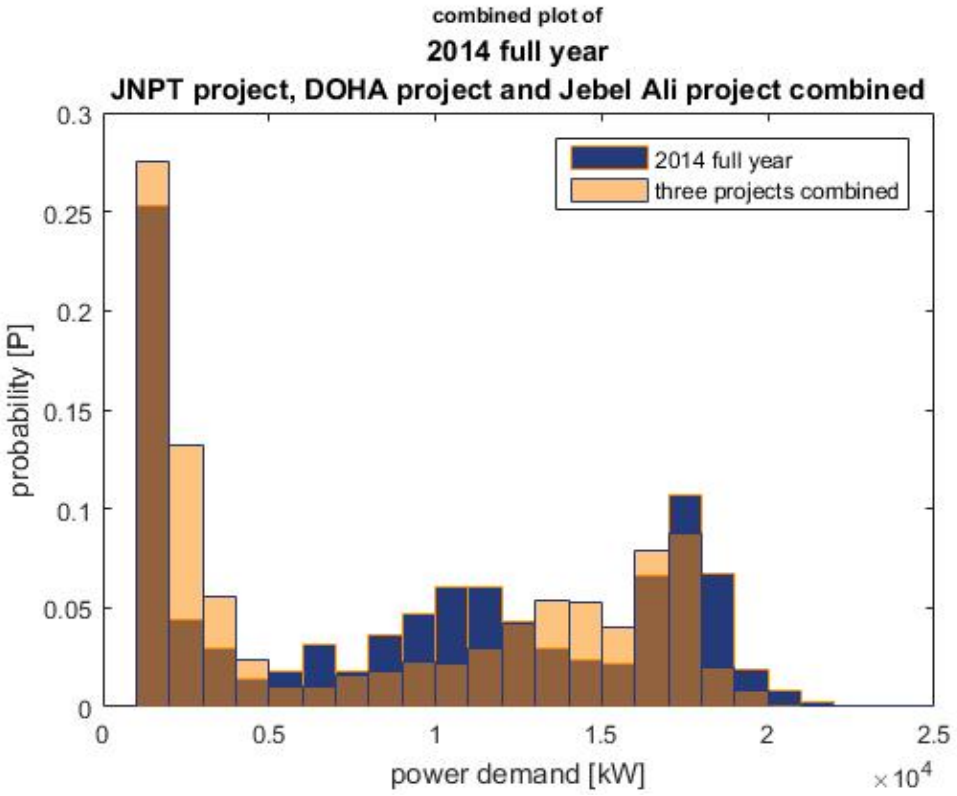

Figure 2.8: Combined plot of *histogram power demand measurements 2014* and *histogram power demand measurements on three different projects* combined

The goal is to develop a working profile of the CSD that is usable for simulation and in the same time representative for the full year operation of a CSD. Therefore it is decided to reject the working profile based on the combination of the three different projects. Although being unsuitable for the development of a generic hybrid system, these three weeks of operation can be used for more specific analysis in the future. An analysis of the variables influencing the power demand is presented in appendix A. It turns out that the power demand and the probability density distribution of this power demand is strongly dependent from soil conditions and the length of the discharge line.

It is proposed to hold on to the data of 2014 as presented in figure 2.6, but search for a time slot with a similar probability density in terms of power demand. To do so a Matlab tool is developed. This tool analyses different lengths of time windows over the total period 2014. The different time windows are moved over the time line with time steps of one day. So for several time windows around 365 options are analysed. Each analysis consist of the construction of a probability distribution and comparing it with the 2014 distribution. The time window with the least RMSE is than stored. The values that are of interest are the time window length, the RMSE and the day the time window starts. An overview of the results of this analysis is presented in table 2.1. The intention of this analysis was to find the shortest representable time frame. A (*local*) optimum is found at a time window with a length of six days starting on the eighth of October.

Note that the RMSE becomes smaller again when longer time intervals are under consideration. This is a trivial result since the time window will approach te 2014 data set more and more as it gets longer. The visual result of this analysis is presented in figure 2.9. Since the simulation will be done in the time domain the time domain signal of the period with the best fit is presented as well. For the time domain signal see figure 2.10

Table 2.1: Results of time window analysis

window length $[days]$	Root Mean Square Error	starting day	date	day
3	0.0237	31	31-Jan-2014	Friday
4	0.0190	281	08-Oct-2014	Tuesday
5	0.0172	281	08-Oct-2014	Tuesday
6	**0.0165**	281	08-Oct-2014	Tuesday
7	0.0172	281	08-Oct-2014	Tuesday
8	0.0180	281	08-Oct-2014	Tuesday
9	0.0181	281	08-Oct-2014	Tuesday
14	0.0177	278	05-Oct-2014	Sunday

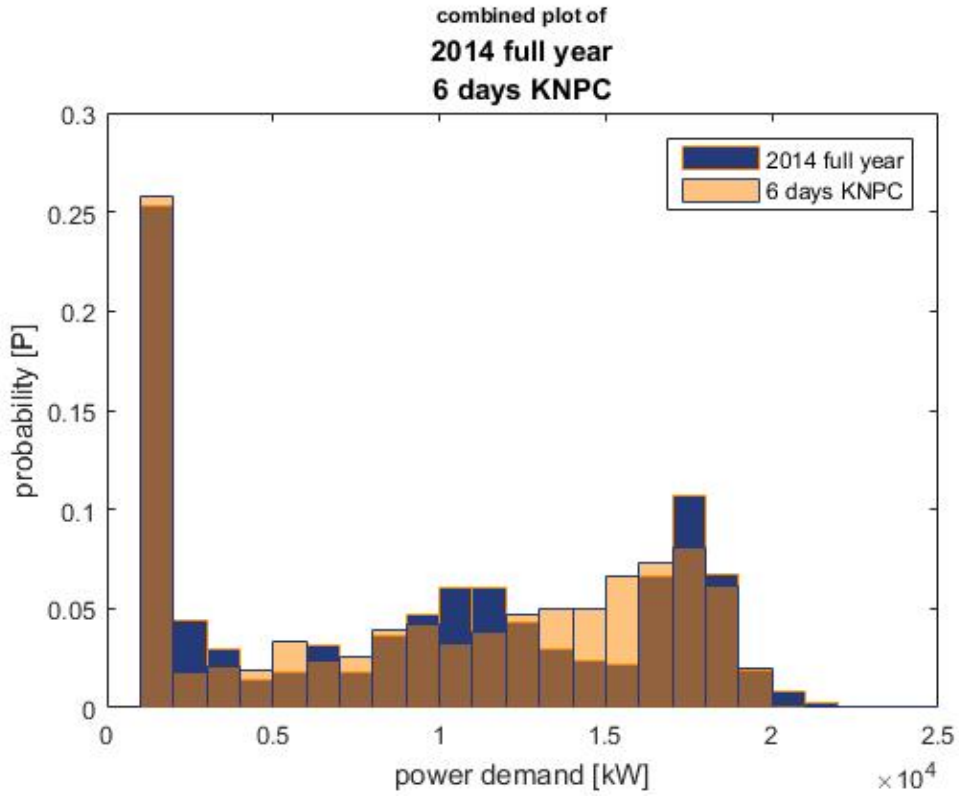

Figure 2.9: Combined plot of *histogram power demand measurements 2014* and *histogram power demand best fit time window*

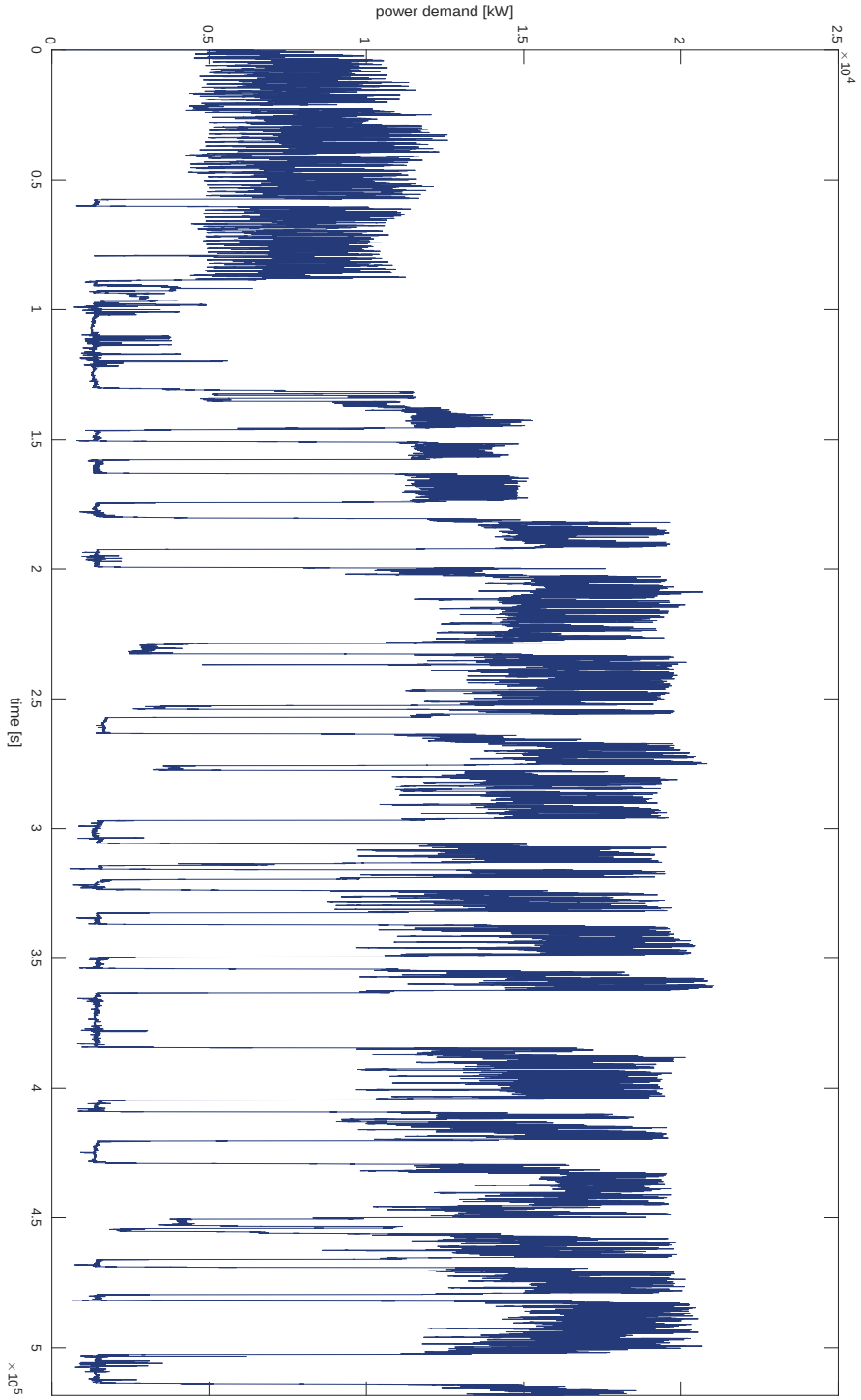

Figure 2.10: Time domain plot of power demand during the six day time window

3

Hybrid systems

This chapter will serve as a small introduction in the developing *hybrid* industry. First of all the definition for hybrid systems will be derived. The definition can be translated to potential gains in the form of fuel reduction and reduction of maintenance. Moreover, this definition is s starting point for deriving different hybrid configurations. The series and parallel hybrid systems will be described. Furthermore the developments in the automotive and maritime industry will briefly be discussed.

3.1. Definition

In the introduction of this thesis the term *(hybrid)* is introduced. It is also stated that in this thesis a hybrid system should at least be comprised out of an internal combustion engine and an energy storage device. However it is still not completely clear what *hybrid* means. The definition of ”hybrid”according to the Cambridge Business English Dictionary [2015] is the following;

Definition 3.1. *Something that is a combination of two different things, so it has qualities relating to both of them*

Since this report focusses on the power generation on board of a cutter suction dredger this definition should be rewritten in a form that includes the generation of power. To ensure the usage of a definition that is valuable and clear for the description of a hybrid power plant on board of a cutter suction dredger the following is proposed;

Definition 3.2. *A system that generates power by using a combination of different energy sources where the overall quality of the system is composed of the individual qualities of the energy sources used*

In this thesis a hybrid system is regarded as a combination of different energy sources. These energy sources may be of chemical composition, electrical or even mechanical. The chemical energy sources that are conventionally used in power generation are fossil fuels, although hydrogen for fuel cells can also be regarded as a chemical energy source. The electrical sources can be divided in two different groups, devices that produce electrical power and devices that store electrical power and feed this power back when needed. For the first category one can think of photo voltaic cells or solar panels. The second category will most probably be in the form of a chemical battery. In this way definition 3.2 is comparable with the definition used in Grimmelius et al. [2011]. In Grimmelius et al. [2011] only energy sources or storage devices that are actually used for power generation are discussed. For example ships equipped with power kites will not be included which should be the case if definition 3.1 is used.

3.2. Hybrid potential

According to definition 3.2 a hybrid system in the sense it is intended in thesis will have a combined quality composed of the individual qualities of the energy sources that are used in the system. The quality of the overall system may be described as supplying power for the dredging process while using a certain amount of fuel and requiring a certain amount of maintenance. One can say that the quality of the system is improved when it requires less fuel and maintenance while performing and achieving the same functionality as was originally intended. Maintenance and fuel consumption can be related to certain cost for operation. If maintenance and fuel consumption is reduced there is a potential cost saving. The potential of the hybrid system for the cutter suction dredger can be expressed as a flow chart and is presented in figure 3.1.

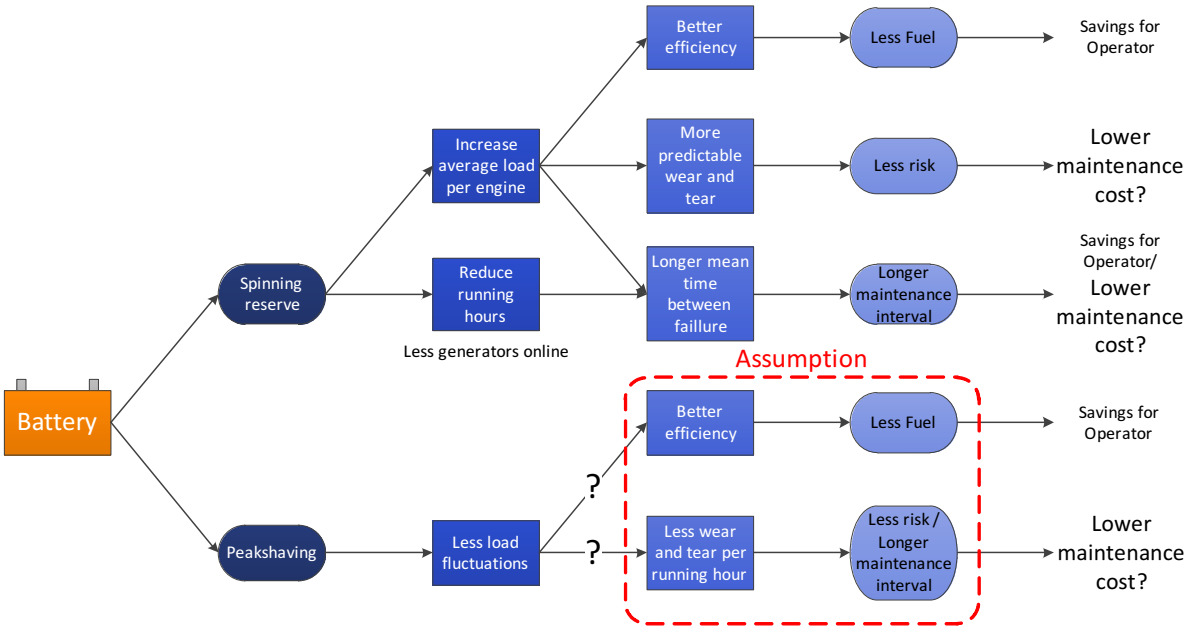

Figure 3.1: Hybrid potential, from battery to reduced cost

3.3. Hybrid configurations

Since the definition of hybrid systems is applicable on almost all combinations of energy sources several options will be described. The description of different hybrid configurations will be the start of a selection process to find the most feasible configuration for a hybrid cutter dredger.

The most common configurations known in the development of hybrid systems are the series and parallel hybrid configuration. These two options are presented in figure 3.2 and figure 3.3 respectively. In these two figures the power is primarily generated by the diesel engine, which is of course an internal combustion engine converting chemical energy to mechanical energy. This block in the figures might be replaced by a fuel cell, a LNG engine or even an petrol engine. However the fuel cell and petrol engine have been found more suitable for smaller applications than shipping, for instance the automotive industry. The battery pack in both configurations might be replaced by another storage device. This can be a different electrical storage device like a super capacitor. The energy might also be stored in the form of mechanical energy by using flywheel technology.

The main difference between the series and parallel system is that in the parallel system the end users is driven mechanically via a gearbox instead of electrically by an electric machine. In fact this is the main drawback of the parallel hybrid system. For each end user a similar system should be developed. In the parallel connected system the only component that can be used for different end users is the storage device. In the case of figure 3.3 the battery pack. The series connected system only needs an electric machine per individual end user. The rest of the system may be centralised which improves

design flexibility.

The Athena and Artemis are equipped with a diesel electric system. This means that there is a central engine room with three diesel generator sets and electric machines powering the end users. The best hybrid solution in this case would be the series hybrid configuration since most of the system is already present in the vessels.

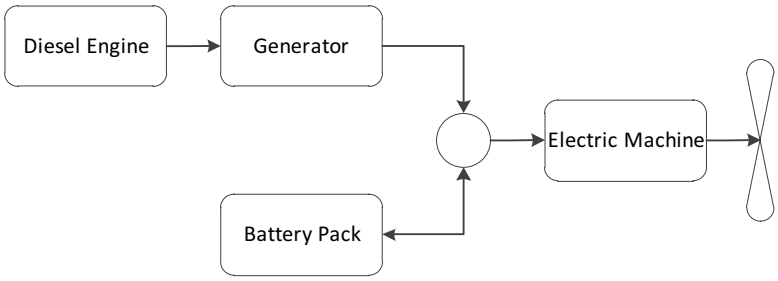

Figure 3.2: Series hybrid configuration

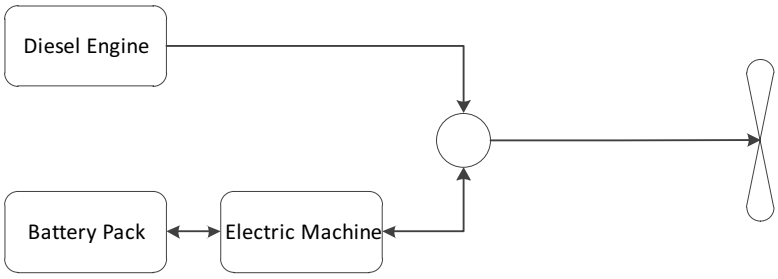

Figure 3.3: Parallel hybrid configuration

3.4. Development in the automotive industry

For several years other industries then the maritime industry are looking into ways to reduce fuel consumption by means of hybrid systems. Most readers will be familiar with the Toyota Prius which was one of the first hybrid applications in the automotive industry. In this section the development of hybrid systems in other industries than the maritime sector will be briefly discussed.

In the automotive industry the concept of hybrid propulsion was developed over the last two decades. Most application of hybrid systems in the automotive industry are based on a combination of an internal combustion engine and a form of electric propulsion. Hybrid configurations that are available today use batteries to provide energy to the electric motor. The energy that is stored in the battery is either generated by the internal combustion engine (in this case the electric motor is used as generator), by means of regenerative breaking or supplied by the domestic electricity grid. Series and parallel hybrid systems are both used in the automotive industry. Multiple adaptations to the general series and parallel system have been developed and tested over the last two decades, however the main principle stays the same. More configurations of hybrid systems in vehicle applications can be found in Gao [2012]. Research papers from Odeim et al. [2014] and Mallouh et al. [2014] describe the development of models and control algorithms for hybrid electrical vehicles that use batteries and a combination of regenerative braking and a power source in the vehicle to charge the battery. In their research the internal combustion engine was replaced by a fuel cell to provide the energy needed. The paper of Sciarretta et al. [2014] focusses on the development of a control benchmark for the energy management of a plug-in hybrid vehicle. So in this research also power from the electrical grid is stored in the battery. It becomes clear that most hybrid vehicle manufacturers and researchers focus on the use of batteries in hybrid applications.

Nevertheless other systems are proposed as well for hybrid vehicles. In Trajkovic [2010] a pneumatic hybrid vehicle is proposed. Instead of storing energy in a heavy battery the surplus of energy is stored in the form of compressed air. The internal combustion engine itself is used as compressor during braking and will pump air to a storage tank. During acceleration this stored compressed air is used to speed up the vehicle without the need for extra fuel injection. Similar hybrid systems can be thought of by using hydraulics and accumulators, although with the addition of a hydraulic pump/motor [Pedersen and Engja, 2010].

3.5. Development in the maritime sector

In the maritime industry the development of hybrid systems follows the developments in other industries. Hybrid system design in shipping differs from automotive mainly due to the large quantities of energy consumed. One can imagine that when a system uses more power, the storage devices have to be scaled up as well. Despite scaling issues more and more companies develop energy storage systems for the marine applications. At this moment several ships equipped with hybrid systems are operational.

In the maritime sector the influence of hybrid systems is mostly seen in ship types with a strongly varying operational profile. This means that for these vessels the energy demand varies significantly over time. Examples of vessels with a varying power demand are tugs, offshore supply vessels, yachts, dredgers and other special ship types.

Examples of the use of hybrid systems in tugboats are given in Grimmelius et al. [2011] and Aspin and Hayman [2009]. In Grimmelius et al. [2011] a hybrid system for a conventional tug with two 1865 kW diesel engines was investigated. In this research the focus lay more on the development of the control system and was done during the early design stages of this tugboat. The actual performance of this tug has proved to be a little disappointing as was presented in an Imarest meeting in spring 2015. The reduction in fuel consumption was marginal where large reductions were predicted. The ”Carolyn Dorothy” which is described in Aspin and Hayman [2009] was designed to be a hybrid tug, combining two smaller 1342 kW diesel engines with two 900 kW electric motors. Both vessels are equipped with a parallel system.

Hybrid systems for passenger and car ferries are developed by Imtech Marine as described by van der Pennen [2015]. The presented system was designed for the ferry that sails between Sconser and Raasay. This system combines three 330 kW generators, two 350 kWh battery packs and two 375 kW electric motors. This is typical example of a series hybrid system.

These examples represent developments from system integrators in the hybrid market. The role of battery producers should not be underestimated in the developing hybrid propulsion market. For example Corvus energy supplied over 25 MWh of battery storage capacity solely for hybrid applications in the marine industry [Rahn, 2015]. In table 3.1 a small overview of the largest battery packs ($>$ 1 MWh)in maritime hybrid applications is presented.

Table 3.1: Overview of the larger battery systems supplied by Corvus energy [CORVUS energy, 2015]

Vessel name	Vessel type	Battery capacity $[MWh]$	Bus Voltage $[V]$	Number of modules
Prins Richard	Passenger and Car Ferry	**2.6**	932	399
Texelstroom	Passenger and Car Ferry	1.6	1050	252
Prinsesse Benedicte	Passenger and Car Ferry	1.6	932	252
Deutschland	Passenger and Car Ferry	1.6	932	252
Folgefonn	Passenger and Car Ferry	1.4	800	221
Deutschland	Super Yacht	1.0	600	156

4

Hybrid component models

In this chapter the development of the individual component models within the hybrid cutter model will be discussed. The assumptions that were made during the development of the mathematical models will be presented. Since the hybrid model will include multiple extra components the EFD will be slightly different when compared with the system introduced in chapter 2. The EFD will be the foundation for the final mathematical model. Therefore the proposed configuration is presented in this introduction as an EFD in figure 4.1. The individual components that have to be modelled are the electrical grid, the diesel generators with there corresponding fuel consumption, the battery with its important features and a power management systems to combine the different models into a working system. The development of these models will be presented in this order.

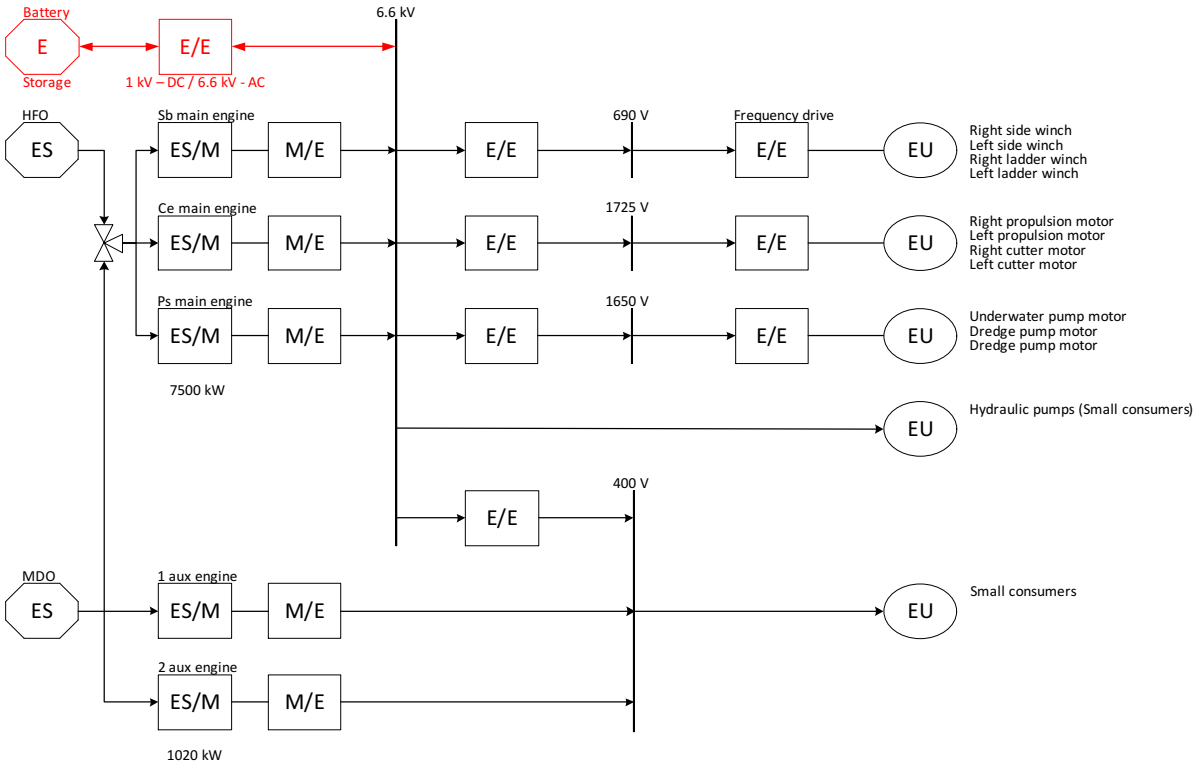

Figure 4.1: Energy flow diagram of the hybrid configuration

4.1. Power demand

The dredging operation of the cutter suction dredger with all its processes requires power. Or in other words the functionality of the CSD demands power. In this section the steps from power demand by the final end users to the diesel engine will be derived. It is important to know where different power measurements are taken. The location of the measurements determines which efficiencies have to be taken into account when determining the power demand from the diesel engines. The power demand measurements are taken on the frequency drives. Figure 4.2 gives an overview of the different efficiencies in the energy distribution network [Klein Woud and Stapersma, 2002]. It turns out that efficiencies of the frequency drive, the electrical grid and the generator should be determined in order to derive the required power output of the diesel engine. Next to the power demand the power supply is measured by the VODAS system. These measurement are taken at the generator terminals. With this information it is possible to determine the combined efficiency of the electric grid and the frequency drive. The generator efficiency is still unknown. This value should be derived while tuning the complete model. These processes are described in chapter 5.

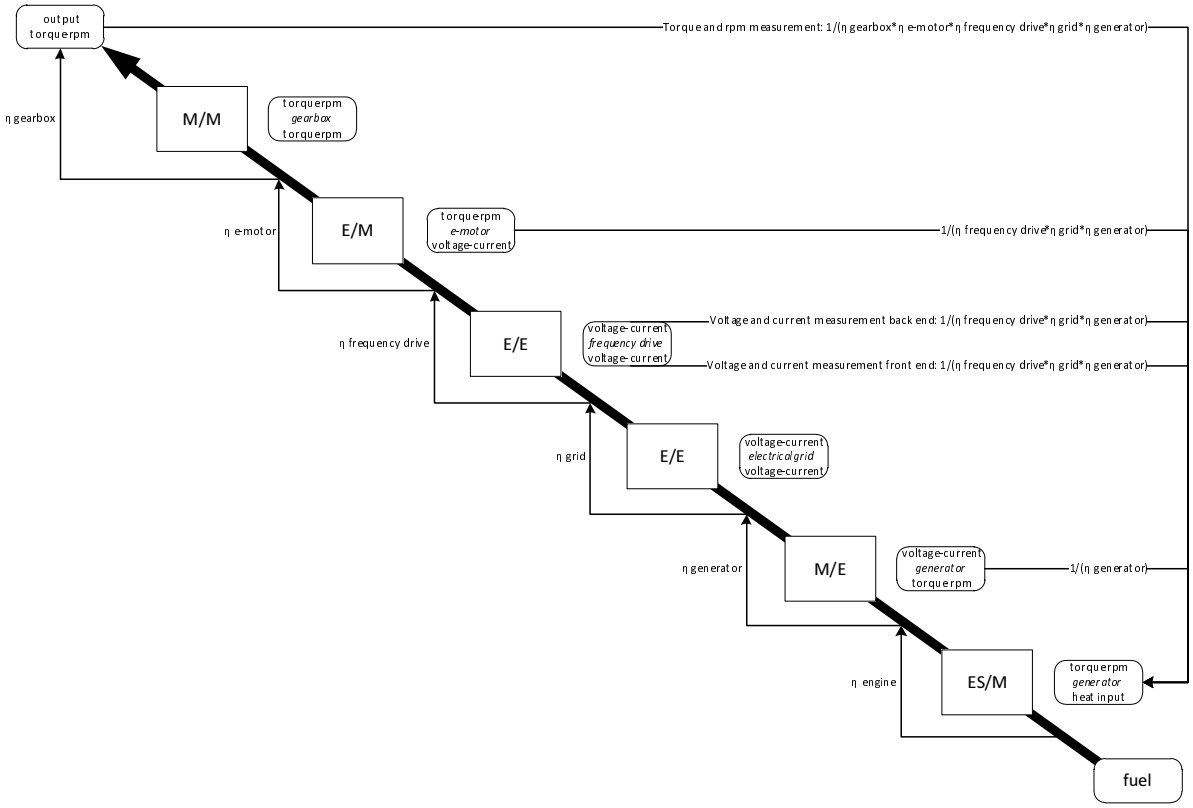

Figure 4.2: Power chain: overview of power and efficiency from fuel to user

4.2. Fuel consumption

Fuel consumption is key in the development of the cutter model. Eventually the fuel consumption of the model should be compared with the actual fuel consumption of a CSD to validate the model that will be developed.

4.2.1. General information and literature on fuel consumption

In this section several terms will be used that might need some explanation. Therefore these terms will be discussed shortly. Specific Fuel Oil Consumption (SFOC) will be used frequently. SFOC is defined as the fuel consumption of a fuel consuming power generating device (in this case a diesel engine) related to its ”brake” (*or ”effective”*) power. The mathematical formulation is presented in equation 4.1 [Stapersma, 2010b]. The unit of SFOC is $[g/KWh]$.

$$sfoc = \frac{\dot{m}_f}{P_b} \tag{4.1}$$

The FAT is the test where the client (*in this case Van Oord*) and the class society give their approval to the product and accept the engine as is.

In Rensen [2014] interesting conclusions were made on the fuel consumption prediction of the VO-CUT program. The main conclusion of this research is that a significant difference is found between the SFOC measured during the FAT and the SFOC that is encountered during actual operation. The trend that the actual SFOC is higher than the SFOC measured during the FAT is noticed by more ship owners becomes clear from Hartkopf Mikkelsen and Grønvald Raun [2015]. In this article it is stated that the Norwegian carrier I.M. Skaugen is suing MAN Diesel and Turbo for the fact that the fuel consumption from six medium-speed four-stroke diesel engines is higher in reality than the fuel consumption that was promised by MAN. Several causes can be found for the difference in fuel consumption of diesel engines between FAT and actual operation. In Rakopoulos and Giakoumis [2009] multiple transient related causes are described. When speaking about transients in this thesis it is meant that the power demand on the diesel engine will fluctuate over time. The transient operation of the diesel engine is probably not the only reason that there is a certain discrepancy between measured and actual fuel consumption figures. MAN Diesel and Turbo [2016] and Wärtsilä Corporation [2015] state multiple causes for increased fuel consumption, it is stated that the fuel consumption increases due to ageing and delayed maintenance.

Rensen [2014] did his research within Van Oord and did not address the affect of transients in the operating profile of the diesel engines. In the papers of Lebedevas et al. [2015] and Lindgren [2005] similar problems are described as what Rensen [2014] was facing. Lebedevas et al. [2015] and Lindgren [2005] did search for a correlation between fuel consumption and transients in the operating profile of the diesel engine.

In the research of Lebedevas et al. [2015] two diesel engines of train locomotives are analysed. The parameters of these diesel engines are presented in table 4.1. In this research only the Caterpillar was actually modelled. It is stated that the MTU would respond the same as the Caterpillar. The increase in total fuel consumption due to transients is 3% according to Lebedevas et al. [2015]. The same research states that this result is only possible since the Caterpillar that was modelled had a variable common rail fuel injection system. The visual result of this research show that the increase in SFOC can sometimes be 800% during transients. As further analysis on the ships from Van Oord will show these spikes in SFOC will not contribute to a noticeable increase in overall fuel consumption.The high transients occur for very short time periods, this might be the reason that the contribution to overall fuel consumption is small. The total fuel consumption is the integral of SFOC multiplied with delivered power over time these short time periods will not contribute much in this integral. Next to that the integral is taken from the product of SFOC and power. In the high power ranges there is not much room for transients since the engine limits will restrict this. Therefore the absolute fuel consumption during transients will be lower than would be expected from the SFOC figures.

Lindgren [2005] did his research on a Valtra 420 DWRE engine which was mounted on a agricultural tractor. The specifications of this engine are presented in table 4.2. In this research attempts were taken to fit a function through experimental data. The diesel engine was tested in transient operation and fuel flow was measured. Lindgren [2005] did measurements on absolute fuel consumption and did not calculate the SFOC of the engine under consideration. However his method for curve fitting is promising since it does not imply any form of modelling constraints.

This is specifically mentioned since the results described in the papers of Lebedevas et al. [2015] and Lindgren [2005] are not applicable on the larger four-stroke medium-speed engines that are of interest for Van Oord and this thesis. Nevertheless the line of thought can be followed to derive functions that can describe the fuel consumption of such large engines in transient operation. The importance of understanding the behavior of larger diesel engines in transient operation is emphasised in Lyu [2016]. In Lyu [2016] a hybrid system is developed for a semi submersible crane vessel. The author states that the real potential of the hybrid system in peak shaving with respect to fuel consumption can only be proven when a proper relation between transients and fuel consumption is developed. To clarify, peak shaving in this sense is actually smoothing out the power demand on the engine. High peaks in power will be reduced by providing power from a different source and troughs in the power demand will be filled by charging the energy storage device.

Table 4.1: Technical parameters of the Caterpillar 3512B-HD and MTU 4000 R41 diesel engines

	Cat 3512B-HD	MTU 4000 R41
Maximum power $[kW]$	1700	1500
Maximum speed $[rpm]$	1800	1800
Number of cylinders	12	12
Bore $[mm]$	170	165
Stroke $[mm]$	215	190

Table 4.2: Technical parameters of the Valtra 420 DWRE diesel engine. [tractordata.com, 2009]

	Valtra 420 DWRE
Maximum power $[kW]$	81
Maximum speed $[rpm]$	2200
Number of cylinders	4
Bore $[mm]$	108
Stroke $[mm]$	120

4.2.2. Fuel measurements and initial analysis

Within Van Oord three ships are equipped with fuel flow sensors. The sensors measure the fuel flow to the engine and the fuel flow in the return line. The fuel flow can also be measured before the booster unit. In the first case the difference between the two measurements is the fuel consumed by the engine. In the second case the fuel consumed by the engine is given by just the single measurement before the booster unit. Note that the fuel sensors are not placed on the direct supply to the fuel pumps, the fact that measurements are taken before the booster unit can introduce a delay in the signal. The measurement equipment is supplied by *VAFinstruments*. Since the volume flow is measured it is necessary to convert the measured values to mass flow. The derived mass flow can then be combined with the power output of a certain engine to develop a SFOC figure.

The fuel volume flow is calculated by substituting equation 4.2 in equation 4.3, in which Δp represents the change in the number of pulses (generated by the sensor) and K_{factor} represents the number of pulses per litre. The K_{factor} is entered in the *VAF* computer by a *VAF* technician. Δt represents the time interval or sampling period in seconds. So the unity of Q is $[l/sec]$.

$$\Delta v = \frac{\Delta p}{K_{factor}} \tag{4.2}$$

$$Q = \frac{\Delta v}{\Delta t} \tag{4.3}$$

As stated before the volume flow has to be converted to mass flow. This is done by multiplying the volume flow with the correct density as is presented in equation 4.6. Since the density is temperature depended an equation should be solved to find the correct density value. Equation 4.5 was adopted from VAF instruments [2015], whereas equation 4.4 was described in Stapersma [2010a]. The difficulty with the *VAF* measurements is that the crew has to pre program the *VAF* computer with the correct density ρ^{15} and the gc value to calculate the correct mass flow. It turns out that quite frequently the settings of the computer are not correct. Possibilities for this problem could be the fact that no density information is available and that the gc value has a uncommon unity i.e. $[\%/s]$.

$$\rho_f^T = \rho_f^{15} - 0.68 \cdot (T - 15) \tag{4.4}$$

$$\rho_f^T = \rho_f^{15.6} \cdot (1 - gc \cdot (T - 15.6)) \tag{4.5}$$

$$\dot{m}_f = Q \cdot \rho_f^T \tag{4.6}$$

Since several possibilities for mistakes based on wrong assumptions are identified it is decided to request the settings from the *VAF* computer on board. It should be possible to derive the measurement temperature. Further calculations can then be done manually. The settings from the computer for two of the vessels are presented in table 4.3. In this table the italic fuel types are the ones that were actually used in the time period that will be analysed. The measurement temperature can be found by rewriting equation 4.6 to equation 4.7. This equation can be substituted in 4.5 which results in equation 4.8. From the last equation the measurement temperature can be derived as is presented in equation 4.9. For the HAM318 the period between March 4 and March 31 2016 is analysed. To be able to compare results the temperature values are also derived for the Vox Maxima albeit for a different period i.e. February 1 till February 25 2016.

$$\rho_f^T = \frac{\dot{m}_f}{Q} \tag{4.7}$$

$$\frac{\dot{m}_f}{Q} = \rho_f^{15.6} \cdot (1 - gc \cdot (T - 15.6)) \tag{4.8}$$

$$T = ((\frac{-\dot{m}_f}{Q \cdot \rho_f^{15.6}} + 1)/gc) + 15.6 \tag{4.9}$$

Table 4.3: VAF computer settings as received from chief engineers

Vox Maxima				
Fuel Type	Spec. Gravity $[kg/l]$	Gravity Change $[\%/C]$	Ref Temp $[C]$	Caloric Value $[MJ/kg]$
HFO 2103	0.9908	0.07	15	40.470
HFO in u	0.9720	0.07	15	40.393
HFO	0.9980	0.07	15	40.870
MDO	0.8450	0.07	15	42.691

HAM 318				
Fuel Type	Spec. Gravity $[kg/l]$	Gravity Change $[\%/C]$	Ref Temp $[C]$	Caloric Value $[MJ/kg]$
HFO 2103	0.9980	0.07	15.6	40.870
HFO in u	0.9970	0.07	15.6	41.230
HFO	0.9960	0.07	15.6	40.570
MDO	0.8900	0.083	15.6	41.830

Unfortunately the results have to be rejected since the temperatures that were found vary between -300 C an 500 C. To illustrate this a histogram with the results of this analysis is presented in figure 4.3. This result shows that the mass flow value calculated by the *VAF* computer is not correct. The flow values measured by *VAF* might be correct, but the calculations have to be done manually. Two assumed temperatures are adopted, 140 degrees Celsius for HFO and 25 degrees Celsius for MDO for further calculations.

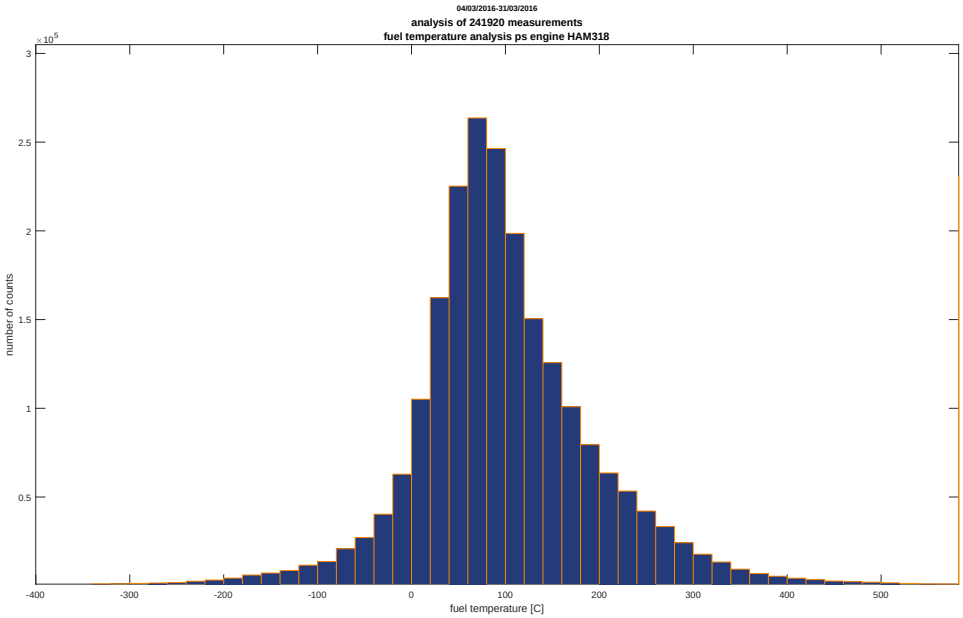

Figure 4.3: Calculated fuel temperature of the portside engine from the HAM318

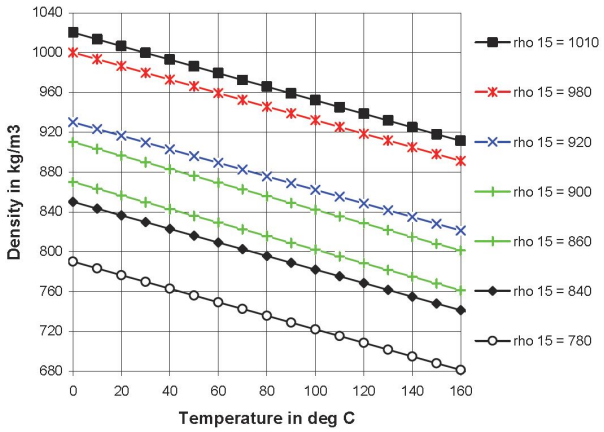

Figure 4.4: Density versus temperature of fuel oils [Stapersma, 2010a]

Since the flow measurements are supposed to be correct it should be possible to derive a comparable mass flow value in $[kg/s]$ using flow data, *assumed* temperature data and the density values as presented in Stapersma [2010a]. Nevertheless the initial density of the fuel should be known. The density ρ_f^{15} is necessary to use equation 4.4 or the regression lines as presented in figure 4.4.

It is proposed to use the energy flow into the engine to compare actual consumption and consumption as presented in the FAT report. At least as an initial step to eliminate the differences in lower heating value between HFO and MDO. The energy flow is presented in equation 4.10 as $\dot{J}$ in $[kJ/s]$.

Note that the Lower Heating Value (LHV) is often presented in the fuel test reports. However, when the LHV is not available in a fuel test report the following approach can be used to find an approximation for the lower heating value;

Besides the LHV the mass fraction of sulphur is often presented in the fuel test reports. The mass fraction sulphur is an important value to determine an approximate LHV of a fuel. This is presented in equation 4.11, in which x_s is the mass fraction sulphur and C/H the ratio carbon and hydrogen atoms of the fuel under consideration. Since the C/H fraction is not presented in fuel test reports one can use equation 4.12. When equation 4.12 is substituted in equation 4.11 the relation between x_s, ρ_f^{15} and LHV is found. This relation is presented in equation 4.13. Equation 4.11 and 4.12 were adopted from Stapersma [2010a].

The energy flow figure is representative for engines running on diesel oil and heavy fuel oil and makes comparison between engines possible. It is assumed that the combustion efficiency of the diesel engines will be the same for both fuel types. In other words the comparison is made fuel independent. Since $[kJ/s]$ is an uncommon unity to compare engine efficiency the decision was made to pick one fuel type with set parameters as density and LHV to calculate the SFOC. A representative fuel could be te fuel that was used during the FAT. Values presented in the FAT report of one of the engines from the HAM318 are presented in table 4.4 [Wärtsilä Corporation, 2000]. This enables comparison between actual performance of an engine and the performance during the FAT.

Table 4.4: Fuel specifications FAT Wärtsilä 12V46C HAM318

Fuel Type	Spec. Gravity $[kg/l]$	Ref Temp $[C]$	Caloric Value $[MJ/kg]$
HFO	0.965	15	41.360

$$\dot{J} = \dot{m} \cdot LHV \tag{4.10}$$

$$LHV = 43300 - 1200 \cdot (C/H - 6) - 27000 \cdot x_s \tag{4.11}$$

$$\rho_f^{15} = 800 + 90 \cdot (C/H - 6) \tag{4.12}$$

$$LHV = 43300 - \frac{1200}{90} \cdot (\rho_f^{15} - 800) - 27000 \cdot x_s \tag{4.13}$$

Before the initial results from the fuel consumption - transient analysis will be presented a short summary of the work will be given. The theoretical background has already been presented in the previous section. These presented formulas are used in the analysis but will not be repeated every time.

The fuel flow for the Vox Maxima and the HAM318 is analysed in the specific periods described earlier. The flow is given in liter per second and liter per hour respectively. The engines of the Vox Maxima were running on HFO with a specific density ρ^{15} of 0.961 kg/l and a LHV of 40581 kJ/kg. The HAM318 ran on MDO with a ρ^{15} of 0.838 kg/l and a LHV of 42828 kJ/kg. Finally the factory acceptance test fuel values from the HAM318 are used to convert back to mass flow. This fuel is presented in table 4.4. The fuel temperature on the Vox Maxima is assumed to be 140 C since it was running on HFO and the fuel temperature on the HAM318 is assumed to be 25 C.

The results of this analysis are presented in figure 4.6 and figure 4.7. These figures represent the specific fuel oil consumption of the engines from the Vox Maxima and the HAM318. The SFOC is plotted on the z-axis against the load factor and the time derivative of the load factor. The Load Factor (LF) is represents the power that is delivered as a percentage of the Maximum Continues Rating (MCR). The time derivative of the LF represents the increase or decrease in power as a percentage of the MCR since the previous time step. In this case the sampling frequency is set to 1 Hz, so the time step is 1 s. An overview of the minimum and maximum specific fuel oil consumptions is given in table 4.6.

It might be clear that the trend shown in figure 4.6 and 4.7 is comparable for both vessels and both engine types. The general specifications of the diesel engines are presented in table 4.5. At this point it is not possible to formulate a conclusions from the figures mentioned. The following reasons can be addressed to why this analysis is not usable to state a hard conclusion;

1. the minimum SFOC found is always lower than the lowest SFOC provided by the manufacturer.

2. there is no clear trend between the minimum and maximum SFOC when this is related to transients.

Table 4.5: Engine specifications Vox Maxima and Ham 318

Engine	manufacturer	type	nominal power $[kW]$	nominal speed $[rpm]$
PS Engine Vox Maxima	MAN diesel	12V46/60B	14400	514
PS Engine HAM318	Wärtsilä	12V46C	12600	514

The fact that the SFOC found from the measurements is lower than the SFOC specified by the manufacturer is strange. Typically an engine manufacturer will present the lowest possible fuel consumption in order to sell its engines. The cause for this discrepancy might be found in the assumed fuel temperatures. Another cause can be that the densities and lower heating values were taken from (*for the period under consideration*) recent fuel test reports. It is of course possible that other bunker tanks with different fuel specifications were used in the period that is analysed. These assumed values might lead to a constant error between observations and factory data. This should not be a problem when the goal is to find trends instead of absolute values.

If one is searching for a trend between transients in power and an increase in specific fuel oil consumption the second point might pose difficulties. It was thought that the specific fuel consumption would increase during transient events. The only thing that can be found from the SFOC figures is that the specific fuel consumption increases during negative transients and decreases with positive transients. This does not stroke with the hypothesis. There is no clear physical explanation for the phenomena found. Common sense tells us that during acceleration more energy is used than during steady state operation (*compare the results with the fuel consumption of your car, a car is less efficient in an urban environment than on the highway…*). It is decided to search for the existence of phase lag in the measured signals. If phase lag is present in the signals this might explain the *strange* results during transients. When the fuel flow signal lags on the power signal one will find high SFOC values during negative transients and low SFOC values during positive transients. Since all the data collected with Vodas is compressed in order to send it via satellite it is smart to use uncompressed data for this phase analysis. A set of uncompressed data is available for the Volvox Asia since a colleague did on board measurements. (*this is the third ship equipped with fuel flow sensors*)

An analysis was done to confirm the suspicion that the flow signal lags the power measurements. It was assumed that the fuel rack, which is measured, should be in phase with the flow measurements. The reason for this is that it can be expected that full flow is measured at 100% rack setting. If the two signals mentioned are not in phase the difference between the two signals gives the phase lag. Result from this analysis are presented in figure 4.5. After figure 4.6 and 4.7 this analysis will be explained further.

Table 4.6: Summary of initial SFOC transient results

Engine	minimum SFOC $[g/kWh]$	maximum SFOC $[g/kWh]$	$[LF]$	$[dLF/dt]$
PS Engine Vox Maxima	140		109.5	0.36
		300	26.5	-0.14
SB Engine Vox Maxima	134		109.5	-1.07
		306	31.0	-7.07
PS Engine HAM318	182		102.5	-1.83
		231	27.0	-2.83
SB Engine HAM318	151		38.5	7.89
		236	39.5	-7.61

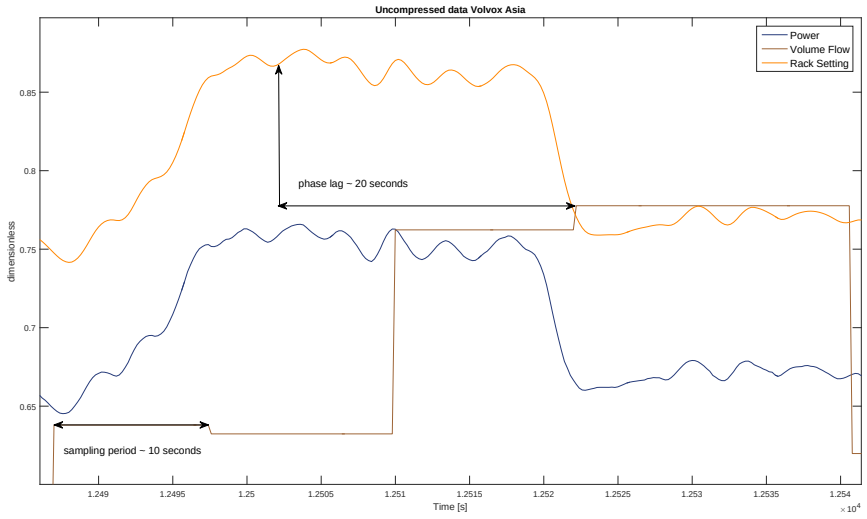

Figure 4.5: Phase lag and sampling period analysis

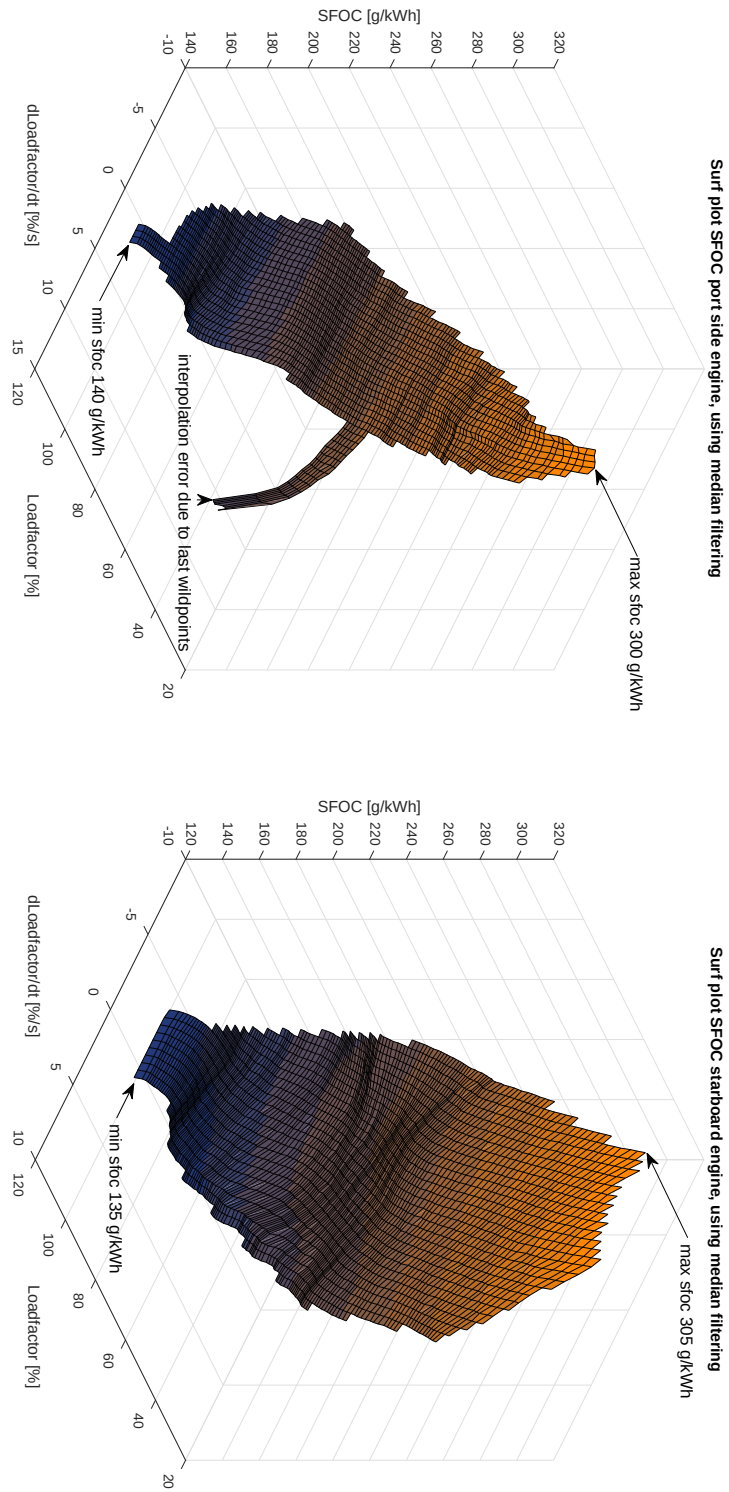

Figure 4.6: SFOC Vox Maxima

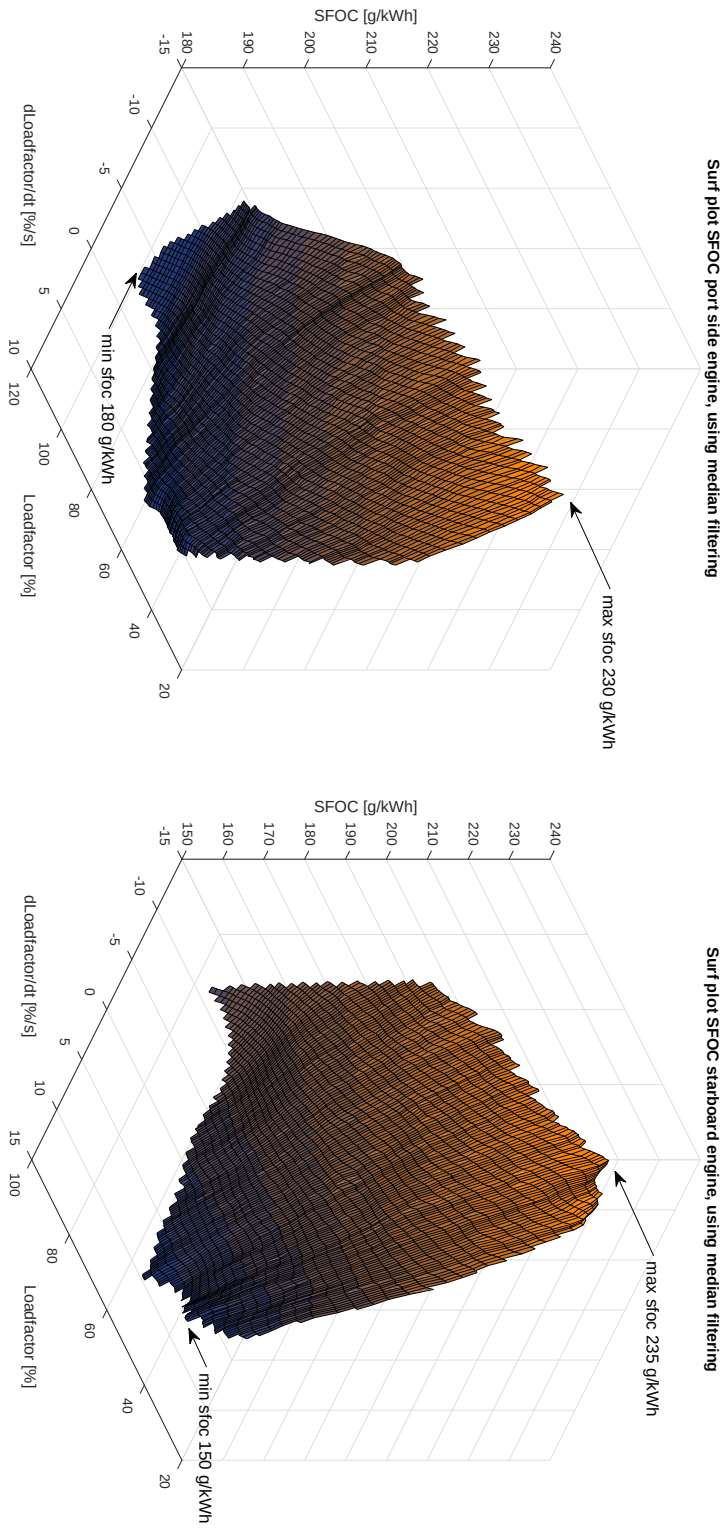

Figure 4.7: SFOC HAM318

The measurement signal analysis was done based on data measured on board of the Volvox Asia. Since it is assumed that the fuel rack should be in phase with the fuel flow these two signals are used to determine the phase lag on the fuel flow signal. By moving the fuel rack signal in time and calculating the RMSE between the fuel rack signal and the fuel flow signal each iteration a value can be found for the phase lag. In other words the phase shift of the fuel rack signal that results in the lowest RMSE compared with the fuel flow signal gives the phase lag of the fuel flow signal. It turns out that the smallest error occurs with a shift of 102 time steps. Since the sampling period is 0.2 second this results in a ultimate phase lag of around 20 seconds. As is presented in figure 4.5. It should be mentioned that a same analysis could be done between the power signal and the fuel rack signal. Though it can be seen from figure 4.5 that this phase difference will be small.

4.2.3. Extended analysis

It is now determined that the initial specific fuel consumption versus transient relation that was found is incorrect. A constant or steady state error can be found due to the fact that certain assumptions have been done on fuel temperature, fuel density and the lower heating value of the fuel. On the other hand there is an error introduced due to the phase lag on the fuel flow signal. Therefore another approach is suggested to determine if there is a relationship between transients and SFOC.

The proposal to use longer time sequences in order to eliminate the effects of phase lag on the measurements. The time sequences under consideration will have a minimum length of 15 minutes or 900 seconds. In this case the maximal error that can be introduced by the phase lag will be 2%. To determine where the usable time windows are situated (*on the time vector*) and how long these time windows are a moving average filter was constructed. This filter has a reset based on the error between the average value and the real measurement. If the maximum error between the real measurements and the average value is exceeded the average filter will start again at the value of the measurement at that time step. To illustrate this the average and real signal for a certain time window are presented in figure 4.8.

Since the initial analysis posed some difficulties with regards to the fuel measurements it should be confirmed that the measurement results over a longer period are indeed correct. Van Oord internally checked the results of the fuel measurements and the gauging of the bunker tanks. It turns out that over the period of a year the measurements are 3.26% lower than the manual findings. This can be explained by the fact that the measurement equipment is situated behind separators and settling tanks, so the water and particles in the fuel are already removed [Paauw, 2016]

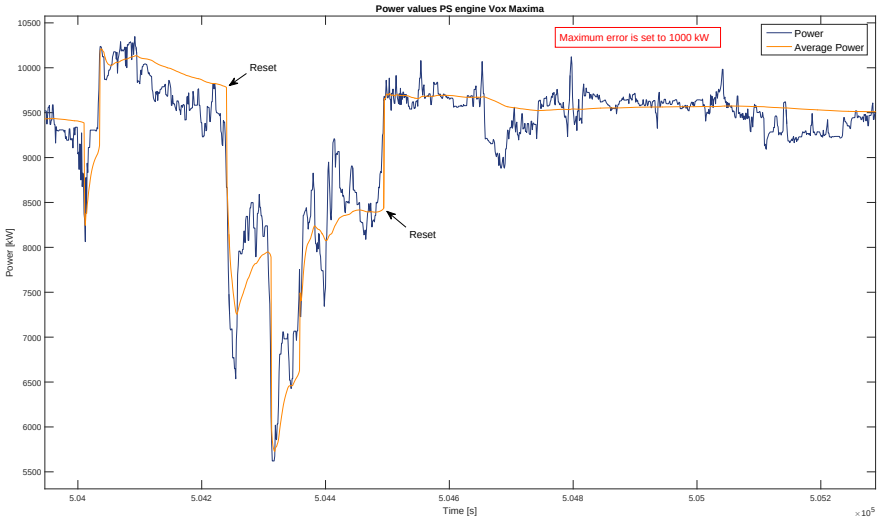

Figure 4.8: Power signal and filtered power signal PS engine Vox Maxima

The filtered power signal is the base for further analysis. As stated earlier, the goal is to find time windows of at least 15 minutes. A period is selected when the average power signal stays within a certain bandwidth. During this analysis the bandwidth was set to 750 kW By doing this a fairly constant average signal is found. This constant signal provides rough information about the average load factor during this time window. The average signal does not provide any information about transients. Therefore the ripple around this average value, the original power signal, is expressed as a variance from the mean value. By integrating fuel mass flow (*determined in previous sections*) a value for the fuel used in the time window is found. The same holds for the amount of power that is generated. According to equation 4.1 an average SFOC can then be found for the time window under consideration. To summarize this section the following values are found for the different time windows;

1. window length $[s]$ (minimal 900 s)
2. average delivered power $[kW]$
3. variance on the delivered power (transients) $[kW]$
4. specific fuel oil consumption $[g/kWh]$

To reduce the effect of the earlier described constant or steady state error introduced by the assumptions on temperature and fuel specifications it was decided to represent the SFOC as a dimensionless value. The found SFOC values are related to the minimum SFOC found during the analysis. In this way the difference in trend between the measured values and the factory acceptance test can be visualized. Besides the SFOC, the delivered power and the transients are made dimensionless as well. Deliverd power is presented as LF as percentage of MCR. The transients are presented as a percentage of the current delivered power. The result of this analysis is presented in figures 4.10 to 4.13.

From the results of the adjusted transient vs. SFOC analysis the following preliminary conclusion can be formulated; *transients in power demand from a stationary diesel engine (generator mode with constant rotational speed) do not affect the efficiency of this diesel engine. The average load factor is still the governing variable in the specific fuel consumption of the diesel engine.*

In order to confirm the conclusion stated above a meeting was held with Wärtsilä Netherlands. During this meeting the results of the transients versus fuel consumption analysis were discussed. It turned out that Wärtsilä could not confirm the results at this instance. The general assumption that transients in the power demand would lead to a higher SFOC was shared by Wärtsilä, unfortunately no measurements or test were available to confirm this hypothesis. On the other hand Wärtsilä could not reject the conclusion either. So unfortunately it is not possible to confirm the conclusion right away.

Interesting to see is that Shi [2013] found similar results as the results presented in figure 4.11 and 4.13 while measuring on board of a trailing suction hopper dredger from Boskalis. Wei Shi presents the results of his measurements in his PHD dissertation. Several load cases were investigated by Wei Shi, including steady state operation and load steps. These load steps can be seen as transient events. A transient event is slightly different from transient operation. Transient operation is a continuous fluctuating power demand whereas a transient event happens in one moment. The steady state measurements resulted in a benchmark on SFOC for different power acceptance of the diesel engine. After the benchmark was set several transient events were initiated such as decelerating, accelerating and a crash stop. It should be mentioned that the tests were executed on two different power configurations, one where the diesel is connected to a Controllable Pitch Propeller (CPP) and the other where the diesel engine drives a CPP and a electrical generator. The conclusion drawn from Shi [2013] is that all the transient events he investigated did not have any effect on the SFOC of the diesel engine. The diesel engine uses the same amount of fuel during a transient event as it would during steady state operation.

It is possible to give an explanation for the behaviour of the diesel engine in transient operation using the generalized efficiency function for the diesel engine. Equation 4.14 represents the general efficiency function for a diesel engine. In this equation the mechanical efficiency η_m, the combustion efficiency η_{comb}, the heat loss efficiency η_{hl} and the thermodynamic efficiency η_{td} is included. These efficiencies are presented in mathematical form in equation 4.15 to 4.18. The individual efficiencies will be discussed with respect to their behaviour under transient conditions. The efficiency explanation is based on knowledge gained from Stapersma [2010a] and Stapersma [2010b]. Information from other authors will be cited individually.

$$\eta_e = \eta_m \cdot \eta_{comb} \cdot \eta_{hl} \cdot \eta_{td} \tag{4.14}$$

$$\eta_m = \frac{W_e}{W_i} = \frac{W_i - mechanical\ losses}{W_i} \tag{4.15}$$

$$\eta_{comb} = \frac{Q_{comb}}{Q_f} = \frac{Q_f - heat\ of\ unburned\ fuel}{Q_f} \tag{4.16}$$

$$\eta_{hl} = \frac{Q_i}{Q_{comb}} = \frac{Q_{comb} - heat\ lost}{Q_{comb}} \tag{4.17}$$

$$\eta_{td} = \frac{W_i}{Q_i} = \frac{\int_{cycle} \tilde{p} \cdot dV}{\int_{cycle} \tilde{T} \cdot dS} \tag{4.18}$$

1. Mechanical efficiency η_m gives the ratio between indicated work (*inside the engine*) and the effective work delivered at the end of the crankshaft. The difference between these two values is the mechanical loss. In a mechanical system the losses are comprised of friction in the bearings, the cylinder liners and other types of friction. Besides friction there is some engine power used for the engine's support systems like cooling water pumps. This is not always the case, but it can be assumed that the power going to these systems will not change dramatically during a transient event (*if it is assumed that the friction is a constant loss, which is valid for a engine running on constant rpm, the efficiency will actually increase at higher power outputs, which can also be seen in the steady state efficiency of a diesel engine*). Finally the inertia of the engine (*and all the other rotating parts connected to the engine*) will play a role in the mechanical efficiency. During most common transient events the engine will have to increase its rotational speed. Energy is then stored in the form of kinetic energy, this energy will not be available at the end of the crankshaft. This will reduce the mechanical efficiency during transients. Although in the case of a dredging application (*as in Shi [2013]*) the engines will be used as stationary machinery running on a constant rpm value. During a load acceptance transient no energy has to be stored as kinetic energy due to the inertia of the system and the mechanical efficiency will stay constant. The effect of the inertia of the system is described in more detail in appendix D. Since some readers may doubt the statement that the friction losses are constant for an engine running on constant speed the author would like to refer to Stapersma [2010b] and Berger [2002].

2. The combustion efficiency η_{comb} presents the ratio between the heat that is released during combustion and the heat that was stored in the injected fuel. The last is the potential heat that enters the cylinder. The combustion efficiency gives a value to the effectiveness of combustion. A low η_{comb} means that not all fuel that is injected is burned. The combustion of fuel is subjected to multiple constraints. The most pronounced constraints for complete combustion are the availability of oxygen and a certain temperature to ignite the fuel. The temperature in the cylinder is determined by the air inlet temperature and the compression ratio. Since during a transient event the compression ratio will not change (*this is geometrical property of the engine*) and the intake temperature is not directly related to any form of transient the combustion efficiency will probably be solely dependent from the availability of oxygen. Oxygen enters the cylinder in the form of intake air. There is a certain ratio between the amount of air (*and therefore oxygen*) and fuel that is needed for complete combustion. This is the so called stoichiometric ratio σ. Normally there is more air available in the combustion chamber than is strictly necessary for complete combustion.

$\lambda = \frac{m^{air}_{available}}{m^{air}_{minimal\ needed}}$ gives the relation between these two values of air and is called the air excess ratio. During a transient event this air excess ratio will change. This might affect the combustion efficiency. According to Rakopoulos and Giakoumis [2009] this effect is most pronounced for turbocharged engines. During a load pick up more fuel is injected in a matter of seconds after the increased load demand is detected by the governor. From the moment that more fuel is injected it takes some time (*can be up to 25 seconds [Rakopoulos and Giakoumis, 2009]*) before the turbo provides the necessary amount of combustion air. During that period the air excess ratio is lower than was intended during the design of the engine. If this air excess ratio drops below the smoke limit there is not enough air and therefore oxygen to combust all the injected fuel. This results in actual smoke coming out of the exhaust. Interesting to see is that during low load operation the diesel engines of the Vox Maxima work as naturally aspirating engines [MAN Diesel SE, 2007]. Hence reducing the effects of turbo lag during transients will not be as present. From figure C.1 in appendix C it can be seen that at a LF of 90% MCR the waste gate opens. This means that the turbocharger provides more combustion air than the cylinder can cope with (*due to pressure constraints*). Since the turbo already produces more air than can be taken up the effect of turbo lag is reduced to zero. To summarize, the combustion efficiency can be worse during a transient event due to turbo lag. If the air excess ratio does not drop below the smoke limit the combustion efficiency will not be substantially affected.

3. η_{hl} or the heat loss efficiency provides a measure to asses the amount of heat that is transferred to the boundaries of the combustion process. After the fuel is ignited heat is released from the fuel. Not all this heat can be converted into work. A certain amount of heat is transferred to the cylinder walls, the piston crown and the cylinder head. This heat transfer is necessary to prevent the engine from melting. Nevertheless it reduces the amount of heat available to convert in actual work. According to Rakopoulos and Giakoumis [2009] the variation of the cylinder wall temperature during a transient event does not affect the performance of the engine. It is also stated that the initial wall temperature (*at the beginning of the event*) has an effect on the response of the engine. In the authors opinion the initial wall temperature can be seen as a steady state value and is therefore not directly related to transients.

4. Finally the thermodynamic efficiency of the engine has to be discussed. η_{td} or thermodynamic efficiency expresses the ratio between the heat available to be converted to mechanical work and the actual mechanical work that is generated. Not all processes in the diesel engine contribute to the generation of mechanical work, think of the scavenge stroke and for example the heat lost in the exhaust gasses. This efficiency is in fact a theoretical efficiency and is based on first principle laws of thermodynamics. The thermodynamic efficiency is not related to transients in the operation. In fact the thermodynamic efficiency should not even be a function of steady state LF.

It seems that the combustion efficiency is the only efficiency that can be affected during a transient event. In the enumeration from the individual efficiencies it is stated that the combustion efficiency is mostly related to the availability of fresh air. To develop the background on the fresh combustion air even further an analysis was done to evaluate the amount of fresh air available in the cylinder. The availability of fresh air in the cylinder can be related to the minimum amount of air that is needed for complete combustion of the injected fuel. This relation is also known as the air excess ratio λ. For the diesel engines of the Vox Maxima (*introduced in table 4.5*) the air excess ratio was calculated for different load factors. The result of this calculation is shown in figure 4.9. For a complete explanation of the air excess ratio analysis refer to appendix B. From figure 4.9 it can be seen that for a LF of 22.8% and higher their is enough air present in the cylinder to satisfy the conditions for complete combustion. Note that the lowest LF in the measurements was 30%. The 22.8% presented here is based on the fitted formula. The engine might have a form of mechanical air supply in the low load area. More interesting to see is that the air excess ratio exceeds a factor two above 60% MCR. This means that at the beginning of a transient, i.e. load pick up the amount of fuel injected may double before dropping below the minimal air to fuel ratio. This taken into account it can be assumed that during a transient event the combustion efficiency η_{comb} will not change significantly.

The preliminary conclusion should be somewhat rephrased. From initial analysis is seemed that transient events do not affect the specific fuel oil consumption of a diesel engine. This result did not coincide with general feeling that was expressed in the literature on this topic. Moreover the result falsified the hypothesis that SFOC would increase during transient events. In this chapter it was mentioned a couple of times that the engines that were investigated are in fact used as stationary engines running on constant Revolutions Per Minute (RPM). This reduced the effect of inertia on the mechanical efficiency of the engine during a transient. Next to that it turned out that the air excess ratio is in most cases high enough to accommodate a load pick up without compromising on combustion efficiency. To summarize, no obvious causes are found for a reduction of the engines efficiency during a transient. Therefore the results as presented in figure 4.10 to 4.13 will be adopted for the further development of the hybrid cutter model.

The conclusion with respect to specific fuel consumption of a diesel engine in transients is as follows; *For turbocharged four stroke diesel engines working in generator mode (constant RPM) with a sufficient high air excess ratio to accommodate complete combustion the specific fuel oil consumption will not increase as result of transients in power demand*

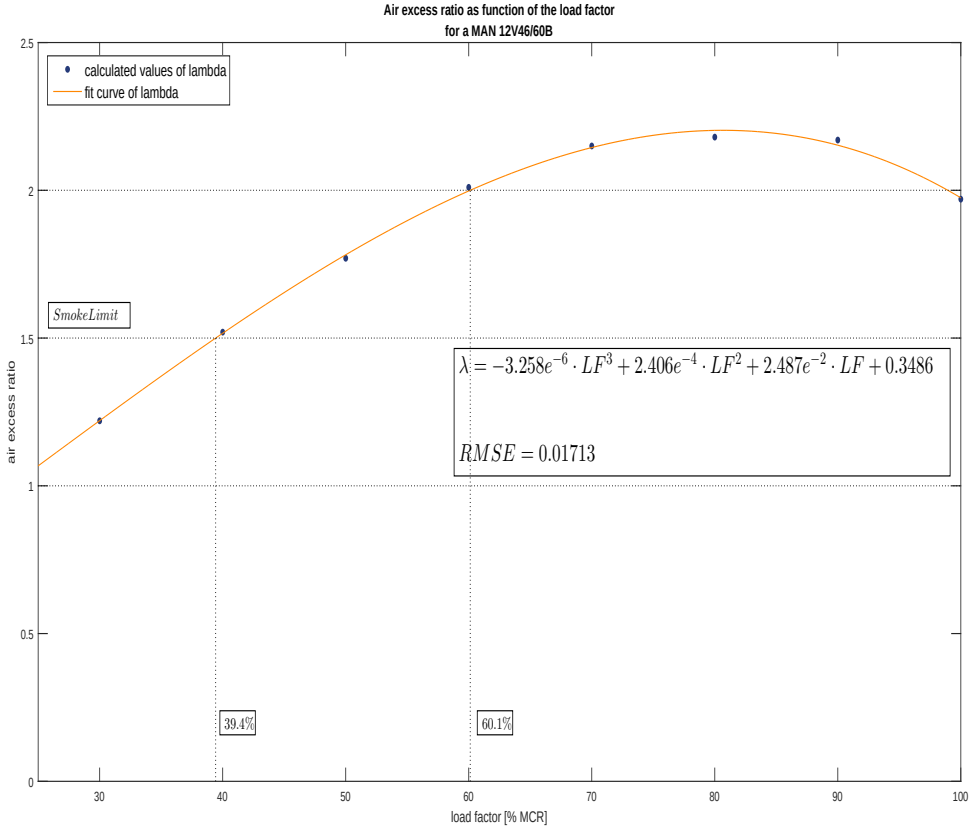

Figure 4.9: The air excess ratio as function of the load factor

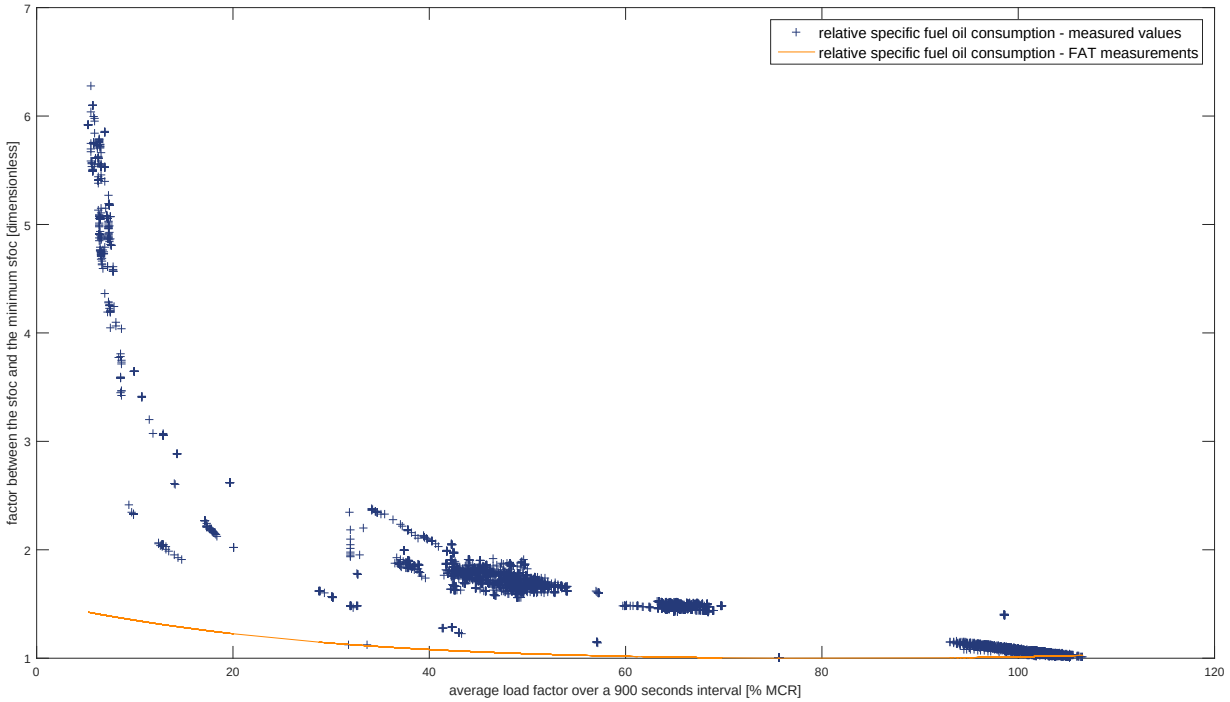

Figure 4.10: Relative SFOC from measurements and FAT - PS engine Vox Maxima

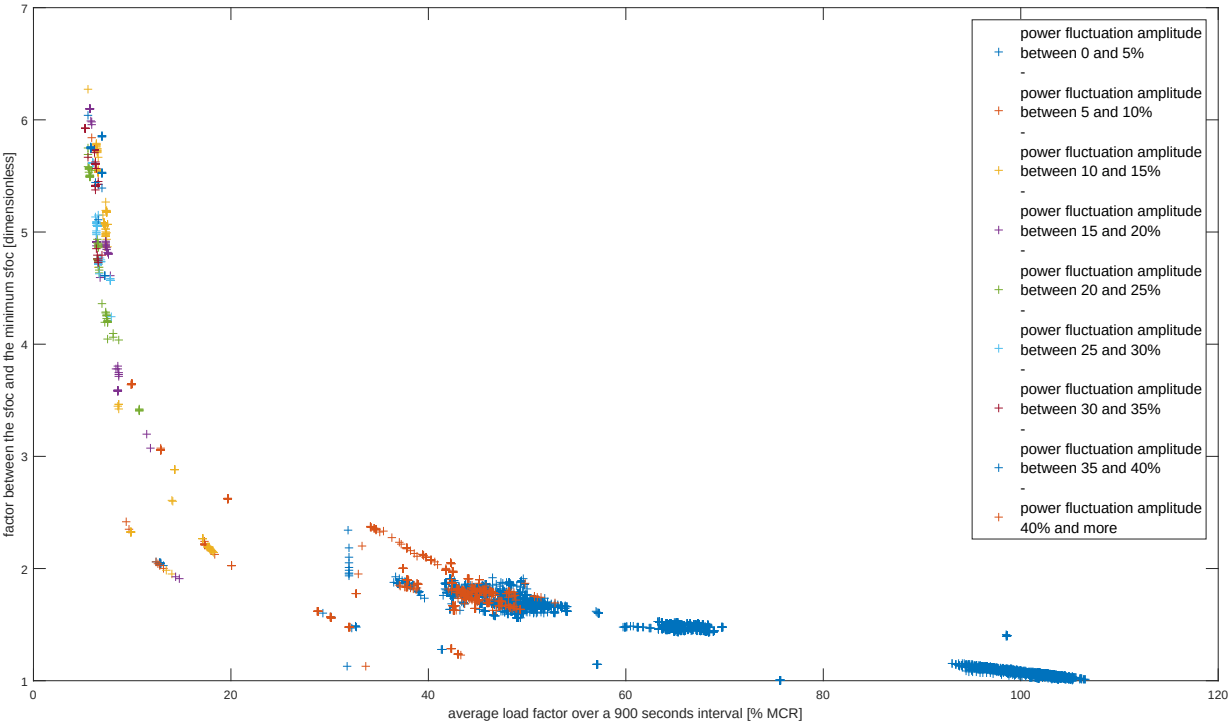

Figure 4.11: Relative SFOC from measurements sort by transients - PS engine Vox Maxima

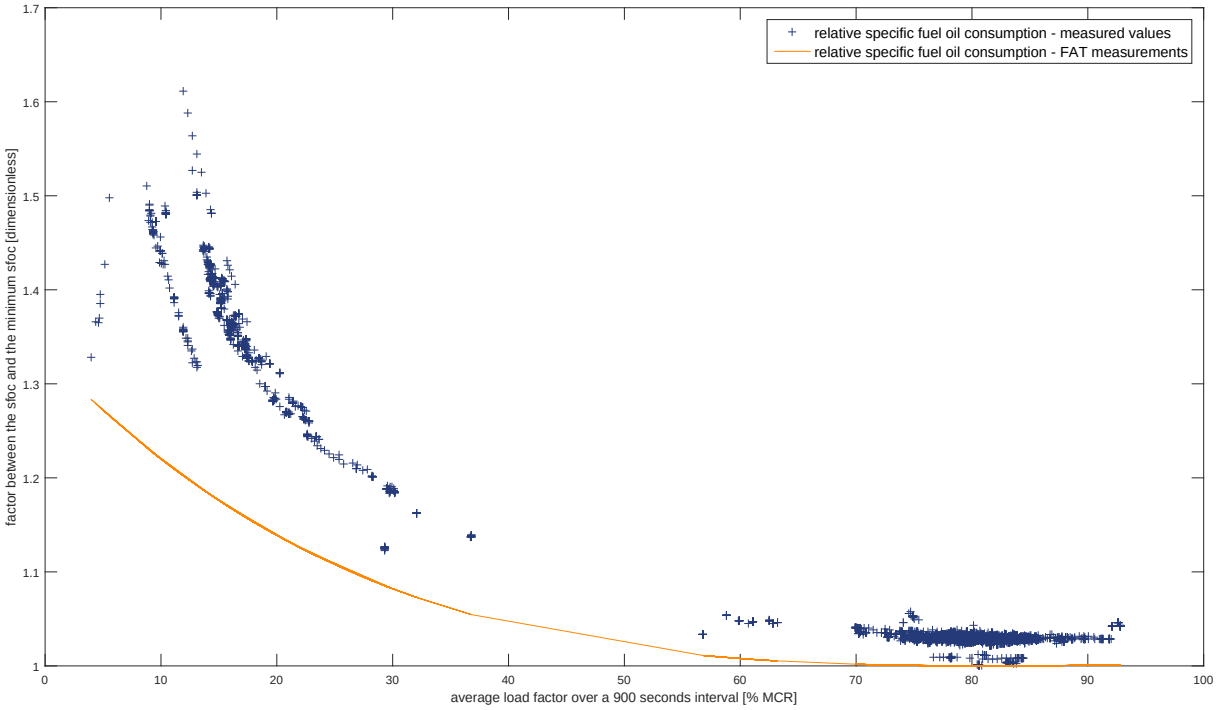

Figure 4.12: Relative SFOC from measurements and FAT - PS engine HAM318

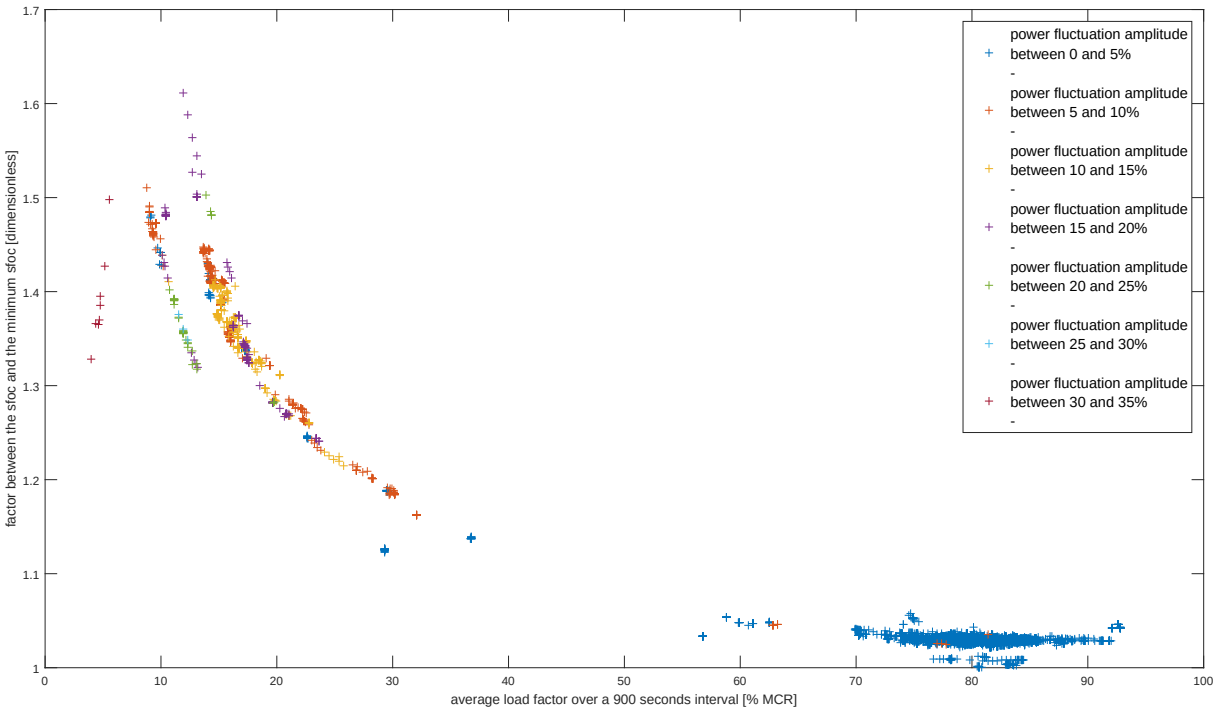

Figure 4.13: Relative SFOC from measurements sort by transients - PS engine HAM318

4.3. Battery

In this section the development of the battery model will de described. The decision is made to work with modern Lithium Ion chemistry electrical batteries. As presented in chapter 3 the Lithium Ion chemistry battery is the chemistry of choice for most hybrid applications in the maritime sector. The specific battery that will be modelled is based on the *XALT 75 Ah HP Superior Lithim Ion Cell* from Xalt Energy as this company is the preferred supplier for Corvus Energy batteries and Spear Power Systems [XALT Energy, 2015]. The performance data of the *XALT 75 Ah HP Superior Lithim Ion Cell* almost equal as the performance of the cells cells from Valence and Super-B (*on low charge and discharge rates*) Super B b.v. [2016]; Valence [2016]. This finding is based on provided performance graphs from different suppliers. Valence and Super-B do not supply information about the behaviour of their batteries at charge and discharge rates higher than two times the nominal rate.

As a start the figures containing discharge rats,charge rates and temperature dependencies of the Xalt 75 Ah cells are converted to data series that can be used for computation in Matlab. The result of this data conversion is presented in appendix E. This data will be analysed in order to create a model in Simulink that represents the behaviour of these specific Lithium Ion (Li-Ion) cells.

After the data extraction from the Xalt specification sheet a conversion is made on the charge data in order to express the charge characteristics in terms of cell voltage as a function of State of Charge (SOC) and charge current. Initially the data is presented as a current and voltage value as function of time as can be seen in figure E.1 in appendix E. The current and the voltage data have been interpolated to a common time vector. This ensures that a correct relation between voltage and current is found. The current data is integrated in time to find the capacity of the battery in ampère hour $[Ah]$. The battery cell under consideration has a nominal capacity of 75 Ah. By dividing the value of the current integral by the nominal capacity a SOC percentage is found. Figure E.2 in appendix E presents the results of this data conversion.

Decisions should be made on the actual modelling of the battery cell. Several types of modelling approaches can be used to create a battery model. Chemical models are available to predict terminal voltage as function of SOC, discharge current and temperature. These models are computational very intensive. Besides the downside that simulation will take a lot of time a real in depth knowledge of the chemical processes within the battery cell is necessary to work with these models [Huria et al., 2012]. Another option to model the behaviour of Li-Ion batteries is to use equivalent circuit models. In this model the behaviour of the battery is simulated using electrical components as resistors and capacitors as is presented in figure 4.14. The RC branch in this model accounts for the dynamic behaviour of the battery. The single resistor R_0 simulates the voltage drop caused by the internal resistance of the battery cell. According to Huria et al. [2012] this type of model can be used for all kinds of battery chemistries. To evaluate the values of the parameters in this model one could create multi dimensional lookup tables in Simulink, in which the values of E_m, R_0, R_1 and C_1 can be found for a certain SOC, discharge current and temperature. These lookup tables can be populated using the parameter estimation toolbox in Matlab Simulink [Jackey, 2012]. The only downside to this approach is that one should have detailed measurements of a certain battery type in order to use the parameter estimation toolbox. Unfortunately no battery supplier has been willing to share detailed test information. For this reason this type of modelling can not be used in this thesis.

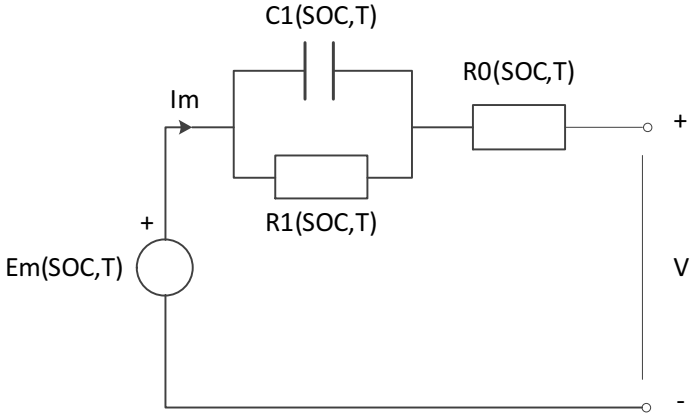

Figure 4.14: Single equivalent circuit block model

Besides the equivalent circuit model approach as was introduced by Huria et al. [2012] the Mathworks provides a generic battery model in its Simscape environment within the Simulink simulation environment. It has been investigated if this model could be used for this thesis. Following the general approach as is described in the *Help* file from this generic battery model the different system parameters are constructed [The Mathworks, 2008]. The parameters that have to be entered into the battery model block are presented in table 4.7. A short summary of the working principle of this battery model will be given before the initial test results will be discussed.

The generic battery model in Matlab is based on the equivalent circuit theory as described earlier. The equivalent circuit that is used in this model is presented in figure 4.15. Four different battery chemistries can be implemented in the generic battery model from Matlab. One can choose between Lead-Acid, Lithium-Ion, Nickel-Cadmium and Nickel-Metal-hydride chemistries. For the Li-Ion batteries the open circuit voltage from the battery as function from current, SOC and temperature is described in equation 4.19 and 4.20 for discharge cycles and charge cycles respectively. In these equations multiple temperature dependent parameters are introduced. These parameters are presented in equation 4.21, 4.22, 4.23 and 4.24. The different variables are explained in 4.25.

$$\begin{aligned} f_1(it, i^*, i, T, T_a) &= E_0(T) - K(T) \cdot \frac{Q(T_a)}{Q(T_a) - it} \cdot (i^* + it) + A \cdot \exp(-B \cdot it) - C \cdot it \\ V_{batt}(T) &= f_1(it, i^*, i, T, T_a) - R(T) \cdot i \end{aligned} \tag{4.19}$$

$$\begin{aligned} f_2(it, i^*, i, T, T_a) &= E_0(T) - K(T) \cdot \frac{Q(T_a)}{it + 0.1 \cdot Q(T_a)} \cdot i^* - K(T) \cdot \frac{Q(T_a)}{Q(T_a) - it} \cdot it + A \cdot \exp(-B \cdot it) - C \cdot it \\ V_{batt}(T) &= f_2(it, i^*, i, T, T_a) - R(T) \cdot i \end{aligned} \tag{4.20}$$

$$E_0(T) = E_0|_{T_{ref}} + \frac{\partial E}{\partial T} \cdot (T - T_{ref}) \tag{4.21}$$

$$K(T) = K|_{T_{ref}} \cdot \exp\left(\alpha\left(\frac{1}{T} - \frac{1}{T_{ref}}\right)\right) \tag{4.22}$$

$$Q(T_a) = Q|_{T_a} + \frac{\Delta Q}{\Delta T} \cdot (T_a - T_{ref}) \tag{4.23}$$

$$R(T) = R|_{T_{ref}} \cdot \exp\left(\beta\left(\frac{1}{T} - \frac{1}{T_{ref}}\right)\right) \tag{4.24}$$

with:

E_0	$Constant\ open\ circuit\ voltage$	$[V]$
E	$Open\ circuit\ voltage$	$[V]$
K	$Polarization\ constant$	$[\frac{1}{Ah}]$
Q	$Maximum\ battery\ capacity$	$[Ah]$
i^*	$Low\ frequency\ current\ dynamics$	$[A]$
it	$Extracted\ capacity$	$[Ah]$
i	$Battery\ current$	$[A]$
A	$Exponential\ voltage$	$[V]$
B	$Exponential\ capacity$	$[\frac{1}{Ah}]$
C	$Nominal\ discharge\ curve\ slope$	$[\frac{V}{Ah}]$
T_{ref}	$Nominal\ ambient\ temperature$	$[K]$
T_a	$Ambient\ temperature$	$[K]$
T	$Cell\ temperature$	$[K]$
α	$Arrhenius\ rate\ constant\ for\ the\ polarization\ resistance$	
β	$Arrhenius\ rate\ constant\ for\ the\ internal\ resistance$	

(4.25)

Some tests have been done with this model in order to check the validity of the model. A simple model was constructed where constant discharge curves could be entered. In that way the relation between voltage and SOC at a certain discharge current could be evaluated. By plotting the values of the actual response and the simulated values in the same figure one can visually check if the model represents reality. The result of this is presented in a simplified form in figure 4.17.

Table 4.7: Matlab generic battery model parameters

Parameter	Value	unit
Nominal voltage	3.7	V
Rated voltage	75	Ah
Initial State-of-charge	100	%
Battery response time	30	s
Maximum capacity	75	Ah
Fully charged voltage	4.2	V
Nominal discharge current	37.5	A
Internal resistance	0.00071	Ohm
Capacity at nominal voltage	70	Ah
Exponential zone [Voltage, Capacity]	[3.96, 10.7]	$[V, Ah]$
Initial cell temperature	23	C
nominal ambient temperature T1	23	C
Second ambient temperature T2	60	C
Maximum capacity *at T2*	79.5	Ah
Initial discharge voltage *at T2*	4.2	V
Voltage at 90 % maximum capacity *at T2*	3.52	V
Exponential zone [Voltage, Capacity] *at T2*	[3.96, 15]	$[V, Ah]$
Thermal resistance, cell to ambient	0.6	C/W
Thermal time constant, cell to ambient	1000	s

It turns out that the modelled behaviour of the battery does not represents the actual behaviour of the battery cell under consideration. The assumptions made in the model on the exponential part of the discharge curve are not that far of, nevertheless the transfer function does not result in good results during the nominal part of the discharge curve. Besides the fact that the model is not working properly in a constant current test there are more arguments to reject this generic Matlab model. The model is based on the assumption that the charge curve and the discharge curve of the battery follow the same pattern. The general shape of the charge and discharge curve is similar as can be seen from figure E.2 and figure E.3 in appendix E. Note that the values at certain points in the figure are not the same. This is caused by the fact that the battery has a certain efficiency. Some of the energy that enters the battery will be converted in heat and this heat can be seen as a loss. In other words, not all the energy that enters the battery can be retrieved from the battery. This results in an efficiency lower than one. It is known that the efficiency of a battery is depending from the charge and discharge current as well as the temperature. The way the efficiency of the battery is related to the charge and discharge current is presented in figure 4.16. This analysis was done by integrating the voltage over the capacity (*in ampère hour*) for different charge and discharge rates. The result of this integration is an amount of energy stored in the battery during a charge cycle and an amount of energy drawn from the battery during a discharge cycle. The ratio between energy $\frac{energy\ in}{energy\ out}$ gives a measure for efficiency. A curve fit was done on the surface that is created in 4.16. This curve fit results in equation 4.26 which can be used to predict the efficiency of a battery. It turns out that the efficiency may drop to 0.7 or 70% in specific cases. Therefore it is important to simulate charge and discharge cycles separately. The last comment on the generic Matlab battery model is based on the simulation of different cell chemistries. During the constant discharge current test the chemistry settings were changed. Four tests were executed, one for every chemistry that can be modelled. It turned out that the response of the model was the same for the four different chemistries. Which actually means that a Lead-Acid cell would perform just as good as a Li-Ion cell. It should be clear that this is not feasible. In order to model the battery in a more realistic way than the generic Matlab model a custom made model is suggested.

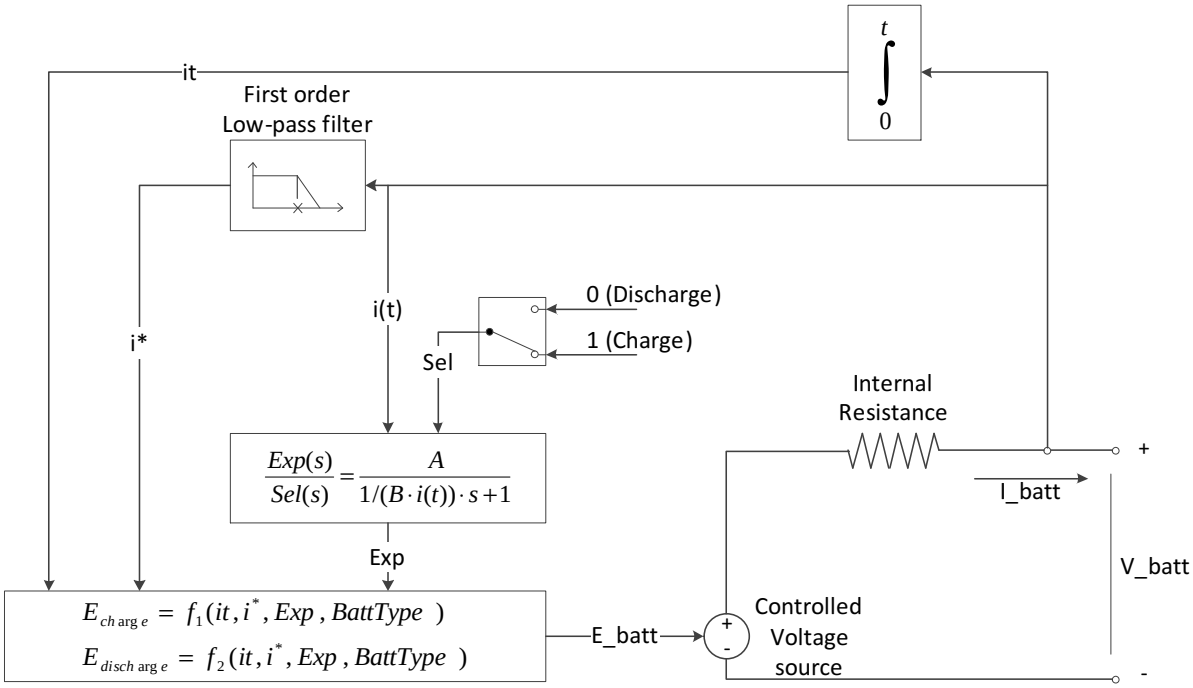

Figure 4.15: Generic Matlab battery model equivalent circuit

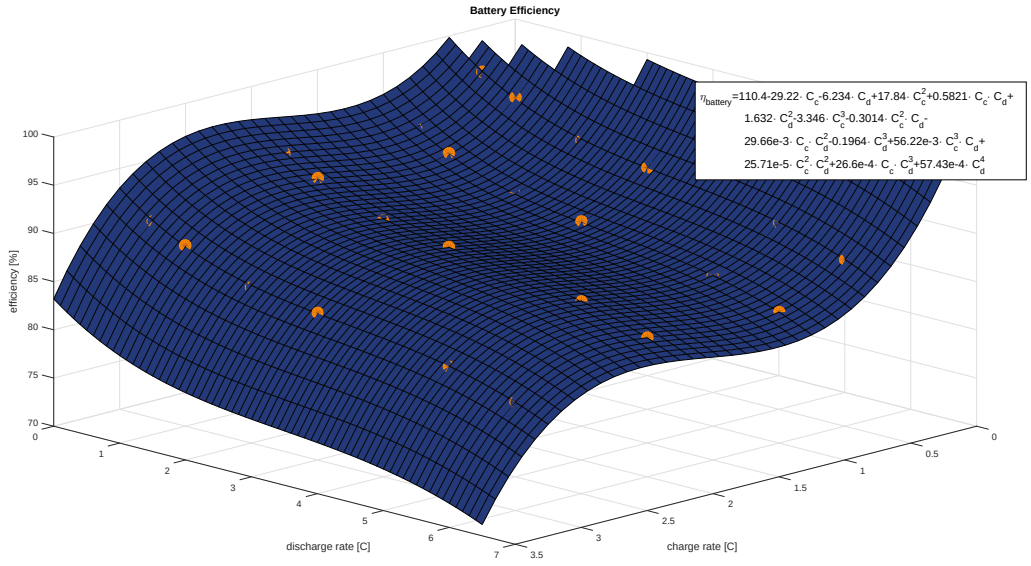

Figure 4.16: Battery efficiency as function from charge and discharge rates

$$\begin{aligned}\eta_{battery} =& 110.4 - 29.22 \cdot C_c - 6.234 \cdot C_d + 17.84 \cdot C_c^2 + 0.5821 \cdot C_c \cdot C_d + \\ & 1.632 \cdot C_d^2 - 3.346 \cdot C_c^3 - 0.3014 \cdot C_c^2 \cdot C_d - \\ & 29.66e-3 \cdot C_c \cdot C_d^2 - 0.1964 \cdot C_d^3 + 56.22e-3 \cdot C_c^3 \cdot C_d + \\ & 25.71e-5 \cdot C_c^2 \cdot C_d^2 + 26.6e-4 \cdot C_c \cdot C_d^3 + 57.43e-4 \cdot C_d^4\end{aligned} \tag{4.26}$$

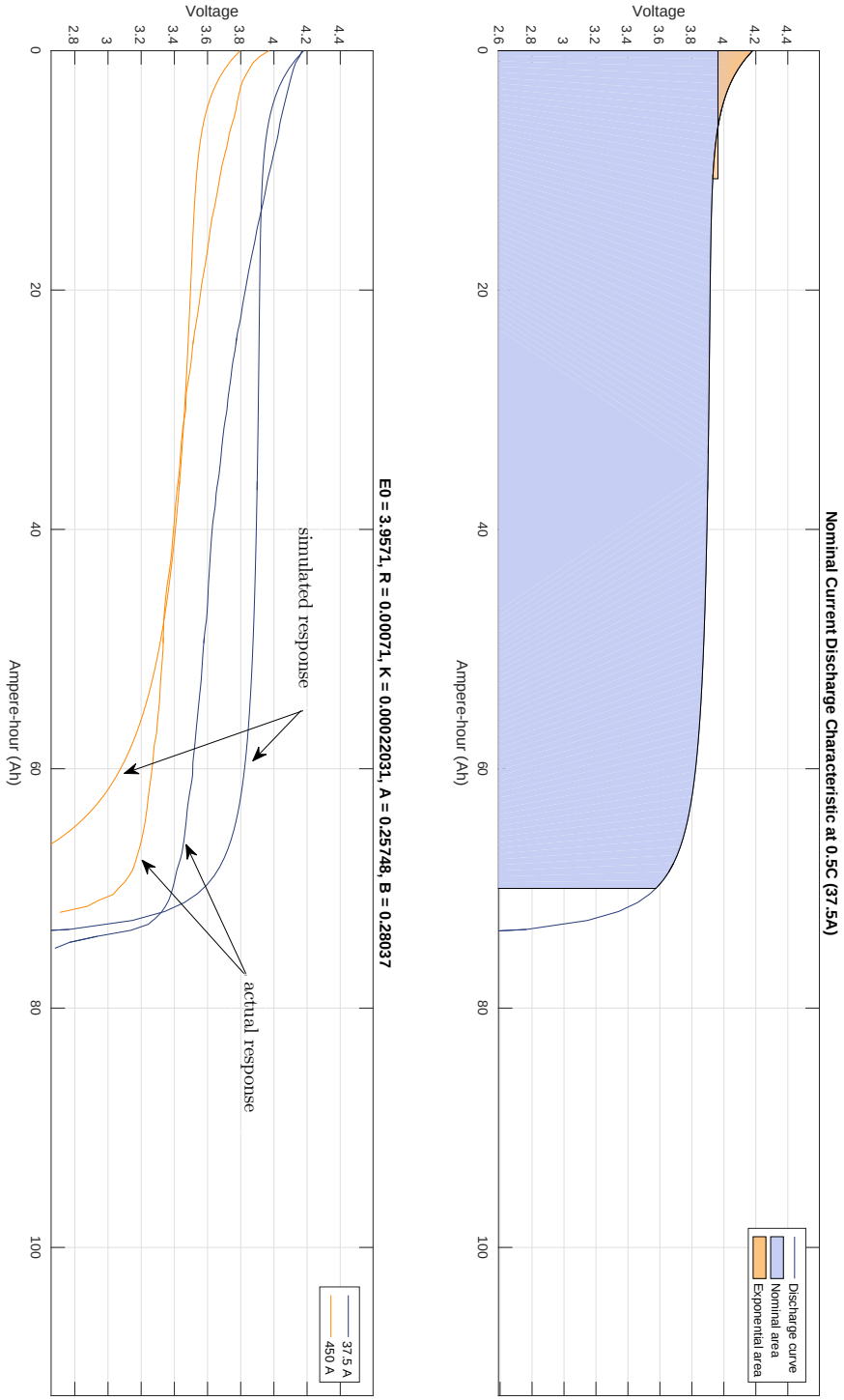

Figure 4.17: Response of the generic Matlab battery model compared with the actual battery response

The custom model that was created in Simulink is based on a combination of the models that were described previously. It is decided to adopt the multi dimensional lookup table approach as has been introduced by Jackey [2012]. Furthermore the difference between charge and discharge characteristics is taken into account as well. This is comparable with the chemical models available for battery modelling. Temperature dependencies will be included in the model as well.

The advantage of this model is that it does not require large amounts of computational effort. Nevertheless all important battery characteristics will be present in the model. For this thesis one of the most important factors of this model is the fact that a certain efficiency between charge and discharge is included. It is shown in figure 4.16 that the efficiency from the battery is far from constant. The importance of taking efficiency into account is also stressed by Kessels [2007]. Kessels [2007] introduces the suggestion to use a weight factor λ to evaluate the fictional fuel consumption of the battery pack. The weight factor λ makes it possible to relate the SOC to a certain (fictional) cost. The weight factor λ is determined with a Proportional Integrator (PI) controller. In Grimmelius et al. [2011] this method was also adopted to evaluate the SOC. The weight factor is a rough estimation for the efficiency of the battery.

The custom battery model will be discussed in the order of the layers the model is build up from. The model mask is presented on page 127 in appendix F. The input and output signals of the model will be discussed separately but an overview is given in table 4.8

Firstly the input to the model will be discussed. It can be seen that the input to the model is a power signal and certain constants. The power signal is determined by other parts of the cutter model and represents the resultant value between generated power by the diesel generators and the electrical power demand from the users. A positive value of this signal represents a power shortage in the system, so a positive power demand from the battery. A negative value means that there is a surplus of energy in the systems so the battery has to store this energy. The constants can be set by the user. The number of battery cells in series connection determines the nominal and maximal voltage of the battery system. The number of parallel connections between the series strings determine the nominal capacity of the batteries in Ah. Furthermore the charge cut-off and discharge cut-off can be set in the constants window. These two values are set as a percentage SOC. These two constants can be arbitrarily set but will affect cycle life of the batteries.

The model develops nine different output signals of which five are time varying signals and four are constants. The five time varying signals are SOC, terminal voltage, current, actual power and the demanded power delivery from or storage in the battery. The constants are nominal capacity in $[kWh]$, nominal capacity in $[Ah]$, maximum bus voltage and nominal bus voltage. The output constants can be used to dimension the power electronics needed to convert the battery energy to usable AC frequency and voltage.

The second layer of the battery model provides an insight in the interconnection between the different subsystems in the model. The actual power that is deliver from or stored in the battery is the product from the terminal voltage and the current through the battery pack. Due to the fact that the current changes sign when switching from charging to discharging the sign of the power changes in a similar way. Note that power drawn from the battery has a positive sign whereas power delivered to the battery has a negative sign.

Underneath the second layer of the model the individual subsystems can be found. The first subsystems that will be discussed are the charge and discharge subsystems. The discharge model is presented on page 129 in appendix F. The discharge model is build around a multidimensional lookup table which represents the terminal voltage as function of three different parameters. The lookup table is in fact a $151x6x6$ matrix. In the first dimension the terminal voltage is given for different values of SOC at a constant discharge current. The second dimension of this matrix represents the terminal voltage for different currents at a constant SOC. The third dimension enables a temperature dependency. A generic form of this lookup table is presented in figure 4.18. The three dimensions of the lookup table represent the input signals that have to be entered into this Simulink block.

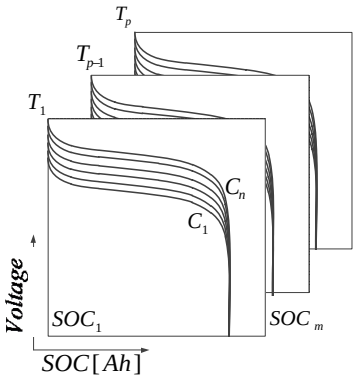

Figure 4.18: Multi dimensional lookup table example

SOC is entered in the lookup table as the capacity at time t in Ah. This enables SOC determination based on a simple integral of the current. The value of this integral is divided by 3600 in order to convert the value from $A \cdot second$ to Ah. The current is determined by dividing the demanded power by the battery terminal voltage. The integral is reset when the power switches sign, so when the cycle is changed from charge to discharge. Several initial conditions have been added to the model. This prevents the simulation to hold due to algebraic loops. It is assumed that the battery cycle will always start fully charged, so with a SOC of 100%. Next to that it is assumed that a charge cycle will always be followed by a discharge cycle immediately. Therefore the initial condition of the SOC integral is always equal to the final SOC of the charge cycle. In order to prevent misinterpretation of the SOC value that is transported via the ”goto” port a switch is added. This switch prevents passing through the ”SOC_discharge” value during a charge cycle. The charge subsystem works in a similar way. The systems are different in two ways. Naturally the lookup tables differ as explained earlier. Next to that it can be seen that the charge subsystem has no temperature dependency. This information is not available and is therefore not included in this model.

Table 4.8: Battery model input and output

signal	unit
Time varying input	
demanded power battery out(+)/in(-)	kW
Constant input	
nr. of cells parallel	#
nr. of cells series	#
Charge cut-off	$\%SOC$
Discharge cut-off	$\%SOC$
Time varying output	
SOC	%
battery terminal voltage	V
current battery out (+)/in(-)	A
actual power battery out(+)/in(-)	kW
demanded power battery out(+)/in(-)	kW
Constant output	
nominal storage capacity	kWh
nominal capacity	Ah
maximum bus voltage	V
nominal bus voltage	V

Note that in the previous paragraphs a temperature dependency is introduced for the discharge model. The temperature is set to a constant value of 23 degrees Celsius. At this temperature the battery performs the best in terms of capacity and cycle life according to XALT Energy [2015]. If one would like to include a varying temperature value to the model this is possible due to the temperature port in the discharge lookup table. To determine the temperature in the battery room it is suggested to use the efficiency value to determine the added heat in the battery room. The loss that is introduced between the charge energy and the discharge energy has to be converted to heat. The loss is created by the internal resistance of the battery and the only product of this resistance is heat. In order to simulate the heat flow as function of time one should acquire more information about the thermal transfer coefficients of the battery casing and the heat transfer between the cells. This information is not available therefore it is decided to work with a constant temperature input.

The final subsystem that will be discussed in this section is the charge/discharge cut-off model. The subsystem is presented in page 131 in appendix F. This model serves as a protection against overloading the battery and draining the battery capacity completely. This measure of protection serves two purposes. The first goal of this subsystem is to make sure that the overall model represents reality. In real life it is not possible to charge the battery more than 100% SOC. Over charging will cause thermal runaway of the battery cells which might lead to fire or explosions. Draining the battery completely will dramatically shorten the lifetime of the battery and is therefore undesirable. The second purpose of this system is to make the model robust. If the model was able to completely discharge the battery the voltage will drop to zero. This will introduce mathematical errors. By keeping the SOC between certain limits it enables us to keep the simulation running for the full time window without introducing algebraic loops which would cause the simulation to fail. The input to the charge/discharge cut-off model is the actual state of charge at $(t-1)$ and the maximum and minimum SOC set-points. The decision to compare the set-points with the state of charge at $(t-1)$ is made to enable the model to work with discontinuities in the SOC signal.

The testing and verification of this model will be discussed in section 5.

The model that has been constructed so far gives insight in the relation between battery terminal voltage, current and state of charge or capacity of the battery. These three values are necessary to simulate the power distribution between the generators, the energy storage device and the end users. This is in turn important to estimate the fuel saving potential of the hybrid system. Nevertheless one important parameter is still missing in order to give final conclusions about the economical feasibility of the hybrid system. To estimate the economical feasibility it is important to know how long the battery pack will last. The lifetime of the battery pack is expressed in Cycle Life (CL). CL gives a number of cycles a battery can undergo before the capacity of the battery is reduced to 80% of its nominal capacity. The cycle life of chemical battery is most of the times expressed as a number of cycles at a certain Depth of Discharge (DOD). An example of such a CL vs. DOD relation is given in figure 4.19. One can imagine that the cycle life will be supplier dependent. Since the battery behaviour was modelled using the *XALT 75 Ah HP Superior Lithim Ion Cell* it would be logical to use the cycle life information for this cell. Unfortunately this information is not available. The reason for this is found in the fact that the Xalt battery cells are used by various battery manufacturers. These battery manufacturers combine the individual cells to create complete batteries. The way these cells are com-

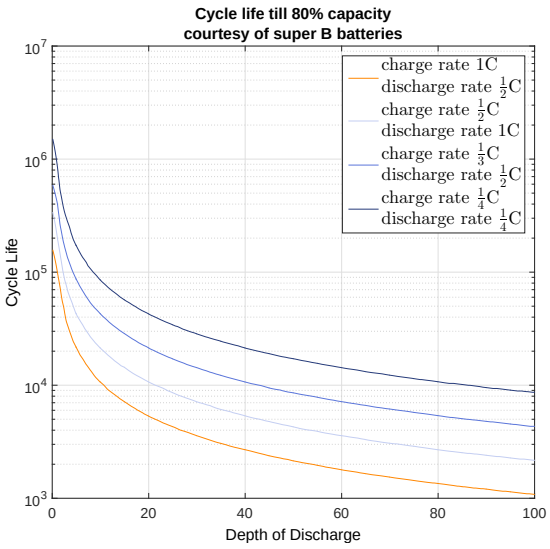

Figure 4.19: Cycle life as function of DOD, charge rates and discharge rates [Super B b.v., 2016]

bined determines the usage of the battery. The battery cells will be selected on internal resistance and impedance. Certain combinations of cells will result in batteries that have a long life expectancy in long cycles at low current rates and others will perform better when used in short cycles at high current rates. For this reason it is assumed that the CL information from Super B b.v. as presented in figure 4.19 can be used in this thesis. Figure 4.19 gives information about cycle life based on different DOD and different charge and discharge rates. However this information is not yet usable for simulation purposes.

In order to make the Super B information usable for simulation purposes as intended in this thesis several steps have to be taken. In Lyu [2016] the approach as presented in Muenzel et al. [2015] is used. The approach suggested in Muenzel et al. [2015] seems very useful for the CL determination as intended for the hybrid cutter. Nevertheless the algorithm as used in Lyu [2016] will be altered to produce a better result. First the general approach as suggested by Muenzel et al. [2015] will be explained. Since most of the time battery manufacturers only provide very limited ageing information it is suggested to extrapolate a set point CL prediction to a multi variable prediction method. In this approach equation 4.27 plays a central role. This approach was again adopted by the authors of Muenzel et al. [2015] from Omar et al. [2014]. In equation 4.27 CL stands for the predicted cycle life to a certain point of degradation. The variable x_1 to x_k represent the variables which can affect the cycle life of the battery. One can think of DOD, charge current, discharge current etc…The subscript nom presents the nominal values of the variables which affect the cycle life. Equation 4.27 can be rewritten to 4.28. Now it becomes clear that CL can be determined as a nominal CL multiplied with certain relative factors which will reflect the actual operation point of the battery.

$$\frac{CL(x_1, \dots, x_k)}{CL(x_{1,nom}, \dots, x_{k,nom})} = \frac{CL(x_1)}{CL(x_{1,nom})} \cdot \dots \cdot \frac{CL(x_k)}{CL(x_{k,nom})} \tag{4.27}$$

$$CL(x_1, \dots, x_k) = CL(x_{1,nom}, \dots, x_{k,nom}) \cdot \frac{CL(x_1)}{CL(x_{1,nom})} \cdot \dots \cdot \frac{CL(x_k)}{CL(x_{k,nom})} \tag{4.28}$$

The life expectancy of a Li-Ion battery is most dependent of the following parameters, temperature T, charging current I_{ch}, discharge current I_d and the maximum and minimum SOC boundaries. The maximum and minimum SOC boundaries can be presented using a average state of charge SOC_{av} and a corresponding depth of discharge DOD. These values can be determined quite easily as can be seen from equation 4.29 and 4.30. In equation 4.30 the subscripts max and min have been replaced by 1 and 2 to account for the difference between charge and discharge cycles. During discharge the sign of DOD will be positive whereas during charging the sign of DOD will be negative. A full cycle will consist of a charge part and a discharge part. Since it has been noted that the cycles encountered in the cutter model are most of the time not uniform (*meaning that the amount of energy charged is not equal to the amount of energy discharged*) the cycles have been evaluated as being a half cycle from a uniform charge-discharge cycle. Finally equation 4.31 presents that SOC_{av} and DOD can not be seen as independent variables.

$$SOC_{av} = \frac{SOC_{max} - SOC_{min}}{2} \tag{4.29}$$

$$DOD = SOC_1 - SOC_2 \tag{4.30}$$

$$SOC_{av} = \frac{|DOD|}{2} + SOC_1 \tag{4.31}$$

Equation 4.28 can now be extended to equation 4.32. In the following paragraph the equations for the individual normalised nCL will be introduced. The normalized CL factors for T, I_d and I_{ch} are derived using equation 4.33, 4.34 and 4.35 respectively. Equation 4.37 gives the normalized CL factor for the SOC_{av} and DOD dependency. In this equation the numerator is equal to equation 4.36 whereas the denominator is actually the same equation with the exception that SOC_{av} and DOD are replaced by there nominal counterparts. In the equations presented so far the following fit coefficients have been introduced, a,b,c,d,e,f,g,h,m,n,o,p,q,s,t,u and v. The authors of Muenzel et al. [2015] have adopted the values for these fit coefficients from Omar et al. [2014] and verified the coefficients with experiments as presented in their paper. In this research the same fit values have been adopted since no detailed cycle life test are available in order to conduct new fit attempts. The values from the fit coefficients are presented in table 4.9.

$$CL(T, I_d, I_{ch}, SOC_{av}, DOD) = CL_{nom} \cdot nCL(T) \cdot nCL(I_d) \cdot nCL(I_{ch}) \cdot nCL(SOC_{av}, DOD) \tag{4.32}$$

$$nCL(T) = \frac{a \cdot T^3 - b \cdot T^2 + c \cdot T + d}{a \cdot T_{nom}^3 - b \cdot T_{nom}^2 + c \cdot T_{nom} + d} \tag{4.33}$$

$$nCL(I_d) = \frac{e \cdot exp(f \cdot I_d) + g \cdot exp(h \cdot I_d)}{e \cdot exp(f \cdot I_{d,nom}) + g \cdot exp(h \cdot I_{d,nom})} \tag{4.34}$$

$$nCL(I_{ch}) = \frac{m \cdot exp(n \cdot I_{ch}) + o \cdot exp(p \cdot I_{ch})}{m \cdot exp(n \cdot I_{ch,nom}) + o \cdot exp(p \cdot I_{ch,nom})} \tag{4.35}$$

$$\begin{aligned} CL(SOC_{av}, DOD) = & q + \left(\frac{u}{2 \cdot v} \cdot (s + 100 \cdot u) - 200 \cdot t\right) \cdot \\ & DOD + s \cdot SOC_{av} + t \cdot DOD^2 + \\ & u \cdot DOD \cdot SOC_{av} + v \cdot SOC_{av}^2 \end{aligned} \tag{4.36}$$

$$nCL(SOC_{av}, DOD) = \frac{CL(SOC_{av}, DOD)}{nCL(SOC_{av,nom}, DOD_{nom})} \tag{4.37}$$

Table 4.9: Cycle life model fit coefficients

coefficient	value
a	0.0039
b	1.95
c	67.51
d	2070
e	4464
f	-0.1382
g	-1519
h	-0.4305
m	5963
n	-0.6531
o	321.4
p	0.03168
q	1471
s	214.3
t	0.6111
u	0.3369
v	-2.295

Equation 4.33 to 4.37 can be substituted in equation 4.32. If than the values from table 4.9 are also substituted in 4.37 a complete formula for the cycle life prediction is found. It is now possible to determine the effect of certain parameters on the cycle life of a battery. However one is still not able to determine the total life time of the battery due to the non-uniform cycling the battery encounters. Therefore the model as presented so far will be slightly extended to fulfil this purpose. As mentioned earlier the battery will encounter different charge and discharge rates within one cycle. This is not incorporated in the model. Nevertheless a solution for this problem can be found in the form of analysing *half* cycles, so differentiate between charging and discharging. During a charge cycle the normalized effect of the charge current is calculated according to equation 4.35. In the same time step the effect of the discharge current is zero, since there is no discharge current. Therefore the normalized effect of the discharge current is set to one. The calculation of the other factors is straight forward. After entering all the values in equation 4.32 the cycle life *for a full cycle* of the battery will be found. The number of cycles will result in a degradation of 20% of the battery capacity according to figure 4.19 [Super B b.v., 2016]. If this 20% is divided by the number of cycles calculated earlier one will find a relative degradation per full cycle. The last step in this calculation is to divide this relative degradation by two since it only addresses half a cycle. The same methodology can be adopted for the discharging part of the full cycle. This approach has been summarized in equation 4.38.

It should be noted that during this whole exercise the normalised effect of temperature on the cycle life of the battery is set to one as if it were that the battery is operating on its nominal temperature all the time. The reason for this is that it was decided to work with a constant temperature in an earlier stage of this research.

$$relative\ degradation_{charge} = \frac{20\%}{2 \cdot (CL_{nom} \cdot 1 \cdot nCL(I_d) \cdot 1 \cdot nCL(SOC_{av}, DOD))} \tag{4.38}$$

Since the relative degradation of the battery cell for one charge or discharge cycle (so effectively half a cycle) is known the final step is to sum all the individual amounts of degradation. In this way a total amount of degradation is found for a certain time period. This is presented in equation 4.39. To recapitulate the time frame under consideration was presented in section 2.2.3. This period of six days was found to be representative for a full year of operation. In this way the result of equation 4.39 can be scaled to find the total life expectancy of the battery to a certain extend of relative degradation of its initial capacity.

$$relative\ degradation_{total} = \sum_{cycle=1}^{cycle=n} relative\ degradation_{cycle\ 1:n} \tag{4.39}$$

4.4. Power management

So far the development of the fuel consumption model and the battery model has been discussed. Besides these two models this chapter has started with the power demand as a continuation on the working principle analysis in chapter 2. What is missing so far is a model that can act as an interface between the power demand signals, the fuel consumption model and the battery. A model that can interact and connect all these signals and different sub models is the power management system. In this section the power management system in general will be discussed as well as the power management system that is developed for this specific research.

As described in Odeim et al. [2014] the advantages of a hybrid system stand or fall with a proper power management system. In Odeim et al. [2014] conducted simulations and tests to develop an power management system for a fuel cell/battery hybrid vehicle.

This research is in that way comparable with the 'hybrid cutter development' research in that way that the research described in Odeim et al. [2014] tries to find a balance between the fuel cell and the battery usage. The battery is used to let the fuel cell perform on its optimum efficiency point. In a way that is the same goal as what is tried to achieve in the 'hybrid cutter development' research, the goal is to use the battery to let the diesel generators run at their respective optimal efficiency point.

In offshore applications power management has always been a hot topic since a proper power management system will make the difference between safe operation and the potential for blackouts. In the offshore sector a power blackout is critical with regards to safety. When a offshore supply vessel looses its dynamic positioning capabilities during a transfer to a drill rig this will instantly put the crew and the operation at risk. In dredging the negative effect of a blackout will not immediately affect the safety of crew, but it will have an effect on the production. A blackout during the cutter process can result in clogging of the discharge pipe with all negative consequences. For this reason there is some experience with power management in dredging as well. As stated before this type of power management focussed on prevention of blackouts and distributing power to the most critical production processes. This type of power management is operating at the demand side of the energy distribution system.

In this research the power management philosophy was shifted from the demand side to the supply side. It is key in the performance of the power generation system that the amount of power from the generators and the battery (or other energy source for that matter) are managed in such a way that not each element on its own performs at its best efficiency point but that an optimum is found in the total operation efficiency of the system as a whole.

Grimmelius et al. [2011] and Sorensen [2014] focus on control algorithms based on feedback control for the power systems. Both suggest that is would be much more efficient for the overall control loop to predict future events, this can either be done by using state estimation or by using feed-forward control. Sorensen [2014] develops several types of control algorithms for Dynamic Positioning (DP) systems of Platform Supply Vessel (PSV) in which state estimation is used. State estimation in case of DP systems is based on dynamic state space equations (similar to a mass spring damper system) to predict the position in the near future. Sorensen [2014] also suggest the use of wind feed forward to adjust for the quick changes in wind speed and direction.

It might be beneficial to incorporate a certain form of feed forward in the cutter model as well. The proposal is to search for time dependences between different power demand signals. In 2.2.2 the operating principle of the CSD is described. Section 2.2.2 explains how the movement of the vessel influences the pressure on the cutter head and therefore the power demand of the cutter motors. The movements of the vessel are induced by the side winches and the spud carrier. This taken into account there might be a way to relate the power going to the cutter motor to the side winch power and the hydraulic power to the spud carrier. In a similar way one can probably also find a dependency between the cutter power and the pump power albeit with some delay. This can be explained by the fact that if the cutter motor power increases the cutter will produce more dredge material. This will in turn result in a mixture with a higher density. A higher density in the pump will result in a higher power demand from the pump motor. Depending from the speed through the pump this increase in power demand will

propagate with a certain speed through all three dredge pumps.

The control system developed for the hybrid model discussed in this thesis will not look into feed-forward control strategies. The control system that will be discussed in this thesis will solely focus on obtaining the best efficiency set-point for the diesel engines. As discussed in the chapter 1 the goal of the hybrid system is to reduce fuel consumption and corresponding emissions as well as reducing running hours. This is also presented in figure 3.1 on page 26.

The main aspects governing the philosophy behind the power management system are the following;

1. Maintain a high average loading of the diesel generators. Preferable 80% MCR to achieve maximum efficiency.
    - Select the optimal number of diesel generators on-line based on power demand. Include auxiliary generators in this equation.
2. Reduce the running hours of the main generators.
    - Shut the main generators down as soon as it is possible.
    - Make more use of the auxiliary generators.
    - Try to extend the off-line period by using battery power.
3. Keep the battery within a specific bandwidth of SOC to ensure a certain lifetime of the battery.
    - Introduce a maximal charge and discharge power based on battery capacity in order to preserve life time of the battery.
4. Prevent starting and stopping of diesel generators for small periods of time since this is not realistic.
    - During normal operation the control signals for the diesel generators is based on a filtered version of the real power demand. This signals is less fluctuation than the actual power demand. Therefore the optimal configuration of diesel generators will change in the same rate as this signal. (*Note that this introduces a certain amount of peak shaving*)
    - The power management system can demand an artificial charge or discharge power to ensure that the SOC stays within its bandwidth. This might trigger the starting or stop procedure of a diesel generator. The generator that is stopped or started has to stay off-line or on-line for a predetermined amount of time. This ensures that a charge or discharge cycle always has a certain minimum length.

The PMS as developed for this thesis is presented in appendix G. The layers of this model will be discussed in chronological order. The first layer of the model as presented on page 133 displays the input and output signals of the PMS system. The input to the model is summarized in table 4.10. The system power demand that is used as input for the model is a filtered version of the original VODAS power demand signal. This results in a more constant signal which makes it possible to control the system in a better way. A certain amount of peak shaving is introduced by this decision. The state of charge of the battery is the next time dependent property. This signals is used to check if the SOC is within the set boundaries. The maximum charge and discharge power are user defined set-points. The values of these parameters are dependent from the chosen battery capacity. The charge power has to be limited in order to ensure a maximum charge rate of $\frac{1}{3}C$. The maximum charge rate is set to prevent excessive generation of heat and to extend the lifetime of the battery. The discharge power follows the same approach, however the discharge rate can be higher than the charge rate, $\frac{1}{2}C$. After the charge and discharge power set-points one will find the MCR values of the main generators and the auxiliary generators. These values are constant system properties. In this case the values found on the Athena and Artemis are entered in the PMS system. However if one would want to investigate the effect of different diesel power configurations these values can be changed. The different load factor set-points

are user defined set-points. It is known that a LF of 80% will result in the most efficient operation of the diesel engines, therefore this is the desired LF. The maximum and minimum load factor influence the power bandwidth of the individual diesel engines. When the power demand falls outside this bandwidth an extra generator will be started or a generator will be shut down. The minimal and maximal SOC values are again user defined. Increasing the SOC bandwidth will reduce running hours of the generators but at the same time this increases the DOD of the battery, influencing the life time of the battery. The last input to the model is the timer limit. When an charge or discharge cycle is demanded this timer value ensures that the charge or discharge cycle will long for a predetermined amount of time. The output of the system is in this layer presented as a set of displays. The interface of the power management system with the other models is the signal *Power from generators*. How these values are determined will be explained when the underlying layers are discussed.

Table 4.10: Input signals for power management system

signal	value	unity	sort
system power demand	0-24540	kW	time dependent signal
SOC	0-100	$\%\ capacity$	time dependent signal
maximum charge power	1500	kW	user defined set-point (*dependent from battery capacity*)
maximum discharge power	2500	kW	user defined set-point (*dependent from battery capacity*)
MCR main generator 1	7500	kW	system constant
MCR main generator 2	7500	kW	system constant
MCR main generator 3	7500	kW	system constant
MCR aux generator 1	1020	kW	system constant
MCR aux generator 2	1020	kW	system constant
desired load factor	80	$\%\ MCR$	user defined set-point
maximal load factor	90	$\%\ MCR$	user defined set-point
minimal load factor	70	$\%\ MCR$	user defined set-point
maximal SOC	90	$\%\ capacity$	user defined set-point
minimal SOC	20	$\%\ capacity$	user defined set-point
timer limit	3600	s	user defined set-point

The second layer of the model is build up from four different sections. This layer contains the actual calculations. An overview of the second layer in the PMS model is presented in appendix G on page 134. The optimisation process itself is conducted in the embedded Matlab function. The same input signals as discussed before are fed through to this function block. The output of the function is an option index, which represents a certain combination of diesel generators. For verification purposes also a best option index is presented. When the SOC is out of its bounds these two indexes should be different. The option index has no physical value in the Simulink model. Therefore it is entered into the *Convert Matlab signal back to Simulink signal using multiport switches* block. The content of this block will be discussed subsequently. Using the available MCR signal and the demanded LF signal one is able to calculate the actual power output of the generators. Besides the blocks just discussed one can notice two feedback signals entering the Matlab function. These to feedback signals keep track of the duration of a charge or discharge cycle.

The third and final layer of the power management model is the *Convert Matlab signal back to Simulink signal using multiport switches* block. The content of this block is presented in appendix G on page 135. The input to this sub model an option index which is determined by the embedded Matlab function. From this index the actual configuration of diesel engines can be determined. This results in a value for the available MCR. When the MCR from an engine is regarded as being available the seconds are integrated to determine the running hours of the individual engines.

As stated before a large part of the PMS system is constructed as a Matlab function embedded in the Simulink model. The general form of the script and assumptions made in the logic relations will be discussed to provide a better understanding of the decision process. In order to decide which configuration would be the best the script should first know which configurations are available. The possible configurations with their corresponding option indices are presented in table 4.11. These different configurations have their own value of available MCR. A matrix is constructed with in the first column the option index and in the second column the available MCR. The MCR value is simply the sum of the MCR of the individual diesel engines as can be seen from equation 4.40. Since the load factor is presented as a percentage of MCR this matrix can easily be converted to a matrix containing desired power per configuration, maximal power per configuration and minimum power per configuration. This is presented in equation 4.41, 4.42 and 4.43 respectively. The minimal and maximal power per configuration for the input parameters as presented in table 4.10 are visualised in figure 4.20.

Table 4.11: Different options used in the power management system

option index	configuration
1	$auxiliary\ generator\ 1$
2	$auxiliary\ generator\ 1+$ $auxiliary\ generator\ 2$
3	$main\ generator\ 1$
4	$main\ generator\ 1+$ $auxiliary\ generator\ 1$
5	$main\ generator\ 1+$ $auxiliary\ generator\ 1+$ $auxiliary\ generator\ 2$
6	$main\ generator\ 1+$ $main\ generator\ 2$
7	$main\ generator\ 1+$ $main\ generator\ 2+$ $auxiliary\ generator\ 1$
8	$main\ generator\ 1+$ $main\ generator\ 2+$ $auxiliary\ generator\ 1+$ $auxiliary\ generator\ 2$
9	$main\ generator\ 1+$ $main\ generator\ 2+$ $main\ generator\ 3$
10	$main\ generator\ 1+$ $main\ generator\ 2+$ $main\ generator\ 3+$ $auxiliary\ generator\ 1$
11	$main\ generator\ 1+$ $main\ generator\ 2+$ $main\ generator\ 3+$ $auxiliary\ generator\ 1+$ $auxiliary\ generator\ 2$

$$MCR_{configuration} = \begin{bmatrix} 1 & \sum_1^1 MCR \\ \dots & \\ n & \sum_1^5 MCR \end{bmatrix} \tag{4.40}$$

$$P_{desired} = \begin{bmatrix} 1 & MCR_{configuration^1} \cdot LF_{des} \\ \dots & \\ n & MCR_{configuration^n} \cdot LF_{des} \end{bmatrix} \tag{4.41}$$

$$P_{maximal} = \begin{bmatrix} 1 & & MCR_{configuration^1} \cdot LF_{max} \\ & \dots & \\ n & & MCR_{configuration^n} \cdot LF_{max} \end{bmatrix} \tag{4.42}$$

$$P_{minimal} = \begin{bmatrix} 1 & & MCR_{configuration^1} \cdot LF_{min} \\ & \dots & \\ n & & MCR_{configuration^n} \cdot LF_{min} \end{bmatrix} \tag{4.43}$$

The general approach is to find the *best* option to satisfy the power demand. To do so one has to find the minimum difference between the power demand and the values in the matrix $P_{desired}$. The index of this value can be used to determine the best option, since this was stored in the first column of this matrix. This is the first step in the decision hierarchy, the system will always try to satisfy the power demand in this way. The result from this is that the generators will run at 80% MCR for most of the time. The second step is to check if the SOC requirements are met. When the SOC value is lower than the minimum SOC set-point a charge cycle will be initiated. This can be achieved in different ways. The first one is to increase the load factor of the diesel engines that are currently on-line. If the power in $P_{maximal}$ for this current configuration is higher than the power demand plus the charge power the PMS will choose this option. If the maximal power of the current configuration is not sufficient to supply the necessary charge power the PMS will search for a new configuration. This will mean that more generators are put on-line. The same approach is followed for a discharge cycle. The PMS will first try to discharge the battery by lowering the load factor of the diesel engines before an attempt is done to take a generator off-line. When a charge or discharge cycle is initiated and there is a change in the option index value a trigger signal will be changed from 0 to 1. The trigger resets an integrator in the Simulink model which acts as timer. The integrator counts seconds from the beginning of the charge or discharge cycle. Until the integrators value has risen above the pre-set timer limit the power management system is not allowed to change the current configuration. So when an engine is started for a charge cycle it has to stay on-line for the time entered in the timer limit. The power management system is allowed to change the load factor of the engines that are on-line. This last condition is the third order in the control hierarchy. A schematic overview of the decision hierarchy is presented in figure 4.21. The code generated to perform these logic operations is presented in appendix G.

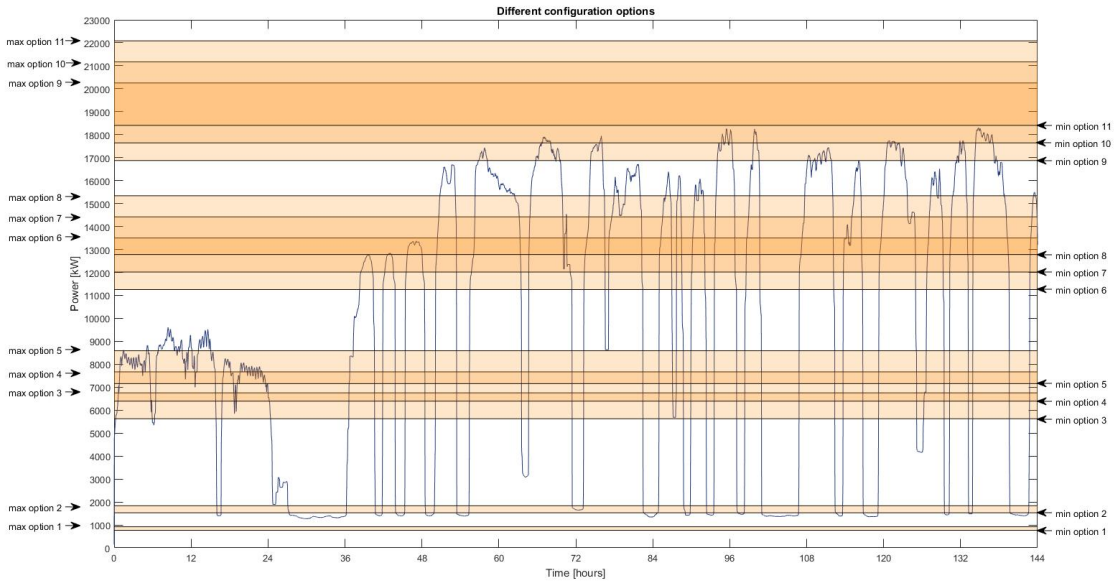

Figure 4.20: Overview power configuration in relation to filtered power demand

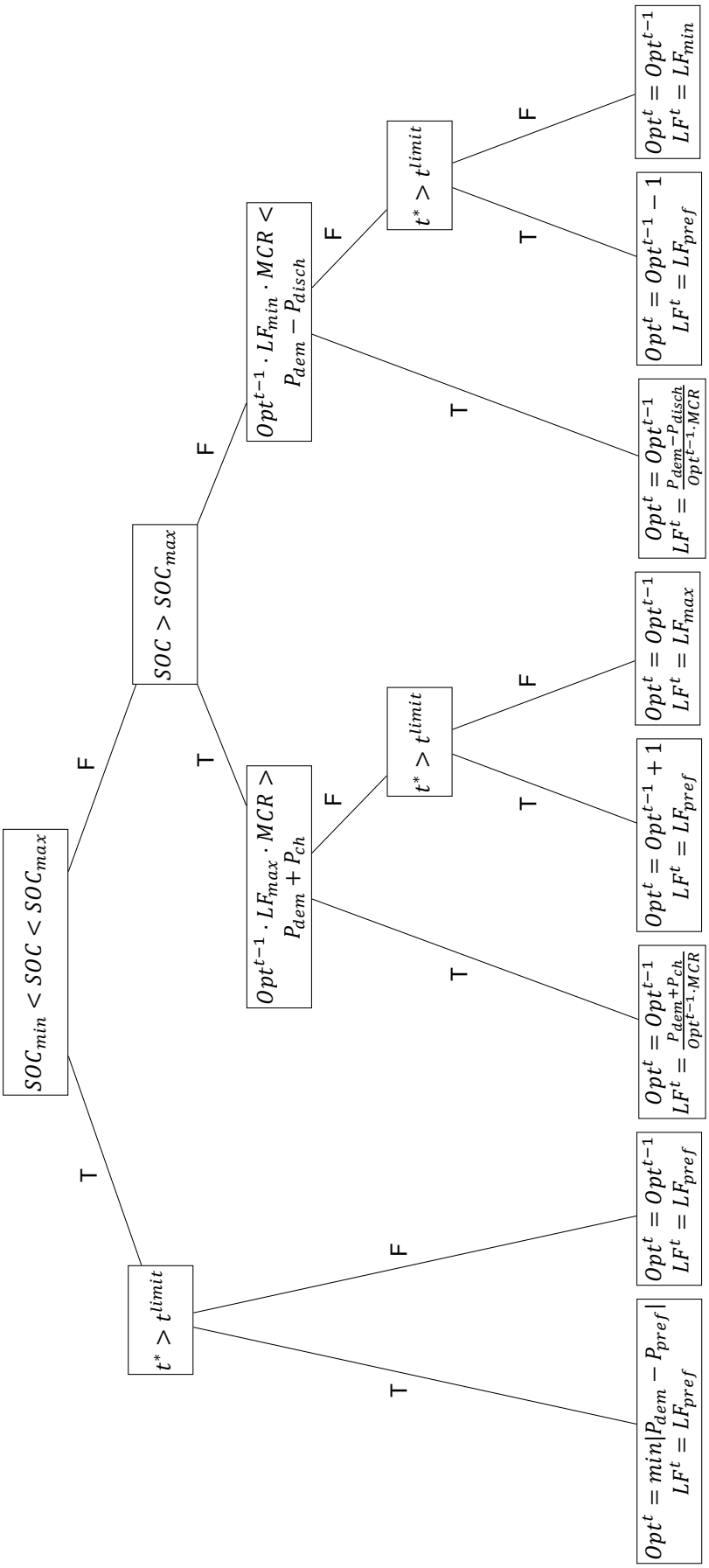

Figure 4.21: Decision tree for the power management system

5

Testing and verification

This chapter will focus on the evaluation of the models as they are developed so far. The goal is to verify the cutter model with measurements done in the field. The most important factor in this is the fuel consumption of the cutter suction dredger as it is operating right now. Further more the validation of the battery model will be discussed step by step.

5.1. Fuel consumption

One of the goals of the development of the hybrid cutter dredger is to reduce fuel consumption. The reduction in fuel consumption should be equal to the fuel consumption of the power generation system without the use of an energy storage device minus the fuel consumption simulated with the hybrid cutter model. In order to prove that the fuel consumption estimation is correct a simple Simulink model has been developed. The test set-up in Simulink is visualized on page 139 and 140 in appendix H. This model uses the power measurements from the three main generators. The power measurements are then converted to a load factor for each generator. The load factor expresses the power produced as a percentage of the maximum continuous rating of the engine. Note that the power measurements take place at the terminals of the generator. A certain generator efficiency should be taken into account to find a value for the actual mechanical power developed by the diesel engine. This generator efficiency is used in the model as a bias. The bias value enables tuning of the model [Sorensen, 2014].

The LF of the individual generators is then fed into a lookup table containing information about specific fuel oil consumption. The lookup table population is based on the findings presented in section 4.2. It is found that the actual SFOC is much higher than the SFOC presented in the FAT test reports. As an initial guess the SFOC values determined for the Wärtilä engines from the HAM318 have been adopted. The engines from the HAM318 and the Athena and Artemis have a lot in common, but the differences should not be overlooked. Most important parameters of both engines are presented in table 5.1 [Wärtsilä Corporation, 2000, 2012]. First of all it is obvious that the power output of both engines is different. The engine of the HAM318 delivers more power than the engines from the Athena and Artemis. Nevertheless the power output per cylinder is quite similar. furthermore the cylinder geometry is equal for both engines. The most important engine parameter that is introduced in table 5.1 is the mean effective pressure. The p_{me} for both engines is almost equal. According to equation 5.1 found in Stapersma [2010b] the mean effective pressure p_{me} gives a certain measure for the efficiency of the engine. Using equation 4.14 one can rewrite equation 5.1 to 5.2. If it is assumed that the trapped air efficiency is more or less equal (*for four stroke engines this value is almost one when no extensive Miller timing is used*) one can see that the engine efficiency is then only influenced by the fractions on the right hand side of equation 5.2. The first fraction, $\frac{h^L}{R_c \cdot T_c}$ is equal for both engines since the charge temperature T_c for both engines is around $50C$ after the charge air cooler (*The heat pick-up from cooler to cylinder is assumed to be equal*). The parameters lower heating value h^L and gas constant R_c are engine independent properties. It seems that only the last fraction in 5.2, can influence the engine efficiency. Although the charge pressure p_c for the 6L46F is higher than the charge pressure for the

12V46C, one can assume that the total fraction $\frac{p_c}{\lambda^* \cdot \sigma}$ is almost equal for both engines. Due to the fact that when the charge pressure increases also the scavenge efficiency will increase and therefore the pseudo air excess ratio λ^*. For that reason the net difference between the most right fraction will be small when both engines are compared. Based on the above explanation, the assumption that the efficiency of both engines is comparable is viable. This is also found back in the fuel consumption figures found in the FAT of both engine types. The SFOC of the engines at 85% MCR is around 180 g/kWh.

$$p_{me} = \eta_{trap} \cdot \eta_m \cdot \eta_{comb} \cdot \eta_{hl} \cdot \eta_{td} \cdot \frac{h^L}{R_c \cdot T_c} \cdot \frac{p_c}{\lambda^* \cdot \sigma} \tag{5.1}$$

$$p_{me} = \eta_e \cdot \eta_{trap} \cdot \frac{h^L}{R_c \cdot T_c} \cdot \frac{p_c}{\lambda^* \cdot \sigma} \tag{5.2}$$

Table 5.1: Wärtsilä 6L46F and Wärtsilä 12V46C comparison

	HAM318	Athena/Artemis
Engine	Wärtsilä 12V46C	Wärtsilä 6L46F
nominal power $[kW]$	12600	7500
nr. cylinders	12	6
power per cylinder $[kW/cyl]$	1050	1250
engine speed $[rpm]$	514	600
cylinder bore $[mm]$	460	460
piston stroke $[mm]$	580	580
mean effective pressure $[bar]$	25.4	25.9

The specific fuel oil consumption as presented in section 4.2 is displayed as a relative value as can be seen from figure 4.12. In the fuel consumption part of this chapter no mathematical representation of the relative SFOC was formed. Since this is necessary to create the lookup table population two fit function were developed. One for the relative FAT SFOC and one from the measured SFOC. Both fit functions are presented in figure 5.1.

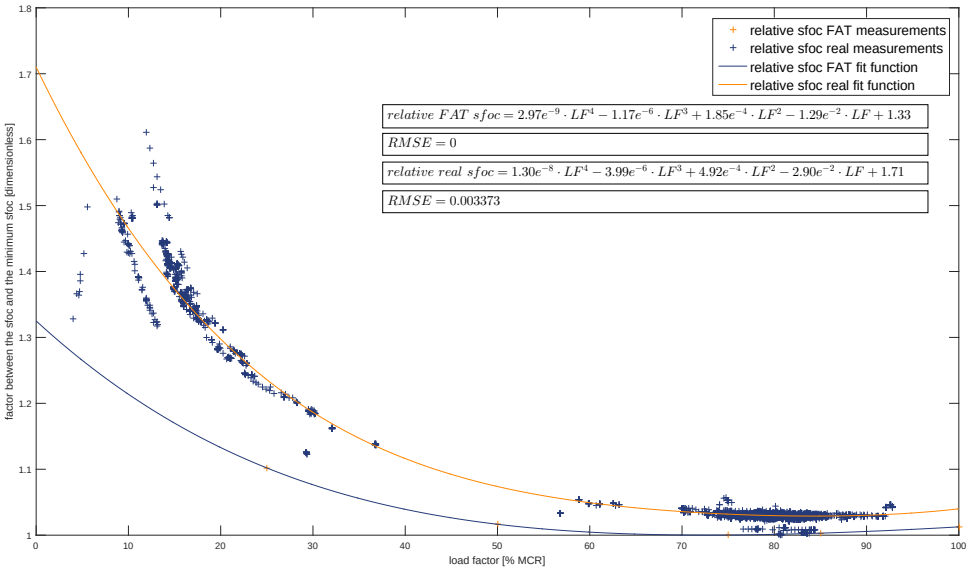

Figure 5.1: FAT and measured relative sfoc figures and their corresponding fit functions

This being said and the important values for the Simulink model introduced it is time to find the *actual* fuel consumption. Fortunately Van Oord keeps a database with all the fuel consumption figures of their vessels. The same holds for the Artemis in the period that is used as benchmark for this thesis. The data that is made available by Van Oord is presented in table 5.2. It can be seen that the fuel consumption is specified as consumption per week. As discussed in section 2.2.3 the period that is best suited for simulation has a length of six days. This means that the weekly data can not be used immediately. Moreover since the measurements that are used for simulation start on a Tuesday instead of a Monday morning. Therefore the fuel consumption presented in the fuel report has to be converted. It is assumed that the fuel consumed is proportional to the amount of energy in kWh. In this way an estimation of the amount of fuel that was burned in the six day time window can be made.

Table 5.2: Fuel database values for the Artemis Van Oord [2014]

Equipment	0241	Artemis				
Week	Fuel total $[Mt]$	HFO Mt	Lub. Oil $[ltr]$	Hydr. Oil $[ltr]$	Grease $[kg]$	CO2 $[Mt]$
Year	2014					
Country	…				Project	…
40	347	331	1200	-	60	1118
41	269	253	1735	-	37	878
42	429	399	2144	20	188	1384
43	425	101	2400	-	60	1348
Totals	1473	1084	7479	20	345	4729

In figure 5.2 the amount of energy produced over time is illustrated. The energy produced is simply the integral of the power output over time. The orange areas in figure 5.2 are not intended to represent the integral but only to visualise the time windows better. The value of the of the plotted line represents the integral. The simple methodology to estimate the fuel consumed is presented in equation 5.3 on page 68. It turns out that around 302 mt of fuel is consumed during the six day period. This is the value that should be produced by the Simulink fuel test model in order to verify the assumptions that were introduced in chapter 4. The way the fuel consumption over six days is calculated is quite rough therefore it is suggested to analyse week 42 as well. Week 42 can be entered as complete week in the simulation so no artificial calculation errors should be introduced.

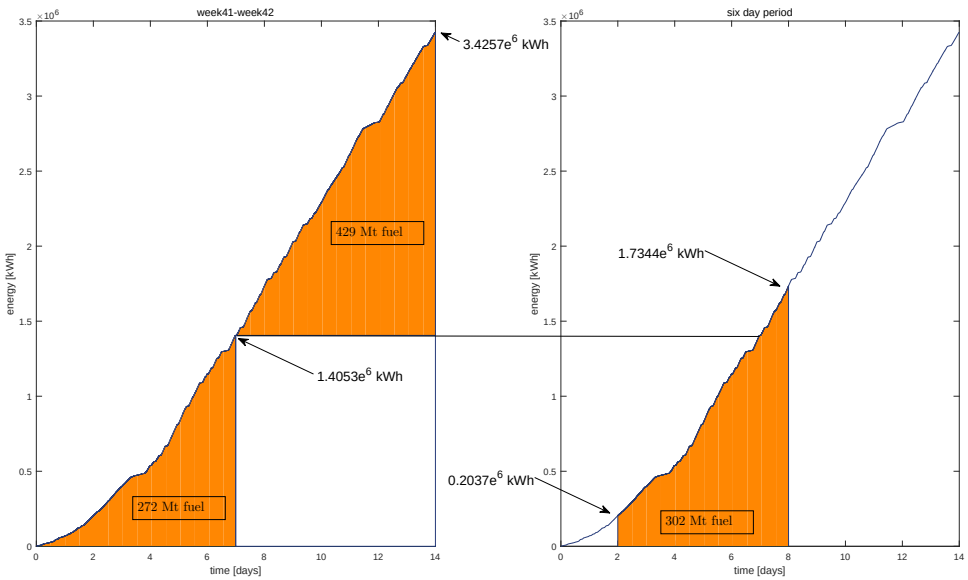

Figure 5.2: Fuel consumption estimation based on the fuel database

$$\frac{272}{1.4053e^6} \cdot (1.4053e^6 - 0.2037e^6) + \frac{399}{(3.4257e^6 - 1.4053e^6)} \cdot (1.7344e^6 - 1.4053e^6) = 302 \tag{5.3}$$

As it turns out the simulation finds values of fuel consumption similar as those measured during actual operation. Besides the fuel consumption some other values were calculated. These values as grid efficiency, running hours and generator efficiency will be used to compare the hybrid system with the original system. The values are presented in table 5.3 and table 5.4. As stated before the generator efficiency is used as a bias to tune the model. The value of 98% efficiency that was found has been confirmed to be realistic by electrical superintendents at Van Oord [Nagy, 2016]. The running hours over week 42 from the main engines have been confirmed to be accurate when they were compared to the values stored in the computerized maintenance management system from Van Oord. Unfortunately the running hours of the auxiliary generators do not correspond to the values found in the maintenance management system. However since the running hours of the main generators seem correct it can be assumed that the running hour estimation of the auxiliary generators is also correct. The only aspect that can cause the discrepancy is the fact that the power output from the auxiliary generators is not logged properly. If this is the case this can also be the cause for the fact that the determined Marine Gas Oil, in this thesis assumed to inherit the same properties as MDO (MGO) consumption is also lower than the values found in the fuel report.

Table 5.3: Results of the model verification test for the six day period

parameter	value
fuel consumption total $[Mt]$	303.4
HFO consumption $[Mt]$	298.3
HFO consumption using FAT measurements $[Mt]$	286.1
MGO consumption $[Mt]$	5.1
grid efficiency η_{grid} $[\%]$	90.67
generator efficiency η_{gen} $[\%]$	97.5
running hours main generator 1 $[h]$	144
running hours main generator 2 $[h]$	125
running hours main generator 3 $[h]$	86
total running hours main generators $[h]$	355
running hours auxiliary generators $[h]$	34

Table 5.4: Results of the model verification test for week 42

parameter	value
fuel consumption total $[Mt]$	404.8
HFO consumption $[Mt]$	399.3
HFO consumption using FAT measurements $[Mt]$	383.5
MGO consumption $[Mt]$	5.5
grid efficiency η_{grid} $[\%]$	91.09
generator efficiency η_{gen} $[\%]$	97.5
running hours main generator 1 $[h]$	166
running hours main generator 2 $[h]$	151
running hours main generator 3 $[h]$	144
total running hours main generators $[h]$	461
running hours auxiliary generators $[h]$	31

5.2. Battery

Similar to the the validation process of the fuel consumption model the battery model should be validated. The developing process and the assumptions made during the development of this model has been discussed in chapter 4. The difference between the verification of the battery model and the fuel consumption model is that there is no actual measured data available. For this reason it is not possible to verify if the response of the model is comparable or equal to a measured dataset. Nevertheless the response of the battery can be broken up in small pieces. When input is compared to the response one should be able to get a good feeling for the validity of the model.

The first test is done with a constant discharge and a constant charge power. This is visualised in figure 5.3. Besides the discharge and charge power the terminal voltage of the battery, the current and the SOC are displayed in this figure. It can be seen that the power graph displays a positive power of 500 W for the first 1800 seconds and a negative power of 500 W for the last 1800 seconds of this test. The positive power is seen as power delivered by the battery, so the first 1800 seconds are part of a discharge cycle. After 1800 seconds the direction of the current is changed and the battery will be charged again. Note that the sign of the current in figure 5.3 does not change. This is done to visualise the non-linear behaviour of the current. It can be seen that the terminal voltage follows a non-linear line when the battery is discharged. This was expected since this is also found in the battery documentation. It is also clear to see that there is a initial voltage drop when a current is drawn from the battery. This voltage drop of around 0.8 volt is also known as the Peukert effect [Jongerden and Haverkort, 2008]. The fact that the battery terminal voltage has a discontinuity when the sign of the power demand is changed is explainable as well. The voltage supplied to the battery should be higher than the voltage at the end of discharge, otherwise the current will not flow in the other direction. The last interesting aspect from this test that is worth discussing is the fact that the state of charge of the battery does not reach the 100% level after the charge cycle. This is as was expected. In chapter 4 it was already discussed that the efficiency of the battery cannot be 100%. The first 1800 seconds of this test 250 Wh was drawn from the battery, the last 1800 seconds 250 Wh of energy was supplied to the battery. Not all this energy is stored in the battery, since it is not fully charged again after 3600 seconds. The efficiency of the battery is properly modelled in this way.

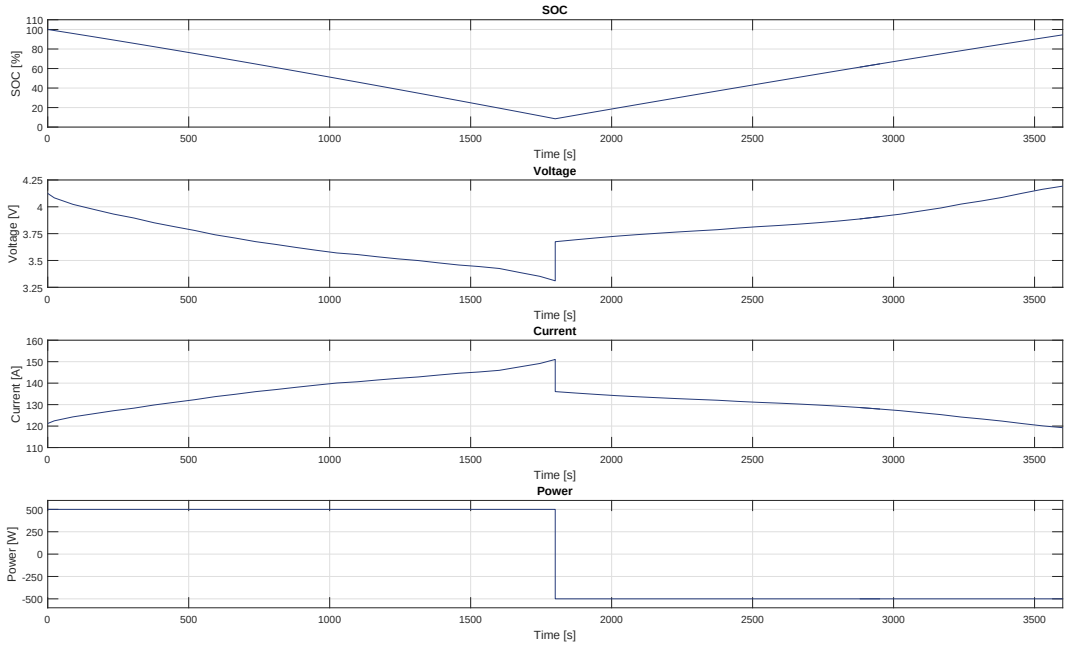

Figure 5.3: SOC, voltage, current and power during first battery model test

The second test that is done has a simulation time of two hours or 7200 seconds. The first hour of the simulation is again a simulation of a constant discharge and charge power. The last hour is simulating a more fluctuating power demand signal. The power signal and the simulation results in terms of SOC, current and terminal voltage are presented in figure 5.4. During this test the battery was scaled to the maximal terminal voltage permitted by battery manufacturers Spear Power Systems and Fry [2016]. This maximal voltage is 1134 volt and relates to a nominal voltage of 999 volt. The other constants entered in this simulation are presented in table 5.5. The discharge power is set to 1000 kW. This means that the battery, which has a capacity of 524.5 kWh would be discharged in somewhat more than 30 minutes. The discharge cut-off signal is set to 50% SOC. This would mean that the discharge cycle should stop around 900 seconds. This is clearly visible in the simulation results. At time is 900 seconds the current is set to zero. It can be seen that the terminal voltage of the battery rises slightly when the discharging is stopped. This effect was to be expected and is referred to as the relaxation effect [Huria et al., 2012]. It can be said that all the important effects in the non-linear behaviour of the battery as described in literature are sufficiently modelled.

Table 5.5: Constants used in the second battery model test

parameter	value
number of batteries in series	270
number of batteries in parallel	7
charge cut-off $[\%SOC]$	100
discharge cut-off $[\%SOC]$	50
nominal storage capacity $[kWh]$	524.5
nominal capacity $[Ah]$	525

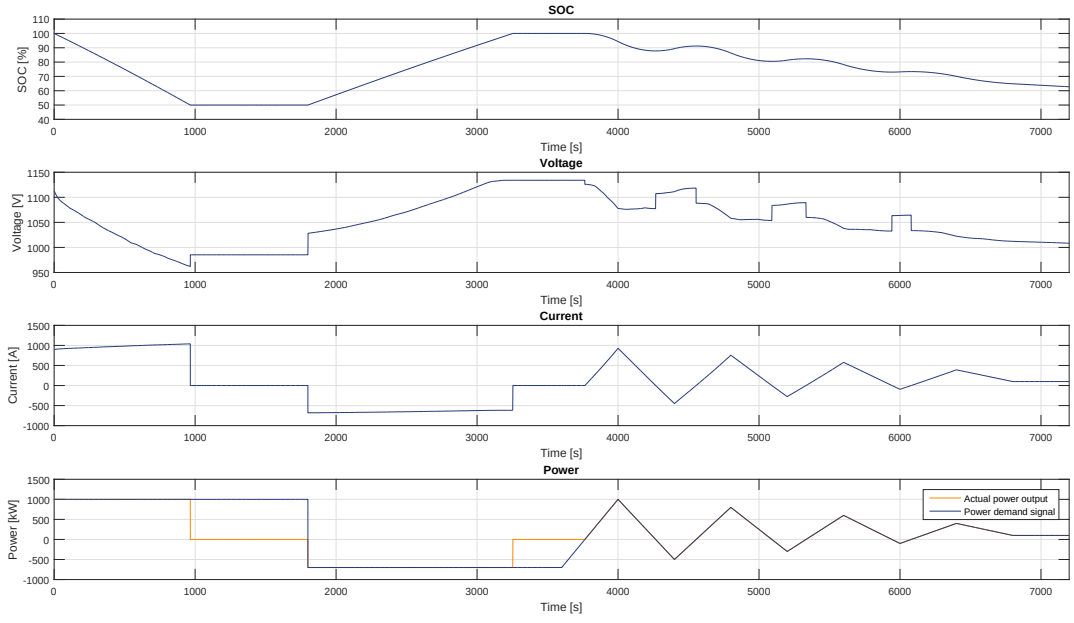

Figure 5.4: SOC, voltage, current, power demand and actual power during second battery model test

5.3. Power management system

The testing of the power management system is basically done in the same way as is done for the battery model. The PMS has to perform as it is intended. The assumptions behind the power management system are discussed in chapter 4.

As a start a sawtooth like power demand was entered into the PMS. The SOC value is set as a constant at 50%. The goal of this simulation is to see if the PMS is able to find the optimal solution for a certain power demand. The optimal solution in this regard is a combination of diesel generators running on 80% MCR (*or another desired load factor*). Such an optimal combination will result in a power output. The input power signal, the time dependent best option and the corresponding delivered power are presented in figure 5.5. As it turns out the PMS is able to find the correct configuration for a power demand varying from 0 to 23000 kW resulting in a step function power supply.

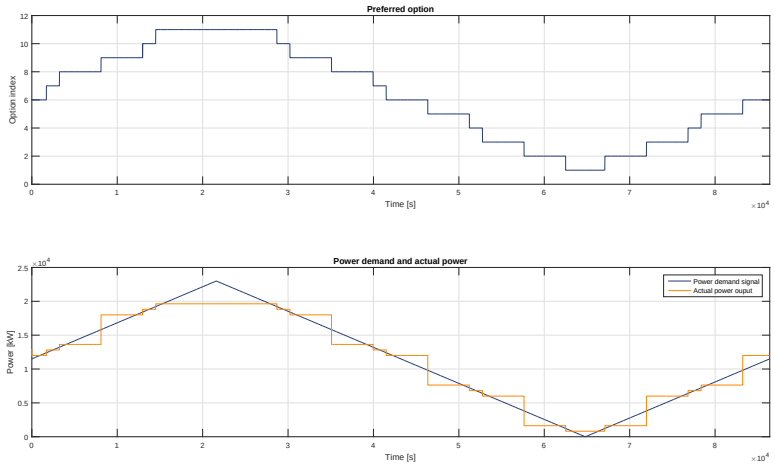

Figure 5.5: Preferred option, power demand and power supply without SOC constraints during PMS test

The PMS works good for a constant value of SOC. In the final simulation the SOC will not be constant, therefore it will also be tested if the PMS reacts properly to a drop in SOC. The second test set-up uses a constant power signal, set on 15000 kW. The intention is to let the SOC signal drop below the minimum state of charge set-point. This will be done at time is 3000 seconds. In this test the minimum SOC is set to 20%. The demanded charge power is set to 1500 kW. The power management system can not supply this charge power by keeping the same configuration of diesel engines. The output signal should be a power supply corresponding with a higher configuration (*more generators on-line*). Next to the fact that the power management system demands more generators on-line it can also be seen that this extra engine is kept on-line for the duration of one hour. The result of this test as well as the input signals is presented in figure 5.6. The power management system reacts as intended.

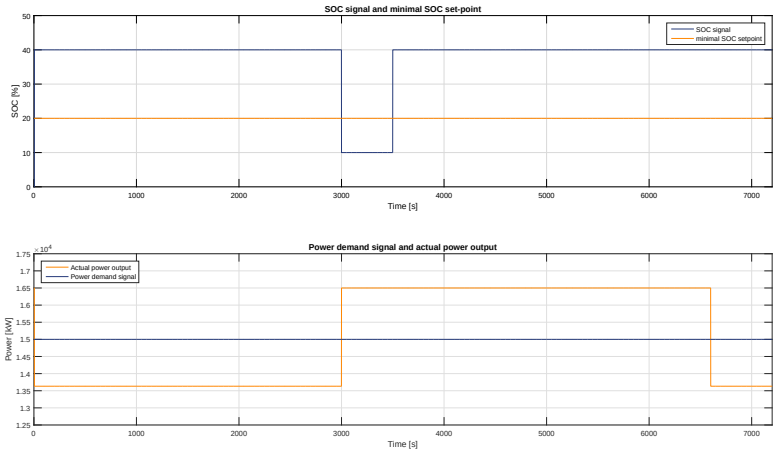

Figure 5.6: Power demand and power supply for a SOC step during PMS test

Finally a more realistic set of input signals is tested. Both power demand and SOC are varied. The state of charge value is build as a step function. The test will simulate 24 hours of operation. During this simulation the limits of the system are searched. One of these limits is to demand a charge cycle when all generators are on-line. In this case the power management system should not hold on to the optimal load factor but increase the load factor to the maximum value allowed. On the other hand when the battery is to high in charge and the power demand itself is already close to zero the demanded load factor should not even be the minimal allowed value, but is should go to zero. Looking to figure 5.7 these two extremes are simulated at 23400 seconds and 66600 seconds respectively. It can also be seen that the power management system first tries to supply more power without switching an extra generator on- or off-line. This is visualised in **Preferred option and actual option** within figure 5.7.

The tests conducted in this chapter should be sufficient to proof that the individual models work as they are intended. The combination of these sub models make up the overall hybrid system model which will be used for the actual sizing of the battery. The input and output of the complete system will be introduced in chapter 6.

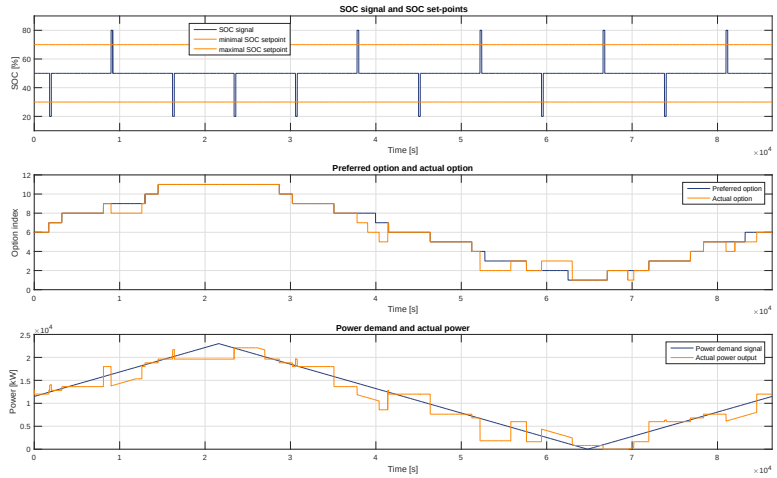

Figure 5.7: SOC, preferred option, actual option, power demand and power supply during PMS test

6

Simulation and results

6.1. input

Before the model can be used to provide useful data one should decide what should be simulated. In other words, what is the input for the models developed so far. To get a proper understanding of the effects of battery size on the overall performance of the system the battery size should be changed for different simulations.

The following strategies are proposed;

1. **simulation with power management system**

   Peak shaving is not a factor that can be influenced while using the power management system. This is caused by the fact that the power management system will always attempt to let the diesel engines run in their optimal efficiency point. These are set options for power output, therefore small fluctuations in power demand will always have to be overcome by battery power.

   Spinning reserve is always minimised using the power management system. If it is possible and allowed by the management strategy to shut down an engine this will be done. As a matter of fact if the state of charge of the battery becomes to high and crosses a certain set-point the power management system will intentionally shut one or more engines down in order to get the battery back to a desired SOC.

   While using the the power management system in the simulation several set-point can be changed. These set-points should be changed to get a better understanding about their effect on system performance and battery life time. Making the bandwidth for the SOC smaller will increase battery lifetime, but will reduce the contribution of the battery to the total power supply. The engines will have to do more, which should be found back in the running hour figures. Further more the set time for charging and discharging can be changed. If an engine is intentionally put on-line to charge the battery it can not be shut down again till it has run for a certain time period. The same holds for shutting a generator down. Last but not least the charge and discharge power to and from the battery can be set. These values are determined by the size of the battery. Charge and discharge rates can be set to a maximum value in order to give the battery a longer and most important more predictable life expectancy.

   In this simulation the battery size will be set at values changing with a constant interval. The different tuning parameters in the power management system will be changed to simulate different system behaviour.

   The set-points and battery capacities used in these simulations are presented in table 6.1.

2. **simulation without elaborate power management system**

   Simulation without any form power management is not possible. The amount of energy available for charging the battery will always be lower than the discharge energy. For this reason a certain form power management should ensure charging of the battery.

   Certain quantities for peak shaving have been developed. This is done by using a median filter to filter the power demand signal over a certain time window. Large spikes in the power demand will be filtered out and will have to be overcome by battery power. Six different time windows are proposed to apply the median filter to. The different time windows are one, five, 15, 30 and 60 minutes. The effect of these filters is visualised in figure I.1 and figure I.2 in appendix I.

   In an iterative way the minimum required battery capacity is determined. This is done using the same capacity intervals as were used during the simulations with power management. The battery capacity should enable peak shaving without reaching a state of charge higher or equal to 100%. If the battery state of charge is to drop below the 30% mark an additional 1000 kW will be supplied by the diesel engines to recharge the battery. The simulation set-points are summarized in table 6.2.

   The minimum amount of battery capacity is determined in an iterative way. No attention has been paid to the lifetime of the battery. The results of these simulations will be used for further analysis in chapter 7. In chapter 7 the battery life time will be determined. The expectation is that the battery lifetime for peak shaving will be lower than with the power management system.

As will be discussed in chapter 7 it turns out that during the initial simulations the auxiliary generators are used a lot. At least way more than in the original situation. In order to verify if it is actually necessary to make use of the auxiliary generators several simulations were done without auxiliary power. It is obvious that the running hours of the auxiliary engines will be zero during these simulations. The auxiliary engines take care of the smaller deviations between power demand and power supply by the main generators. It turns out that the options for power generation are to limited when the main generators are bound by their maximal and minimal load factor of 90% and 70% respectively. Therefore it is decided to lower the minimal load factor for smaller battery capacities. Otherwise the batteries limits will be reached to often to maintain a reasonable life expectancy. The set-points for these simulations are presented in table 6.3.

For simulation 1 to 24 the power management is used in the way it is designed. The minimal and maximal load factor of the diesel engines are set to 70% MCR end 90% MCR respectively. The desired load factor, to which the power management will optimize, is set to 85% MCR. The state of charge set-points are systematically changed from 40%, 30%, 20% and 60%, 70%, 80% for the minimal SOC and the maximal SOC respectively. Note that during these simulations the auxiliary generators contribute to the power generation as well.

Simulation 25 to 30 represent the system behaviour for peak shaving operation. During these simulations no extensive power management system is used. A simple filter is applied to determine the output power from the diesel generators. The deficit between this power supply and power demand is deliver by or stored in the battery. The only artificial signals that is introduced during these simulations is an extra power supply by the generators of 100 kW when the battery state of charge drops below 30%.

Finally simulation 31 to 38 make use of the first power management strategy. However, the use of auxiliary generators is disabled since this turns out to be really expensive. The SOC limits have been set to 20% and 80% for minimal and maximal SOC respectively. Furthermore, the minimal and maximal load factor are tuned in a iterative way. This is a result of the decision that is made, not to use the auxiliary generators.

Table 6.1: Input set-points for power management system simulations

Simulation number	desired battery capacity $[kWh]$	actual battery capacity $[kWh]$	number of cells parallel	time limit $[s]$
1	2500	2547.45	34	3600
2	2500	2547.45	34	3600
3	2500	2547.45	34	3600
4	5000	5019.98	67	3600
5	5000	5019.98	67	3600
6	5000	5019.98	67	3600
7	7500	7492.50	100	3600
8	7500	7492.50	100	3600
9	7500	7492.50	100	3600
10	10000	10039.95	134	3600
11	10000	10039.95	134	3600
12	10000	10039.95	134	3600
13	12500	12512.48	167	3600
14	12500	12512.48	167	3600
15	12500	12512.48	167	3600
16	15000	14985.00	200	3600
17	15000	14985.00	200	3600
18	15000	14985.00	200	3600
19	2500	2547.45	34	3600
20	5000	5019.98	67	3600
21	7500	7492.50	100	3600
22	10000	10039.95	134	3600
23	12500	12512.48	167	3600
24	15000	14985.00	200	3600

Simulation number	charge power $[kW]$	discharge power $[kW]$	minimal SOC $[\%]$	maximum SOC $[\%]$
1	500	500	40	60
2	1000	1000	30	70
3	1250	1250	20	80
4	1000	1000	40	60
5	2000	2000	30	70
6	2500	2500	20	80
7	1500	1500	40	60
8	3000	3000	30	70
9	3750	3750	20	80
10	2000	2000	40	60
11	4000	4000	30	70
12	5000	5000	20	80
13	2500	2500	40	60
14	5000	5000	30	70
15	6250	6250	20	80
16	3000	3000	40	60
17	6000	6000	30	70
18	7500	7500	20	80
19	750	750	45	55
20	1000	350	40	60
21	1000	500	40	60
22	1250	750	40	60
23	1500	1000	40	60
24	2000	1000	40	60

Table 6.2: Input set-points for peak shaving simulations

Simulation number	filter window length $[min]$	actual battery capacity $[kWh]$	charge power $[kW]$	charge duration $[s]$	minimal SOC $[\%]$	maximal SOC $[\%]$
25	1	2547.45	1000	7200	30	100
26	5	2547.45	1000	7200	30	100
27	15	2547.45	1000	7200	30	100
28	30	5019.98	1000	7200	30	100
29	45	5019.98	1000	7200	30	100
30	60	5019.98	1000	7200	30	100

Table 6.3: Input set-points for simulations without auxiliary generators

Simulation number	actual battery capacity $[kWh]$	charge power $[kW]$	discharge power $[kW]$	time limit $[s]$
31	2547.45	1250	1250	3600
32	5019.98	2500	2500	3600
33	7492.50	2500	2500	3600
34	10039.95	5250	5250	3600
35	10039.95	2500	2500	7200
36	12512.48	6250	6250	3600
37	12512.48	3000	3000	7200
38	14985.00	7500	7500	3600

Simulation number	minimal SOC $[\%]$	maximal SOC $[\%]$	minimal LF $[\%]$	maximal LF $[\%]$
31	20	80	30	90
32	20	80	50	90
33	20	80	70	90
34	20	80	75	95
35	20	80	75	95
36	20	80	75	95
37	20	80	75	95
38	20	80	75	95

6.2. results

The results from the simulation done till now are presented in the following tables. Table 6.4, 6.5, 6.6, 6.7, 6.8 and 6.9 present the results from the first round of simulations. These tables represent simulations for 2.5MWh, 5MWh, 7.5MWh, 10MWh, 12.5MWh and 15MWh battery capacities respectively. The goal here is to find a relation between battery capacity and reduction of running hours and fuel consumption. Furthermore the effect of peak shaving on fuel consumption and running hours has been simulated. The results for these simulations are presented in table 6.2. It turned out from the first simulation round that it is best to set the power management system on a minimal SOC of 20% and a maximum SOC of 80% with regards to fuel consumed by the main generators. The contribution of the auxiliary generators to the reduction of fuel consumption and running hours did not become clear from the initial simulations. Therefore extra simulations have been done without the use of auxiliary generators and only for the SOC held between 20% and 80%. The results of these simulations are presented in table 6.11

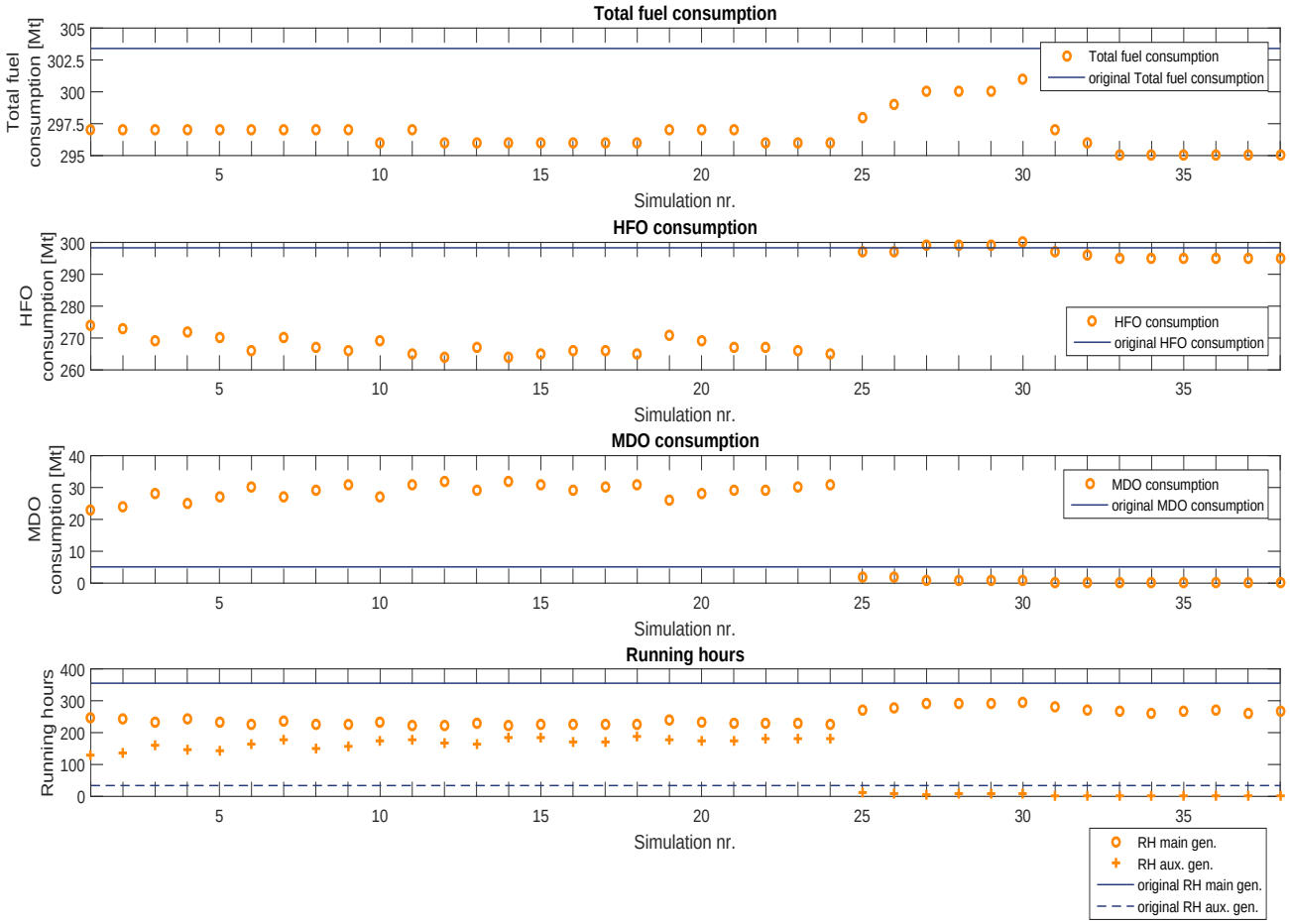

Figure 6.1: Visualised summary of the simulation results per simulation

Table 6.4: Simulation results with 2.5 MWh battery pack

Simulation number	fuel consumption total $[Mt]$	HFO $[Mt]$	MGO $[Mt]$
1	297	274	23
2	297	273	24
3	297	269	28
19	297	271	26

Simulation number	running hours main generator 1 running hours main generator 2 running hours main generator 3	total running hours main generators	running hours auxiliary generators
1	116 81 50	248	129
2	114 81 49	243	137
3	107 80 47	234	162
19	109 82 50	241	146

Table 6.5: Simulation results with 5 MWh battery pack

Simulation number	fuel consumption total $[Mt]$	HFO $[Mt]$	MGO $[Mt]$
4	297	272	25
5	297	270	27
6	297	266	30
20	297	269	28

Simulation number	running hours main generator 1 running hours main generator 2 running hours main generator 3	total running hours main generators	running hours auxiliary generators
4	112 81 49	242	143
5	107 80 46	233	163
6	102 79 45	226	177
20	104 79 50	233	149

Table 6.6: Simulation results with 7.5 MWh battery pack

Simulation number	fuel consumption total $[Mt]$	HFO $[Mt]$	MGO $[Mt]$
7	297	270	27
8	297	267	29
9	297	266	31
21	297	267	29

Simulation number	running hours main generator 1 running hours main generator 2 running hours main generator 3	total running hours main generators	running hours auxiliary generators
7	109 80 47	235	157
8	103 79 44	226	173
9	103 78 45	225	178
21	104 78 59	231	166

Table 6.7: Simulation results with 10 MWh battery pack

Simulation number	fuel consumption total $[Mt]$	HFO $[Mt]$	MGO $[Mt]$
10	296	269	27
11	297	265	31
12	296	264	32
22	296	267	29

Simulation number	running hours main generator 1 running hours main generator 2 running hours main generator 3	total running hours main generators	running hours auxiliary generators
10	107 80 45	232	163
11	103 79 42	223	186
12	101 77 46	223	185
22	104 78 48	230	170

Table 6.8: Simulation results with 12.5 MWh battery pack

Simulation number	fuel consumption total $[Mt]$	HFO $[Mt]$	MGO $[Mt]$
13	296	267	29
14	296	264	32
15	296	265	31
23	296	266	30

Simulation number	running hours main generator 1 running hours main generator 2 running hours main generator 3	total running hours main generators	running hours auxiliary generators
13	104 81 43	228	171
14	100 79 43	222	188
15	101 76 49	225	178
23	102 78 49	228	173

Table 6.9: Simulation results with 15 MWh battery pack

Simulation number	fuel consumption total $[Mt]$	HFO $[Mt]$	MGO $[Mt]$
16	296	266	29
17	296	266	30
18	296	265	31
24	296	265	31

Simulation number	running hours main generator 1 running hours main generator 2 running hours main generator 3	total running hours main generators	running hours auxiliary generators
16	103 80 42	226	174
17	104 77 44	226	181
18	103 74 48	225	181
24	101 77 47	225	180

Table 6.10: Simulation results for peak shaving simulation

Simulation number	fuel consumption total $[Mt]$	HFO $[Mt]$	MGO $[Mt]$
25	298	297	2
26	299	297	2
27	300	299	1
28	300	299	1
29	300	299	1
30	301	300	1

Simulation number	running hours main generators	running hours auxiliary generators
25	271	11
26	276	10
27	290	5
28	292	7
29	291	7
30	294	7

Table 6.11: Simulation results for simulations without auxiliary generators

Simulation number	HFO $[Mt]$	running hours main generator 1 running hours main generator 2 running hours main generator 3	total running hours main generators
31	297	127 91 64	281
32	296	120 87 62	269
33	295	118 86 63	267
34	295	109 88 66	262
35	295	118 86 64	267
36	295	110 95 63	269
37	295	116 84 62	262
38	295	108 93 64	266

7

Analysis of simulation results

The analysis of the simulation result as presented in the previous chapter will be done according a step by step approach. The strategy for analysing the results is presented in figure 7.1.

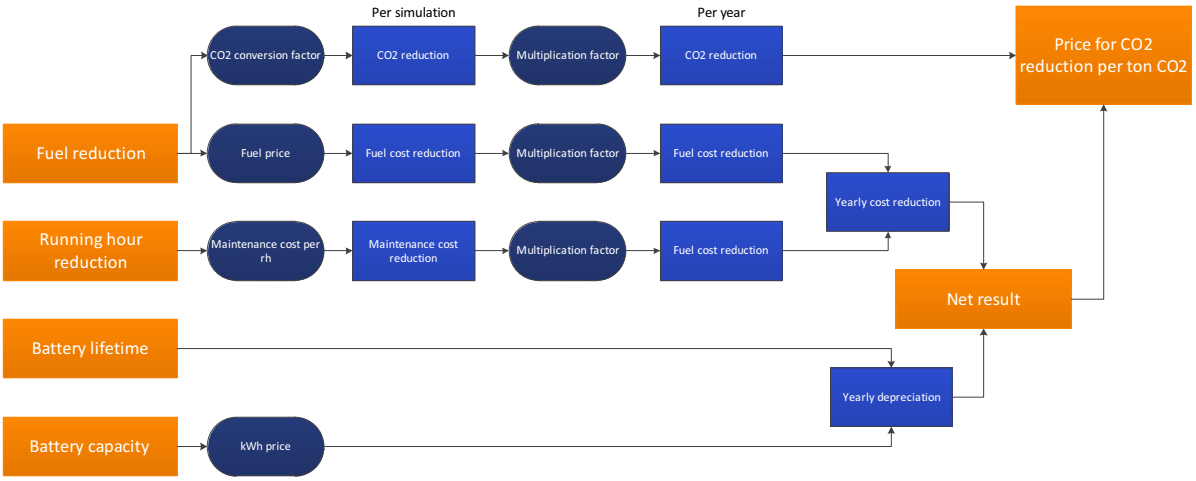

Figure 7.1: Strategy for analysing simulation results

7.1. Financial analysis

Before one can start the financial analysis of the simulation results some financial parameters should be set. In the first part of this section the cost of running hours and the fuel prices that are used will be introduced. The cost of running hours and the fuel price will be used to calculate the potential savings of the hybrid system. This cost reduction should be compared with the investment cost that come with the proposed hybrid system. In order to calculate the investment cost a battery price as function of battery capacity is introduced. The cost of the hybrid system per year will be expressed as the depreciation of the battery system. To do so the period over which the battery is depreciated should be known, it is assumed that the battery will be depreciated linearly over its lifetime. Since this research is primarily done to reduce CO_2 one should know the amount of CO_2 that is actually reduced. The reduction in fuel consumption is known. Conversion factors to calculate the CO_2 emission from the fuel consumption will be introduced in this section as well.

7.1.1. Price of potential savings

In order to determine the financial impact of the reduction of running hours a price per running hour should be determined. The maintenance cost of a diesel engine are direct dependent of the running hours of this diesel engine. All the wear parts in the diesel engine have a certain expected lifetime. This lifetime is expressed in hours. Based on the running hours the engine manufacturer can determine

which wear parts have to be replaced. Since the wear parts have a certain price and the technician which does the maintenance has a certain price as well the engine manufacturer can determine a maintenance price per running hour. The engine manufacturer can offer long term maintenance contracts with a certain price. This enables us to determine the cost of running hours. An example of such a long term maintenance contract or frame agreement is presented in table 7.1 which was derived from Bertens [2014]. The figures presented in table 7.1 are based on a frame agreement with Wärtsilä for three engines with 6000 running hours annually. Table 7.1 can be translated to table 7.2. Taking into account that the frame agreement was based on 6000 operational hours fro three main engines. Therefore the values presented in table 7.1 should be divided by 18000 hours. The increase in price per year will be slightly less since the operational hours have been reduced to 4000 hours. The 4000 operational hour figure is derived from data over 2012, 2013 and 2014 [Bertens, 2014]. The values presented in table 7.2 are derived using a price indexation of 1%. For the actual calculations in this thesis an average value will be used for cost per running hour. The cost per running hours is set to €32.70.

Table 7.1: Maintenance cost per year based on frame agreement proposal from Wärtsilä

Running hours per year	6000
Year	cost [€]
0	570180
1	575882
2	581641
3	587457
4	593332
5	599265
6	605258
7	611310
8	617423
9	623597
10	629833

Table 7.2: Maintenance cost per running hour

Year	cost per running hour for 6000 hours per year [€]	cost per running hour for 4000 hours per year [€]
0	31.68	31.68
1	31.99	31.84
2	32.31	31.99
3	32.64	32.31
4	32.96	32.48
5	33.29	32.64
6	33.63	32.96
7	33.99	33.13
8	34.30	33.29
9	34.64	33.63
10	34.99	33.80

Besides the potential savings in running hours there will also be a reduction in fuel consumption. The reduction in fuel consumption can be expressed as a potential cost saving by simply multiplying the amount of fuel with the fuel price. The fuel price is a fluctuation value determined by market circumstances. It is decided to use the current fuel price to determine the financial impact of the fuel savings at this moment. Besides the fuel prices at the moment of writing it is interesting to evaluate the effect of very high fuel prices. The highest fuel price recorded in Rotterdam was in 2012. The price of one metric ton of HFO was €572.9 in March 2012. In order to evaluate the effect of varying fuel prices it is decided to work with price ranges from €100 to €700 with steps of €200 per metric ton of HFO. To find a corresponding MDO price it is decided to evaluate the ratio between HFO and MDO price. Fuel prices from 1990 to 2016 are analysed and an average ratio HFO/MDO is 1.75. The fuel prices are presented in table 7.3. The current fuel prices used are the prices in Rotterdam and taken from S and P Global, Platts [2016]. The highest fuel price and the HFO/MDO price ratio have been derived from National Institute of Statistics and Economic Studies [2016a] and National Institute of Statistics and Economic Studies [2016b].

Table 7.3: Fuel prices per metric ton

Date	Heavy Fuel Oil [$€/Mt$]	Marine Diesel Oil [$€/Mt$]
Friday August 19, 2016	222.1	379.6
March, 2012	572.9	775.7

7.1.2. Investment cost

The investment cost for the hybrid system is mainly determined by the price of the battery. Since the simulations are done for different battery capacities it is advised to determine a battery price per kWh. A quotation has been provided by Corvus Energy for two battery storage systems [Hauso, 2015]. This system is a concept design for a trailing suction hopper dredger. However, a price per kWh can be determined using this information. The price quotation is given in dollars. Since Van Oord is a Dutch company the decision is made to convert these prices to euros. The following exchange rate has been adopted; $1\$ = €0.89$ [Currency-Converter.net, 2016]. The battery prices and the price per kilowatt hour is presented in table 7.4.

Table 7.4: Battery prices

Battery capacity [kWh]	Price [$]	Price per kilowatt hour [$€/kWh$]
1229	1920323	1391
1502	2099770	1244

In chapter 6 the input parameters for the simulations have been presented. Six different battery capacities have been used for simulation. The battery capacities range from 2500 kWh to 15000 kWh. Scale effects will certainly influence the price of the batteries per kWh. It is assumed for this financial analysis that the price per kWh will drop to a certain limit when the battery capacity is increased further. It is assumed that this limit (*which can be seen as a horizontal asymptote*) is around €700 per kWh [Wärtsilä Corporation, 2016] [Super B and Pot, 2016]. If this is combined with the information supplied by Corvus [Hauso, 2015] one can estimate the price per kWh for the different battery capacities. The result of this estimation is presented in figure 7.2. With the equation presented in figure 7.2 it is possible to determine the price of the battery pack capacities as introduced in chapter 6. The price per simulation option is summarized in table 7.5.

7.1.3. Battery cycle life

In order to calculate the total potential savings possible with a hybrid system one should know the life expectancy of the battery in this system. In chapter 4 the method for determining the battery lifetime has been introduced. For all simulations that have been executed the SOC during the simulation has been logged. So a time varying signal of the battery SOC is known. This signal is analysed using the formulas introduced in chapter 4. The results of the battery lifetime calculations are presented in table J.1 in appendix J. Since the result as they are presented in appendix J are not very intuitive it is decided

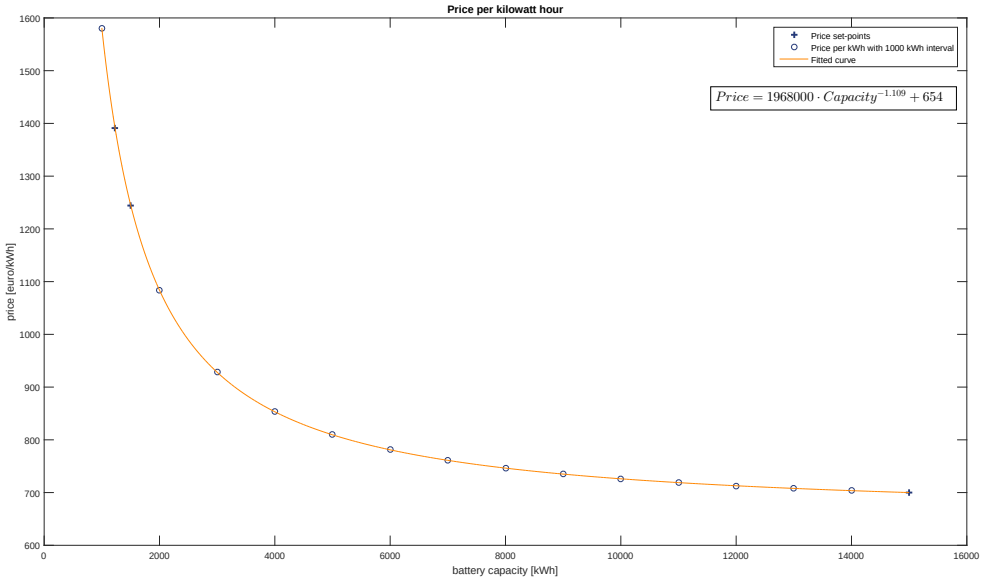

Figure 7.2: Price per kilowatt hour versus battery capacity

Table 7.5: Estimated battery prices

Battery capacity $[kWh]$	Price per kilowatt hour $[€/kWh]$	Total price $[€]$
2547.45	928.59	2365537
5019.98	808.86	4060461
7492.50	753.33	5644325
10039.95	725.80	7286996
12512.48	710.24	8886864
14985.00	700.05	10490249

to visualise the results in graphs before analysing the results.

The actual simulation is split in three different strategies. These strategies will have different results. Therefore the visualisation of the results is split in three different graphs. Figure 7.3 presents the battery life time as function of the battery capacity and the depth of discharge. The depth of discharge is related to the power management settings minimal SOC and maximal SOC. It turns out that a small depth of discharge (*SOC between 40% and 60%*) has a large negative effect on the battery lifetime for smaller battery capacities. Nevertheless the small DOD provides better life expectancies for the larger battery capacities than larger DOD values. Furthermore it can be seen that a certain limit is found in battery lifetime. This can be explained by the fact that the battery has such a large capacity that it can easily cope with the small cycles, the only cycles that are of importance here are the artificial charge and discharge cycles. These cycles are induced when an engine is shut down for example. In the case of a large battery (*$10MWh$ and larger*) the smaller DOD set-points might prolong the battery lifetime since the average SOC will be kept closer to the optimal 50%.

The battery lifetime found for the peak shaving simulations are presented in figure 7.4a. As was expected the battery lifetime is much shorter then when a proper power management system would be used. The reason for this lies in the fact that the battery in case of peak shaving is only charged when it hits its lower limit SOC. The rest of the time the average SOC of the battery is not monitored and actively influenced. In case of the one minute peak shaving filter the state of charge of the battery reaches the 100% quite often. Fully charged the battery ages really quick. When the filter is made longer, for instance the five and fifteen minute filters the life expectancy of the battery increases. The power to be delivered by and stored in the battery will increase, however the average state of charge

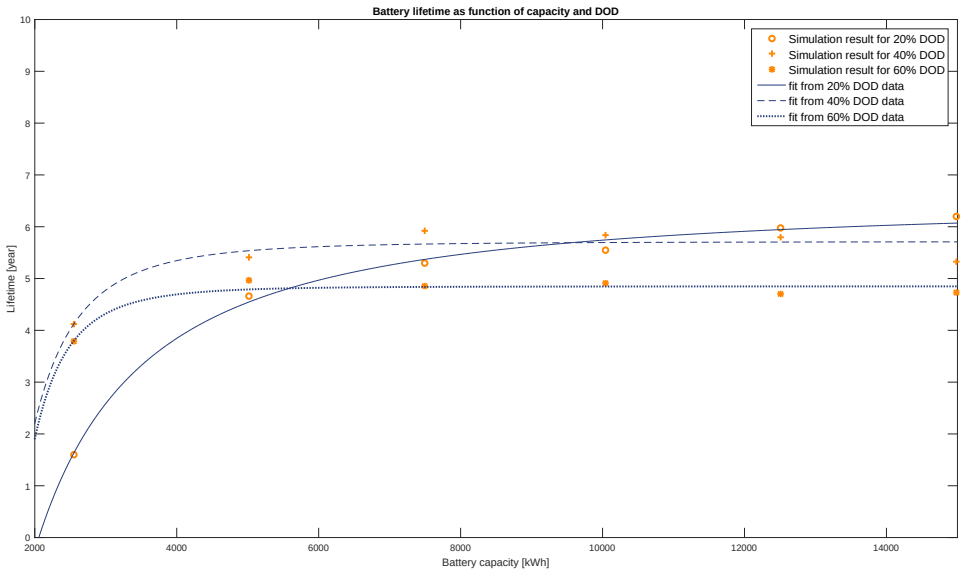

Figure 7.3: Battery lifetime as function of battery capacity and depth of discharge

will be further away from the maximum state of charge. This is beneficial for the cycle life of the battery. From the 15 minute filter onwards the battery capacity had to be increased to around $5MWh$ to enable the delivery and storage of the larger amounts of energy. With regards to cycle life the peak shaving function with a battery is not viable. For this purpose the use of super capacitors would be better. There is no clear fuel saving potential in peak shaving as was discussed in chapter 4 and no running hour reduction is possible, or very limited. This information combined with the rapid ageing of the battery makes investing in batteries for peak shaving unfavourable. For this reason the results of simulation 25 to 30 will not be discussed any further.

The last graph with lifetime values is presented in figure 7.4b. The results presented here were derived from the simulations without auxiliary generators. It should be noted that these simulations have been individually tuned. For this reason the lifetime found in this graph is somewhat higher than the values found in figure 7.3.Again it is clear that for small battery capacities the optimization of the engines creates a power gap that is to large for the batteries. The effect of the generators not meeting the actual power demand and leaving a power gap for the battery is less of influence for the larger batteries. Nevertheless it seems that this effect becomes less and less when increasing the battery capacity further than $12500kWh$.

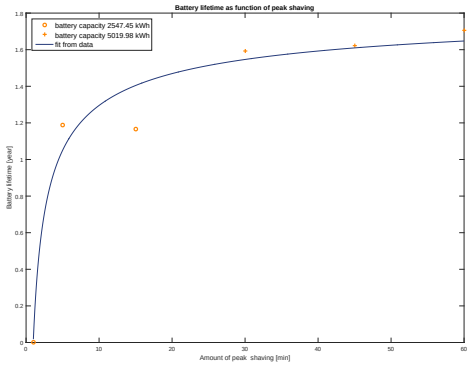

(a) Battery lifetime as function of the amount of peak shaving

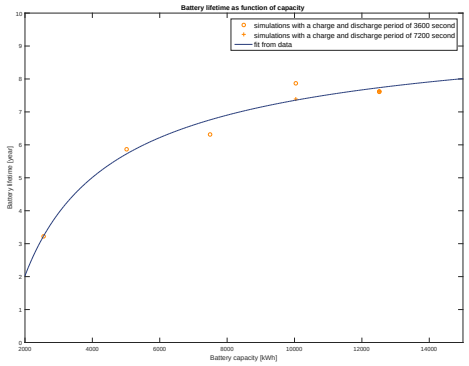

(b) Battery lifetime as function of its capacity for simulations without auxiliary generators

7.1.4. Carbon dioxide

In the introduction of this section the need for a CO_2 conversion factor was expressed. When the composition of a fuel is known one can calculate the amount of CO_2 that is emitted if such a fuel is completely burned. However with heavy fuel oil this composition is not constant. The fuel composition depends from bunker moment and bunker port. This same problem is also noticed by the International Maritime Organisation (IMO) when they developed new legislation on energy management and emission control. The IMO proposes fixed conversion factors to convert metric tonnes of fuel to metric tonnes of CO_2. These conversion factors are adopted for this thesis in order to relate CO_2 reduction to potential savings or increased cost. The conversion factors are found in Coordinator of the discussion at MEPC69 [2016] and presented in table 7.6.

Table 7.6: CO_2 conversion factors

Fuel type	Conversion factor $[Mt\ CO_2\ /\ Mt\ Fuel]$
HFO	3.114
MDO	3.206

In the following sections the term “cost per ton of reduced carbon dioxide”, or $€/Mt\ CO_2$, will be introduced. As it turns out, the hybrid system will not necessary lead to an increased profit for Van Oord. This means that the hybrid system will increase the cost of the CSD. However, since there is a reduction in fuel consumption there will also be a reduction in CO_2 emission. The “cost per ton of reduced carbon dioxide” will give a handhold to determine the most cost effective way to reduce carbon dioxide emission. Strictly speaking the cost per ton CO_2 reduced is the price that Van Oord has to pay for less greenhouse gas emission. This should not be mistaken for the Social Cost of Carbon (SCC) as it is introduced in numerous climate change studies [Daniels et al., 2012; EPA, 2015]. The SCC is an estimated value of the cost for society if no emission reduction is achieved. Although SCC is different than the “cost per ton of reduced carbon dioxide” it is still worth mentioning. In fact, increased cost for Van Oord while reducing CO_2 emission, might result in reduced cost for society on the long run! In Daniels et al. [2012] multiple criteria are used to determine the cost of carbon dioxide emission for society, therefore there is a wide margin for uncertainty in the results. Social impact of a ton CO_2 emitted in 2020 might range from $€17/Mt\ CO_2$ to $€157/Mt\ CO_2$. This figure can increase to $€224/Mt\ CO_2$ in the year 2050. These values can be used to put the simulation results in perspective.

7.1.5. Simulation 1-24

As discussed earlier, the simulation is split in three different strategies. The first part of the simulation was done to investigate the influence of power management settings on the overall performance of the system. The results of simulation one to 24 have been presented in chapter 6. These results combined with the information and financial parameters as derived in this chapter give insight in the effects of the different PMS settings.

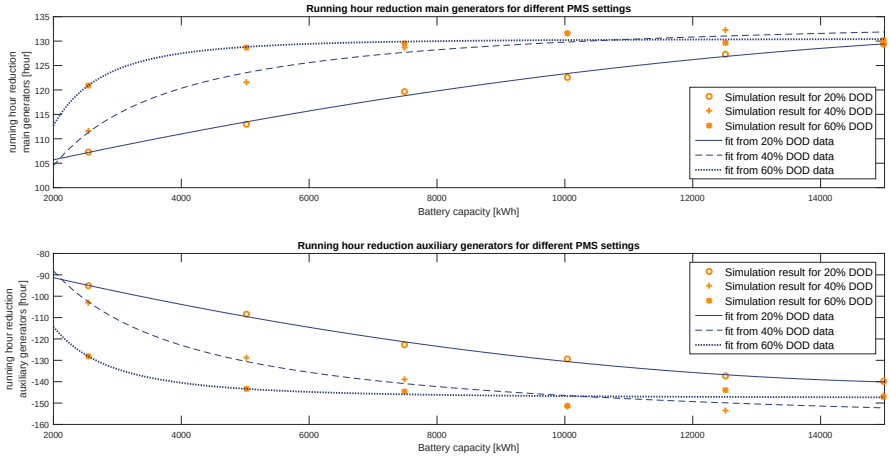

Figure 7.5: Running hour reduction as function of battery capacity and PMS settings

In figure 7.5 the reduction of running hours is presented for different battery capacities and three different PMS set-points. In simulation one to 24 the auxiliary generators are used in combination with the main generators. This results in more running hours for the auxiliary generators than in the original system. It can be seen from figure 7.5 that the reduction in running hours for the auxiliary generators is therefore presented as negative value. As it turns out the PMS setting where the depth of discharge is set to 60% results in the highest running hour reduction for the main generators. However this effect is counteracted by the increase in running hours from the auxiliary generators. Actually the same effect is visible for the fuel consumption figures. The fuel consumption figures are presented in figure 7.6. Again the 60% DOD set-point will result in the highest reduction of HFO. Due to the fact that the running hours of the auxiliary generators will increase also the fuel consumption of these generators will increase.

Figure 7.6 gives an insight in the effect of the different PMS settings on the fuel consumption of the main generators and auxiliary generators separately. This does not give enough information to see if the different configurations actually have an effect on the net fuel consumption. The net fuel consumption is presented in figure 7.7. It is decided to show the results here without the different power management settings. It would not be wise to compare fuel reduction in this way since both HFO and MDO are combined in this figure and this figure gives no information about the ratio between the two types of fuel.

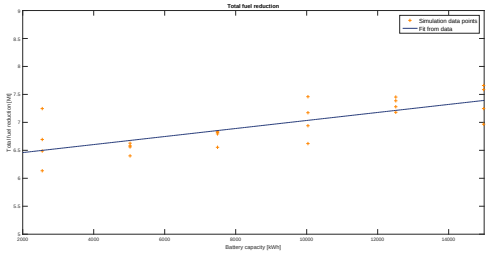

Figure 7.7: Total fuel reduction as function of battery capacity

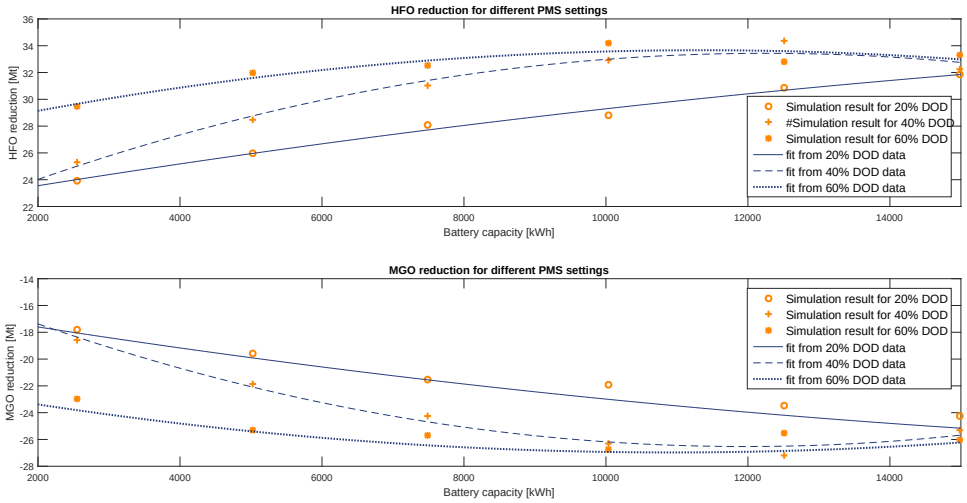

Figure 7.6: HFO and MDO reduction as function of battery capacity and PMS settings

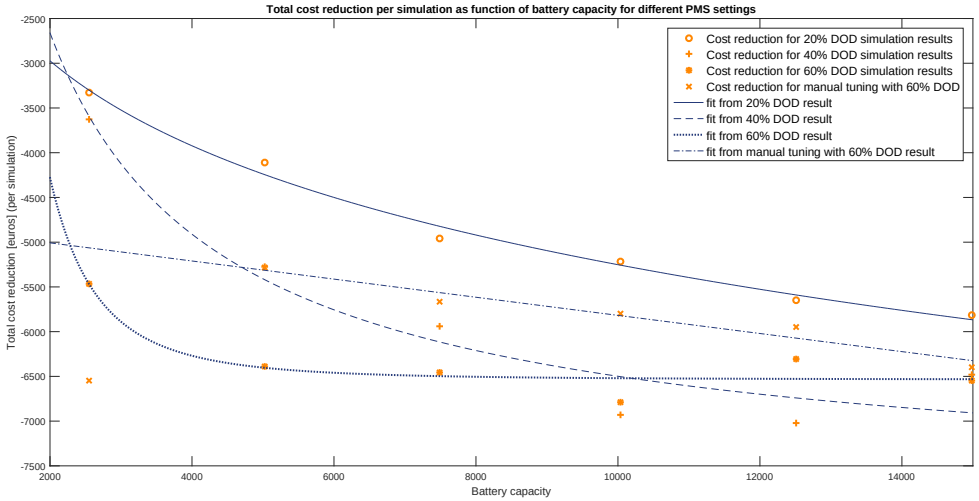

Figure 7.8: Total cost reduction as function of battery capacity and PMS settings

As explained the fuel consumption figure for these simulation is actually a combination between to different types of fuel. The fuel price that was introduced is different for HFO and MDO. The same should hold for the cost of running hours. One running hour with a Caterpillar is more expensive with regards to maintenance than a running hour with one of the main generators. According to engineers at Van Oord with experience in the engine room a factor of 1.75 can be used as an approximation. This means that one hour with the auxiliary set is 1.75 times as expansive as one hour with one of the main generators. This can easily be explained, first of all the auxiliary generators are high speed diesel engines which wear out quicker than medium speed engines. The auxiliary generators have more cylinders as well. As a rule of thumb the maintenance cost are related to the number of cylinders. The last point which explains the difference in maintenance cost is that every 500 hours the oil should be refreshed for a Caterpillar whereas lubrication oil of the Wärtsilä main generators is run through separators. The difference in maintenance cost and the difference in fuel price is clearly visible in the total cost reduction. Figure 7.8 represents the total cost reduction for the different simulations. It can be seen that the cost reduction is displayed negative, in fact there is only an increase in cost. For this reason it is decided that it does not make sense to extrapolate these figures to full year operation. The investment cost have not been added to the total financial result. It can be concluded that is not a good

idea to let the auxiliary generators participate in the overall power generation system. Simulation one to 24 however give information about the PMS settings. The highest potential in reducing fuel consumption and running hours of the main generators is found with a DOD setting of 60%. To recapitulate 60% DOD means a minimal state of charge of the battery of 20% and a maximal state of charge of 80%. These settings are used as input for simulation 31 to 38.

7.1.6. Simulation 31-38

The result of simulation 31 to 38 is comparable with the results of simulation one to 24. The main difference is that the use of auxiliary generators is disabled. During these simulations the depth of discharge setting in the power management system is set to 60% DOD. In the first round of simulation it turned out that this setting yielded the best result in terms of reduction of running hours and reduction of fuel consumption for the main generators. For simulation 31 to 38 the minimal load factor of the main generators had to be changed. The reason for this change in settings was previously introduced in chapter 6 but will be shortly recapitulated here. The minimal load factor had to be lowered for smaller battery capacities since otherwise the gap between power demand and power supply from te generators would become to large for the battery to overcome. In previous simulations this gap was limited due to the use of the auxiliary power. It could be seen that with an increasing battery capacity the minimal load factor can be brought back to its intended 75% MCR. From figure 7.9a and figure 7.9b it can be seen that this changing of the minimal load factor has an influence on the reduction of running hours and fuel consumption respectively. Naturally a constant reduction in running hours and MDO is achieved since the auxiliary generators are not used at all. This result is a substantial reduction in running hours and fuel consumption.

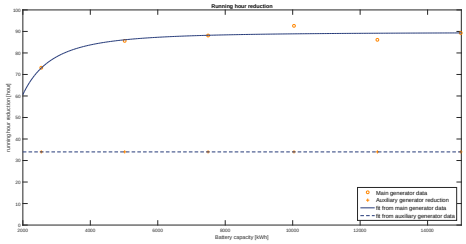

(a) Running hour reduction as function of battery capacity

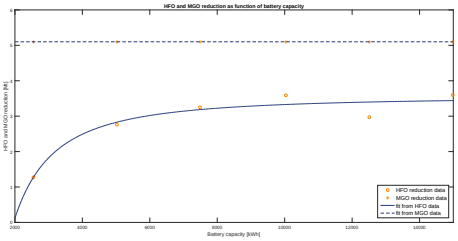

(b) Fuel consumption reduction as function of battery capacity

Combining the reduction in fuel consumption and running hours with the derived prices for fuel and running hours one is able to construct lines of cost reduction as function of battery capacity. This is done for the current fuel prices and for a range of potential future fuel prices. In this analysis it is assumed that the maintenance cost related to running hours is not subjected to change. The result of this calculation is presented in figure 7.10. The values visualised in figure 7.10 are extrapolated to values for a full year of operation. The results of one simulation are extrapolated using the so called multiplication factor mf. This multiplication factor is determined using the values as presented in table 7.7.

Table 7.7: Extrapolation multiplication factor

days simulated	6
hours simulated	144
yearly operational hours	4000
multiplication factor	$mf = \frac{4000}{144} = 27.7$

Similar to the potential cost reduction the investment cost is related to yearly cost. From figure 7.2 the battery price can be determined. The battery lifetime is presented in figure 7.4b. Both battery price and battery lifetime are presented as function of battery capacity. In order to relate the investment cost to a certain cost per year it is decided to express these yearly cost as depreciation of the battery. For

this analysis it is assumed that the battery is linearly depreciated over its calculated lifetime. The yearly depreciation is than the initial battery price divided by its lifetime. Since the depreciation is a function of the battery price per kWh and battery lifetime it is decided to plot results for different battery prices and or different life expectancies. The yearly depreciation as function of battery capacity for different scenarios is visualised in figure 7.10.

Note that the battery lifetime is expressed as the amount of years that is takes to reach 80% of its initial capacity. This means that a battery with a capacity of 5 MWh still has a capacity of 4 MWh after its calculated lifetime. If the power management system settings are changed accordingly the battery might be used for a longer time, increasing its potential

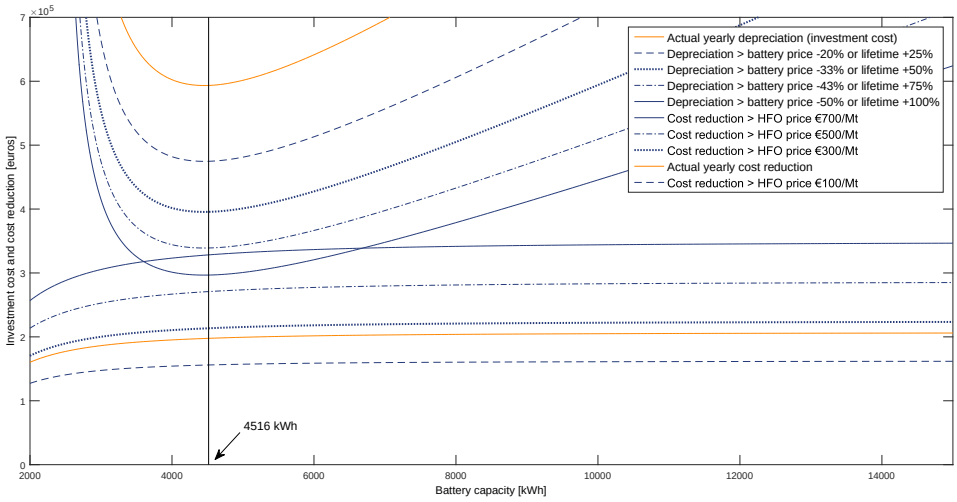

Figure 7.10: Total yearly cost reduction and yearly depreciation as function of battery capacity

From figure 7.10 it can be seen that there is a certain optimum in terms of battery capacity. Notice that the potential yearly cost savings are lower than the yearly depreciation. However the difference between depreciation and savings is minimal at a battery capacity of around 4500 kWh. At this capacity the actual cost for fuel reduction and corresponding CO_2 reduction is the lowest. The values of fuel reduction, CO_2 reduction, running hour reduction, investment cost, battery lifetime and other interesting constants are presented in table 7.8. Note that the reduction values presented here are totals for one year of operation.

Table 7.8: Financial results for the optimal battery capacity

battery capacity	4516	$[kWh]$
investment cost	3,045,700	[€]
battery lifetime	5.13	$[years]$
depreciation	593,430	[€]
running hour reduction		
main generators	2366	$[hours]$
auxiliary generators	944	$[hours]$
HFO reduction	74.65	$[Mt]$
MDO reduction	141.67	$[Mt]$
CO_2 reduction	687	$[Mt]$
price per ton CO_2 reduced	576.31	$[€/Mt\ CO_2]$

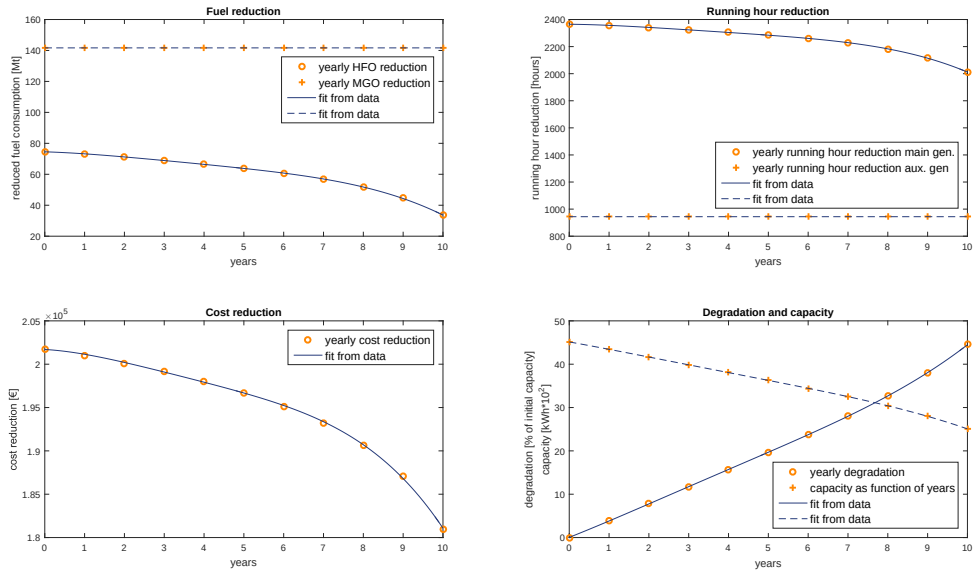

Figure 7.11: Fuel reduction, running hour reduction, cost reduction and battery capacity in case of battery lifetime extension

It is decided to continue on the side note that it might be possible to extend the battery lifetime. The battery lifetime extension can be achieved by degrading the battery further than 20%. This can be done since the original power plant of the Athena and Artemis has not been changed. The battery is actually an extra feature. This implies that the system can still work properly with a battery that is degraded to zero percent of its initial capacity.

Using the trend lines presented in figures 7.4b, 7.9a and 7.9b the yearly degradation, the reduction in running hours and the reduction in fuel consumption can be found as function of battery capacity. Since the battery will loose capacity over the years it is decided to analyse the behaviour of the battery every year, so with different capacities. In figure 7.11 the effect of the degradation of the battery is presented. It can be seen that the fuel reduction, the running hour reduction and the corresponding cost reduction will become less over the years. It is found out that with the initial battery capacity of 4516 kWh the battery will last around ten years. After that period the system will require more fuel than in its original form, so from that point it does not make sense to use the battery any longer.

In the previous sections general relations for fuel consumption and CO_2 emission were derived. Using this relations and the values presented in figure 7.11 a value for the total CO_2 reduction over ten years can be determined. Besides that the totals for fuel reduction and running hour reduction can be found. These values are presented in table 7.9. As was expected the use of batteries will not result in a profit however, when the battery is used to its maximum valuable lifetime the cost per ton of CO_2 reduction can be reduced. When the battery is used over a period of ten years the cost per ton CO_2 that is **NOT** emitted is around €125. This price is approximately 4.5 times lower than was found in the initial result.

7.1.7. Special cases of operation

During the research the question was raised how the hybrid system would perform if the CSD had to operate solely on MDO. This question is valid in the sense that the CSD operates in ports close to urban environments which might be subjected to Emission Control Area (ECA) regulations. An ECA implies that in such an area rules and regulation restrict the emission of certain pollutants. If the CSD has to operate in a Sulphur emission Control Area (SECA) it can not run on HFO since this would result in high values of sulphur emission. In that case the dredger has to operate on a lighter fuel like MDO which has a low sulphur content. For the machinery this is no problem however, it will result in higher operating cost since MDO is around 1.75 times as expensive as HFO.

Table 7.9: Financial results for the optimal battery capacity with extended lifetime

battery capacity	4516	$[kWh]$
investment cost	3,045,700	[€]
battery lifetime	10	$[years]$
depreciation	304,570	[€]
running hour reduction		
main generators	24770	$[hours]$
auxiliary generators	10384	$[hours]$
HFO reduction	666	$[Mt]$
MDO reduction	1558	$[Mt]$
CO_2 reduction	7069	$[Mt]$
price per ton CO_2 reduced	127.60	$[€/Mt\ CO_2]$

In order to calculate the fuel consumption and fuel reduction when running on MDO one should convert the HFO values to representative MDO values. For this conversion it is proposed to use values for density and LHV as derived in chapter 4. The values used for this conversion are presented in table 7.10. This small analysis will be based on the values derived for simulation one to 38 which are presented in table 7.8. The results for running on MDO are presented in table 7.11. It turns out that even when running on MDO there is no profit potential in the hybrid system. However, it will result in a lower cost per ton CO_2 emission that is reduced. The difference between running on HFO and MDO per ton CO_2 reduction is €22.63. Interesting to see is that besides the fact that the CO_2 conversion factor for HFO and MDO are different, the total yearly CO_2 reduction is equal for running on HFO and MDO.

Table 7.10: Fuel properties used to convert HFO consumption to MDO consumption

fuel type	density ρ^{15} $[kg/m^3]$	LHV $[kJ/kg]$
HFO	965	41360
MDO	838	42828

Table 7.11: Fuel and CO_2 reduction while running on MDO

values for simulation duration		
original HFO consumption	298.3	$[Mt]$
simulated HFO consumption	295.6	$[Mt]$
original consumption converted to MDO consumption	288.1	$[Mt]$
simulated consumption converted to MDO consumption	285.5	$[Mt]$
simulated MDO reduction (*main gen.*)	2.6	$[Mt]$

values extrapolated to one year operation		
MDO reduction (*main gen.* + *aux. gen*)	214.4	$[Mt]$
CO_2 reduction	687.5	$[Mt]$
price per ton CO_2 reduced	553.68	$[€/Mt\ CO_2]$

Besides the *general* working profile which was derived in chapter 2 three other working profiles were used as input for the hybrid model. These three projects were also introduced in chapter 2. The three projects, JNPT, Jebel Ali and DOHA are analysed in terms of soil conditions and discharge line configuration in appendix **??**. The three projects have been simulated using the hybrid cutter model with a battery capacity of 4516 kWh. The results of these simulations together with the results of the general working profile simulation in terms of fuel and running hour reduction are presented in table **??**. The results are presented as an absolute value and a relative value. The relative reduction of running hours and fuel consumption gives a better representation than the absolute values since the original fuel consumption and running hours differ per project. The reduction of MDO and auxiliary generator running hours will not be presented in a relative way since these reduction values are always 100%.

As it turns out, the hybrid system performs better in projects like the JNPT project where the power demand is low. If power demand is increased it is clear that the potential savings achieved with the hybrid system become less. In previous sections the lifetime of the battery for different capacities was derived. This is also done for the three individual projects that are simulated. The lifetime of the battery (*to 80% initial capacity*) is 27, 18 and two years for the JNPT, Jebel Ali and DOHA project respectively. If it is assumed that the fuel price and maintenance cost will not change over the coming years (*which is of course not realistic, prices will probably go up*) and the simulated project represent a full year operational profile, the payback time of the hybrid system can be calculated. The payback time for the JNPT, Jebel Ali and DOHA project is 10, five and 17 years respectively. With this information it can be concluded that the hybrid system may be a profitable investment if the yearly power demand distribution approaches the power demand of the JNPT and especially the Jebel Ali project.

Table 7.12: Performance of the hybrid system for different projects

Project	HFO reduction $[Mt]$	HFO reduction $[\%]$	running hour reduction main generators $[hours]$
KNPC (*general working profile*)	2.7	0.9	85
JNPT	20	23	72
Jebel Ali	12	4.6	86
DOHA	34	8.6	35

Project	running hour reduction main generators $[\%]$	MDO reduction $[Mt]$	running hour reduction aux. generators $[hours]$
KNPC (*general working profile*)	24.1	5	34
JNPT	49.7	3	20
Jebel Ali	26.5	22	139
DOHA	9.4	7	41

7.2. Physical impact of the chosen battery capacity

In the previous section a battery capacity of 4516 kWh was found to be the most cost effective possibility to save fuel and reduce CO_2 emission. However, no information has been shared about the physical impact of such a battery on the ships design. The size and weight of the battery actually follows a linear relation. The battery pack is build up from individual battery units. The total system can be scaled to achieve a desired battery capacity. Since the independent batteries have a certain weight and geometry the total weight and space requirement can easily be derived.

Different suppliers offer different battery packs. It is interesting to see that the technology they use does not result in extreme differences in weight and volume. The weight of the total 4516 kWh battery pack will be between the 40 and 60 tons whereas the footprint will vary from 20 to 40 square metres. Precise results of the weight, volume and footprint calculations are presented in table 7.13. The values derived for the batteries of Spear Power Systems, Corvus Energy and Super B were taken from Eppler [2014]; Fry [2016]; Hauso [2015]; Super B b.v. [2016] respectively.

Table 7.13: Physical properties of a 4516 kWh battery from different suppliers

Supplier	weight $[Mt]$	volume $[m^3]$	footprint $[m^2]$	number of racks
Spear Power Systems	43.2	50.4	35.2	32
Corvus Energy	55.8	48.9	22.2	36
Super B	57.6	62.9	40.1	86

8

Final conclusion and recommendations

In the introduction of this thesis a main research question was derived. The main goal of this thesis has been to answer the research question in order to give Van Oord insight in the potential of hybrid technology with the use of batteries for their large cutter suction dredgers. This chapter will finalise this research by providing an answer to the research question in the form of a conclusion. The sub-questions as presented in chapter 1 will be discussed as well. After the conclusion is presented the final result will be discussed and put into perspective. This chapter will end with recommendations for further research in the hybrid field with special focus on the dredging industry.

8.1. Conclusion

To end up with an answer on the main research question, the sub-questions will be answered first. The goal of these sub-questions was to provide an understanding of the individual components in a hybrid system and how they interact with each other. The three sub-questions that will be answered are stated below.

1. *What are the main variables determining the size of the battery?*
2. *Which variables influence the fuel consumption in a hybrid system?*
3. *Which variables determine the running hours of the diesel generators in a hybrid system?*

The first sub-question has a trivial answer, the size of a battery in terms of volume and weight is linearly dependent from the capacity. However, the coefficients in these relations are dependent from the chosen manufacturer. The answers to the second and third sub-question are more interesting to discuss. The fuel consumption of the hybrid system is dependent from the battery capacity up to a certain point. Small battery capacities force the PMS to allow a wider load factor bandwidth, resulting in a lower average load factor. This is necessary to ensure a reasonable battery lifetime (*with the current state of the art batteries*). The lower average LF reduces the potential to operate the diesel generators at their best efficiency point, thus reducing the fuel savings. However, a really large battery will not increase the fuel saving potential either. At a certain capacity, the optimal system efficiency is reached. In other words, the engines run at their best efficiency point as much as possible. Increasing the battery capacity further than this optimal capacity will not increase the fuel savings. This result is found by evaluating the results of simulation 31 to 38. In these simulations the battery capacity has been increased in a systematic way to derive trends between battery capacity and fuel savings. A similar trend is found for the running hour reduction. An optimal battery capacity can be found in terms of running hour reduction. Increasing the capacity further will not influence the running hours of the generators. This can be explained by the fact that the battery has to be charged as well. A really large battery will allow a longer off-line period for the generators. However, the on-line period to recharge the batteries will be longer as well.

During the process of investigating the parameters that influence the fuel consumption of a hybrid system special attention is given to peak shaving. Peak shaving is in fact a filter which shaves the peaks and troughs from a power demand signal. This filter can be a battery, which supplies power during a peak and stores power during a trough. The effect of such a system is that the transients in the power demand are reduced, or filtered out completely. During this study it is found that transients in the load profile of the diesel engines do not affect the efficiency of these diesel engines. This is mainly caused by the fact that the mechanical efficiency and the combustion efficiency will not change due to transients. The mechanical efficiency is dependent from the rotational speed and this speed is constant (*generator mode*). Due to the fact that the engines under consideration have a sufficiently large air excess ratio, the combustion efficiency will not be influenced by transients either. The conclusion that was stated is that the efficiency of a diesel engine running on a constant speed with a sufficient charge air pressure is not affected by transients in its load profile. Based on this conclusion it can be said that peak shaving with a battery will not reduce the fuel consumption of a hybrid CSD. Simulations 25 to 30 confirmed that the reduction of fuel consumption by peak shaving is minimal or even non existent. Next to the fuel consumption figures, it turns out that the battery lifetime is reduced significantly when the battery is used for peak shaving. Battery lifetimes from almost zero to 1.8 years are found for the different peak shaving simulations.

In the preliminary stage of this study several simulation strategies have been proposed. First of all simulations have been done with the whole system operational. This means that main generators and auxiliary generators are both used in the simulation. Using a systematic iteration approach the response of the system was analysed for different power management settings and different battery capacities. The minimal and maximal SOC set-points in the power management system were varied. It turned out that due to the relatively expensive running hours and fuel of the auxiliary generators this set-up was not viable. However, important information about the battery lifetime in relation to the PMS settings was found. It proves to be beneficial to use the battery in a range from 20% SOC to 80% SOC with regards to battery lifetime.

From this point it has been decided to evaluate the system without the use of the auxiliary generators. This proved to be beneficial for the reduction of operating cost, both in terms of fuel consumption and in reduction of running hours. The structure of the simulations is again based on a systematically increase of battery capacity. Furthermore the load factor set-points have been changed according to the battery capacity. Smaller battery capacities required more flexibility in terms of minimal and maximal load factors. The SOC set-points were kept on 20% and 80% for minimal and maximal SOC respectively. This combination enabled a trend analysis in which reduction of fuel consumption and reduction of running hours is related to battery capacity. This trend analysis is used to answer the main research question.

The main research question as proposed in the beginning of this report was the following;

What should be the size and capacity of a battery in a hybrid electrical grid of a cutter suction dredger to reduce fuel consumption and running hours of diesel engines in such a way that it is cost effective?

The optimal battery capacity is found to be 4516 kWh. At this capacity, the best balance is found between investment cost, battery lifetime, fuel savings and reduction in running hours. Together with this capacity, the following optimal power management settings are found: a minimal SOC of 20%, a maximal SOC of 80%, a desired load factor of the diesel engines of 85% MCR with the possibility to fluctuate between 75% and 95% MCR and a minimal off-line period for an engine of one hour.

This optimal battery capacity was derived for an operational profile which represents a full year operational profile in the best way possible. However, with this battery capacity the hybrid system has been analysed for three different operating conditions as well. It can be concluded that the potential of the hybrid system is the highest during barge-loading operation. In this “off-design” condition a relative fuel reduction of around 23% was achieved, together with a running hour reduction of around 50%. The potential of the hybrid system for the general working profile is much lower. The relative reduction in fuel consumption and running hours for the general working profile is around 4.5% and 24% respectively.

The conclusion answers the main research question as strict as possible. However, it provides very little insight in the effects and future potential of the hybrid system. Furthermore, the main research question states that the system should be cost effective. At this moment the system will not contribute to an increased profit. This is caused by three factors. First of all the fuel price is low at this moment, which diminishes the cost saving potential of reduced fuel consumption. The second aspect is the high investment cost, which is related to the battery price. Finally the lifetime of the battery is not as high as anticipated, reducing the time to earn back the investment. In order to understand these effects it was decided to calculate the financial result for different fuel prices, different battery prices and different battery cycle life values. It turns out that the hybrid system will break even when the fuel price reaches €700 per ton HFO and the battery price drops to €414 per kWh. The current fuel and battery price are €222 and €828 respectively. It is assumed that the break even prices will not be reached soon, therefore the system will not be cost effective in the near future.

Keeping in mind that the system is strictly speaking not cost effective, another measurement criterion is introduced. The main driver of this research has not been a potential higher profit, but cleaner operation of the cutter suction dredger. The hybrid system is able to reduce fuel consumption. Therefore it also reduces carbon dioxide emission. For this reason, it is decided to evaluate the price that Van Oord has to pay, in order to reduce one ton CO_2 with a hybrid system. The battery capacity of 4516 kWh will result in the lowest cost per ton CO_2 reduced. The annual carbon dioxide emission reduction will be 687 tons, which is an emission reduction of approximately three %. This translates to a cost of €575 per ton of CO_2 emission that is reduced. If one would change the fuel type from HFO to MDO this price tag is reduced to €554 per ton CO_2 reduction. Further analysis has proved that if the battery lifetime is extended, by adapting the power management settings to the actual residual battery capacity, the cost for CO_2 reduction can be lowered. This is a trivial result, since less carbon dioxide is emitted for a longer period, while keeping an equal investment. It is very beneficial to extend the battery lifetime in this way, the cost per ton CO_2 reduction can become as low as €128 per ton. The three % CO_2 reduction is found for the general working profile, which represents a full year of operation. For individual projects the CO_2 reduction can be as high as 26% (*see appendix A for the JNPT project*).

These cost per ton of reduced CO_2 emission can be put in perspective by presenting the social benefits of CO_2 reduction. The reduction of one ton CO_2 in the year 2020 can save the Dutch society €17 to €157. These figures are estimates for the cost for society as result of climate change. It is expected that the effects of climate change will increase exponential over the years, therefore the reduction of one ton CO_2 in 2050 might save society up to €224.

8.2. Discussion

In this section, the conclusion as presented in the previous section will be put in perspective. What happens if the boundary conditions on which the conclusion was based change?

First of all the influence of the fuel price should be looked at. It is known that the fuel price is very low at this moment. The financial analysis has been executed for fuel price of €500 per ton of HFO. This value was the highest fuel price recorded in Rotterdam since 1990. Even with this fuel price the hybrid system will not be cost effective. The same holds for a lower battery price. It is expected that the price for batteries will become lower in the coming years. For this reason, different battery prices have been examined. It turns out that even when the battery prices halves over the coming year,s the hybrid system will not be cost effective (*with current fuel prices*). The hybrid system in this configuration will only be cost effective if the battery prices halves (*or lifetime doubles at the same price*) **AND** the fuel price reaches a value of around €700 per metric ton of HFO. This seems to be an unrealistic prognosis for the nearby future.

The conclusion is based on a battery lifetime as presented by battery manufacturers. Most battery suppliers state that their batteries reach their end of life when the capacity has dropped to 80% of the “new” capacity. The cutter suction dredgers under consideration in this thesis still have their fully equipped engine rooms and thus can always fall back on their original functionalities. This opens the possibility to degrade the batteries to the capacity where they do not contribute to fuel reduction and running hour reduction any more. It turns out that the battery lifetime is then extended from five years to ten years. This increases the saving potentials significantly, whilst keeping the investment cost equal. This process can be optimized since power management settings were derived for a wide range of battery capacities. Unfortunately, with this approach the hybrid system still does not become cost effective. After ten years around 2.1 million Euros is saved whereas the investment stays around three million. However, the cost for CO_2 reduction can be minimised. Over the ten-year lifetime of the battery,a reduction of around 7069 ton of CO_2 emission is achieved. This results in an increased cost, for Van Oord, of €128 per ton CO_2 reduction.

Until now, all the analyses have been based on a way of operating that has the highest probability to occur. The system will run most of the time on heavy fuel oil and will most probably encounter a working profile as has been developed in this thesis. This working profile is referred to as the *general* working profile. However, it might be possible that the cutter suction dredger will have to work under different circumstances, like operation on marine diesel oil. This MDO is more expensive than HFO, which might influence the business case of the hybrid cutter dredger. After analysing the change from HFO to MDO, the same result was found as for a higher fuel price. A higher fuel price alone is not enough to result in a potential profit. It has been found that running on MDO will reduce, the price per ton CO_2 reduction, from €575 to €554.

The operational profile of the cutter suction dredger has been established as a *general* operational profile that approaches the actual full year operational profile power distribution as close as possible. This has resulted in an optimal battery capacity for a hybrid system. Interesting to see is how this hybrid system would perform under different circumstances. In other words what will be the results of the hybrid cutter model, for different power demand signals. It turns out that the hybrid system performs much better for the power demand signals that were logged during the JNPT project. Fuel reductions reach values of around 25% and running hour reduction of around 50%. If this is expressed in payback time, the battery will earn itself back in around ten years. The battery lifetime will be around 27 years, meaning that there are 17 years left to make a profit. The reason that the hybrid system performs better on this project is the fact that the average power demand is low. Only the submerged pump was used during the JNPT project. This was possible since the barge loading system was used, resulting in a short discharge line and thus limiting required pump power. Furthermore, the rock was easy to cut, therefore limiting the required cutter power. To top it all of, since the barge loading system was used there were quite some delays in between arrivals of the barges. The low average power demand resulted in stable charge and discharge cycles increasing battery lifetime. Due to the low power demand during the simulation, it was possible to shut engines down for a longer period and only work with power from the battery. The Jebel Ali project had a higher average loading of the diesel engines. This reduces the potential of the battery somewhat when compared with the JNPT project. During the Jebel Ali project the potential savings on the main generators are lower than in the JNPT project. The savings on diesel oil and auxiliary generator running hours on the other hand are much higher. The battery power can substitute the power from the auxiliary generators, resulting in high cost savings. If the payback time is calculated for the Jebel Ali project one will find a payback time of five years. The DOHA project has the highest average power demand. This results in limited savings potential when using the hybrid system. The high average power is not beneficial for the lifetime of the battery. The life expectancy of the battery is two years when simulating with the DOHA load profile.

8.3. Recommendations for future work

During this research several thoughts came up about interesting topics affiliated with the hybrid industry. In this section the topics of interest for hybrid applications in the dredging industry will be discussed. However, these topics might also be of interest for other branches in the maritime industry.

In the introduction of this thesis it is mentioned that several new techniques are available at today's market to reduce carbon dioxide emission. One of these techniques is the use of LNG as fuel. This possible solution for reducing carbon dioxide has not been looked into in this thesis. The reason for this is that the aim of the author has been to increase the efficiency of the cutter suction dredger. This is not necessarily achieved when making the transition form liquid fuels to LNG. However, this does not mean that one should not investigate the possibilities of the use of LNG in dredging applications. The last few months there has been made some effort within Van Oord to look into the possibilities for the use of LNG on their vessels. Interesting to see is that the response of an LNG fuelled engine is much slower than the response of an original diesel engine. The response of a gas engine compared with a diesel engine is visualised in figure 8.1 [MAK, 2014]. This might pose problems when operating in a dynamic environment in which frequent and large transients occur, such as operating an engine in a dredging application. One would expect that even a gas-fuelled engine would cope with high transient loadings better when running on a high average load. The contrary is true. According to Cimac Working Group "GAS ENGINES" [2011] the response of the gas engine will be worse when running on a higher average loading. To make matters even worse, the ability of the gas engine to cope with load steps is further decreased when the engine is operated at constant speed (*generator mode*). This inability of the gas engine to provide an instant response when power is demanded asks for an alternative solution. One option is to change the load profile in such a way that the power demand does not inhabit large transients. However, this might influence the production capabilities of the piece of dredging equipment. Another option to overcome the gap between power demand and power supply might be using additional energy storage devices. As is showed in this thesis, batteries might be the answer to this problem. Further research should be done on the combination of LNG powered machinery and electrical storage devices, thus a LNG hybrid system. Interesting in this is that the business case of the hybrid system will change significantly. The use of energy storage devices will no longer be an extra feature, but it will become a necessity.

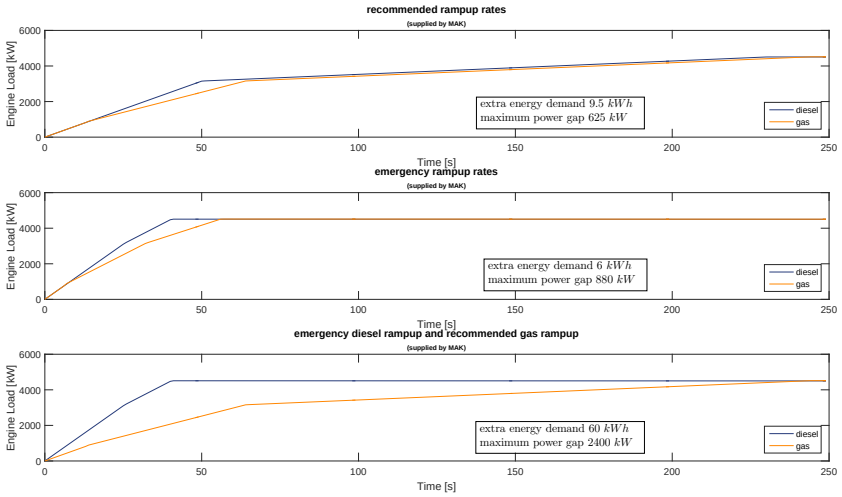

Figure 8.1: Difference in load acceptance for a gas and diesel engine

Another trend in the maritime industry is the use of a common Direct Current (DC) bus. According to ABB the common DC bus will result in significantly lower fuel consumption than conventional Alternating Current (AC) systems [Hansen et al., 2011]. The main reason for this is that the generator (*either diesel or LNG fuelled*) can adapt its speed to the power demand. So when little power is required by the system and the generator has to provide less power, it can lower its rpms. By lowering the speed of the generator the combustion engine will have a higher efficiency. This can be related back to the explanation given in chapter 4 about the efficiencies of a diesel engine in relation with transients in the load profile. The mechanical efficiency η_m of the engine will be higher when the speed is lowered, since the friction will decrease with lower rotational speed [Berger, 2002; Stapersma, 2010b]. This statement about the mechanical efficiency is partly true, since the dynamic mechanical efficiency will change when fluctuations in rpm values are allowed. In chapter 4 an introduction was given to the effect

of inertia on the performance of a diesel engine. This was further elaborated on in appendix D. For the Athena and Artemis it was determined that at nominal rpm around 44500 kJ of energy was stored in the diesel engines and their connected generators. If it is assumed as a side note that one wants to ramp up the engines from the Athena/Artemis from 300 rpm to 600 rpm in five seconds, this will require around 6500 kW of power just to overcome the rotational inertia! (*to prevent misinterpretation; the 6500 kW figure presents power. In a period of five seconds this translates to 32500 kJ which is around 9 kWh of energy.*) This same amount of power will be dissipated during ramp down. In the authors opinion this type of operation has a chance of being more efficient than the current system, only if a certain form of energy storage is used. Otherwise too much energy will be lost in the process of changing the engines' speed. Further research in this topic should provide figures about the actual fuel consumption of the system as a whole. Furthermore, the effect of changing rotational dynamics on the maintenance of the diesel engines should be taken into account. Only then one is able to say if a common DC grid with energy storage devices is viable.

It is already mentioned that there is not enough knowledge about the effect of changing rotational speeds on the maintenance of a diesel engine. During literature research it was noticed that there is very little known about the parameters determining wear and tear of a diesel engine in general. Not only changing rotational dynamics might influence the wear of an engine, but also the change in loading might cause increased wear and tear. Suppliers of hybrid systems claim that a hybrid system and especially when it is used for peak shaving can reduce maintenance cost. However, this cannot be proven at this point. The only information about this topic that was retrieved from a source working at Wärtsilä, is that a higher average loading of an engine increases wear. Still no quantities and hard figures were found. It is a fact that a hybrid system will reduce transients in the load profile. The reduction of transients is clearly visualised in appendix K. In this appendix the power output of the generators is plotted for the original system and for the simulated hybrid system. Further research into the cause of wear and tear, especially the effect of transients in the load profile on the wear and tear of the engine should be done. This will most probably influence the potential of a hybrid system in a positive way!

In this thesis efforts have been made to determine the effects of transients in the load profile of a diesel engine. The conclusion states that transients in a load profile of a diesel engine running on constant rpm with an air excess ratio that is sufficiently high will not affect the efficiency of that engine. In chapter 4 the results of this analysis were presented. It was seen that the overall specific fuel oil consumption was higher than would be expected from the factory acceptance test results. It would be interesting to find out which factors (*in our uncontrolled measurement environment*) caused this result. Furthermore it might be worthwhile to do controlled experiments to investigate the effect of transient loading on fuel consumption. The author can imagine that this would be a kind of research that can be done on the MAN installed in the test facilities of the NLDA in Den Helder.

To finalise this section of recommendations, the effect of engines types in the hybrid system will be discussed. During simulations it was found that the largest savings were gained if the auxiliary engines were shut down. These engines have a relatively high specific fuel oil consumption and are more expensive in maintenance. It is proposed to do further research into the performance of the hybrid system incorporated in a smaller CSD. The smaller cutter suction dredgers are equipped with smaller high-speed diesel engines instead of large medium speed engines. The benefits and potential savings of the hybrid system might be more distinct than was found in this thesis. In the same line of thought it is also proposed to adept the hybrid model to incorporate different engines. By changing the number of installed engines and the engine output power more configurations of hybrid systems can be evaluated. It turned out that the Athena and Artemis are rather efficient machines. However, dredgers with a less advanced power generation system might have more benefit of a hybrid system.

I wish everyone taking on these proposed (*further*)research topics the best of luck! The author.

A

Background on the working profile

In chapter 2 several dredging projects are introduced. These projects are executed with CSD Artemis. For the different projects histograms are constructed to get a feeling for the power demand distribution. It turned out that the power demand distributions were really different from project to project. In this appendix the projects will be reviewed once more to find an explanation for the difference in power demand.

The first project that was adopted from Rensen [2014] and introduced in chapter 2 is the JNPT project. During this project the CSD Artemis was chartered by another dredging company. The work was executed in India, in the sheltered bay of Mumbai. Interesting from this project is that the barge loading installation was used. This means that there is no long discharge line connected to the dredger. The soil consist of weathered rock and fresh rock, mostly columnar basalt. The soil was in fact easy to cut due to the high vertical fracturing. The teeth were more used as chisel than for cutting [Geus, 2013].

The power demand during the JNPT project was mainly low (<$7000\ kW$). The following reasons can be addressed;

1. Use of the barge loading system, which means a short discharge line. So limited pump power is required, in fact only the underwater pump is used.
2. Soil conditions are favourable, limiting the cutter power that is required.

The average power distribution is presented in the form of a Sankey diagram in figure A.1. From figure A.1 it can be seen that the total average power consumption is low. This was already found in chapter 2 and is confirmed again. The three megawatt input from the main generator results in an average loading of the main generator of around 40%, whereas for the auxiliary input the auxiliary generator is loaded for 49%. In this case it would be wise to shut the auxiliary generator down and work only with one main generator. It might be possible that the response of system is to slow in that case according to the operator. Proving the potential of the battery pack. In order to investigate the response of the hybrid system as derived in chapter 7 two simulations were done. One simulation to investigate the original behaviour of the system during the JNPT project and one simulation to see how the hybrid system would perform. The results of both simulations are presented in table A.1.

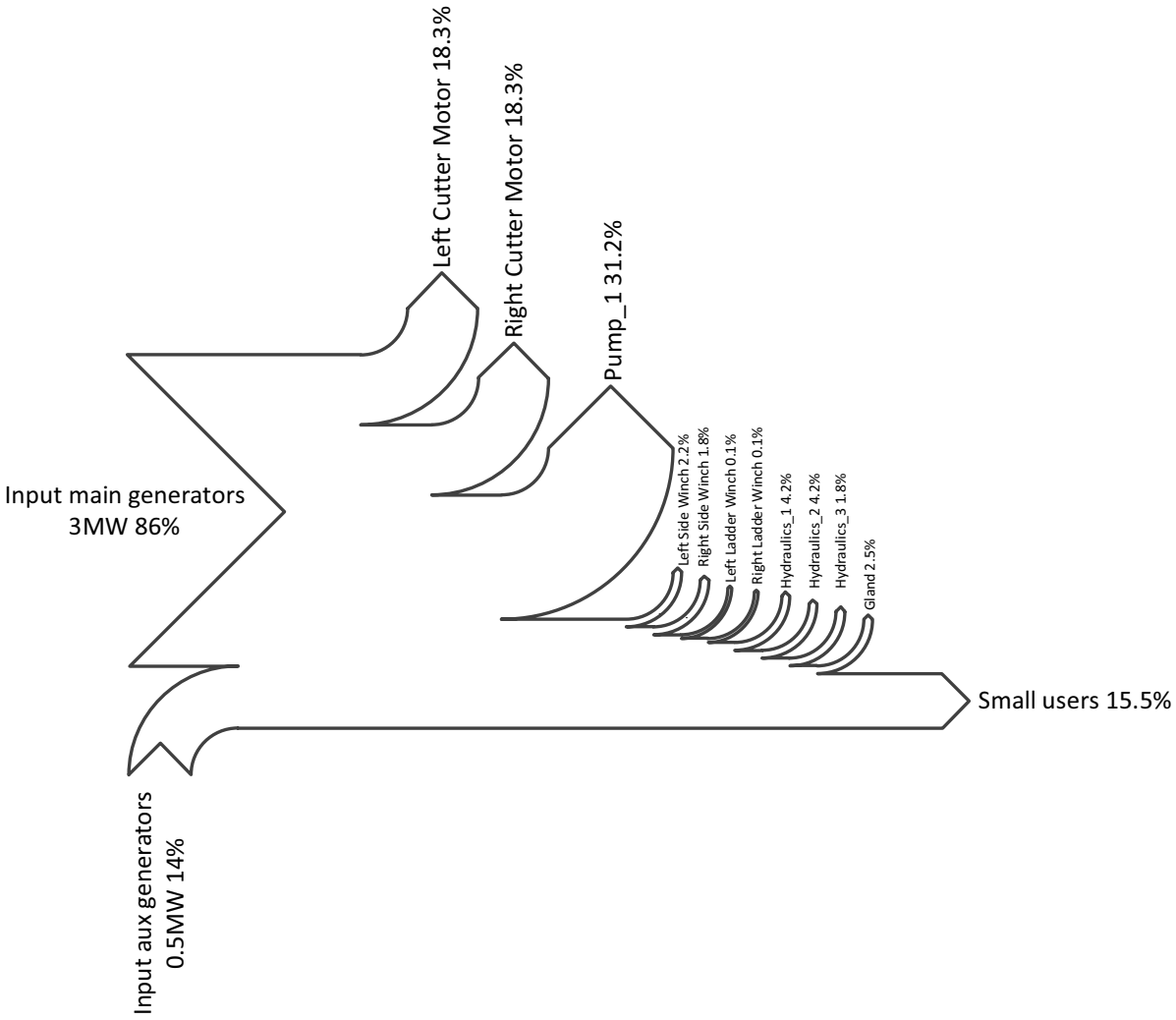

Figure A.1: Sankey diagram JNPT project

Table A.1: Simulation results for the JNPT project

Original performance

HFO $[Mt]$	MGO $[Mt]$	running hours main generators	running hours auxiliary generators
87	3	145	20

Hybrid performance

HFO $[Mt]$	MGO $[Mt]$	running hours main generators	running hours auxiliary generators
67	0	73	0

Potential savings

HFO $[Mt]$	MGO $[Mt]$	running hours main generators	running hours auxiliary generators
20	3	72	20

Battery lifetime	27 $years$

The second project evaluated is the Jebel Ali port construction project [Geus, 2014b]. During this project CSD Artemis was used to dredge a new harbour pocket in the Jebel Ali port. Contrary to the JNPT project the dredged material was transported via a discharge line. This requires more pump power compared with the barge loading system. The soil that was dredged consisted out of a top layer of cap rock and a subsequent layer of sand stone. During the cap rock removal a six blade cutter with stone ring had to be used, limiting the use of the full cutting capacity. The cap rock required more actual cutting action resulting in a higher cutter power than was found during the JNPT project.

The power demand during the Jebel Ali project was situated around the power output of two main generators (*14000* kW). The following reasons can be addressed;

1. Use of a discharge line, requiring more pump capacity. Actually two pumps were used.
2. Soil conditions required working with limited cutter power due to a stone ring and a six bladed cutter (*3000* kW).

The average power demand and distribution for the Jebel Ali project is visualised in the form of a Sankey diagram in figure A.2. In the report that was written after a work visit from the Engineering and Estimating department from Van Oord the concern was shared that the power distribution was not optimal. It turned out that the engines were mostly running on low average loading. The reason for this was that getting an additional engine on-line required to much time. Therefore the average power of 14000 kW was generated by three generating sets instead of two. Additional the auxiliary generators were used for a lot of hours as well. Resulting in an overall inefficient operation. This is also presented in table A.2. It seems that even when power demand is higher the hybrid system has potential. In this case especially since expansive auxiliary running hours can be reduced.

Table A.2: Simulation results for the Jebel Ali project

Original performance			
HFO $[Mt]$	MGO $[Mt]$	running hours main generators	running hours auxiliary generators
259	22	325	139
Hybrid performance			
HFO $[Mt]$	MGO $[Mt]$	running hours main generators	running hours auxiliary generators
247	0	239	0
Potential savings			
HFO $[Mt]$	MGO $[Mt]$	running hours main generators	running hours auxiliary generators
12	22	86	139
Battery lifetime		19 $years$	

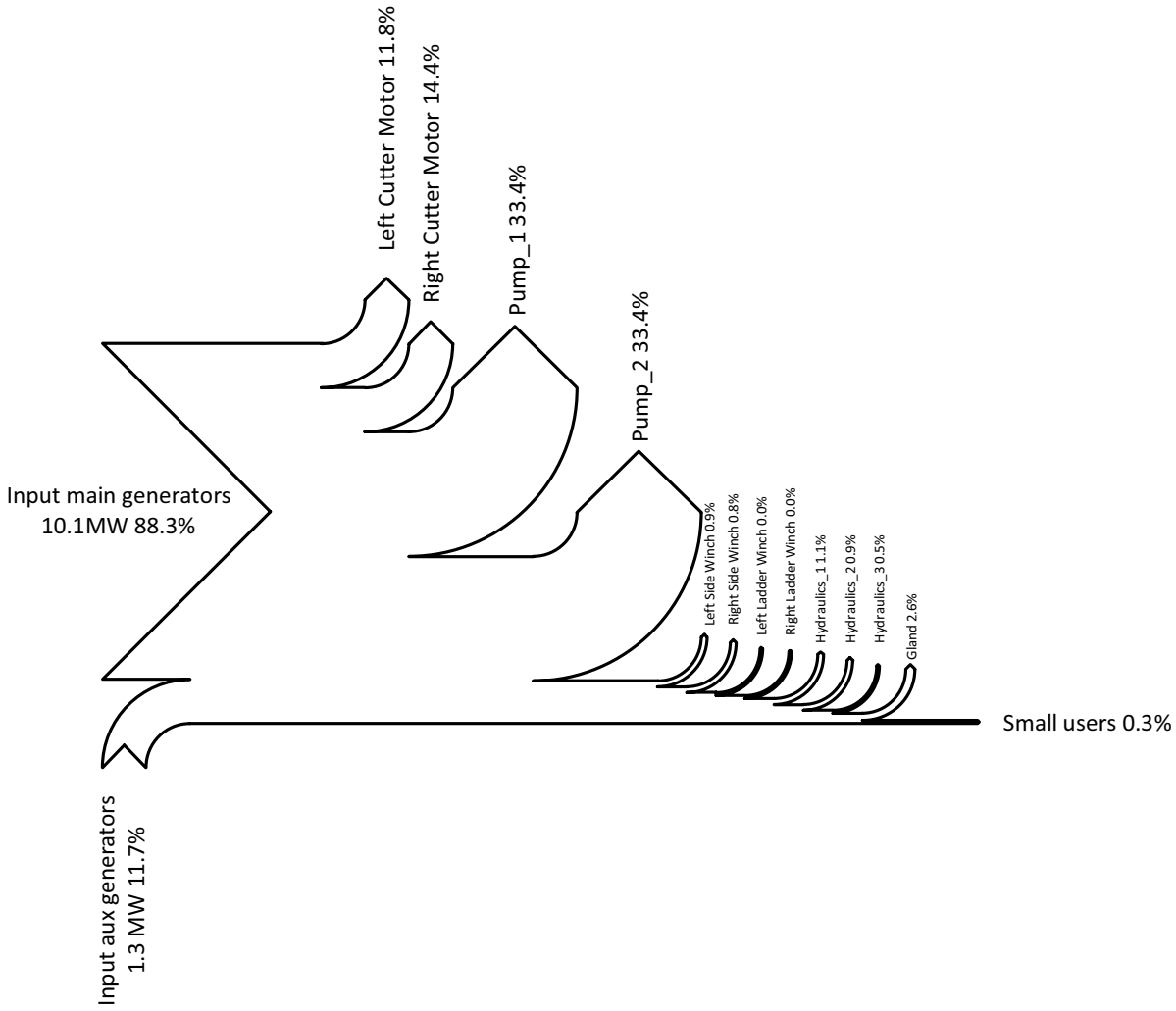

Figure A.2: Sankey diagram Jebel Ali project

The third and last individual project that will de described is the DOHA project. Unfortunately this project cannot be elaborated on as was done for the previous two projects since no dedicated work report for this project has been found. Nevertheless this project has been simulated in the same way as the two previously described projects. The result of these simulations are presented in table A.3. During the DOHA project the average load on the generators was higher than during the JNPT and the Jebel Ali project. This was already shown in chapter 2. As it turns out the potential of the hybrid systems is quite low in this situation. The average load factor of the main generators is high, so no gain in efficiency can be achieved by increasing the load factor to 85%. When working with a high average loading of the main generators there is not much room in power output to charge the batteries. A similar result was found for the peak shaving simulations in chapter 6. It turned out that in peak shaving operation the battery lifetime would decrease dramatically, the same is found for the DOHA project simulation.

The final working profile that is proposed to use for the simulations is a week of operation during the KNPC project. This week turned out to represent the full year operation in the best way with regards to power demand. The KNPC project is again different from the other projects described previously. During the KNPC project the CSD Artemis was used as cutter whereas CSD Athena was used as booster station. The power demand histogram presented in chapter 2 for the KNPC project was based on measurements done on board of the Artemis and thus representing actual cutter operation. During this operation the discharge line had a length of 6565 meters [Geus, 2014a]. This required the use of all three of Artemis' pumps. The material to be cut was a medium sand and did not require the full power of the cutter motors on the cutter head. The distribution of the power over the different end users is

Table A.3: Simulation results for the DOHA project

Original performance			
HFO $[Mt]$	MGO $[Mt]$	running hours main generators	running hours auxiliary generators
394	7	374	41
Hybrid performance			
HFO $[Mt]$	MGO $[Mt]$	running hours main generators	running hours auxiliary generators
360	0	339	0
Potential savings			
HFO $[Mt]$	MGO $[Mt]$	running hours main generators	running hours auxiliary generators
34	7	35	41
Battery lifetime		2 $years$	

presented as a Sankey diagram in figure A.3. In terms of power demand and power supply the KNPC project seems to be an average of the Jebel Ali and DOHA project. However due to some testing with the set-up of the booster station Athena low power demand was also encountered during the week that is simulated.

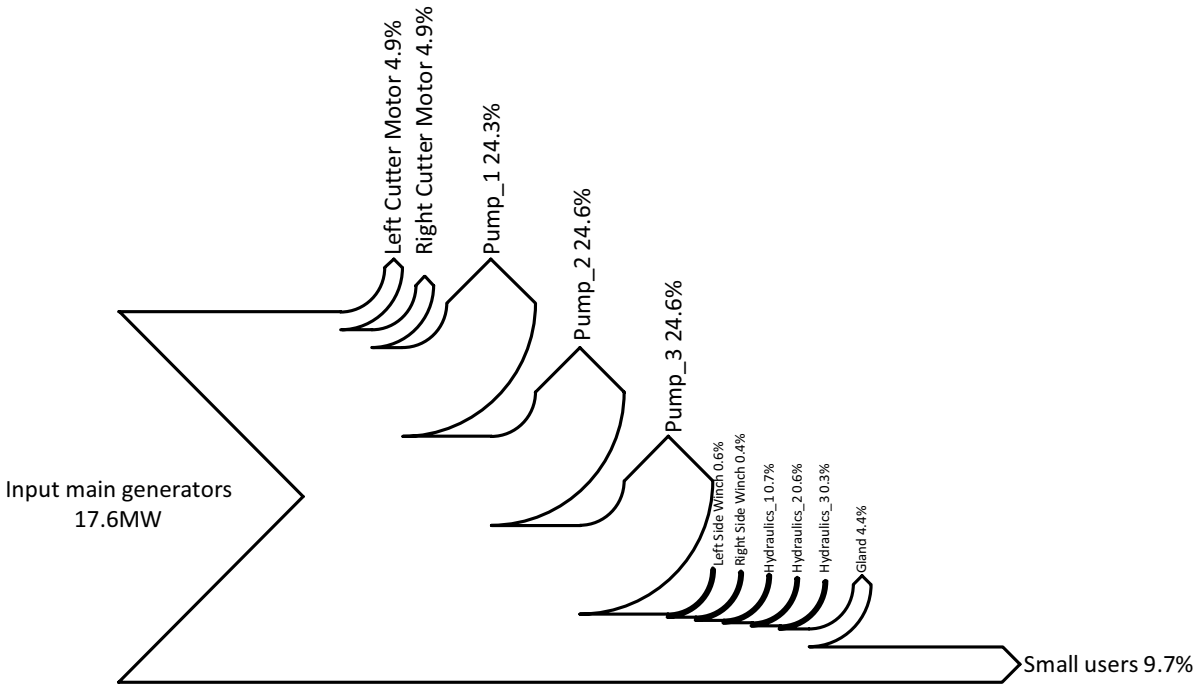

Figure A.3: Sankey diagram KNPC project

The influence from the length of the discharge line on the power demand is visualised in figures A.4 and A.5. These two figures were reproduced from IHC Holland [1985]. Visible is that with a longer discharge line the resistance becomes higher, increasing the required pump power. When the discharge line is lengthened even further the density of the mixture should be lowered. In order to do so the cutter should cut less soil, thus reducing the required cutting power. These effects were also noticed in the four projects described in the beginning of this appendix.

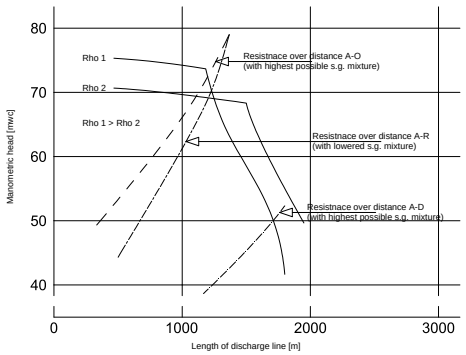

(a) Discharge line resistance and pump curves

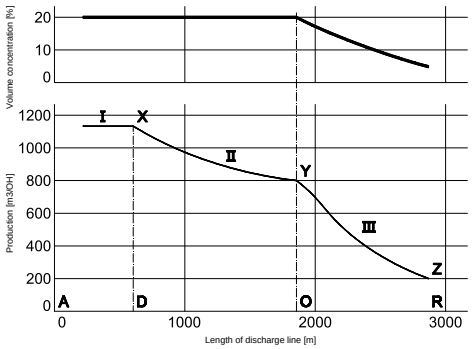

(b) Discharge line production and concentration curves

Figure A.4: Resistance, production and concentration curves for different discharge line configurations

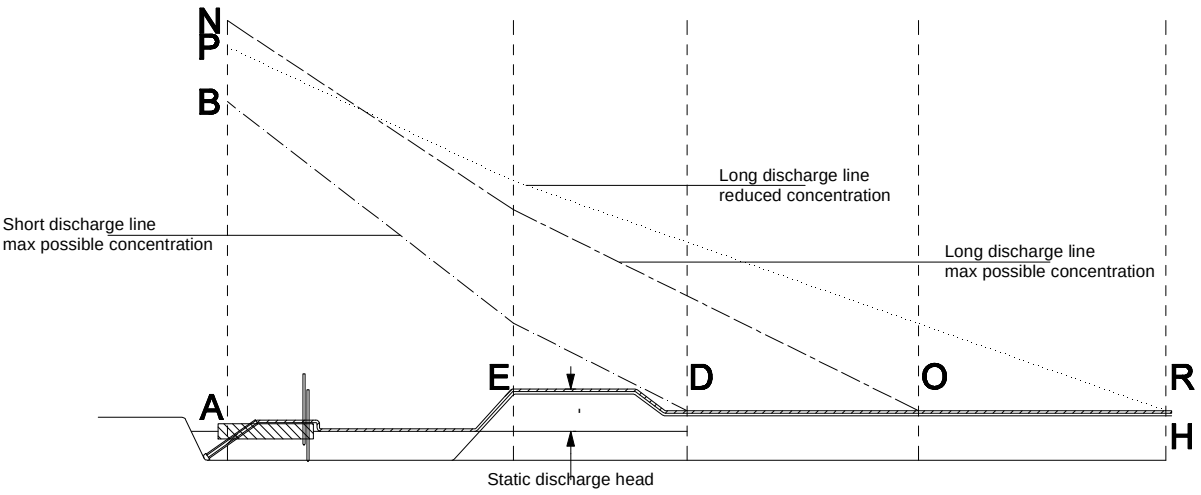

Figure A.5: Discharge line overview

B

Air excess ratio calculation

In this appendix the air excess ratio calculation for the engines of the Vox Maxima will be explained. These calculations were executed to prove the suspicion that during a transient operation of the engine there will always be enough fresh air in the cylinder to ensure complete combustion of the injected fuel. In table B.1 the general parameters of the engine under consideration are presented.

Table B.1: Engine specifications Vox Maxima

Engine	manufacturer	type	nominal power $[kW]$	nominal speed $[rpm]$
PS Engine Vox Maxima	MAN diesel	12V46/60B	14400	514

For this analysis several formulas from Stapersma [2010a] and Stapersma [2010b] will be used. Furthermore, the test protocol from the MAN 12V46/60B is used to find engine specific values [MAN Diesel SE, 2007]. Finally several geometrical parameters from the diesel engine had to be entered in the different equations. The geometrical properties like bore, stroke and valve timing were adopted from the technical documentation delivered with the engine [MAN Diesel SE, 2008].

Table B.2: Constants used in the air excess ratio calculation

parameter	symbol	value	unit
number of cylinders	$n_{cylinder}$	12	
k-factor	k	2	
Bore	B	480	mm
Stroke	L_s	600	mm
Geometric compression ratio	ε	15.3	
Start of compression	$\angle_{crank}^{inlet\ valve\ closed}$	14	$^\circ\ crank\ angle$
Gas constant dry air	R_1	287.058	J/kgK
Stoichiometric ratio	σ	13.75	

Table B.3: Values as read from turbo performance parameters (see appendix C) MAN Diesel SE [2007]

Load Factor $[\%MCR]$	Power $[Kw]$	$P_1\ [Pa]$	$T_1\ [K]$	SFOC $[g/kWh]$
30	4320	68000	304	213
40	5760	106000	305	201
50	7200	149000	306	193
60	8640	201000	308	190
70	10080	249000	309	188
80	11520	284000	309	185
90	12960	320000	310	185
100	14400	328000	310	188

First of all the different formulas will be explained. Figure B.2 will serve as an explanation for equation B.1. In equation B.1 the compression ratio ε is presented as a function of stroke volume V_s and the volume in the cylinder above Top Dead Centre (TDC) V_{TDC}. The stroke volume can be calculated by entering the bore B and the stroke L_s in equation B.2. Then by substituting equation B.2 in equation B.1 and some rewriting the equation for V_{TDC} can be found as presented in equation B.3. V_s and V_TDC determine the value of V_1. V_1 is the volume in the cylinder at the moment that the inlet valve is closed. From that point on the compression stroke will start. V_1 is determined in equation B.5. It can be seen that a certain parameter X is introduced. X is a value for the effectiveness of the compression stroke. If the inlet valve is closed at bottom dead centre which can be the case with naturally aspirated engines the value of X is one. For turbo charged engines the inlet valve can close after bottom dead centre, as is the case for the MAN under consideration. Than the value of X is determined according to equation B.4. The inlet valve closes 14 degrees crank angle after Bottom Dead Centre (BDC) for this MAN engine as can be seen in figure B.3. When V_1 is known one can estimate the mass contained in the cylinder by using equation B.6. In equation B.6 p_1 is the pressure in the cylinder the moment the inlet valve closes, as presented in table B.3. R_1 is the gas constant for dry air (assumed to behave as a ideal gas). T_1 indicates the temperature of the air that has entered the cylinder before the inlet valve closes. Finally V_1 is a value that was already explained. Note that besides the fact that the intake air is assumed to behave as an ideal gas there are more simplifications in this approach. It is assumed that to whole volume V_1 is fresh air that is available for combustion. In reality there will always be some residual gas in the cylinder. This amount is expressed in the so called “purity” factor. This purity factor is assumed to be equal to one, so no residual gas will be present in the cylinder. This assumption is a valid approximation for a four stroke engine. A four stroke engine is not only dependent from the scavenging process. A four stroke engine will always refresh the volume in the cylinder by its exhaust and intake stroke. Next to that the engine under consideration scavenges the volume V_{TDC} due to its valve overlap.

$$\varepsilon = \frac{V_s + V_{TDC}}{V_{TDC}} \tag{B.1}$$

$$V_s = \frac{1}{4} \cdot \pi \cdot B^2 \cdot L_s \tag{B.2}$$

$$V_{TDC} = \frac{\frac{1}{4} \cdot \pi \cdot B^2 \cdot L_s}{\varepsilon - 1} \tag{B.3}$$

$$X = 1 - \frac{\angle_{crank}^{inlet\ valve\ closed}}{\angle_{crank}^{180}} \tag{B.4}$$

$$V_1 = V_{TDC} + X \cdot V_s \tag{B.5}$$

$$m_1 = \frac{p_1 \cdot V_1}{R_1 \cdot T_1} \tag{B.6}$$

$$m_{fuel} = \frac{SFOC \cdot Power}{rpm \cdot 60 \cdot \frac{1}{k}} \cdot \frac{1}{n_{cylinder}} \tag{B.7}$$

$$\lambda = \frac{m_1}{m_{fuel} \cdot \sigma} \tag{B.8}$$

The mass of air in the cylinder is now determined. The last step before calculating the actual air excess ratio is to determine the mass of fuel injected in the cylinder. The values of SFOC given in the test report is a continues flow property. To establish the air excess ratio λ, which is a in cylinder property, the SFOC value has to be converted in a discrete in cylinder value. The question to be answered is, what is the amount of fuel injected each cycle per cylinder? To convert the continues SFOC value to a discrete in cylinder value equation B.7 is used. In this equation $SFOC$ times $Power$ gives mass flow per hour. By multiplying the revolutions per minute rpm with 60 minutes and the inverse of the k factor the amount of working cycles per hour is found. The k factor compensates for the fact that a four stroke engine has one combustion stroke per two revolutions of the crankshaft. When dividing the fuel mass flow per hour by the number of working cycles per hour the amount of fuel per working cycle is found. This value is than divided by the number of cylinders and the mass of fuel per injection is known.

The final result of this process is to determine the air excess ratio for different load factors. This is done by using equation B.8. In this equation numerator is a value for the mass of air present in the cylinder. The denominator gives a figure for the minimal amount of air needed for complete combustion. This value is comprised of the mass of fuel injected times the so called stoichiometric ratio σ. σ is based on the chemical composition of the fuel and the air. This ratio ensures that the minimal amount of oxygen is present for complete combustion.

The calculated values are presented in table B.4. From the data in table B.4 a figure B.1 was created in which a fit function for the air excess ratio is presented.

Table B.4: Calculated values from the air excess ratio analysis

Load Factor $[\%MCR]$	$m_1\ [g]$	$m_{fuel}\ [g]$	$m_\sigma\ [g]$	λ
30	84	5	68	**1.22**
40	130	6	86	**1.52**
50	183	8	103	**1.77**
60	245	9	122	**2.01**
70	302	10	141	**2.15**
80	345	12	158	**2.18**
90	387	13	178	**2.17**
100	397	15	201	**1.97**

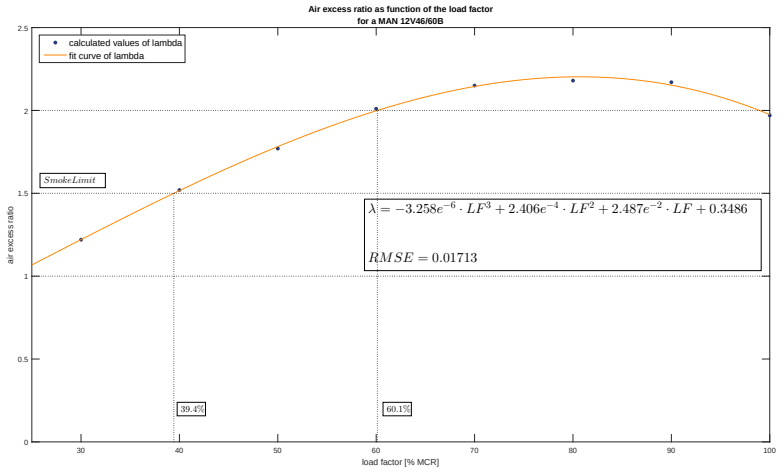

Figure B.1: The air excess ratio as function of the load factor

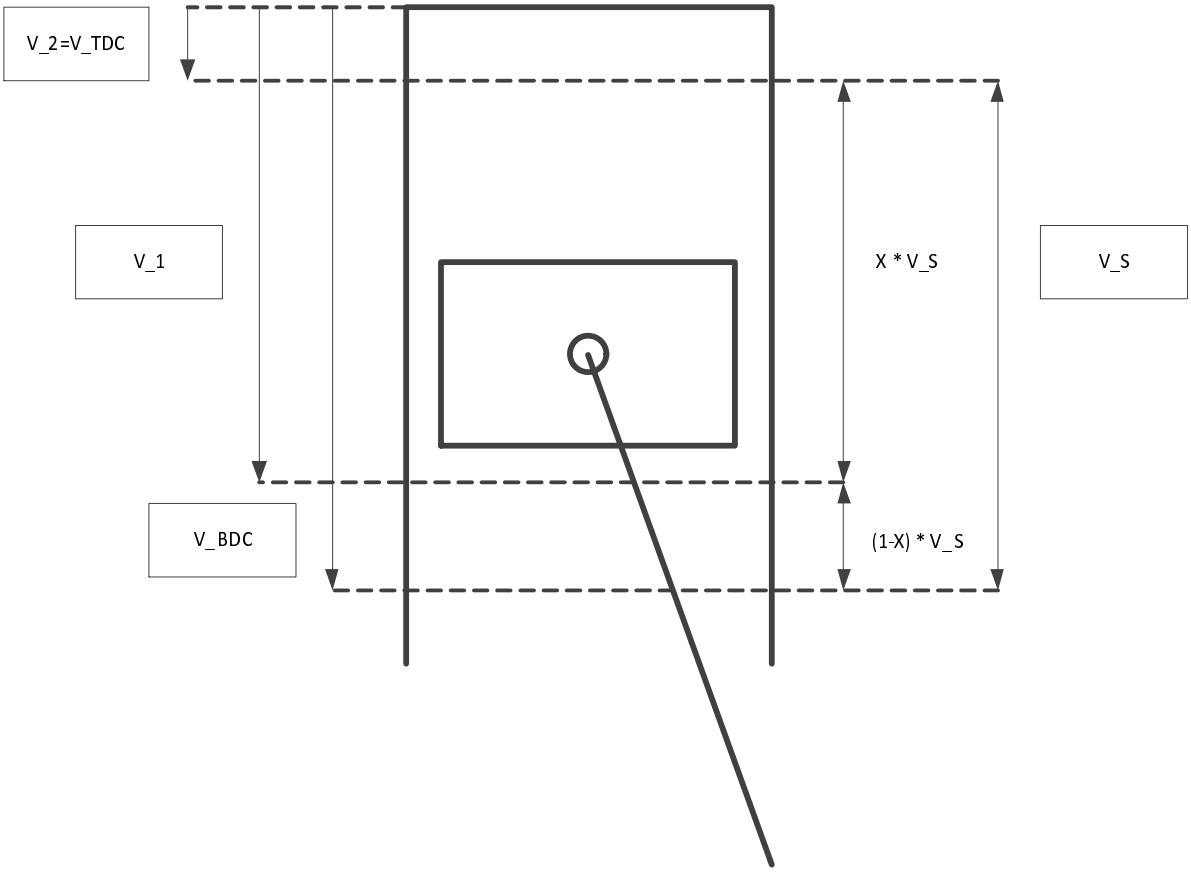

Figure B.2: Stroke volume during in cylinder process

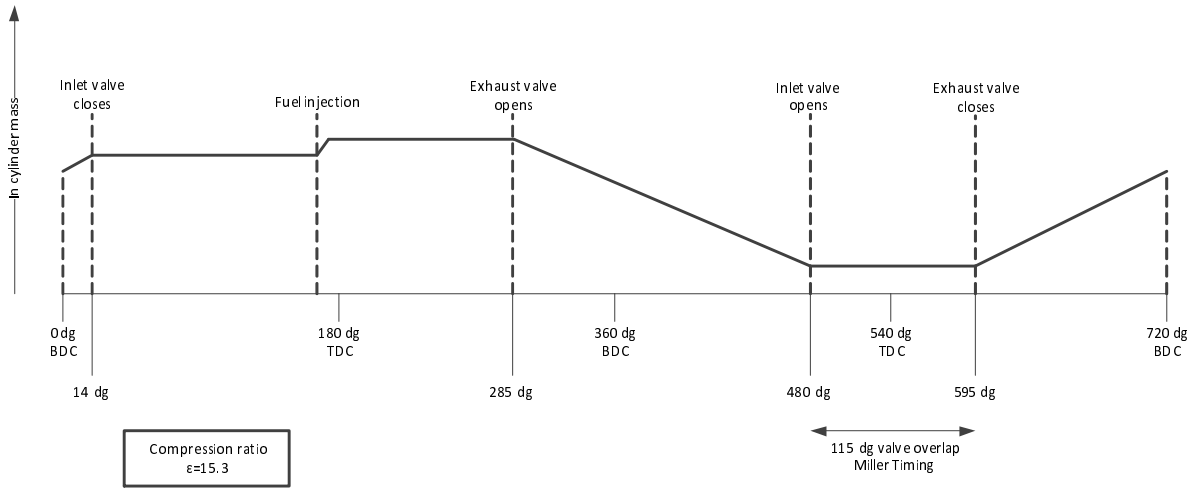

Figure B.3: In cylinder mass and valve timing during full four-stroke cycle

C

turbo performance parameters

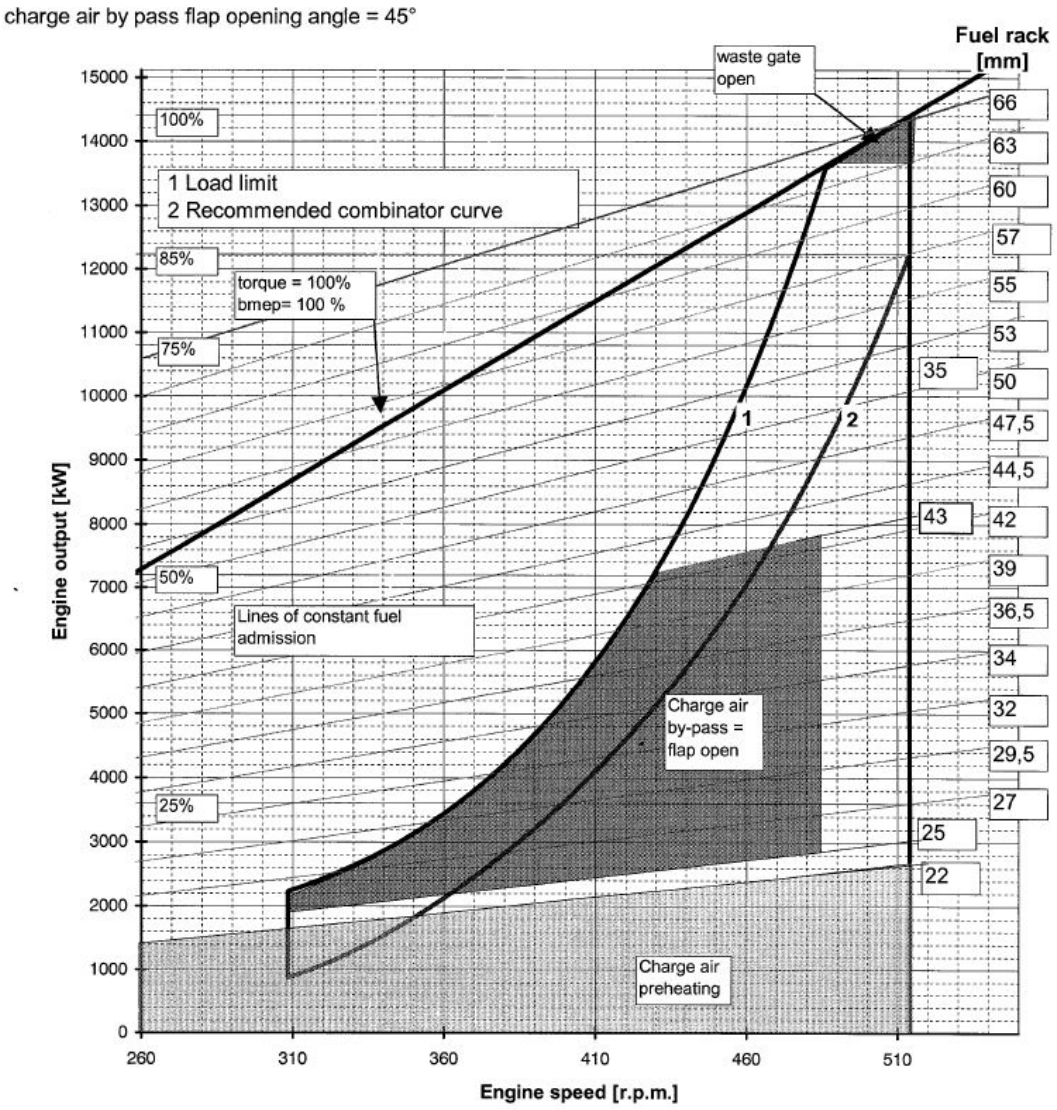

Figure C.1: Turbo operating test report - PS engine Vox Maxima MAN Diesel SE [2007]

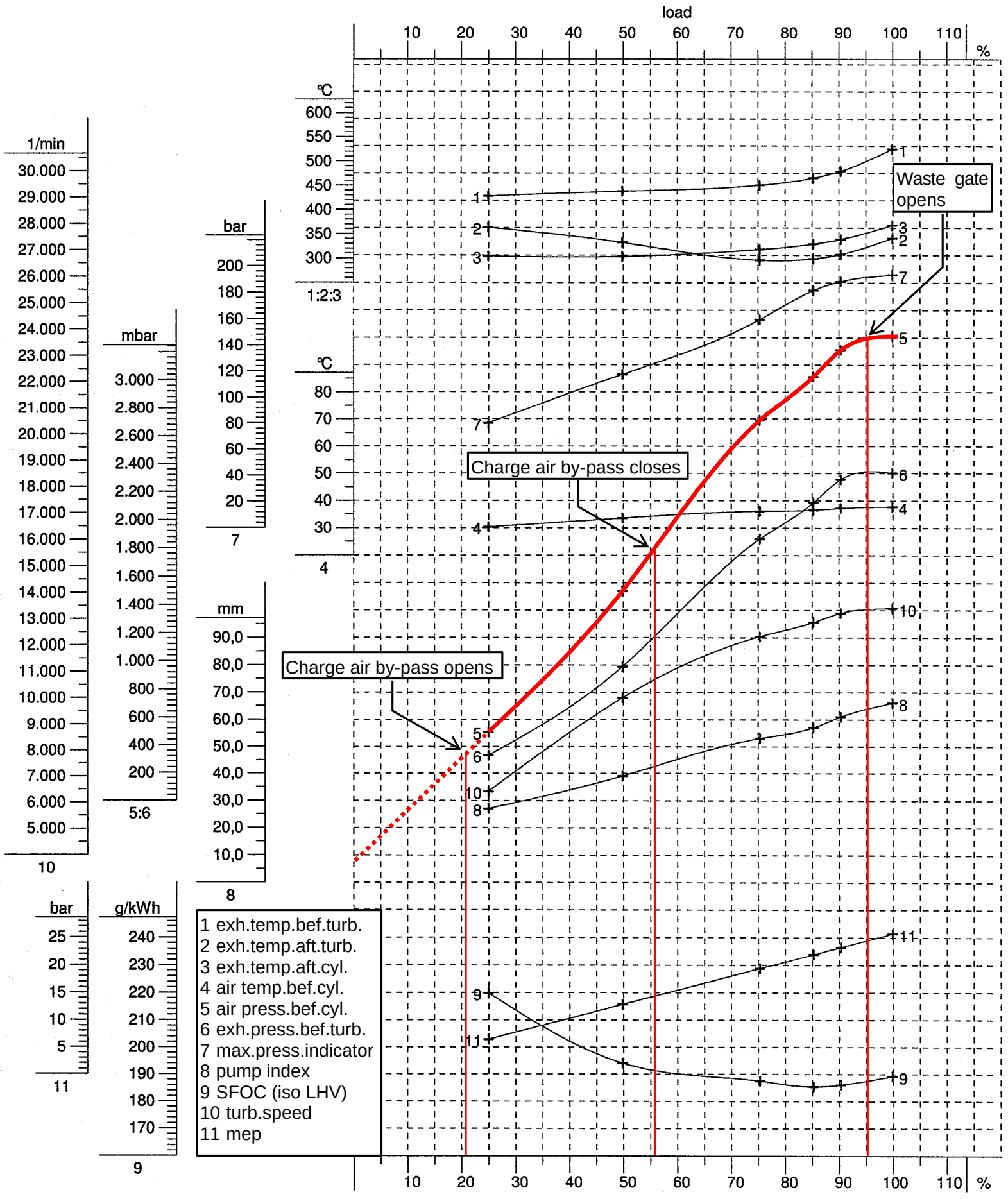
load
10 20 30 40 50 60 70 80 90 100 110 %
℃
600 550 500 450 400 350 300
1:2:3
℃
80 70 60 50 40 30
4
bar
200 180 160 140 120 100 80 60 40 20
7
mbar
3.000 2.800 2.600 2.400 2.200 2.000 1.800 1.600 1.400 1.200 1.000 800 600 400 200
5:6
1/min
30.000 29.000 28.000 27.000 26.000 25.000 24.000 23.000 22.000 21.000 20.000 19.000 18.000 17.000 16.000 15.000 14.000 13.000 12.000 11.000 10.000 9.000 8.000 7.000 6.000 5.000
10
mm
90,0 80,0 70,0 60,0 50,0 40,0 30,0 20,0 10,0
8
bar
25 20 15 10 5
11
g/kWh
240 230 220 210 200 190 180 170
9
Waste gate opens
Charge air by-pass closes
Charge air by-pass opens
1 exh.temp.bef.turb.
2 exh.temp.aft.turb.
3 exh.temp.aft.cyl.
4 air temp.bef.cyl.
5 air press.bef.cyl.
6 exh.press.bef.turb.
7 max.press.indicator
8 pump index
9 SFOC (iso LHV)
10 turb.speed
11 mep

D

Rotational energy calculation

In this appendix the kinetic energy stored in the power generation system is analysed. The idea is to compare the kinetic energy stored in the system of the HAM318 with the kinetic energy stored in the system of the Athena or Artemis. The amount of kinetic energy at nominal engine speed might be assumed to act as a first buffer (*peak shaving device*) between the power demand and the power supply of the diesel engines. One can compare the kinetic energy in the overall power generation system with an external flywheel energy storage device. The same principles of operation apply.

The kinetic energy that is stored in the two different systems is related to the rotational moments of inertia of individual rotating components in the system. For both vessels the most important rotating components with their corresponding rotational inertias have been summarized in table D.1. When rotational moments of inertia were not provided they are calculated according to equation D.1 [Hibbeler, 2010]. The systems of the HAM318 and Athena/Artemis are schematically visualised in figure D.1 and figure D.2 respectively.

$$J = \frac{1}{2} \cdot m \cdot r^2 \tag{D.1}$$

Table D.1: Rotating components and rotational inertias

HAM318			
Component	Inertia J $[kgm^2]$	nominal speed ω $[rad/s]$	source
Wärtsilä 12V46C	4660	53.83	Wärtsilä, Ship Power Technology [2013]
Gearbox input gear	491	53.83	Floren [2000]
Gearbox PTO gear	28	105.98	Floren [2000]
Generator	2250	105.98	ABB Industry Oy / Machines [2000]
Gearbox output gear	7380	12.07	Floren [2000]
Propeller shaft	2964	12.07	Grevink [2000]
Propeller	25735	12.07	IHC HOLLAND NV. [2000]

Athena/Artemis			
Component	Inertia J $[kgm^2]$	nominal speed ω $[rad/s]$	source
Wärtsilä 6L46F	3620	62.83	Wärtsilä, Ship Power Technology [2013]
Coupling	520	62.83	Francesco et al. [2009]
Generator	3387	62.83	Francesco et al. [2009]

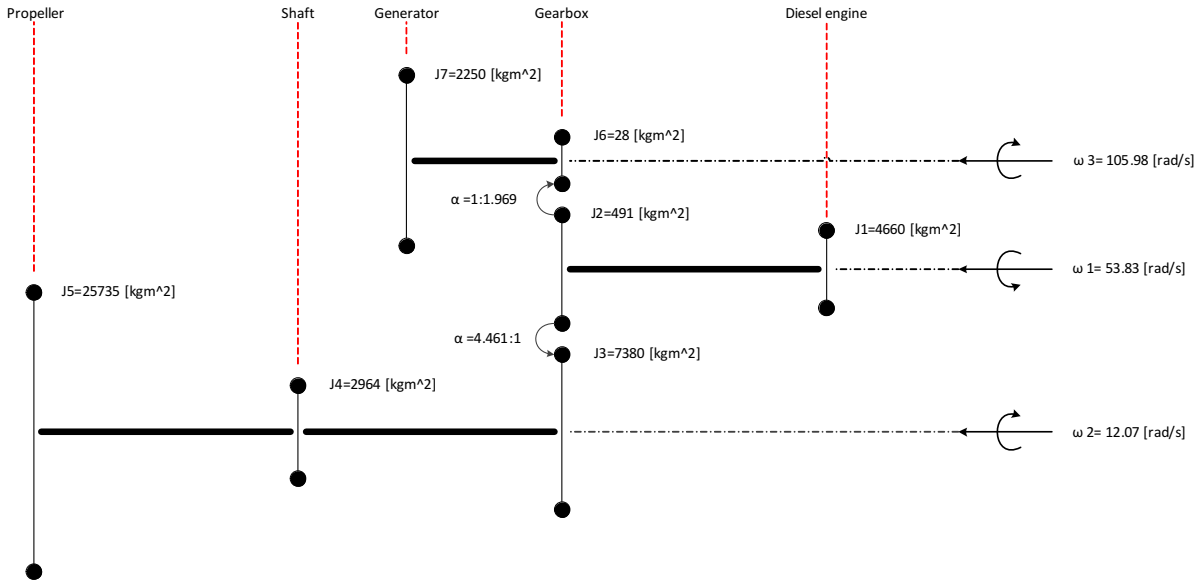

Figure D.1: Simplified rotational dynamics in the power plant of the HAM318

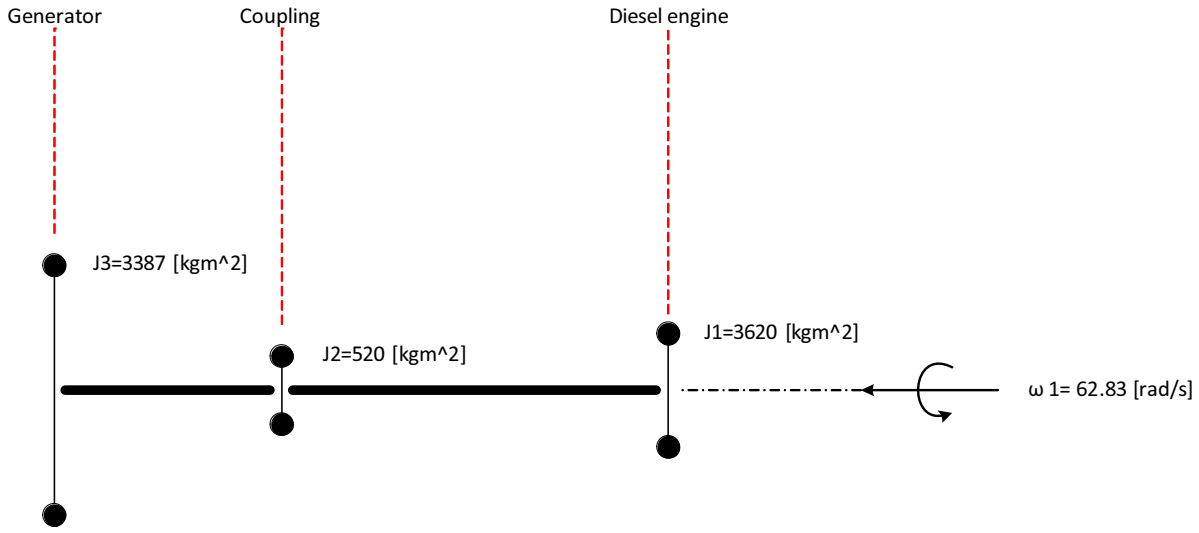

Figure D.2: Simplified rotational dynamics in the power plant of the Athena

In order to understand how much energy is stored in the rotating parts of the two different systems one should calculate the kinetic energy. The kinetic energy in a rotating body can be calculated using equation D.2 [Hibbeler, 2010]. The total kinetic energy stored in the system is simply the sum of the kinetic energy stored in the individual bodies. Since it is not only interesting to know the kinetic energy at nominal engine speed it is decided to calculate the kinetic energy for a 1.5% drop in rpm and a 1.5% overshoot in rpm as well. The value of 1.5% was derived from load acceptance tests done during the new building of the Athena Pernice [2009]. The results of this analysis are presented in table D.2. Here the kinetic energy stored in the systems as presented in figure D.1 and D.2 are displayed in the second column. The third column represents the total kinetic energy. The total kinetic energy is a multiplication of the kinetic energy in the second column of the table. For the HAM318 the multiplication factor is two, since the ship is equipped with two similar systems. The multiplication factor for the Athena and Artemis is three since three generator sets are installed in these vessels.

Not only the energy stored in the form of rotational kinetic energy is important. Maybe even more important is the difference in kinetic energy between the different rotational speeds. This difference is

either supplied as power from the rotating parts to the energy consumers in case of a drop in rpm or power has to be supplied by the engine to the rotational parts in the case of an increase in rpm. The delta energy for the rotational speeds that are analysed is presented in table D.3. Since this thesis is expressing energy in terms of kWh, the delta kinetic energy values are also presented in this unit. From the load acceptance test it turns out that the drop in rotational speed takes more or less one second. The time to restore the desired net frequency takes about three seconds. With this information the power supplied by the flywheel effect and the extra power needed to restore original speed can be calculated. Since the cutter dredger is analysed in this thesis this calculation will be done for the Athena/Artemis. During the speed drop 1327 kW is provided from the rotational inertia to the system, which holds approximately **442** kW per generator set. In the three second period in which the rotational speed is restored to its desired value the speeding up of the rotational part requires an extra power from the diesel engines of around **150** kW per generator set.

$$T = \frac{1}{2} \cdot J \cdot \omega^2 \tag{D.2}$$

Table D.2: Kinetic energy calculation results

HAM318		
rpm	kinetic energy $[kJ]$	total kinetic energy $[kJ]$
506	22217	44433
514 *(nom.)*	22872	45744
522	23537	47073

Athena/Artemis		
rpm	kinetic energy $[kJ]$	total kinetic energy $[kJ]$
591	14415	43246
600 *(nom.)*	14858	44573
609	15307	45920

Table D.3: Delta kinetic energy

HAM318		
rpm_1-rpm_2	Δ total kinetic energy $[kJ]$	Δ total kinetic energy $[kWh]$
506-514	1310	0.36
514-522	1330	0.37

Athena/Artemis		
rpm_1-rpm_2	Δ total kinetic energy $[kJ]$	Δ total kinetic energy $[kWh]$
591-600	1327	0.37
600-609	1347	0.37

It turns out that the total kinetic energy stored in the rotating parts of the power generation system of the HAM318 and the Athena/Artemis is almost equal. This is different than was expected. It was expected that the HAM318 would have more kinetic energy stored since the inertia of its propulsion system is higher than that of the Athena and Artemis. The fact that the main gear of the gearbox, the propeller shaft and the propeller itself rotate at a much lower speed than the rest of the system is reason for the *low* kinetic energy. Besides that it becomes clear that having three generator sets in the Athena and Artemis increases the stored energy significantly, whereas the HAM318 has only two systems that contribute to the total inertia. Furthermore it is noticed that due to the small variation of rotational speed *(since the net frequency should stay within predetermined bounds)* the energy available for initial peak shaving is much lower than expected. The values of 0.37 kWh are not comparable with the proposed energy storage in the electrical battery which lies around the 5 MWh mark.

E

Battery specifications

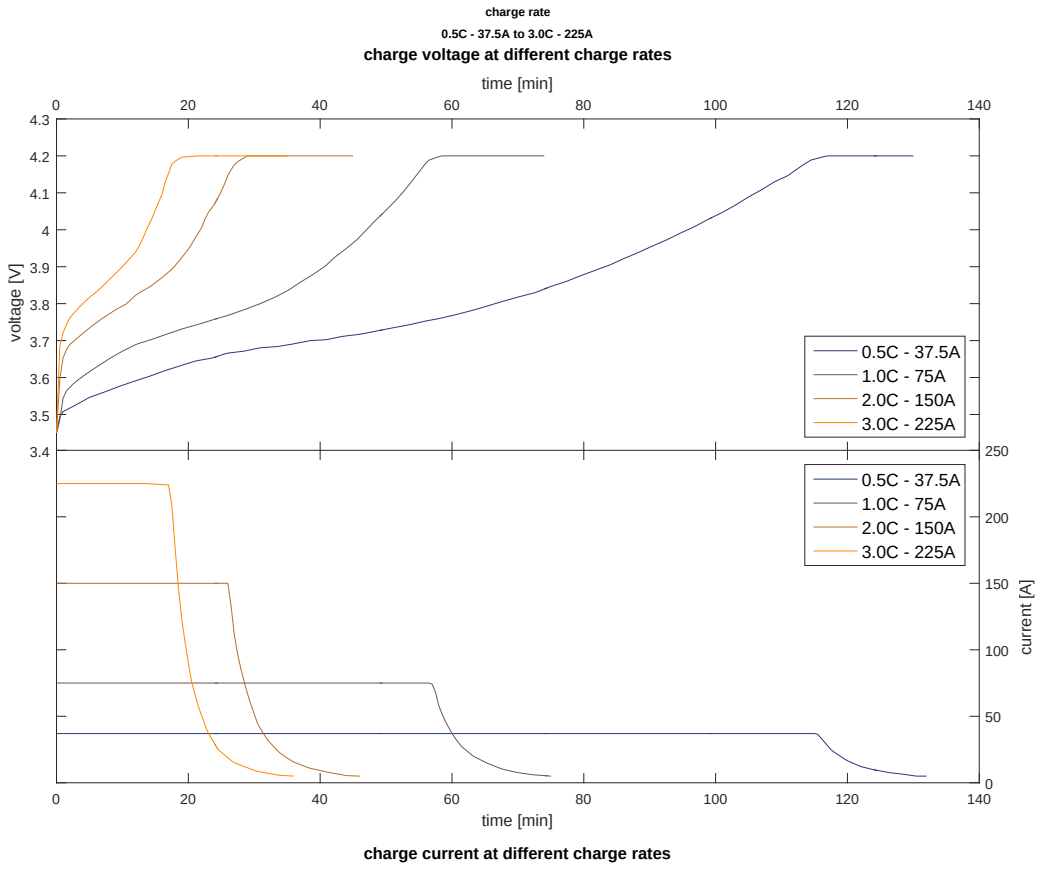

Figure E.1: Voltage and current for different charge rates

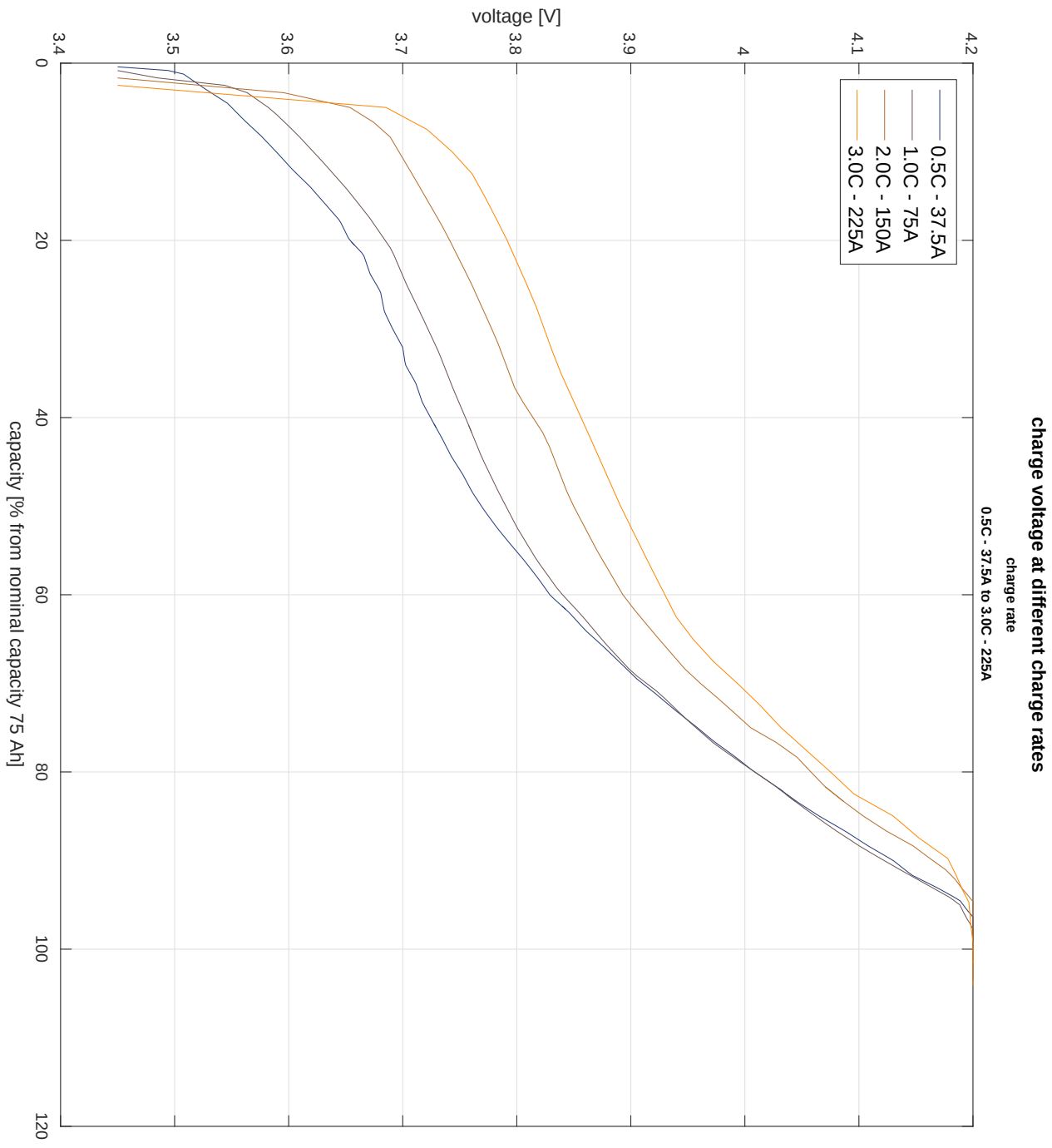

Figure E.2: Voltage vs. capacity for different charge rates

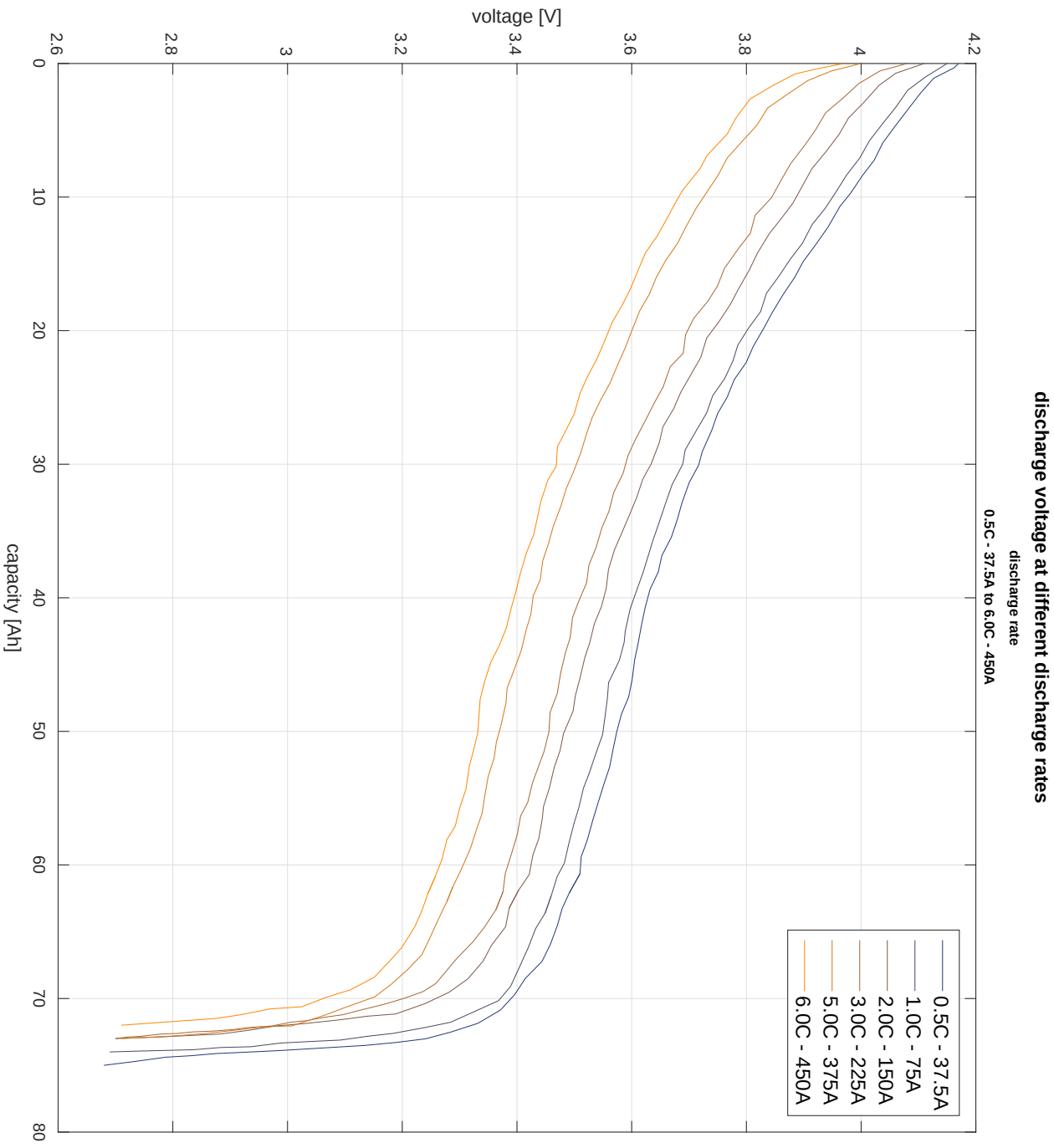

Figure E.3: Voltage and capacity for different discharge rates

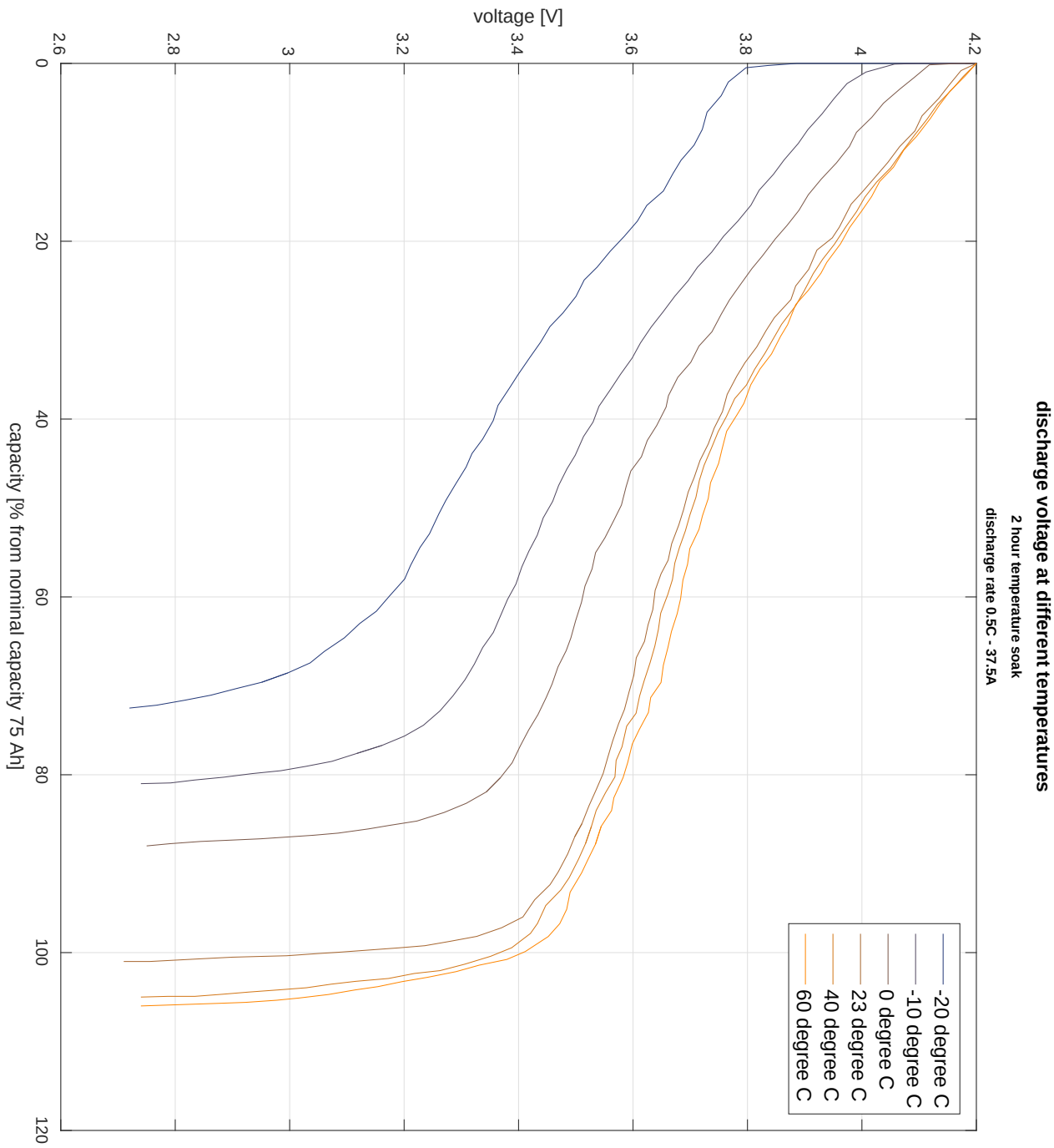

Figure E.4: Voltage and capacity for discharge under different temperatures

Superior Lithium Ion Cell

Charge Curves – Rate Dependence

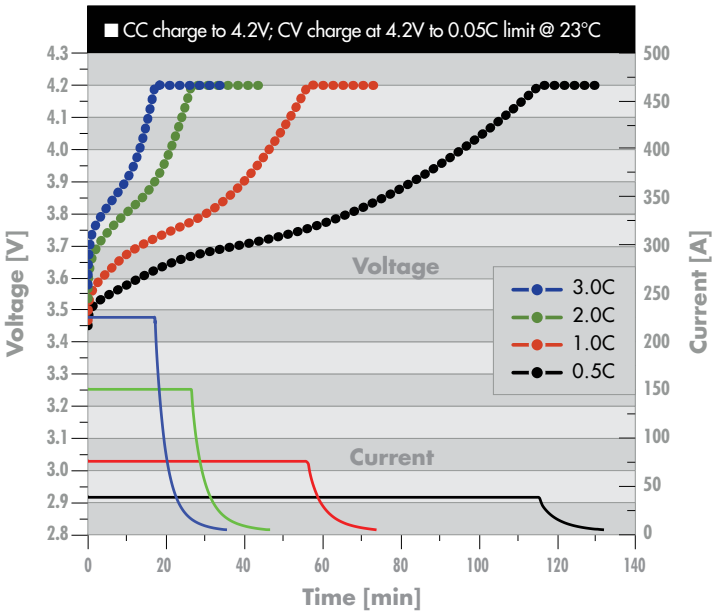

Discharge Curves – Rate Dependence

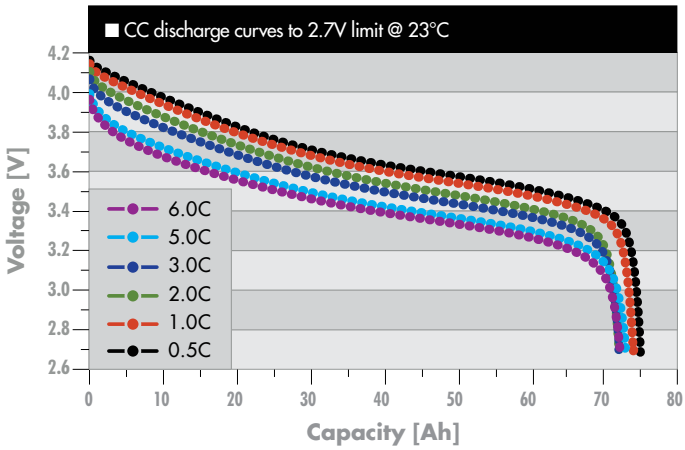

Discharge Curves – Temperature Dependence

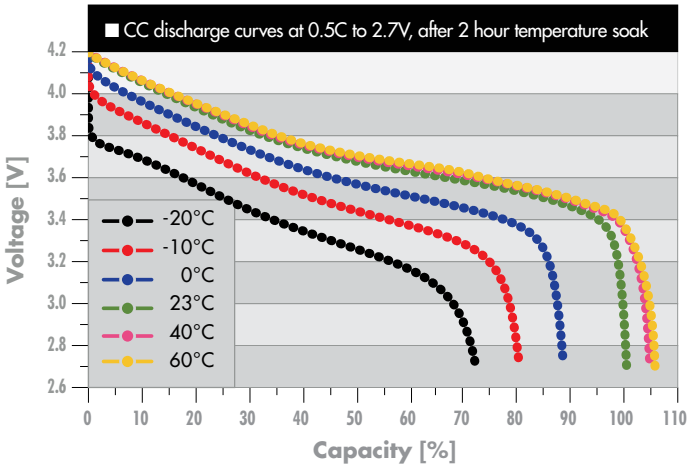

Mechanical Characteristics

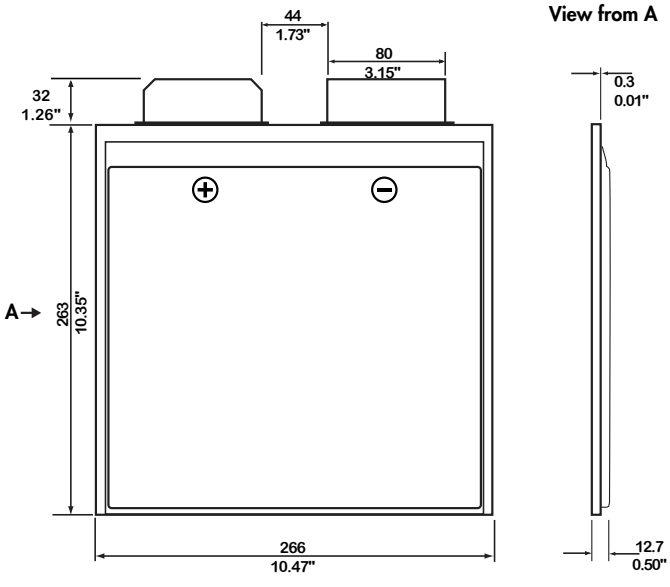

Note: dimensions shown in mm and inches (")

XALT Energy
2700 S. Saginaw Road, Midland, MI 48640 • +1 (989) 486-8501
Email: powerup@xaltenergy.com
Web: xaltenergy.com
Made in USA

F

Battery model in Simulink

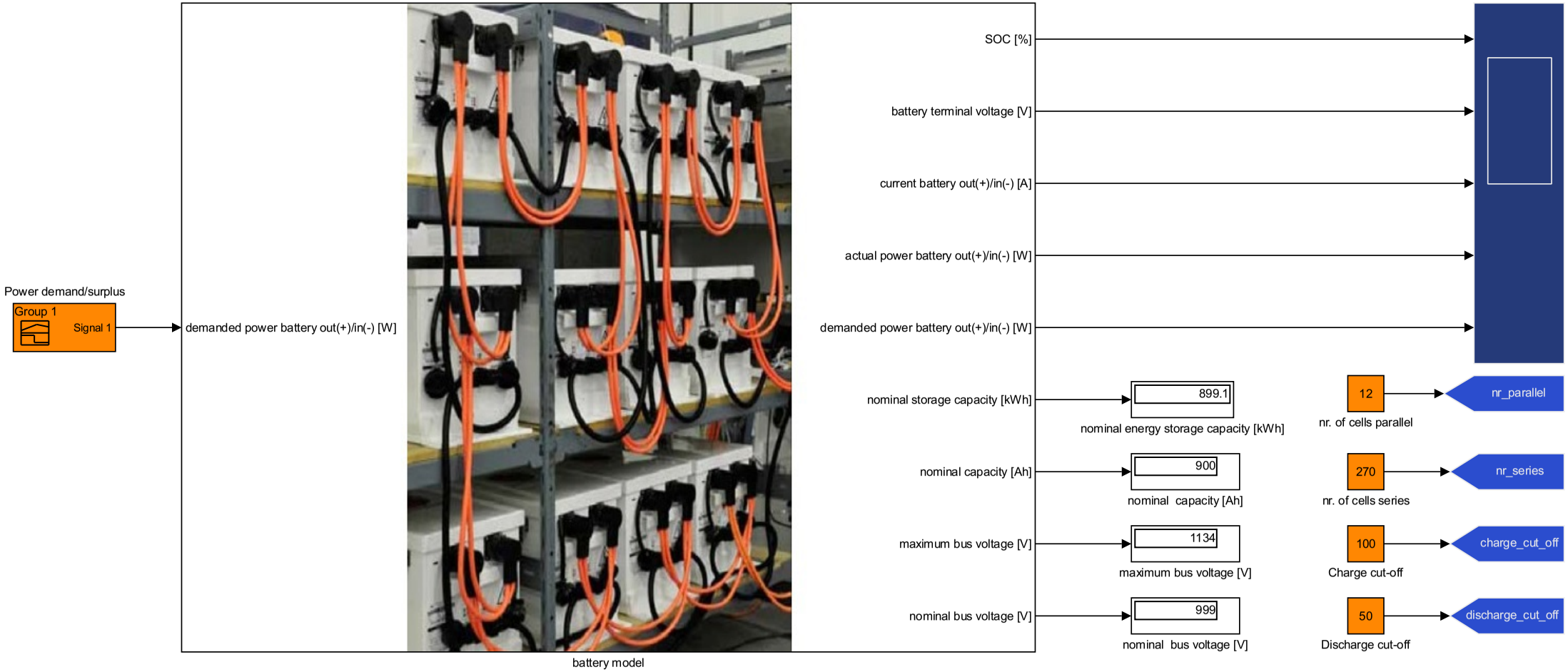
Power demand/surplus
Group 1
Signal 1
demanded power battery out(+)/in(-) [W]
SOC [%]
battery terminal voltage [V]
current battery out(+)/in(-) [A]
actual power battery out(+)/in(-) [W]
demanded power battery out(+)/in(-) [W]
nominal storage capacity [kWh]
899.1
nominal energy storage capacity [kWh]
nominal capacity [Ah]
900
nominal capacity [Ah]
maximum bus voltage [V]
1134
maximum bus voltage [V]
nominal bus voltage [V]
999
nominal bus voltage [V]
12
nr. of cells parallel
nr_parallel
270
nr. of cells series
nr_series
100
Charge cut-off
charge_cut_off
50
Discharge cut-off
discharge_cut_off
battery model

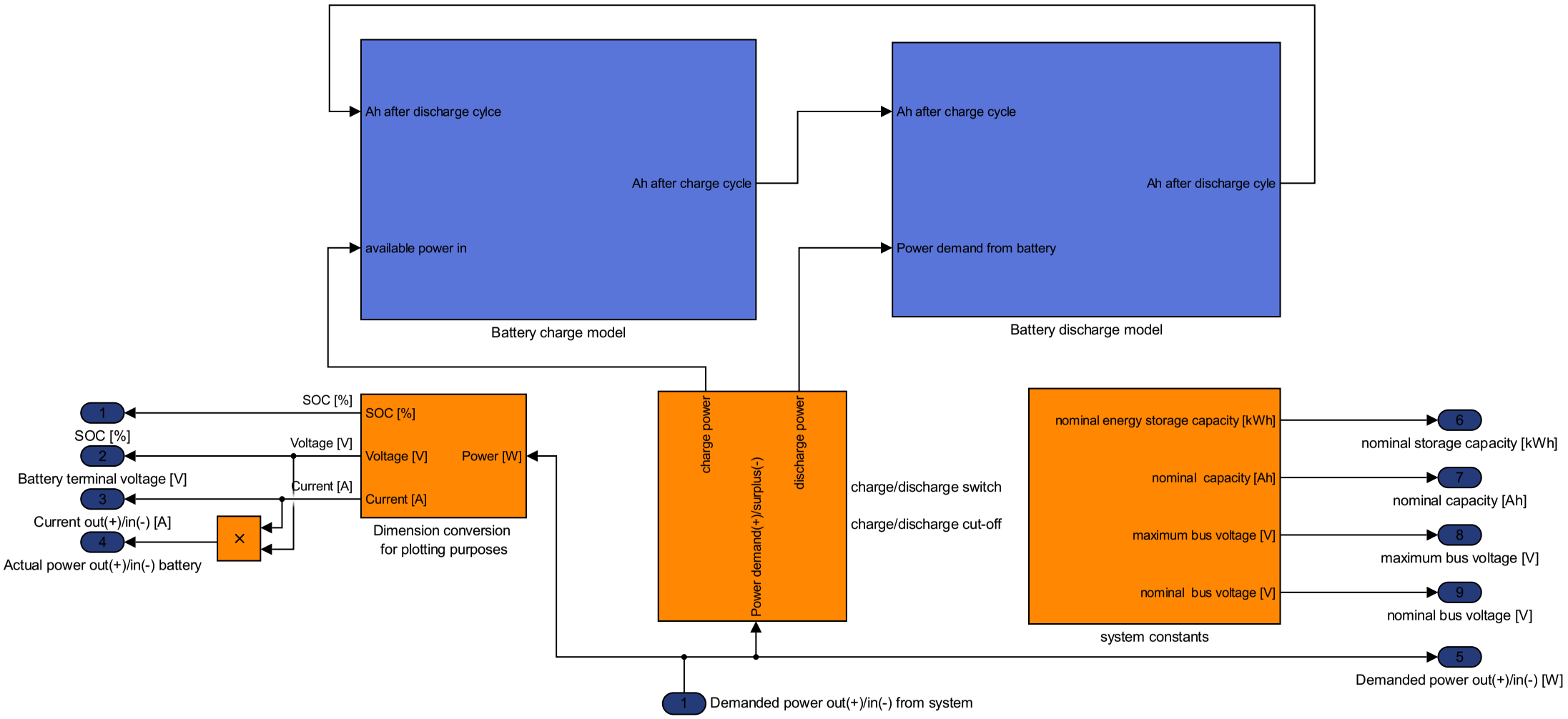
Ah after discharge cylce
Ah after charge cycle
available power in
Battery charge model
Ah after charge cycle
Ah after discharge cyle
Power demand from battery
Battery discharge model
SOC [%]
Voltage [V]
Current [A]
Dimension conversion
for plotting purposes
charge power
discharge power
Power demand(+)/surplus(-)
charge/discharge switch
charge/discharge cut-off
nominal energy storage capacity [kWh]
nominal capacity [Ah]
maximum bus voltage [V]
nominal bus voltage [V]
system constants
1
SOC [%]
2
Battery terminal voltage [V]
3
Current out(+)/in(-) [A]
4
Actual power out(+)/in(-) battery
6
nominal storage capacity [kWh]
7
nominal capacity [Ah]
8
maximum bus voltage [V]
9
nominal bus voltage [V]
5
Demanded power out(+)/in(-) [W]
1
Demanded power out(+)/in(-) from system

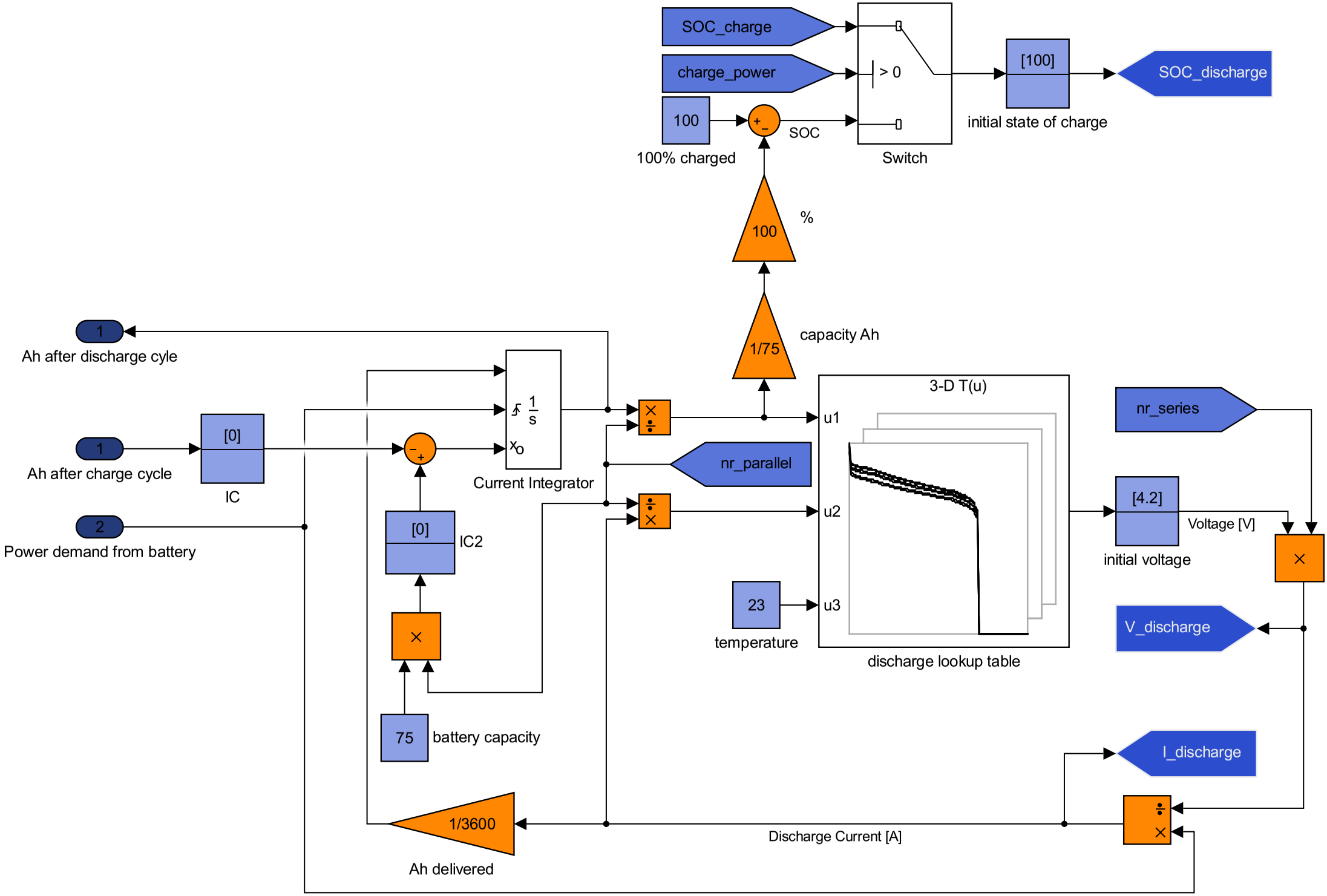
SOC_charge
charge_power
> 0
[100]
SOC_discharge
100
SOC
100% charged
Switch
initial state of charge
100
%
1/75
capacity Ah
1
Ah after discharge cyle
1
Ah after charge cycle
[0]
IC
2
Power demand from battery
Current Integrator
nr_parallel
3-D T(u)
u1
u2
u3
nr_series
[4.2]
Voltage [V]
initial voltage
23
temperature
discharge lookup table
V_discharge
[0]
IC2
75
battery capacity
I_discharge
1/3600
Ah delivered
Discharge Current [A]

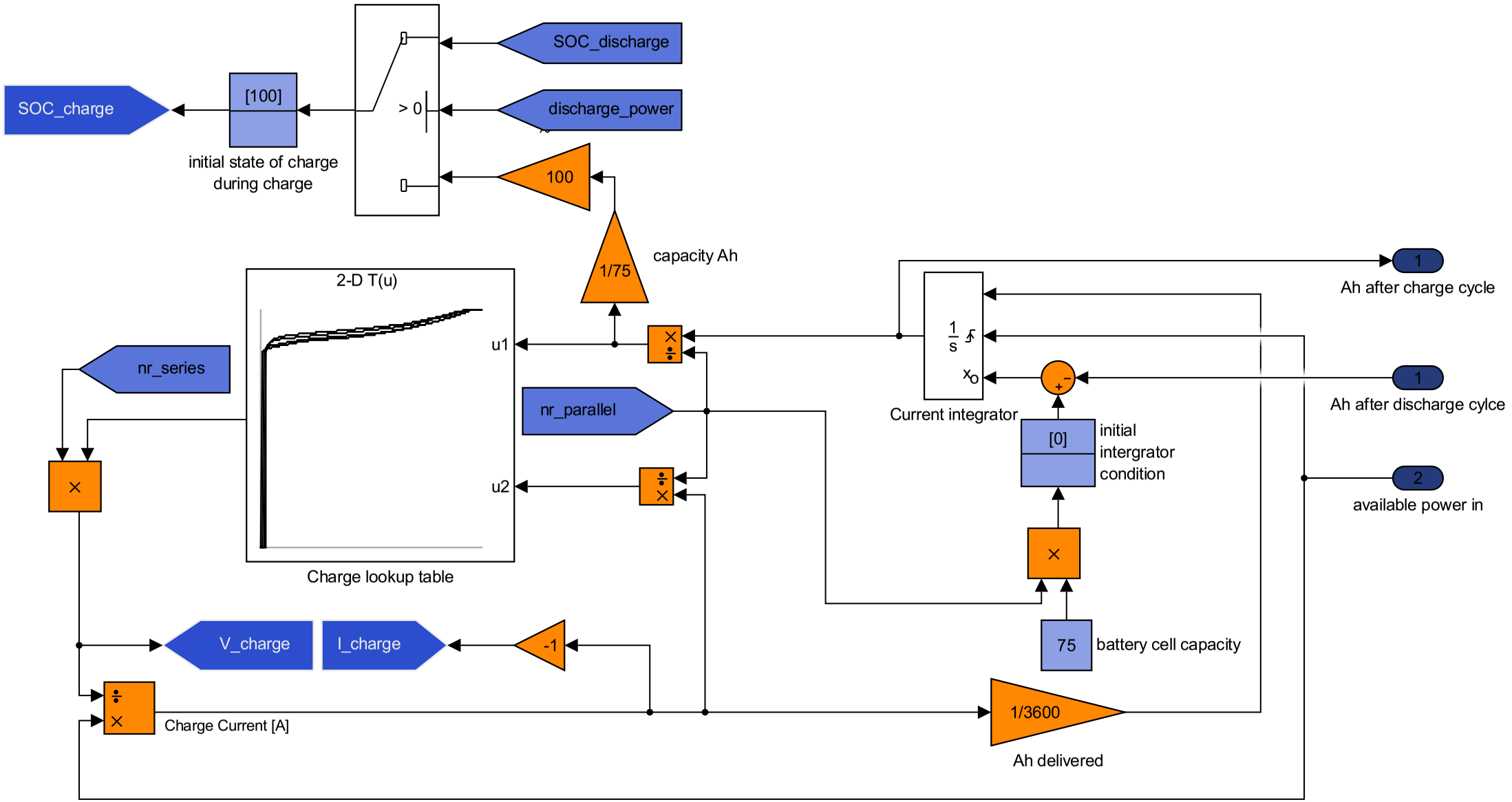
SOC_charge
[100]
initial state of charge during charge
> 0
SOC_discharge
discharge_power
100
1/75
capacity Ah
2-D T(u)
u1
u2
Charge lookup table
nr_series
nr_parallel
Current integrator
[0]
initial intergrator condition
1
Ah after charge cycle
1
Ah after discharge cylce
2
available power in
75
battery cell capacity
1/3600
Ah delivered
V_charge
I_charge
-1
Charge Current [A]

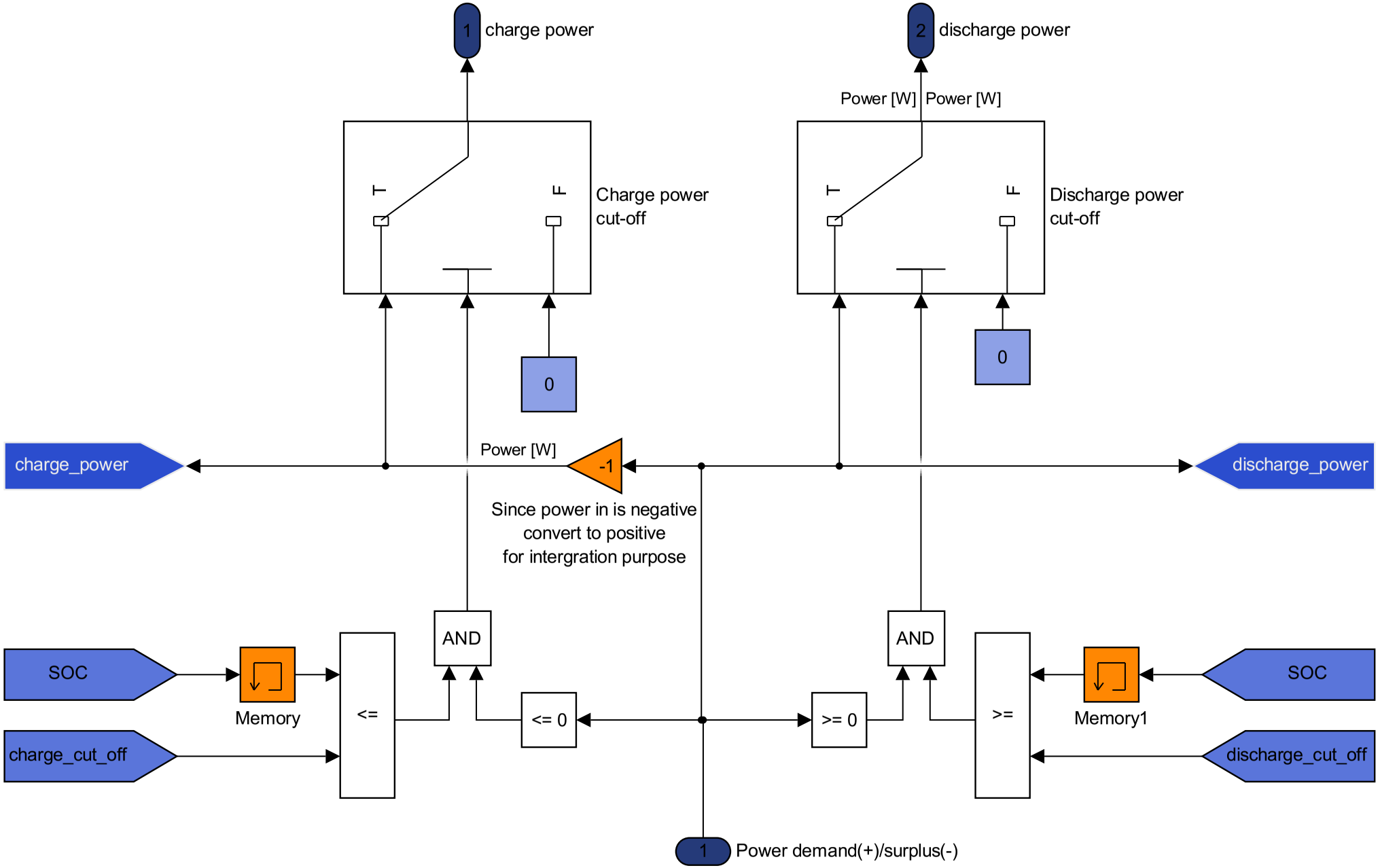
1
charge power
2
discharge power
Power [W]
Power [W]
T
F
Charge power
cut-off
T
F
Discharge power
cut-off
0
0
charge_power
Power [W]
-1
discharge_power
Since power in is negative
convert to positive
for intergration purpose
AND
AND
SOC
Memory
<=
<= 0
>= 0
>=
Memory1
SOC
charge_cut_off
discharge_cut_off
1
Power demand(+)/surplus(-)

G

Power management model in Simulink

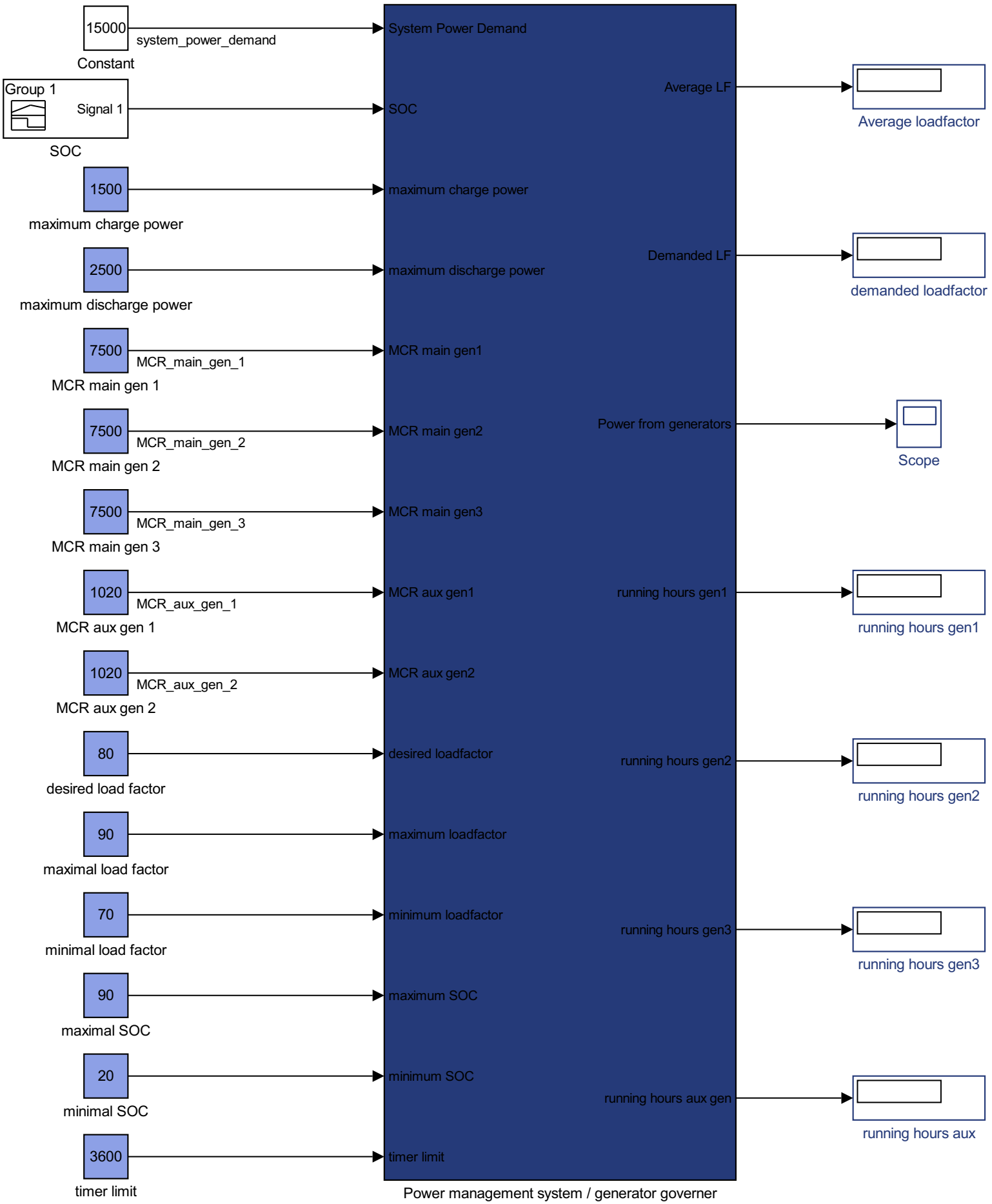
15000
system_power_demand
Constant
Group 1
Signal 1
SOC
1500
maximum charge power
2500
maximum discharge power
7500
MCR_main_gen_1
MCR main gen 1
7500
MCR_main_gen_2
MCR main gen 2
7500
MCR_main_gen_3
MCR main gen 3
1020
MCR_aux_gen_1
MCR aux gen 1
1020
MCR_aux_gen_2
MCR aux gen 2
80
desired load factor
90
maximal load factor
70
minimal load factor
90
maximal SOC
20
minimal SOC
3600
timer limit
System Power Demand
SOC
maximum charge power
maximum discharge power
MCR main gen1
MCR main gen2
MCR main gen3
MCR aux gen1
MCR aux gen2
desired loadfactor
maximum loadfactor
minimum loadfactor
maximum SOC
minimum SOC
timer limit
Power management system / generator governer
Average LF
Demanded LF
Power from generators
running hours gen1
running hours gen2
running hours gen3
running hours aux gen
Average loadfactor
demanded loadfactor
Scope
running hours gen1
running hours gen2
running hours gen3
running hours aux

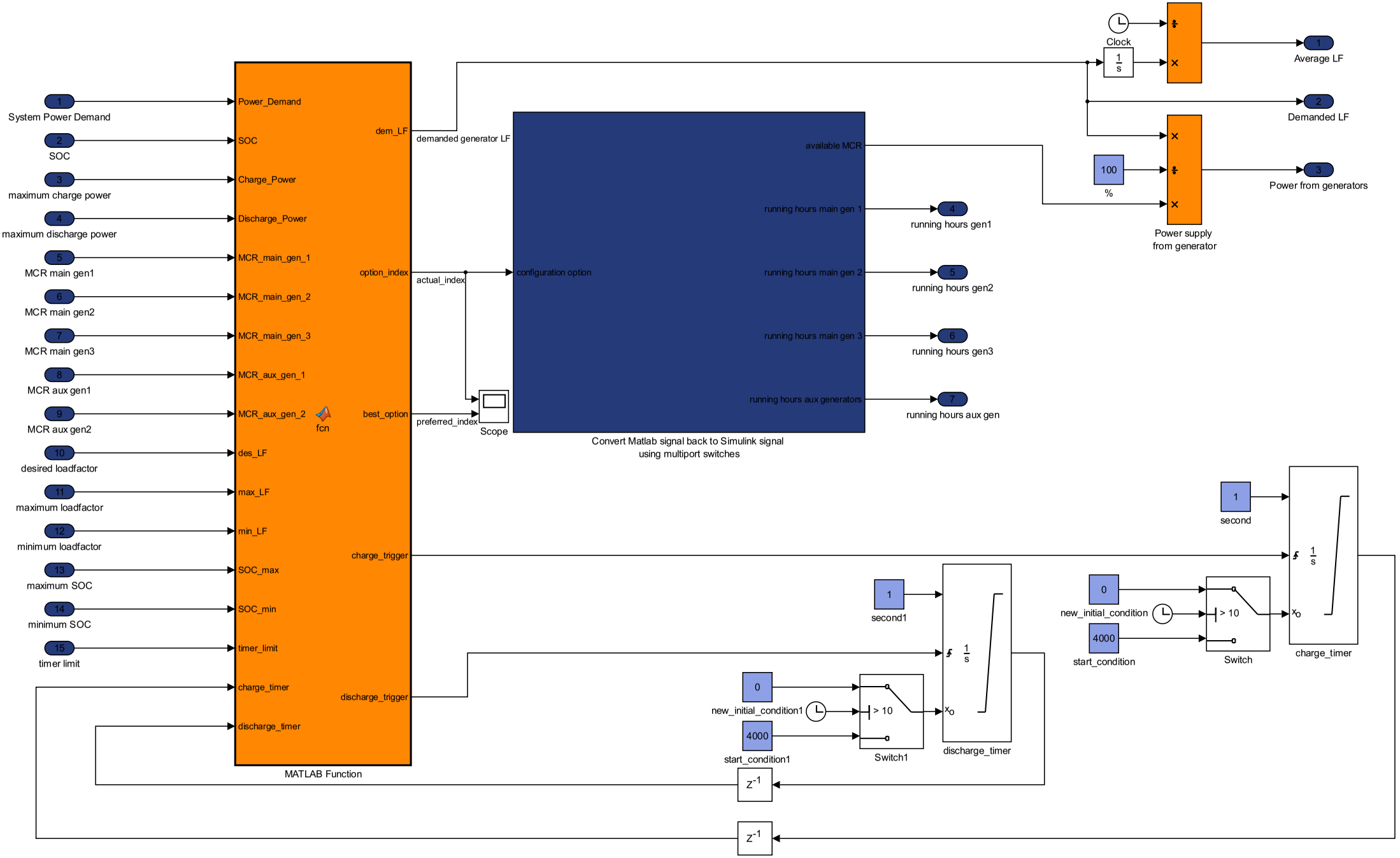
1
System Power Demand
2
SOC
3
maximum charge power
4
maximum discharge power
5
MCR main gen1
6
MCR main gen2
7
MCR main gen3
8
MCR aux gen1
9
MCR aux gen2
10
desired loadfactor
11
maximum loadfactor
12
minimum loadfactor
13
maximum SOC
14
minimum SOC
15
timer limit
Power_Demand
SOC
Charge_Power
Discharge_Power
MCR_main_gen_1
MCR_main_gen_2
MCR_main_gen_3
MCR_aux_gen_1
MCR_aux_gen_2
fcn
des_LF
max_LF
min_LF
SOC_max
SOC_min
timer_limit
charge_timer
discharge_timer
dem_LF
option_index
best_option
charge_trigger
discharge_trigger
MATLAB Function
demanded generator LF
actual_index
preferred_index
Scope
configuration option
available MCR
running hours main gen 1
running hours main gen 2
running hours main gen 3
running hours aux generators
Convert Matlab signal back to Simulink signal
using multiport switches
4
running hours gen1
5
running hours gen2
6
running hours gen3
7
running hours aux gen
Clock
1
s
1
Average LF
2
Demanded LF
100
%
3
Power from generators
Power supply
from generator
1
second
1
second1
0
new_initial_condition1
4000
start_condition1
> 10
Switch1
discharge_timer
0
new_initial_condition
4000
start_condition
> 10
Switch
charge_timer
z-1
z-1

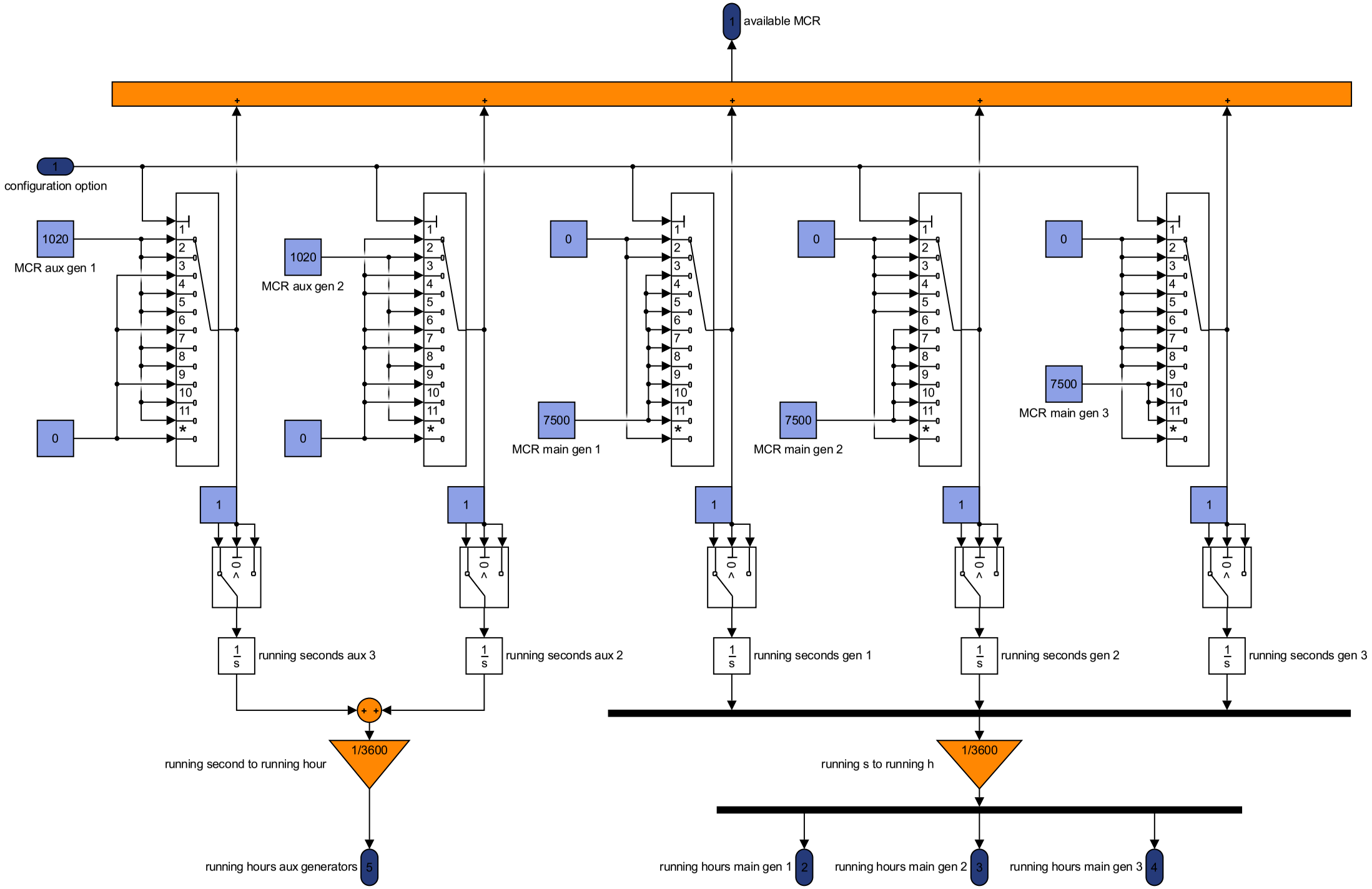
1
available MCR
1
configuration option
1020
MCR aux gen 1
0
1020
MCR aux gen 2
0
0
7500
MCR main gen 1
0
7500
MCR main gen 2
0
7500
MCR main gen 3
1
1
1
1
1
running seconds aux 3
running seconds aux 2
running seconds gen 1
running seconds gen 2
running seconds gen 3
1/3600
running second to running hour
1/3600
running s to running h
running hours aux generators
5
running hours main gen 1
2
running hours main gen 2
3
running hours main gen 3
4

```
[~, option_index]=min(abs(Power_Demand-P_des_a(:,2)));
%selection criterea
max_BOP=P_max_a(option_index,2);
min_BOP=P_min_a(option_index,2);
MCR_100_BOP=P_MCR_100(option_index,2);

%%
if charge_timer<timer_limit %keep on charging
    charge_trigger=0;
    discharge_trigger=0;

    if (P_max_a(10,2)-(Power_Demand+Charge_Power))<=0 ||(P_max_a(10,2)-(Power_Demand+Charge_Power))<=0
        option_index=11;
    else
        vector=P_max_a(:,2)-(Power_Demand+Charge_Power);
        a=vector<0;
        vector(a)=max(vector);
        [~,option_index]=min(vector);
    end

    MCR_100_BOP=P_MCR_100(option_index,2);

    dem_LF=(Power_Demand+Charge_Power)/MCR_100_BOP*100;

    if dem_LF>=max_LF
        dem_LF=max_LF;
    end
elseif discharge_timer<timer_limit %keep discharing
    charge_trigger=0;
    discharge_trigger=0;

    if (Power_Demand-Discharge_Power)<=0
        dem_LF=0;
    else
        vector=(Power_Demand-Discharge_Power)-P_min_a(:,2);
        a=vector<0;
        vector(a)=max(vector);
        [~,option_index]=min(vector);

        MCR_100_BOP=P_MCR_100(option_index,2);

        dem_LF=(Power_Demand-Discharge_Power)/MCR_100_BOP*100;

        if dem_LF>=max_LF
            dem_LF=max_LF;
        end
    end
else
    if SOC<=SOC_min                                                    %charging, so oversupply of power

        if max_BOP>=(Power_Demand+Charge_Power)
            dem_LF=(Power_Demand+Charge_Power)/MCR_100_BOP*100;
        else
```

```
 54             vector=P_max_a(:,2)-(Power_Demand+Charge_Power);
 55             a=vector<0;
 56             vector(a)=max(vector);
 57             [~,option_index]=min(vector);
 58
 59             BOP=P_des_a(option_index,2);
 60             MCR_100_BOP=P_MCR_100(option_index,2);
 61
 62             dem_LF=(Power_Demand+Charge_Power)/MCR_100_BOP*100;
 63
 64             charge_trigger=1;                                          %↙
triggers an integrator to keep track of time
 65             discharge_trigger=0;
 66
 67             if dem_LF>=max_LF
 68                 dem_LF=max_LF;
 69             end
 70         end
 71     elseif SOC>=SOC_max                                               %↙
discharging, so shortage of power
 72
 73         if min_BOP<=(Power_Demand-Discharge_Power)
 74             dem_LF=(Power_Demand-Discharge_Power)/MCR_100_BOP*100;
 75         else
 76             if (Power_Demand-Discharge_Power)<=0
 77                 dem_LF=0;
 78             else
 79                 vector=(Power_Demand-Discharge_Power)-P_min_a(:,2);
 80                 a=vector<0;
 81                 vector(a)=max(vector);
 82                 [~,option_index]=min(vector);
 83
 84                 BOP=P_des_a(option_index,2);
 85                 MCR_100_BOP=P_MCR_100(option_index,2);
 86
 87                 dem_LF=(Power_Demand-Discharge_Power)/MCR_100_BOP*100;
 88
 89                 charge_trigger=0;
 90                 discharge_trigger=1;
 91
 92                 if dem_LF>=max_LF
 93                     dem_LF=max_LF;
 94                 end
 95             end
 96         end
 97     else
 98         dem_LF=des_LF;
 99         charge_trigger=0;
100         discharge_trigger=0;
101     end
102 end
```

H

Fuel consumption validation model in Simulink

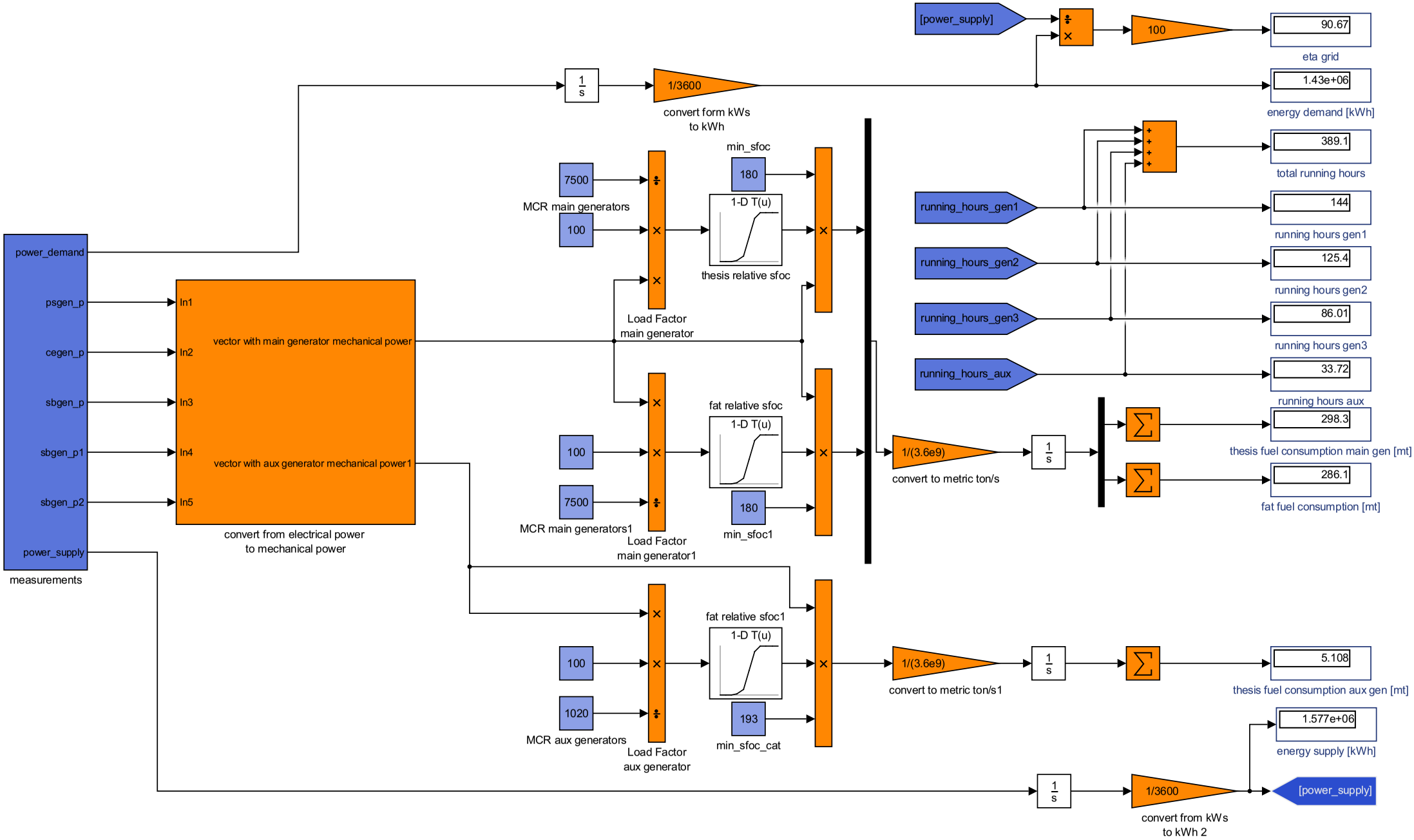
power_demand
psgen_p
cegen_p
sbgen_p
sbgen_p1
sbgen_p2
power_supply
measurements
In1
In2
In3
In4
In5
vector with main generator mechanical power
vector with aux generator mechanical power1
convert from electrical power
to mechanical power
1
s
1/3600
convert form kWs
to kWh
7500
MCR main generators
100
Load Factor
main generator
min_sfoc
180
1-D T(u)
thesis relative sfoc
100
7500
MCR main generators1
Load Factor
main generator1
fat relative sfoc
1-D T(u)
180
min_sfoc1
100
1020
MCR aux generators
Load Factor
aux generator
fat relative sfoc1
1-D T(u)
193
min_sfoc_cat
[power_supply]
100
90.67
eta grid
1.43e+06
energy demand [kWh]
running_hours_gen1
running_hours_gen2
running_hours_gen3
running_hours_aux
389.1
total running hours
144
running hours gen1
125.4
running hours gen2
86.01
running hours gen3
33.72
running hours aux
1/(3.6e9)
convert to metric ton/s
298.3
thesis fuel consumption main gen [mt]
286.1
fat fuel consumption [mt]
1/(3.6e9)
convert to metric ton/s1
5.108
thesis fuel consumption aux gen [mt]
1.577e+06
energy supply [kWh]
1/3600
convert from kWs
to kWh 2
[power_supply]

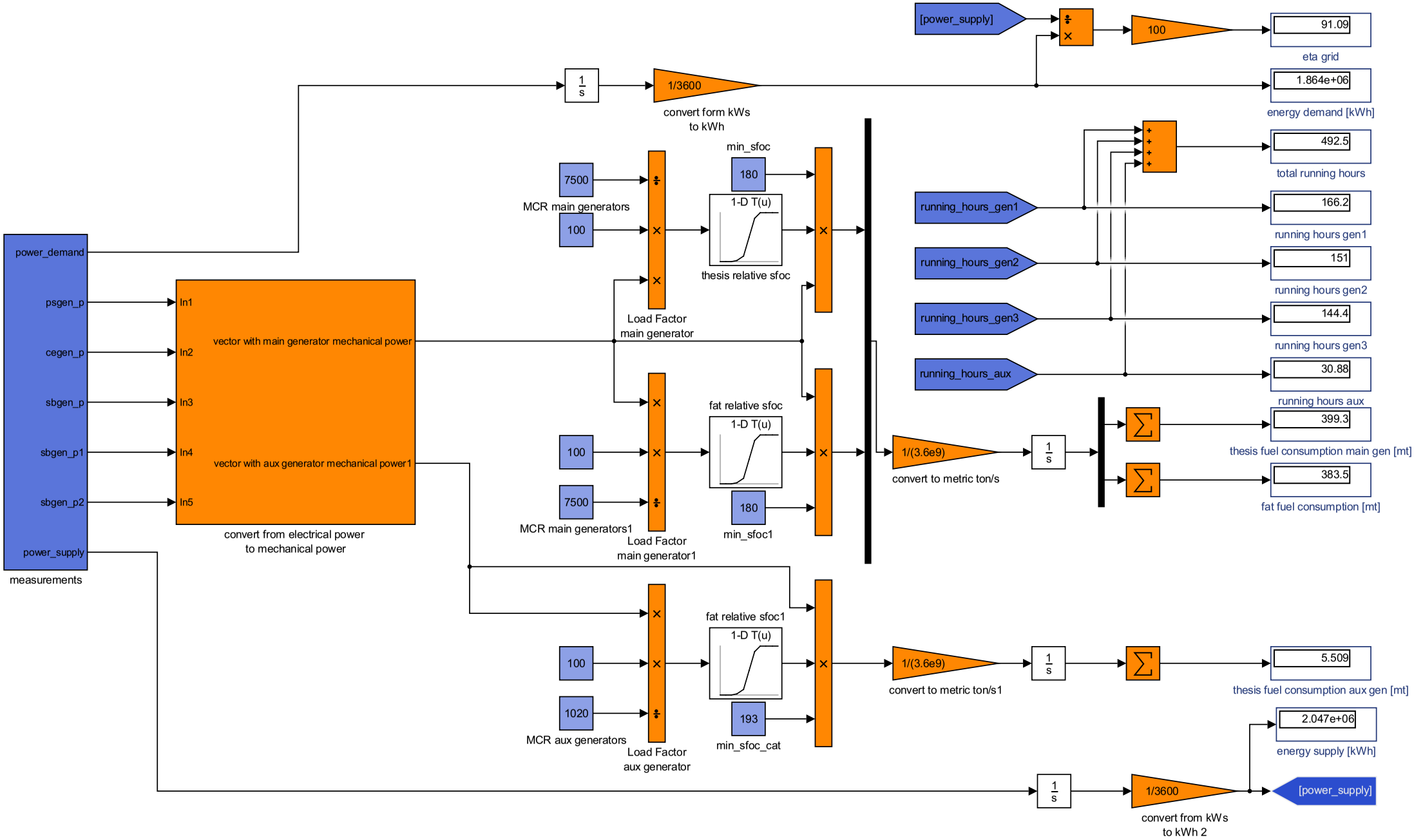
power_demand
psgen_p
cegen_p
sbgen_p
sbgen_p1
sbgen_p2
power_supply
measurements
In1
In2
In3
In4
In5
vector with main generator mechanical power
vector with aux generator mechanical power1
convert from electrical power to mechanical power
1/s
1/3600
convert form kWs to kWh
7500
MCR main generators
100
Load Factor main generator
min_sfoc
180
1-D T(u)
thesis relative sfoc
100
7500
MCR main generators1
Load Factor main generator1
fat relative sfoc
1-D T(u)
180
min_sfoc1
100
1020
MCR aux generators
Load Factor aux generator
fat relative sfoc1
1-D T(u)
193
min_sfoc_cat
[power_supply]
100
91.09
eta grid
1.864e+06
energy demand [kWh]
running_hours_gen1
running_hours_gen2
running_hours_gen3
running_hours_aux
492.5
total running hours
166.2
running hours gen1
151
running hours gen2
144.4
running hours gen3
30.88
running hours aux
1/(3.6e9)
convert to metric ton/s
399.3
thesis fuel consumption main gen [mt]
383.5
fat fuel consumption [mt]
1/(3.6e9)
convert to metric ton/s1
5.509
thesis fuel consumption aux gen [mt]
2.047e+06
energy supply [kWh]
[power_supply]
1/3600
convert from kWs to kWh 2

Filtered power demand signals

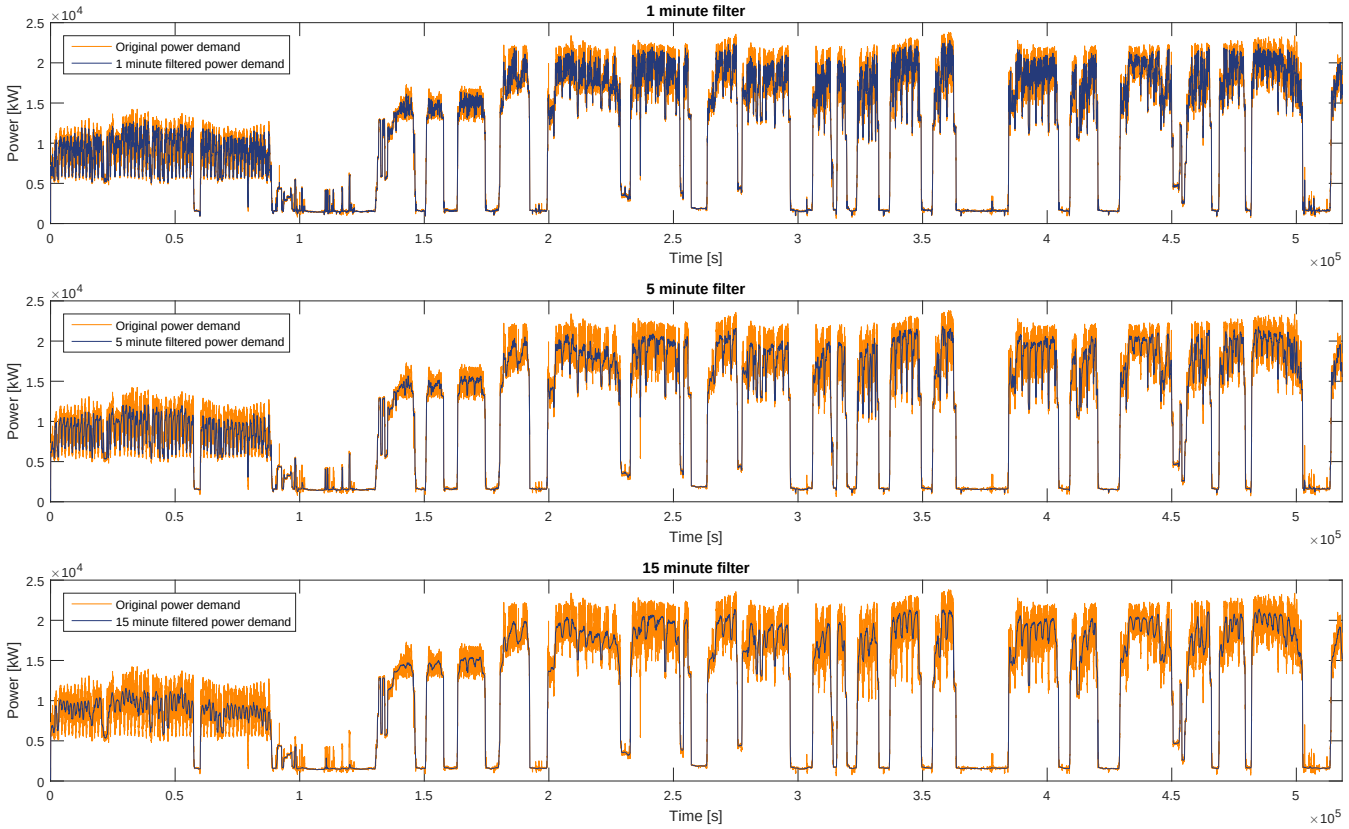

Figure I.1: 1, 5 and 15 minute peak shaving filters

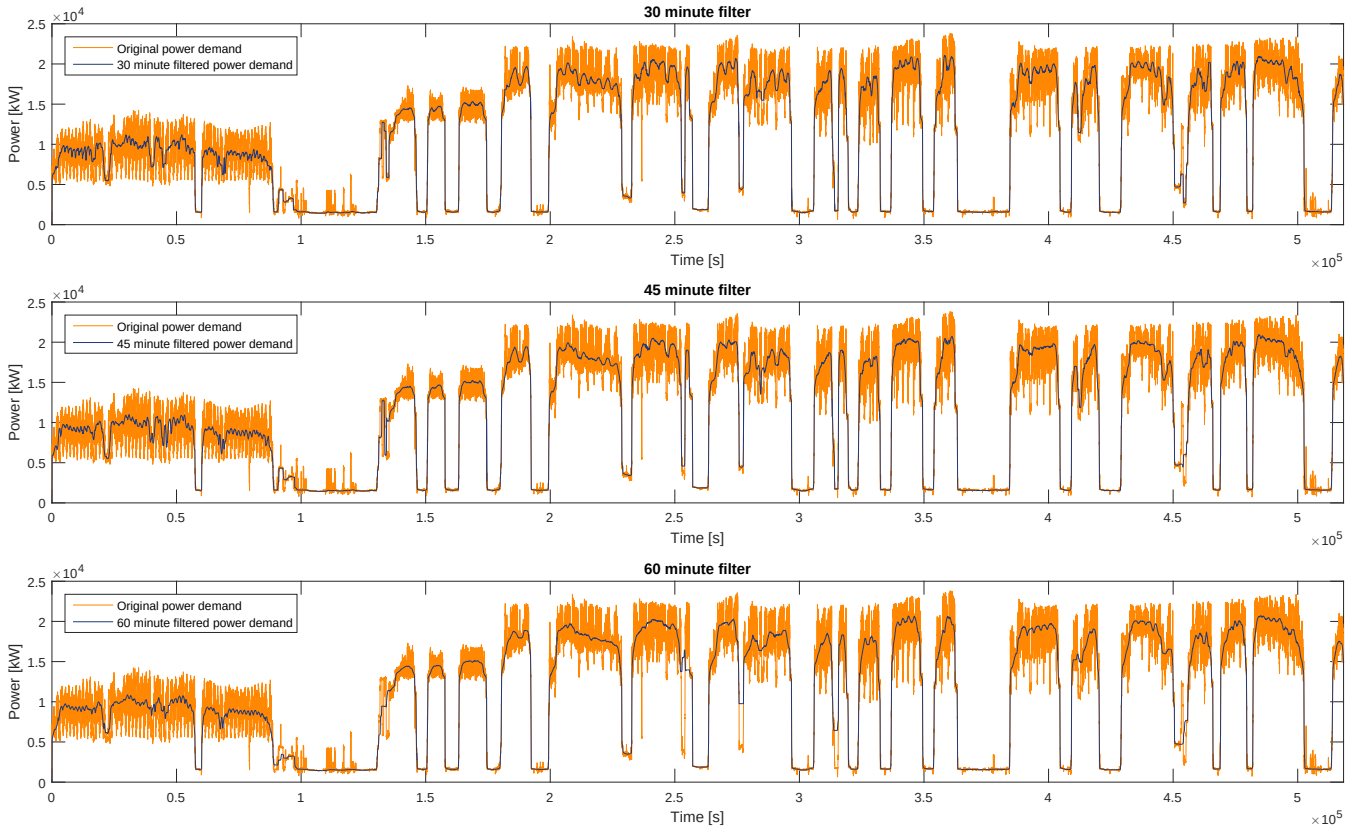

Figure I.2: 30, 45 and 60 minute peak shaving filters

J

Battery lifetime calculation results

Table J.1: Estimated battery lifetime

Simulation number	battery lifetime $[year]$	simulation number	battery lifetime $[year]$
1	1.6	20	3.8
2	4.1	21	4.5
3	3.8	22	4.7
4	4.7	23	4.9
5	5.4	24	4.9
6	5.0	25	0.9
7	5.3	26	1.2
8	5.9	27	1.2
9	4.9	28	1.6
10	5.5	29	1.6
11	5.8	30	1.7
12	4.9	31	3.2
13	6.0	32	5.9
14	5.8	33	6.3
15	4.7	34	7.9
16	6.2	35	7.4
17	5.3	36	7.6
18	4.7	37	7.6
19	4.0	38	8.0

K

Original and hybrid generator power

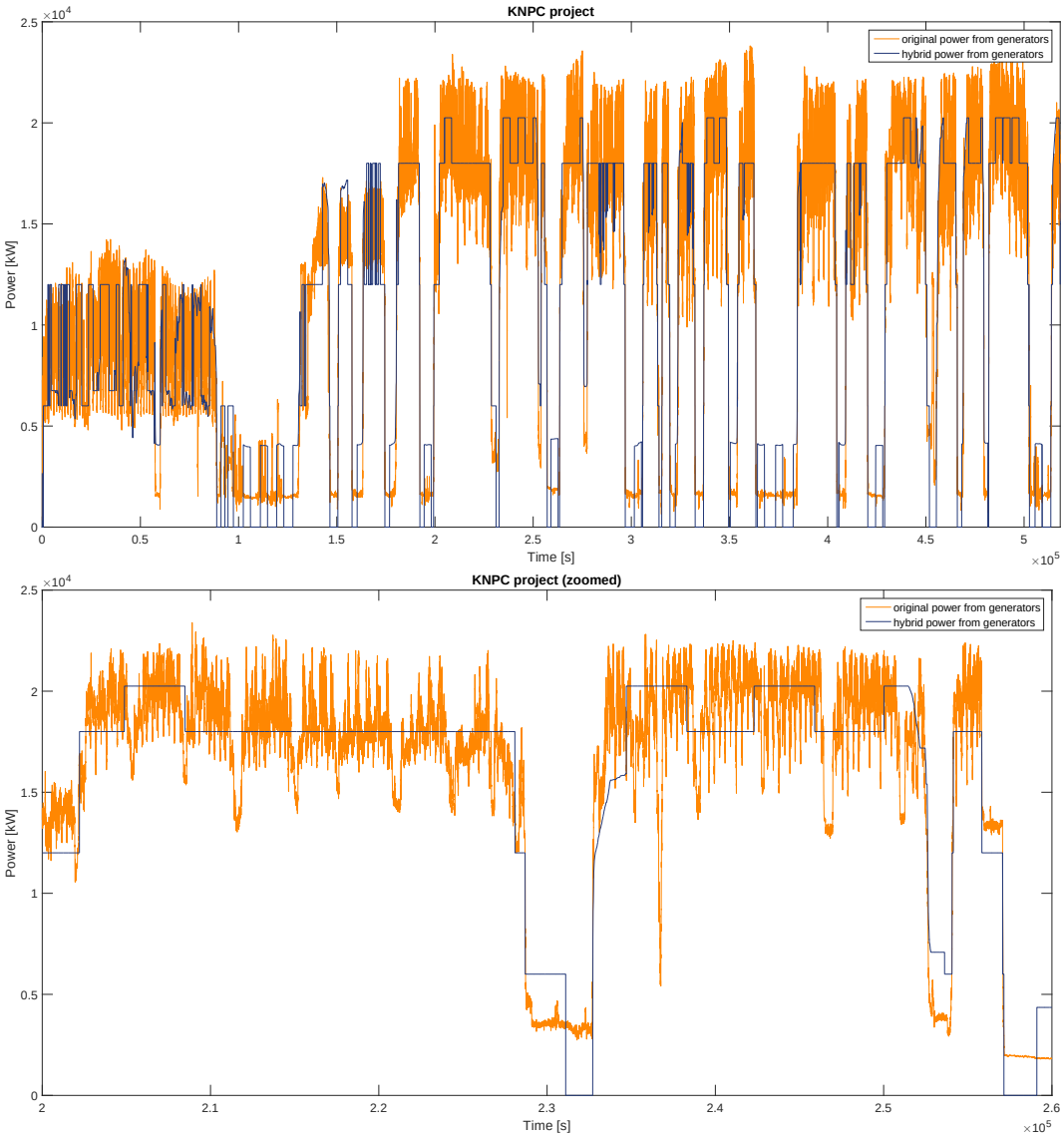

Figure K.1: Original and hybrid generator power output for the *general* working profile

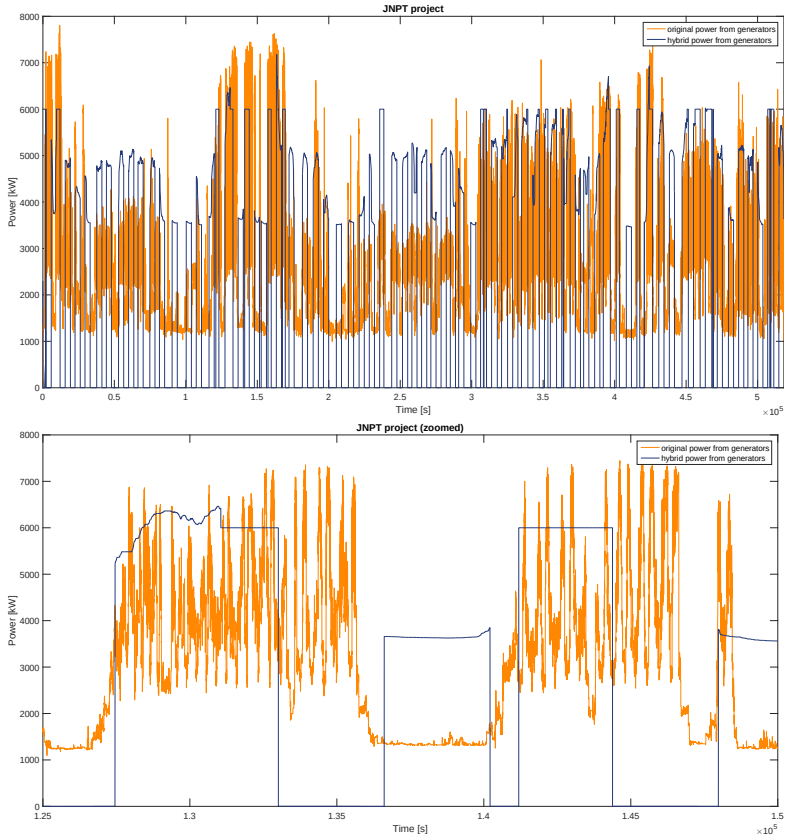

Figure K.2: Original and hybrid generator power output for the JNPT working profile

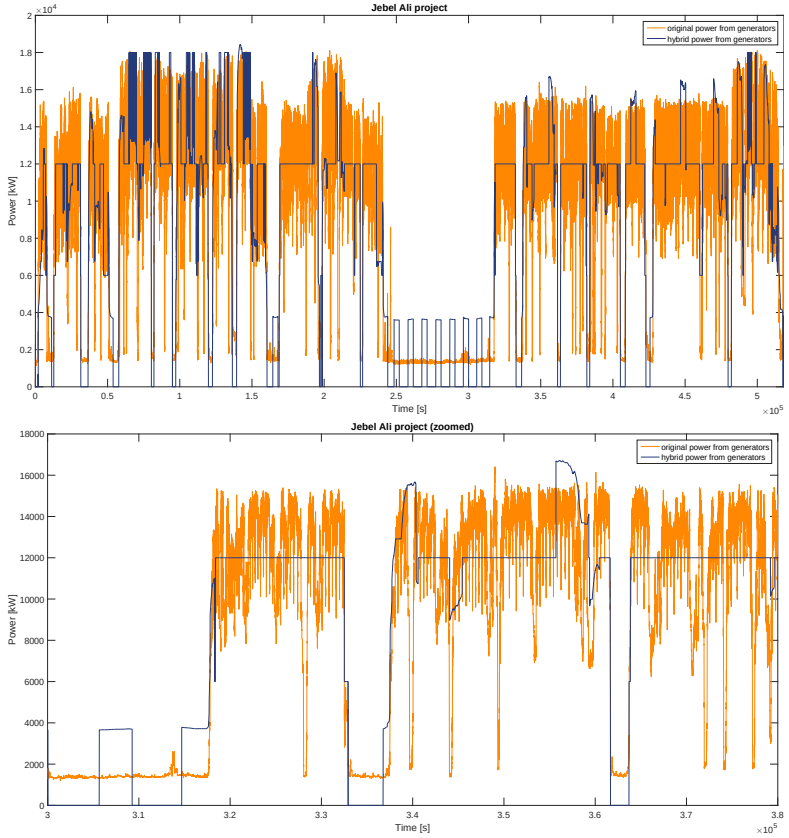

Figure K.3: Original and hybrid generator power output for the Jebel Ali working profile

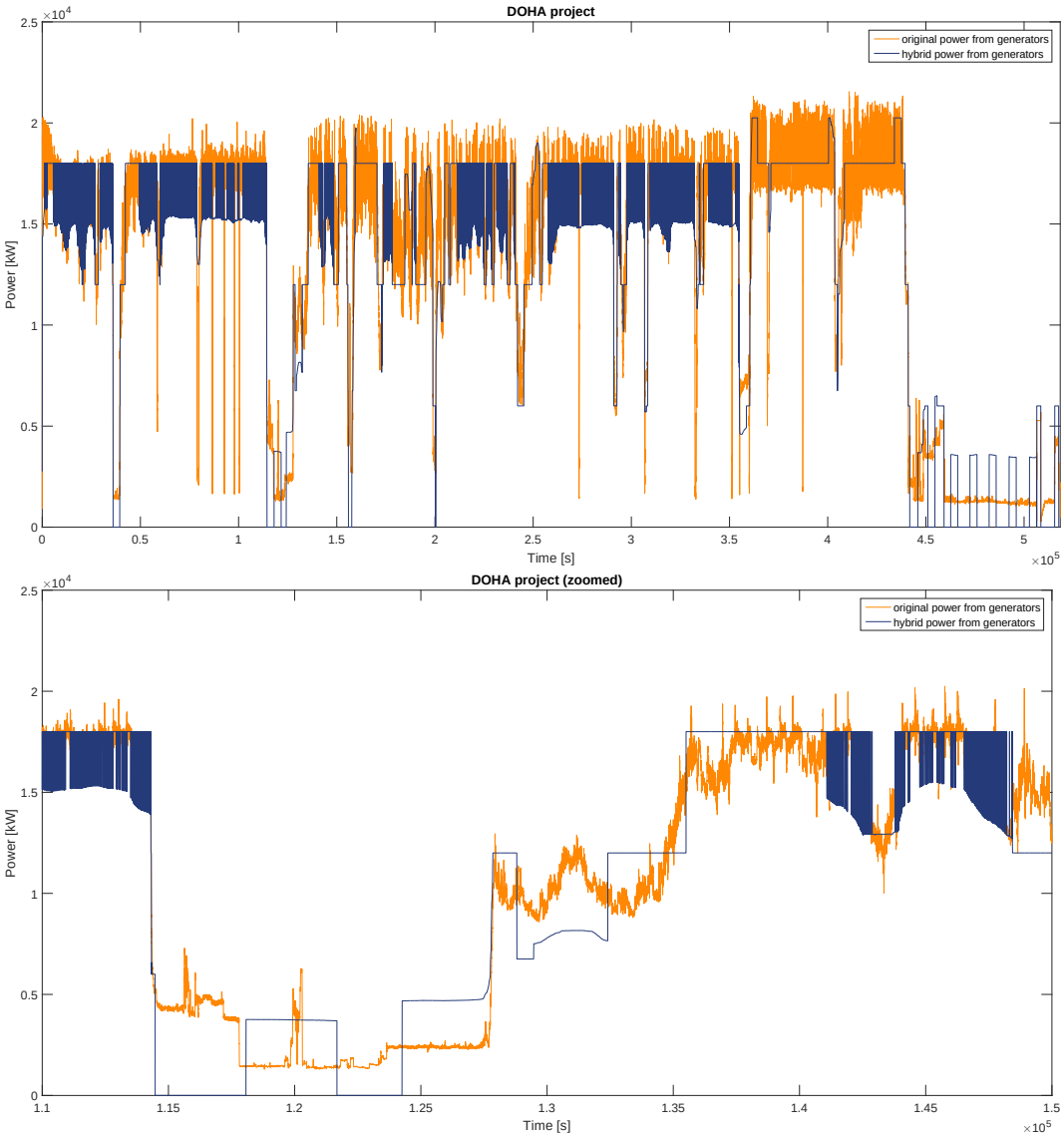

Figure K.4: Original and hybrid generator power output for the DOHA working profile

Bibliography

ABB Industry Oy / Machines (2000). Synchronous machine amg 1120mr06 lsea. Technical report, ABB TURBOCHARGER B.V. used for generator moment of intertia HAM318.

Aspin, J. and Hayman, S., editors (2009). *The Hybrid Tug Reality - The Business Case for Green Technology in the Tugboat Industry*, 2. TUGNOLOGY'09, ABR company Ltd.

Berger, E. (2002). Friction modeling for dynamic system simulation. *American Society of Mechanical Engineers*, 55, no. 6:535–577.

Bertens, J. (2014). Evaluation opex life cycle costs diesel engines tshd's - mph9.0. Technical report, Van Oord.

Cambridge Business English Dictionary (2015). "hybrid" in business english. internet. `http://dictionary.cambridge.org/dictionary/english/hybrid`.

Cimac Working Group "GAS ENGINES" (2011). Transient response behaviour of gas engines. Technical report, International Council on Combustion Engines. Position Paper.

Coordinator of the discussion at MEPC69 (2016). Appendix b - a sample form of a ship energy efficiency management plan - part ii - fuel consumption data collection plan. e-mail correspondence. Shared document from K.A. van Dijk (Van Oord).

CORVUS energy (2015). Market segments - merchant marine. internet. `http://corvusenergy.com/merchant_marine/`.

Currency-Converter.net (2016). Usd/eur exchange rate. internet. `https://currency-converter.net/?gclid=CjwKEAjwxeq9BRDDh4_MheOnvAESJABZ4VTqxLfzIQ4ovEXC9H-r5VVmpmWPDtiAPujNjHMk1HywlxoCVsHw_wcB`.

Daniels, B., Tieben, B., Weda, J., Hekkenberg, M., Smekens, K., and Vethman, P. (2012). Kosten en baten van co2 emissiereductie maatregelen. *ECN beleidsstudies*.

Dredgepoint.org (2012). Brasil. internet. `https://www.dredgepoint.org/dredging-database/equipment/brasil`.

EPA (2015). Social cost of carbon.

Eppler, A. (2014). In the bank. *Electric and Hybrid Marine Technology International*, October 2014:41–42.

Floren (2000). Torsional vibration scheme. Technical report, A. Friedr. Flender AG. used for gerabox moment of intertia HAM318.

Francesco, L., Giampaolo, F., and Vilson, L. (2009). Torsional vibration calculation ihc co1261. Technical report, Wärtsilä Italia SpA. used for generator moment of intertia Athena.

Fry, G. (2016). Rom quote. e-mail correspondence. Spear Power Systems provided a price quotation for a 5620 kWh battery.

Gao, Y. (2012). *Encyclopedia of Sustainability Science and Technology*, chapter Electric, Hybrid Electric and Fuel Cell Vehicles, Architectures of, pages 201–213. Springer Science+Business Media Llc. 978-978-1-4419-0851-3.

Geus, M. (2013). Work visit csd artemis and spread (wk48 till wk50 2013). Technical report, Van Oord.

Geus, M. (2014a). Work visit csd artemis and booster athena (4 days, wk41 2014). Technical report, Van Oord.

Geus, M. (2014b). Work visit csd artemis and spread (4 days, wk28 2014). Technical report, Van Oord.

Grbovíc, P. (2014). *ULTRA-CAPACITORS IN POWER CONVERSION SYSTEMS, APPLICATIONS,ANALYSIS AND DESIGN FROM THEORY TO PRACTICE*. John Wiley and Sons Ltd., The Atrium, Southern Gate, Chichester, PO198SQ West Sussex.

Grevink, J. (2000). Lips technical report t2000-129 shaft line whirling analyses and alignment calculations. Technical report, John Crane-Lips. used for prop. shaft moment of intertia HAM318.

Grimmelius, H., de Vos, P., Krijgsman, M., and van Deursen, E. (2011). Control of hybrid ship drive systems. *Proceedings of the 10th Conference on Computer and Its Application in the Maritime Industry*, pages 1–14.

Hansen, J., Lindtjorn, J., Myklebust, T., and Vänskä, K. (2011). Onboard dc grid. internet. `https://library.e.abb.com/public/b4f3f099e9d21360c1257a8a003beac2/ABB%20Generations_20%20Onboard%20DC%20grid.pdf`.

Hartkopf Mikkelsen, J. and Grønvald Raun, K. (2015). Man sued in dispute about fuel cheating software. internet. `http://shippingwatch.com/secure/carriers/article8111661.ece`.

Hauso, H. (2015). Corvus price proposal. e-mail correspondence. Initial proposal with price quotation from Corvus Energy for concept design of a hopper dredger.

Hibbeler, R. (2010). *Engineering Mechanics DYNAMICS*. Prentice Hall, Pearson Eductaion South Asia Pte. Ltd., 23/25 First Lok Yang Road, Jurong, Singapore 629733, 12 edition.

Huria, T., Ceraolo, M., Gazzari, J., and Jackey, R. (2012). High fidelity electrical model with thermal dependence for characterization and simulation of high power lithium battery cells. *Electric Vehicle Conference (IEVC), 2012 IEEE International*, pages 1–8.

IHC Holland (1985). *Centrifugaal Baggerpompen*, volume 6, chapter Centrifugaal baggerpompen 10, pages 59–64. IHC Holland, Postbus 1, 2960AA Kinderdijk.

IHC HOLLAND NV. (2000). Arrangement of prop. and gen. drive. drawing - Van Oord archive. used for propeller moment of intertia HAM318.

Jackey, R. (2012). Lithium battery model with thermal effects for system-level analysis. internet. `http://nl.mathworks.com/videos/lithium-battery-model-with-thermal-effects-for-system-level-analysis-81886.html?form_seq=conf1302&elqsid=1467374748134&potential_use=Student&country_code=NL`.

Jongerden, M. and Haverkort, B. (2008). Battery modeling. internet. `http://doc.utwente.nl/64556/1/BatteryRep4.pdf`.

Kessels, J. (2007). *Energy Management for Automotive Power Nets*. PhD thesis, Technical University Eindhoven.

Klein Woud, H. and Stapersma, D. (2002). *Design of Propulsion and Electric Power Generation Systems*. IMarEST, 80 Coleman Street, London EC2R 5BJ, 2008 reprint edition.

Lebedevas, S., Dailydka, S., Jastremskas, V., and Rapalis, P. (2015). The influence of locomotive diesel engine transient operating modes on energy usage. *Transportation Research Part D*, 34:219–229.

Lindgren, M. (2005). A transient fuel consumption model for non-road mobile machinery. *Biosystems Engineering*, 91:139–147.

Luyendijk, J. (2015). *DIT KAN NIET WAAR ZIJN*, chapter Other People's Money 4, page 60. Uitgeverij Atlas Contact, Amsterdam/Antwerpen, 13 edition. Dutch edition, quoted phrase is freely translated from Dutch to English.

Lyu, Z. (2016). Concept design of hybrid crane vessel. this thesis is available at `http://repository.tudelft.nl/`.

MAK (2014). M34df project guide / propulsion.

Mallouh, M., Abdelhafez, E., Salah, M., Hamdanl, M., Surgenor, B., and Youssef, M. (2014). Model development and analysis of a mid-sized hybrid fuel cell/battery vehicle with a representative driving cycle. *Journal of Power Sources*, 260:62–71.

MAN Diesel and Turbo (2016). Influence from total engine running time and service intervals on fuel oil consumption. *MAN 48/60CR IMO Tier III, Project Guide - Marine, EN*, 2:88.

MAN Diesel SE (2007). Shop test protocol. Technical Report 1, MAN Diesel SE. Test report, place and date; Saint-Nazaire 30.11.2007, approved by; Bureau Veritas,IHC Dredgers BV, MAN Diesel.

MAN Diesel SE (2008). Technical documentation engine operating instructions b1. Technical Report 1, MAN Diesel SE. Engine; 12V 48/60 B, Work No; 1135376/377, Plant No; 4300155.

Maxwell Technologies (2009). Product guide maxwell technologies boostcap ultracapacitors. Technical report, Maxwell Technologies. Doc. No. 1014627.1.

Muenzel, V., Brazil, M., de Hoog, J., Vishwanath, A., and Kalyanaraman, S. (2015). A multi-factor battery cycle life prediction methodology for optimal battery management. *ACM e-Energyl*.

Nagy, Z. (2016). confirmation generator efficiency. meeting. Z. Nagy is electrical-Technical Superintendent at the E-Technical Department within Van Oord Ship Management Department.

National Institute of Statistics and Economic Studies (2016a). International prices of imported raw materials - domestic diesel heating oil (rotterdam) - prices in euros per tonne - cif - 1% of sulfur. internet. `http://www.insee.fr/en/bases-de-donnees/bsweb/serie.asp?idbank=001565199`.

National Institute of Statistics and Economic Studies (2016b). International prices of imported raw materials - heavy fuel oil (rotterdam) - prices in euros per tonne - fob - 1% of sulfur. internet. `http://www.insee.fr/en/bases-de-donnees/bsweb/serie.asp?idbank=001642885`.

Odeim, F., Roes, J., Wülbeck, L., and Heinzel, A. (2014). Power management optimization of fuel cell/battery hybrid vehicles with experimental validation. *Journal of Power Sources*, 252:333–343.

Omar, N., Monem, M., Firouz, Y., Salminen, J., Smekens, J., O, H., Gaulous, H., Mulder, G., van den Bosche, P., Coosemans, T., and van Mierlo, J. (2014). Lithium iron phosphate based battery - assessment of the ageing parameters and development of cycle life model. *Applied Energy*.

Paauw, J. (2016). Fuel measurement verification. derived from a meeting.

Pedersen, E. and Engja, H. (2010). *Mathematical Modelling and Simulation of Physical Systems*. 2. NTNU, Department of Marine Technology, Nardoveien 12, 7005 Trondheim.

Pernice, D. (2009). W6l46f van oord dredger application de-imotier1 load profile test on 8l46f. Technical report, Wärtsilä.

Rahn, D. (2015). Electric and hybrid marine awards supplier of the year winner: Corvus energy. *Electric and Hybrid Marine Technology International*, October:40.

Rakopoulos, C. and Giakoumis, E. (2009). *Diesel Engine Transient Operation*. Springer-Verlag London Limited. National Technical University of Athens, School of Mechanical Engineering, 9 Heroon Polytechniou St., 15780 Athens.

Rensen, M. (2014). Research into fuel consumption estimation in vocut. Technical Report 1, Van Oord, Department of Estimating and Engineering and Department of Equipment and Process Technology.

S and P Global, Platts (2016). Bunkerwire. Technical Report 40, Platts. Bunkerprices on Friday, August 19, 2016.

Sciarretta, A., Serrao, L., Dewangan, P., Tona, P., Bergshoeff, E., Bordons, C., Charmpa, L., Elbert, p., Eriksson, L., Hofman, T., Hubacher, M., Isenegger, P., Lacandia, F., Laveau, A., Li, H., Nüesch, T., Onori, S., Pisu, P., Rios, J., Silvas, E., Sivertsson, M., Tribioli, L., van der Hoeven, A.-J., and Wu, M. (2014). A control benchmark on the energy management of a plug-in hybrid electric vehicle. *Control Engineering Practice*, 29:287–298.

Shi, W. (2013). *Dynamics of Energy System Behaviour and Emissions of Trailing Suction Hopper Dredgers*. PhD thesis, Delft University of Technology. ISBN: 978-90-6562-315-7.

Sorensen, A. J. (2014). *Marine Control Systems*. NTNU, Department of Marine Technology, Nardoveien 12, 7005 Trondheim. Lecture Notes TMR4240.

Spear Power Systems and Fry, G. (2016). Battery information. e-mail correspondence. Gordon Fry was so kind to provide answers on questions raised during the development of the battery model.

Stapersma, D. (2010a). *DIESEL ENGINES*, volume Part 3:Combustion. NLDA and Delft UT, 8 edition.

Stapersma, D. (2010b). *DIESEL ENGINES*, volume Part 1: Diesel engines A - Performance analysis and turbocharging. NLDA and Delft UT, 8 edition.

Super B and Pot, R. (2016). Battery information. e-mail correspondence. René Pot was so kind to provide answers on questions about battery prices.

Super B b.v. (2016). User manual sb12v160e-zc lithium iron phosphate battery. Technical report, Super B b.v. Provided by René Pot, Super B batteries.

The Dutch Association of Contractors in Dredging, S. a. B. P. (2010). *Snijkopzuiger*, volume 5a. The Dutch Association of Contractors in Dredging, Shore an Bank Protection, Kampenringweg 45, 2800 AL Gouda. Lesboek Voortgezette Opleiding Uivoering Baggerwerken.

The Mathworks (2008). Help file battery sim power systems. internally Matlab.

Thoolen, F. (2014). Ccm flywheel technology. information leaflet. published by: CCM centre for concepts in mechatronics.

tractordata.com (2009). Valmet 6650 - engine. internet. `http://www.tractordata.com/farm-tractors/001/9/0/1903-valmet-6650-engine.html`.

Trajkovic, S. (2010). *The Pneumatic Hybrid Vehicle A New Concept for Fuel Consumption Reduction*. PhD thesis, Lund University, Devision of Combustion Engines, Department of Energy Sciences, Faculty of Engineering, Lund University, P.O. Box 118, SE-22100 Lund. Printed by Tryckeriet i E-huset.

UNFPA (2016). A framework for the assessment of population risk and resilience to climate change. internet. `http://www.unfpa.org/sites/default/files/resource-pdf/Poster_A_Framework_for_the_Assessment_of_Population_Risk_and_Resilience_to_CCf.pdf`.

VAF instruments (2015). Technical manual: 665 pem 3 propulsion efficiency monitor.

Valence (2016). Xp datasheet july 2016. Technical report, Valence.

van der Pennen, W. (2015). Energy management system Find the Optimum from design until operation. presentation. presentation during: Seminar Elektrische Installaties op schepen en offshore : Ontwikkelingen in de IEC Normen.

Van Oord (2014). Fuel and lub reporting. Technical report, Van Oord. Fuel and Lub Reporting for the Artemis, period 2014 week 40 until 2014 week 43.

Wärtsilä Corporation (2000). Delivery documents for wÄrtsilÄ 46-engine. Technical Report 1, Wärtsilä Finland Oy. Test report, place and date; Turku 03.10.2000, approved by; Bureau Veritas, HAM international dredging, Wärtsilä.

Wärtsilä Corporation (2012). WÄrtsilÄ 46f record book of engine parameters. Technical Report 1, Wärtsilä Finland Oy. Test report, place and date; Trieste 04.12.2009, approved by; Bureau Veritas, IHC DREDGERS B.V., Wärtsilä.

Wärtsilä Corporation (2015). Improving engine fuel and operational efficiency. *Wärtsilä Services Bussiness White Paper*, pages 1–7.

Wärtsilä Corporation (2016). Presentation on li-ion batteries. received from Dick Heidelberg. presentation on trends in the Li-ion battery market.

Wärtsilä, Ship Power Technology (2013). WÄrtsilÄ 46f product guide. Technical report, Wärtsilä Finland Oy. used for diesel engine moment of intertia.

XALT Energy (2015). Xalt 75 ah hp superior lithium ion cell. Technical report, XALT Energy Llc. Provided by Jacob Hauge, Sales and Service Engineer at Corvus Energy.